Université de Montréal

Synthèse de nouveaux matériaux conducteurs comportant des unités aromatiques conjuguées et analyse de leurs propriétés physico-chimiques

par
Stéphane Dufresne

Département de chimie
Faculté des Arts et des Sciences

Thèse présentée à la Faculté des études supérieures
en vue de l'obtention du grade de doctorat en chimie

Décembre, 2010

Université de Montréal
Faculté des études supérieures

Cette thèse intitulée :

Synthèse de nouveaux matériaux conducteurs comportant des unités aromatiques conjuguées et analyse de leurs propriétés physico-chimiques

présentée par :
Stéphane Dufresne

a été évaluée par un jury composé des personnes suivantes :

Christian Reber, président-rapporteur
Will Skene, directeur de recherche
James D. Wuest, membre du jury
Timothy P. Bender, examinateur externe
Nicole St-Louis, représentante du doyen de la FES

Résumé

Les matériaux conjugués ont fait l'objet de beaucoup de recherches durant les dernières années. Les nouveaux matériaux présentent des propriétés intéressantes que ce soit au niveau optique, électrique, mécanique ou même les trois en même temps. La synthèse reste la difficulté principale dans la fabrication de dispositifs électroniques. Les méthodes utilisées pour y parvenir sont l'électropolymérisation, le couplage de Suzuki ou de Wittig. Ces techniques comportent encore de nombreuses contraintes et s'avèrent difficilement réalisables à grande échelle. Les thiophènes, les pyrroles et les furanes ont démontré une bonne conductibilité et une bande de conduction basse due à une conjugaison accrue. L'objectif ici est de synthétiser des oligomères principalement composés de thiophènes dans le but d'en caractériser les propriétés spectroscopiques, électrochimiques et de conduction. La synthèse est souvent l'étape délicate de la fabrication de matériaux conjugués. Nous présentons ici une méthode de synthèse simple par modules avec des unités hétérocycliques. Les modules complémentaires sont attachés par condensation entre un aldéhyde et une amine menant à la formation d'un lien robuste, l'azomethine. Les résultats des propriétés photophysiques et électrochimiques de ces matériaux conjugués seront présentés.

En ayant recours à différents groupes électrodonneurs et électroaccepteurs, en variant le degré de conjugaison ou en utilisant différents hétérocycles, les propriétés spectroscopiques, électrochimiques et de bande de conduction peuvent être adaptées à volonté, ce qui en fait des matériaux aux propriétés modelables. Ces nouvelles molécules seront analysées pour en déceler les propriétés recherchées dans la fabrication d'OLED. Nous explorerons les domaines de l'oxidation electrochimique réversible et de la polymérisation menant à la fabrication de quelques prototypes simples.

Mots-clés : Chimie, Synthèse, Imines, Matériaux conducteurs, Électrochromisme, Diodes organiques électroluminescentes.

Résumé en anglais (Abstract)

Conjugated materials have received much attention recently as they show promise for industrial applications. These materials are interesting because of the many new possibilities for devices combining unique optical, electrical and mechanical properties. The synthesis is the major difficulty in the fabrication of electronic devices. Usual methods to do so are electropolymerisation, Suzuki or Wittig coupling. Those techniques are full of constraints and are difficult to scale-up. Thiophenes, pyrroles and furans demonstrated good conductibility and low band-gap due to increased conjugation. Our main goal is to synthesize oligomers made principally of thiophene to characterize their spectroscopic, electrochemical and conduction properties. Synthesis is the most important step in the making of conjugated material. A synthetically simple and modular route to novel conjugated material consisting of heterocyclic units is presented. These complementary modules are linked by condensing aldehydes and amines leading to robust azomethine bonds. The resulting photophysical and electrochemical properties of these conjugated materials will be presented.

Through the use of different electron donor and acceptor groups, degree of conjugation or by using different heterocycles, the spectroscopic, electrochemical and band-gap properties can be tailored leading to materials with tunable properties. Those new molecules will be analysed to detect properties suitable for OLED fabrication. This presentation will also address the electrochemical reversible oxidation and polymerization of these compounds leading to the making of simple devices.

Keywords : Chemistry, Synthesis, Azomethines, Conducting materials, Electrochromism, Organic light emitting diodes.

Sigles et abbréviations

1D, 2D	une dimension, deux dimensions
abs	absorbance
Bu	butyl
CCDC	Cambridge Crystallographic Data Centre
CIF	Crystallographic Information File, format de fichier texte en cristallographie
CP	Case postale
CROUS	Centre régional des œuvres universitaires et scolaires
ΔE	gap énergétique absolu
ΔG	variation d'enthalpie
DABCO	1,4-diazabicyclo[2.2.2]octane
DCM	dichlorométhane
DFT	density functional theory
DG	discovery grant; acronyme anglais de subventions à la découverte
DIBAL	diisobutylaluminium hydride; acronyme anglais de hydrure de diisobutylaluminium
DMF	diméthylformamide
DMSO	diméthylsulfoxyde
Dr	docteur
ε	coefficient d'extinction molaire
e^-	électron
EA	electron affinity; acronyme anglais d'affinité électronique
E_g	gap énergétique entre la bande de valence et la bande de conduction
E_g^{elect}	gap énergétique déterminé électrochimiquement
E_g^{spect}	gap énergétique déterminé spectroscopiquement
em	émission

E_{pa}	potentiel d'oxydation
E_{pc}	potentiel de réduction
eq	équivalent
ESI	electrospray ionization; acronyme anglais de ionisation par électronébulisation
eV	electron volts
Φ	rendement quantique
f, fl	fluorescence
fig.	figure
HOMO	highest occupied molecular orbital; acronyme anglais d'orbitale moléculaire la plus haute occupée
HRMS	high resolution mass spectrometry; acronyme anglais de spectrométrie de masse haute résolution
IC	internal conversion; acronyme anglais de conversion interne
ICT	internal charge transfer; acronyme anglais de transfert de charge intramoléculaire
IP	ionization potential; acronyme de potentiel d'ionisation
ISC	intersystem crossing; acronyme anglais de croisement intersystème
ITO	indium tin oxide; acronyme anglais d'oxyde d'étain et d'indium
K	kelvin
k_{NR}	constante de désactivation non-radiative
k_o	constante de désactivation de la molécule
k_q	constante de désactivation intermoléculaire
k_R	constante de désactivation radiative
K_{SV}	constante de Stern-Volmer
λ	longueur d'onde (presque toujours) ou énergie de réorganisation de solvant

LFP	laser flash photolysis; acronyme anglais de photolyse par impulsion laser
LUMO	lowest unoccupied molecular orbital; acronyme anglais d'orbitale moléculaire la plus basse vacante
M.p.	melting point; acronyme anglais de point de fusion
Me	méthyl
min	minute
MS	mass spectrometry; acronyme anglais de spectrométrie de masse
Nd-YAG	neodymium-doped yttrium aluminium garnet; acronyme de l'anglais de grenat d'yttrium-aluminium dopé au néodyme
NMR	Nuclear magnetic resonance; acronyme anglais de résonance magnétique nucléaire
NSERC	Natural Sciences and Engineering Research Council of Canada; acronyme anglais du Conseil de recherches en sciences naturelles et en génie du Canada
OLED	organic light emiting diode; acronyme anglais de diode électroluminescente organique
PET	photoinduced electron transfer; acronyme anglais de transfert d'électron photoinduit
phos	phosphorescence
poly	polymère
Prof	professeur
ROMP	ring-opening metathesis polymerization; acronyme anglais de polymérisation de type métathétique par ouverture de cycle
RSC	Royal Society of Chemistry
RT	room temperature; acronyme anglais de température ambiante
RTI	research tools and intruments grant; acronyme anglais de subvention d'outils et d'instruments de recherche

SCE	saturated calomel electrode; acronyme anglais de électrode au calomel saturé
SRG	standard research grant; acronyme anglais de subvention ordinaire de recherche
succ.	succursale
τ	temps de vie
T	triplet
TBA	tétrabutylammonium
THF	tétrahydrofuranne
TFA	tetrafluoroacetic acid; acronyme anglais d'acide tétrafluoroacétique
UV	ultraviolet
XRD	X-ray diffraction; acronyme anglais de diffraction des rayons X

Table des matières

Liste des tableaux

Liste des figures (Charts, Figures, Schemes)

À mon très cher Québec,
comme je le connaissais jadis…

Remerciements

Je tiens tout d'abord à exprimer toute ma gratitude au professeur Will Skene sans qui cette étude n'aurait pas été possible. Merci de m'avoir accueilli dans le laboratoire il y a de cela au moins sept ans alors que je n'étais encore qu'un néophyte en chimie et de m'avoir enseigné les rudiments du métier ce qui m'a permis de bien commencer dans la voie de la recherche. Merci de s'être grandement impliqué dans ce projet par ses directives et ses suggestions.

Mes remerciements vont aussi aux membres du groupe Skene qui ont su mettre une ambiance conviviale au sein du laboratoire, à savoir stagiaires post-doctoraux, étudiants au doctorat, étudiants à la maîtrise et stagiaires. Je ne saurais faire la liste exhaustive des membres du groupe à travers les années. Je ne mentionnerai que les acteurs les plus importants de cette thèse.

Je me dois de commencer par nul autre qu'Andréanne Bolduc, seule autre québécoise à avoir eu le courage de s'engager à long terme dans ce groupe de recherche. De par sa bonne humeur et ses péripéties roman-feuilleton, ma voisine de bureau a su mettre de la gaieté dans chacune de ces journées passées au laboratoire. Un merci tout particulier à Alex Bourque qui fût mon comparse de soirées bien arrosées. Merci à Sergio Pérez de m'avoir montré les chemins de la vie. Merci à Marie Bourgeaux, première doctorante graduée du groupe, qui a tenté de me montrer une technique de travail, en vain.

Merci à Pierre Ménard-Tremblay pour toute son aide technique, mais surtout son attitude professionnelle.

Merci à l'Université de Montréal, et plus spécifiquement au département de chimie quant à ses services d'analyses. Notamment, le service de spectroscopie par résonance magnétique nucléaire, le service de spectroscopie de masse, le laboratoire de diffraction des rayons X, les services d'ateliers mécaniques et électroniques pour les nombreux services rendus.

Je voudrais remercier le professeur Garry Hanan et son groupe de recherche pour certaines collaborations, l'emprunt de produits et l'utilisation d'appareil. Il a bien su écrire une lettre de recommandation, et ce, à plusieurs reprises.

Merci au soutien financier du CRSNG. Premièrement, de m'avoir refusé quatre fois de suite, sans quoi je n'aurais pas pu être accepté la cinquième fois et recevoir la bourse Alexander-Graham-Bell, l'une des plus importantes au pays.

J'aimerais remercier les membres du jury qui ont accepté d'évaluer cette thèse et de me faire part de leurs commentaires justes qui ont contribués au présent travail.

Je ne manquerais pas non plus de dire un grand merci à mes parents et amis qui m'ont suivi au cours de cette aventure. Certains amis en chimie ont fait le même parcours que moi et l'encouragement mutuel a fait le plus grand bien. Merci à ma copine Audrey avec qui on peut toujours se permettre de rêver. Merci à la meilleure correctrice qui m'a été donnée d'avoir, Annaïch.

Malgré toute l'aide dont j'ai pu disposer lors de ces années d'études, je suis néanmoins le seul responsable de tous les oublis, les fautes ou les lacunes de ce manuscrit et de cette recherche.

0. Introduction

INTRODUCTION GÉNÉRALE

Les polymères conducteurs font aujourd'hui l'objet de nombreuses études. Plusieurs dates importantes marquent l'histoire de la recherche sur les polymères conducteurs. Les premiers polymères conjugués remontent au milieu du 19^{e} siècle lors de la découverte de l'aniline et du poly(aniline)[1]. Par contre, rien n'a été exploité. Les premiers tests de conductivité ont été réalisés un siècle plus tard en prenant des polymères au hasard et en les mélangeant avec des métaux[2]. Les recherches sur les matériaux conjugués ont réellement débuté lorsque Heeger, MacDiarmid et Shirakawa (1977) ont pensé doper le polyacetylène avec de l'iode et qu'il était doté d'une bonne conductivité[3]. On a attribué un prix Nobel à ces trois chercheurs pour la découverte et le développement des polymères conducteurs en 2000[4]. Cette date coïncide approximativement avec le début de la recherche intensive sur les propriétés des polymères conjugués. On a vu alors en eux un remplacement pour les métaux utilisés dans l'électronique. Ces exemples positifs ont démontré que les matériaux conjugués avaient des propriétés de semi-conducteurs et qu'ils pourront éventuellement remplacer les composés inorganiques dans tous les domaines de l'électronique.

En 1990, Richard Friend a utilisé le poly(*p*-phénylène vinylène) dans une diode électroluminescente[5]. À ce moment, l'utilisation d'oligomères et de polymères conjugués s'intensifiait dans ce qui allait devenir « l'électronique organique ». Francis Garnier utilisait

déjà des oligothiophènes dans des transistors organiques en 1989, mais ce travail n'a pas retenu la même attention[6].

Inutile de dire que le travail réalisé à ce jour sur les oligomères et les polymères conjugués à l'état neutre (semi-conducteur) et à l'état dopé (conducteur) est colossal[7]. Il peut s'agir de différents travaux dans l'amélioration de leur solubilité, de leur mise en œuvre ou de leur structure moléculaire. Les solutions magiques réglant tous ces problèmes ne sont toutefois pas encore arrivées dans le cas des polymères conjugués. Commençons avec certaines définitions et théories qui permettront de se familiariser avec les polymères conjugués.

POLYMÈRES CONJUGUÉS

Les polymères conducteurs regroupent les polymères ioniques et électroniques[7a, b]. La conductivité du premier cas vient de la mobilité d'ions répartis à travers la matrice de polymère. Le présent texte ne fera état que de la deuxième famille où les porteurs de charge migrent à travers la matrice polymère grâce à la présence d'un système d'électrons π-délocalisés. On parlera dans ce cas de polymères conjugués. Ceux-ci sont connus depuis longtemps, mais leur étude a été reportée à plus tard par manque d'intérêt. La plupart des premiers polymères présentaient une solubilité limitée. Leur synthèse aboutissait souvent à un matériau mal défini, plein de défauts, pas très stable et difficilement reproductible. Au cours du temps, la recherche a tenté de résoudre ces problèmes graduellement.

La plupart des polymères conducteurs sont de type π-conjugués. Il s'agit de polymères comportant une alternance de simples et doubles liaisons. Cela permet une délocalisation des électrons sur toute la chaîne le long du polymère. La largeur de la bande interdite est souvent du domaine du visible (quelques eV, 400-700 nm). Cette structure résulte souvent en un polymère rigide et difficilement soluble. Les polymères conducteurs peuvent être regroupés en différentes sous-catégories : les polymères polyèniques, les polymères aromatiques, les polymères hétérocycliques aromatiques, les systèmes mixtes, etc. Des exemples de polymères principalement utilisés au début de la recherche sur les polymères conducteurs sont illustrés à la figure 0-1. Plusieurs dérivés de ces polymères ont été développés au cours du temps. On peut aussi faire des copolymères en introduisant des unités différentes. Cette avenue semble être celle privilégiée au moment d'écrire ces lignes[8]. Dans l'optique de cette thèse, la compréhension des polythiophènes sera la cible principale en se basant sur leur large passé[7a, b, 9].

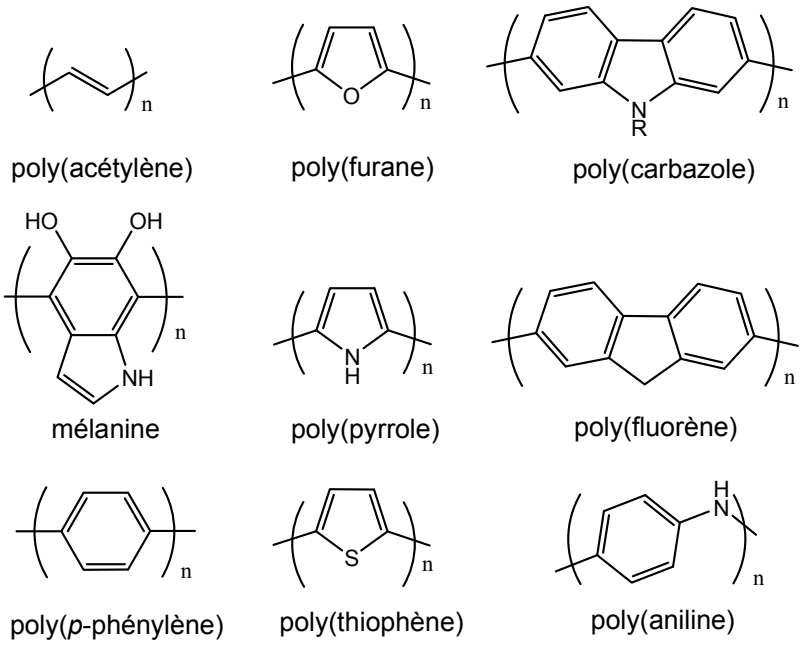

Figure 0-1. Différents polymères conducteurs.

Pour faciliter leur utilisation ou répondre aux propriétés recherchées, les polymères conjugués doivent plus souvent qu'autrement être solubles dans un solvant volatil, faciles à synthétiser, stables face à l'oxydation ou la réduction, avoir les propriétés de fluorescence voulues, ainsi qu'avoir une bonne conductivité et mobilité des porteurs de charge. Chaque application requiert différentes propriétés.

La modulation des propriétés des polymères se fait majoritairement par la fonctionnalisation[10]. Beaucoup de travail a été fait pour synthétiser des dérivés des polymères montrés précédemment[8]. Cette approche s'avère facilement réalisable dans le cas des poly(thiophènes) ou poly(phénylène vinylènes) mais plutôt impossible avec les

poly(anilines) ou poly(acétylènes) sans détruire complètement leurs propriétés de conduction.

Certaines contraintes proviennent parfois du fait de la synthèse du monomère, mais aussi de la polymérisation. Il s'agit habituellement de polymérisation par addition[11], par condensation[12] ou par oxydation[13]. On choisit la méthode selon le monomère choisi et selon les substituants de celui-ci. Plusieurs composés de départ sont offerts sur le marché pour la fonctionnalisation ou la substitution. Pour arriver à un produit aromatique intéressant, il n'est pas toujours nécessaire de procéder à de nombreuses étapes de synthèse.

La synthèse des polymères substitués est souvent orientée vers des polymères plus solubles. On utilise souvent la technique d'ajout de groupements latéraux tels que les groupes alkyles[14]. Leurs propriétés de donneurs d'électrons influencent rapidement la densité électronique des monomères ou comonomères et ainsi leur réactivité. La polymérisation ou copolymérisation s'en voit alors davantage compliquée.

La préparation des polymères mixtes comportant plusieurs unités différentes nécessite la synthèse de macromolécules. L'ajout des différents blocs devra s'effectuer dans un ordre bien précis dans le but de bien contrôler la régiorégularité[15]. Les réactions utilisées pour ce faire font souvent intervenir des catalyses métalliques ou organométalliques. On peut penser au couplage de Suzuki[16], Stille[17] ou Kumada[18]. De même, on peut préparer des

oligomères en appliquant de manière itérative ces méthodes. On trouve des exemples de synthèse très élaborés dans la littérature[19].

Pour ce qui est des polymères, on trouvera plusieurs types de polymérisation[20]. On peut nommer les polymérisations de type métathétique par ouverture de cycle (ROMP)[21], par condensation[12], ou par catalyse (Ziegler-Natta[22], Suzuki[23], etc.). Toutes les méthodes comportent des avantages et des inconvénients. Les problèmes reliés à la purification et aux défauts de structures sont récurrents sans oublier les conditions expérimentales difficiles. Certains, comme la réaction de Wittig[24], forment aussi des produits secondaires en grande quantité difficilement purifiables. Par ailleurs, les catalyseurs métalliques se retrouvent bien enchevêtrés dans le polymère. Les défauts de structures (saturation de la chaîne carbonée) limitent souvent les propriétés des polymères. Dans la présente thèse, la synthèse d'oligomères à base d'hétérocycles par condensation sera priorisée. Pour leurs parts, les polymères seront synthétisés par polymérisation anodique.

La polymérisation par oxydation a été la première méthode utilisée pour l'obtention de poly(thiophène). La figure 0-2 présente le mécanisme. L'électropolymérisation par application d'un potentiel constant ou par cyclage voltampérométrique sont deux options potentielles. Il est aussi possible d'effectuer les mêmes couplages de manière chimique. Pour les polythiophènes, on note l'utilisation de $FeCl_3$[25]. Bien que l'oxydation soit une méthode efficace de polymérisation, le polymère résultant est la plupart du temps

régioaléatoire dans les monomères non-symétriques. Cet effet peut être observé dans les monomères les plus simples comme le 3-alkylthiophène et les propriétés finales obtenues sont complètement différentes. On peut voir de quoi il en est à la figure 0-2.

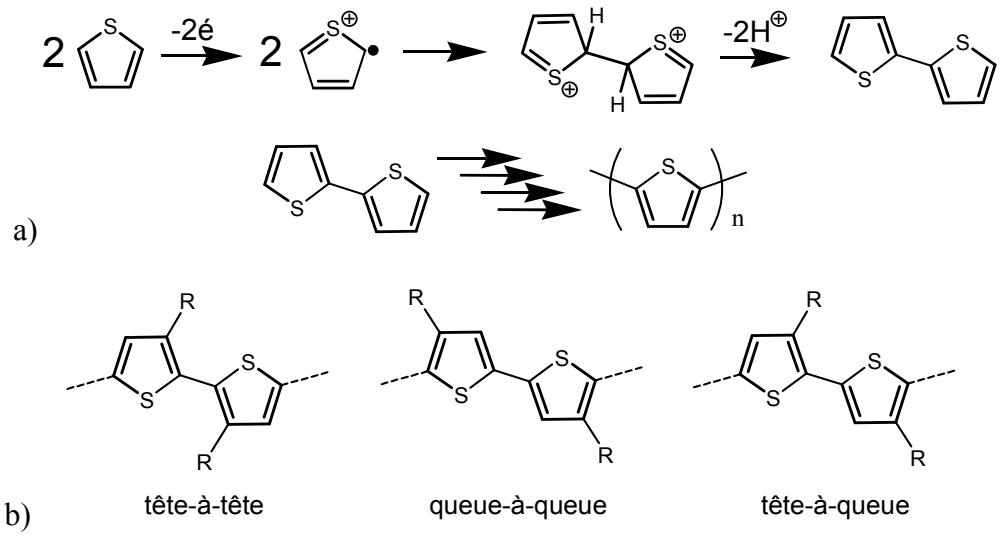

Figure 0-2. a) Mécanisme de couplage anodique et b) régiospécificité des polythiophènes.

Les polymères dits conducteurs ne le sont qu'une fois dopés. À l'état neutre, on les considère comme semi-conducteurs. La conductivité à l'état neutre se situe dans l'ordre de 10^{-10}-10^{-8} S.cm^{-1} [26]. Le dopage est souvent effectué de façon redox même si certains dopages acido-basiques peuvent être faits, notamment dans le cas de la poly(aniline). Le dopage fait en sorte que les porteurs de charge (soit électron ou trou) peuvent se déplacer et augmenter ainsi la conductivité de plusieurs ordres de grandeur jusqu'à 10^{4}-10^{5} S cm^{-1} [27]. La disposition des polymères et l'effet interchaîne sont des facteurs importants qui influent

sur les résultats de conductivité obtenus[28]. Leurs effets, souvent considérables, agissent sur leur efficacité dans les applications électroniques.

APPLICATIONS

Les débouchés sont aussi importants pour la forme semi-conductrice que pour la forme conductrice. Les polymères conducteurs peuvent remplacer les semi-conducteurs inorganiques. Ils peuvent posséder des conductivités comparables aux métaux tout en étant aussi faciles à mettre en œuvre et flexibles.

Les polymères dopés sont utilisables dans deux types d'applications. Lorsqu'ils changent d'état d'oxydation, on peut parler des électrodes de piles électrochimiques ou des détecteurs[29]. Dans le cas où aucun changement d'état d'oxydation n'a lieu, on pourrait penser aux applications de blindage électromagnétique[30] ou aux applications de transporteurs de charge : anode transparente dans une diode luminescente, cathode dans un condensateur électrolytique ou revêtement anti-statique.

Les polymères non-dopés sont l'équivalent organique des semi-conducteurs inorganiques. Ils peuvent remplacer ces derniers dans différents dispositifs électroniques dont les diodes électroluminescentes[5], les transistors à effet de champ[6], les cellules photovoltaïques[31] et les lasers polymères[32]. L'avantage de leur utilisation est surtout lié à

leur mise en œuvre peu complexe (transformabilité) et à leur flexibilité de même qu'à la modulation aisée de leurs propriétés grâce à l'introduction de substituants[33].

Les polymères dont le dopage est réversible peuvent faire l'objet de plusieurs autres applications intéressantes. On n'a qu'à penser à l'électrochromisme, au camouflage, aux sondes chimiques biochimiques et thermiques, aux batteries rechargeables ou encore aux nerfs et aux muscles artificiels.

Les polymères conducteurs sont devenus au fil du temps un champ de recherche autant pour les chimistes, les physiciens que pour les ingénieurs. Les travaux deviennent ainsi multidisciplinaires et nécessitent une certaine expertise dans tous ces domaines ou appellent, à tout le moins, la collaboration entre les chercheurs. Néanmoins, à peine 30 ans après leurs découvertes, les polymères conjugués sont utilisés dans de multiples dispositifs électroniques. On peut penser alors aux diodes électroluminescentes ou aux cellules photovoltaïques. Dans ces exemples, les matériaux utilisés doivent avoir des propriétés de niveaux électroniques (gap énergétique) complémentaires à celle des électrodes. Les propriétés recherchées pour ces applications sont évaluées par des techniques spectroscopiques et électrochimiques[34].

PROPRIÉTÉS SPECTROSCOPIQUES ET ÉLECTROCHIMIQUES

Les méthodes spectroscopiques sont des méthodes rapides pour évaluer les propriétés des composés. On peut approximer les gaps énergétiques (E_g^{spect}), la différence entre les niveaux d'énergie HOMO-LUMO. On peut aussi évaluer la conjugaison des composés. L'énergie la plus basse de l'absorbance d'une molécule est souvent reliée au niveau d'énergie de la bande HOMO.

Les propriétés optiques des polythiophènes sont principalement dues à la transition π-π* de la chaîne conjuguée principale. Quelques facteurs peuvent influencer les longueurs d'onde d'absorbance et de fluorescence. Outre l'homogénéité structurelle et chimique de l'échantillon, l'influence des substituants et les effets stériques sont les plus importants. Un déplacement vers les longueurs d'onde de plus faible énergie sera qualifié de bathochromique (*red shift*) tandis qu'on appellera un déplacement vers les plus petites longueurs d'onde hypsochromique (*blue shift*).

Les propriétés électrochimiques sont souvent déterminées avec la voltampéro-métrie cyclique. On fait varier le potentiel entre une électrode de travail et une électrode auxiliaire pour ensuite observer l'évolution du courant. À partir des potentiels d'oxydation et de réduction obtenus, on peut déduire les niveaux énergétiques HOMO et LUMO en calibrant avec le couple ferrocène/ferrocènium. La réversibilité de ces processus est primordiale pour les diverses applications en électronique. Le dopage/dédopage se doit

d'être parfaitement réversible. La figure 0-3 illustre un voltampérogramme caractéristique d'un cas parfaitement réversible. Dans la plupart des poly(thiophènes), une suroxydation recouvre partiellement le pic de dopage, ce qui diminue la réversibilité de ce processus. L'intensité du pic E_{pc} sera beaucoup moindre que celle du pic E_{pa}. Celui-ci représente l'oxydation du composé relatif à l'électrode de référence.

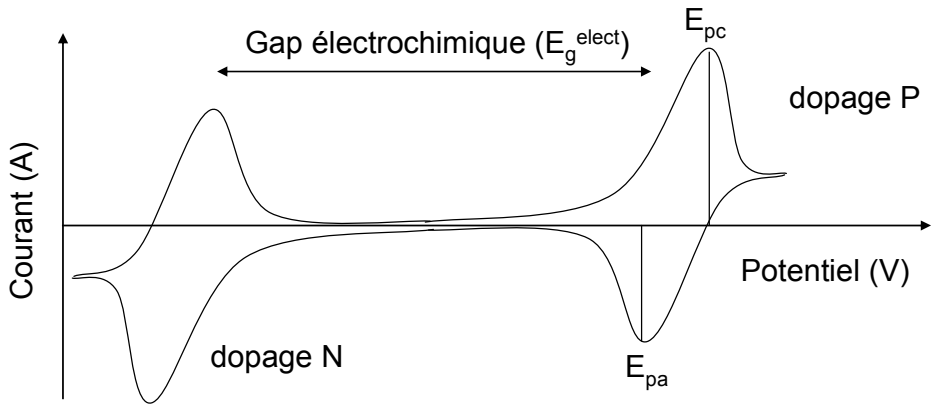

Figure 0-3. Voltampérogramme caractéristique.

La création de polarons et bipolarons (*vide infra*) change significativement les spectres électroniques. Le dopage d'un poly(thiophène) mène habituellement à la disparition du pic de la transition π-π* et à l'apparition de nouvelles bandes dues au dopage. Les études spectroélectrochimiques renseignent sur les différents processus en suivant par absorbance l'évolution du changement de potentiel. En appliquant différents potentiels croissants et en analysant les spectres, on en vient à déduire les processus de dopage et les potentiels correspondants. Aucune autre réaction non désirée ou

décomposition ne se présentera dans le système si on voit l'apparition d'un point isobestique. Seulement deux espèces (neutre, dopée) sont alors présentes en solution.

DOPAGE REDOX

Le dopage peut être effectué de manière chimique ou électrochimique. De plus, le dopage redox peut se faire de deux façons, de type P ou de type N. Le dopage de type P consiste en une oxydation du système. Il s'agit d'une perte d'électrons qui résulte en une transformation des chaînes en polycations. La neutralité électrique est faite en injectant une quantité correspondante d'anion du dopant. Le type N est exactement le contraire avec la transformation des chaînes en polyanions et l'injection de cation. Certains polymères comme le poly(acétylène) ou le poly(*p*-phénylène) possèdent un caractère amphotérique, c'est-à-dire qu'on peut les doper P ou N. La stabilité des polymères dopés P est souvent plus élevée que celle du type N. Ces derniers sont souvent instables en présence d'une faible quantité d'eau ou d'autres sources de protons. Les polymères hétérocycliques sont souvent dopés P comme le montre la figure 0-4. Le dopage N nécessite souvent des potentiels négatifs élevés et n'est souvent pas réversible complètement.

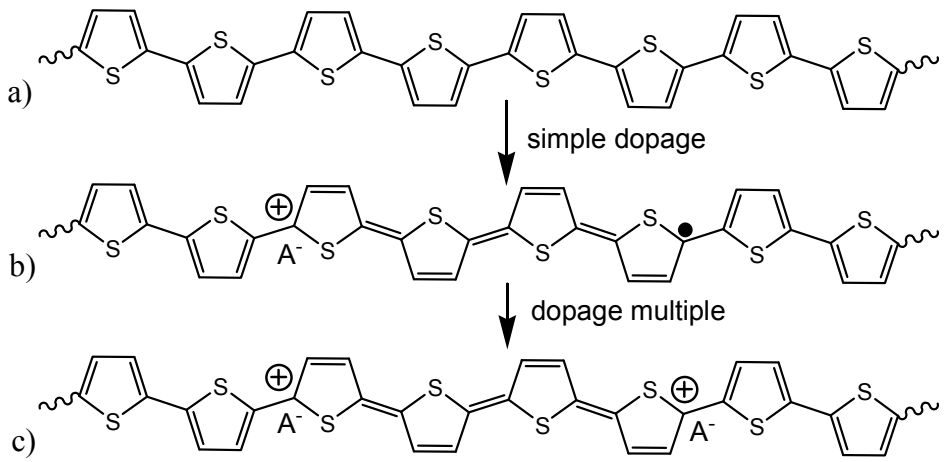

Figure 0-4. Étape successive du dopage de type P du poly(thiophène). a) Polymère neutre, b) formation d'un polaron (cation radicalaire) et c) d'un bipolaron (bication).

Le porteur de charges lors d'un dopage peut être de différents types selon la nature des liaisons et leur symétrie. Les propriétés des matériaux dopés doivent être étudiées tout autant que le matériau semi-conducteur de départ. Dans le cas des polymères hétérocyliques étudiés ici, on retrouvera la formation de polarons et de bipolarons[35]. Les structures de bandes correspondantes sont représentées à la figure 0-5. Ces bandes peuvent être modifiées pour régler les propriétés selon les besoins.

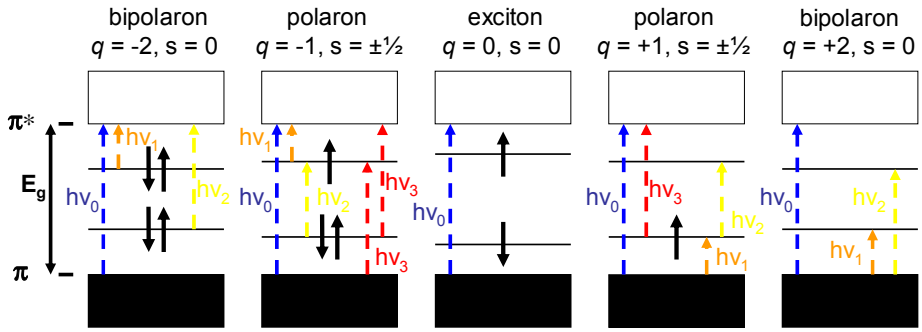

Figure 0-5. Structure de bande d'un polymère conjugué lors d'un dopage de type P ou N. Les charges (q) et les spins (s) des espèces produites y sont montrés avec leurs noms.

RÉGLAGE DES PROPRIÉTÉS

Les différentes propriétés spectroscopiques ou électrochimiques peuvent être réglées à notre guise grâce à différentes stratégies. La conjugaison est un facteur important. Elle est reliée principalement au recouvrement des orbitales[19]. Plus la molécule sera conjuguée, plus l'énergie des transitions sera basse. On pourra penser qu'une molécule plane est plus susceptible de conjugaison.

L'ajout de groupements électrodonneurs et électroaccepteurs en périphérie de la chaîne principale change considérablement les propriétés résultantes[33]. Les substituants électrodonneurs influenceront principalement les niveaux de la bande de valence (HOMO) en les abaissant et les substituants électroaccepteurs, quant à eux, agiront sur les niveaux de la bande de conduction (LUMO) en les augmentant. Les unités constituant la chaîne

principale peuvent aussi jouer le rôle de donneurs et d'accepteurs[7c, d]. Par exemple, ceci peut se faire en faisant l'alternance d'unités aromatiques riches et pauvres en électrons.

L'encombrement stérique affectera principalement la transition π-π* de manière à ce que son absorbance soit déplacée hypsochromiquement à cause d'un mauvais recouvrement des orbitales π. Par exemple, on observe un déplacement de l'ordre de 100 nm entre le poly(alkylthiophène) couplé tête-à-tête-queue-à-queue contrairement au même couplé tête-à-queue régiorégulier[14a, b] (voir figure 0-2). L'emplacement de tous les groupements joue un rôle névralgique sur les propriétés observées[14c]. Encore une fois, la structure joue un rôle de première importance sur les propriétés obtenues.

Les polymères auront souvent des propriétés différentes en solution versus l'état solide[36]. La formation d'excimères ou d'interactions π à l'état solide stabilise la structure et abaisse considérablement les distances de bande. De même, la concentration peut être un facteur des différentes propriétés trouvées. Aussi, les propriétés changeront en chauffant ces polymères si on assiste à un changement de conformation.

PROBLÉMATIQUE

Les molécules conjuguées sont étudiées depuis quelques décennies. Elles étaient attendues comme une révélation dans le domaine électronique organique étant donné qu'elles combinaient de bonnes propriétés optiques, électriques et mécaniques. L'emphase

a été mise sur l'unité thiophène qui a un faible potentiel d'oxydation et une petite distance de bande (E_g). Ces caractéristiques sont recherchées pour la fabrication de dispositifs électroniques efficaces. Beaucoup d'efforts ont été investis dans le thiophène et ses dérivés afin de l'utiliser comme comonomère pour synthétiser de nouveaux matériaux avec des propriétés supérieures à ce qui existe.

Malgré les nombreux efforts, il est très difficile d'établir des tendances entre des molécules apparentées et encore plus entre des ensembles de molécules différentes. Le résultat pour certaines applications est souvent relatif à l'ingénierie de la fabrication des dispositifs. C'est pourquoi le domaine de la chimie des matériaux est une chimie combinatoire et évolue un peu de façon aléatoire. Les nombreuses études structures/propriétés ont été faites dans le but d'obtenir les propriétés optimales pour des applications électroniques précises. Les efforts ont abouti à l'optimisation des propriétés et à l'optimisation des dispositifs, ce qui demeure un défi d'ingénierie. Par contre, des propriétés améliorées peuvent être trouvées grâce à la préparation de nouveaux matériaux dans lesquels d'autres connections que le traditionnel aryle-aryle sont employés. L'utilisation de nouveaux comonomères arrive à un point où leur disponibilité se raréfie.

Les matériaux conjugués sont habituellement synthétisés en utilisant de contraignantes réactions telles que celles énumérées précédemment. Ces réactions doivent être faites avec des catalyseurs métalliques, sous atmosphère inerte et sans lumière. Il en

résulte de nombreux sous-produits, ce qui requiert plusieurs purifications. Dans le cas d'une polymérisation, le produit obtenu est toujours difficile à purifier et les propriétés sont souvent différentes. Cela complexifie d'une part les études précises sur les propriétés en fonction de la structure, et d'autre part rend la prédiction de la synthèse de nouveaux composés ayant les propriétés désirées encore plus ardue.

Comment être sûr de la composition et de la structure d'un polymère composé de deux comonomères, voire plus. La réactivité de chacun est peut-être l'esquisse d'une réponse. C'est en fait une limitation réelle de la copolymérisation. Le polymère résultant peut être un polymère bloc et les propriétés trouvées ne seront pas nécessairement une combinaison de celles des deux comonomères. Même dans le cas où on trouve un système qui conduira à un polymère alterné, il faudra faire attention au divers ratio des comonomères. Ceci est valide autant pour la polymérisation chimique que pour l'électropolymérisation. Dans ce dernier cas, on peut voir l'apparition de sous-produits résultants de couplages non désirés. Une grande importance est donnée au bon contrôle de la formation des polymères.

Les travaux avec les polymères sont difficiles à réaliser en raison des explications données précédemment, mais aussi à cause de leur solubilité. Il faut tenir compte de la masse molaire des polymères pour faire des études de type structure/propriétés. En premier

lieu, il est préférable de bien contrôler les propriétés sur des oligomères et ensuite de transposer aux polymères les connaissances acquises.

OBJECTIFS

Notre but est de développer une nouvelle façon d'obtenir de nouveaux comonomères qui conduira à une étude fiable et méthodique des propriétés par rapport aux structures. Une stratégie où on pourra prédire les propriétés des nouveaux composés synthétisés est à préconiser. Le laboratoire Skene a exploré une nouvelle approche pour la préparation de matériaux conjugués. Le lien imine (azométhine) sera utilisé comme un bloc de construction pour de nouveaux matériaux. Notre recherche récente est connue pour la synthèse d'un lien imine stable menant à des matériaux conjugués d'une manière très contrôlée. Cette manière d'obtenir des matériaux conjugués peut se faire en très peu d'étapes et très facilement.

Le but ultime est d'être capable de mélanger et d'assortir les propriétés désirées des différentes unités dans un seul et même comonomère. Ce comonomère devrait aussi favoriser le recouvrement d'orbitale pour maximiser la conjugaison. La disposition des groupements est aussi la clé dans l'atteinte de la régiorégularité qui permet l'obtention de propriétés accrues et reproductibles.

STRATÉGIE

Il existe donc toujours une nécessité de préparer des matériaux qui auront constamment les mêmes propriétés chaque fois qu'ils seront synthétisés, d'avoir des matériaux avec des propriétés optoélectroniques intéressantes, de fabriquer ces matériaux facilement comparé à leurs analogues carbonés et même d'espérer des propriétés meilleures que ceux-ci.

Pour répondre à ces problématiques, le laboratoire Skene se penche sur une nouvelle approche mettant en jeu la synthèse d'imines. Les imines sont faciles à fabriquer puisqu'elles sont le résultat d'une condensation entre une amine et un aldéhyde. C'est une réaction qui n'a pas beaucoup été exploitée dans le passé dans le domaine des matériaux conjugués. Les reproches toujours évoqués contre le lien imine sont son hydrolyse, son instabilité et sa décomposition face à l'oxydation ou la réduction. On retrouve souvent les imines comme groupement protecteur des amines de par leur formation réversible[37]. C'est pourquoi la stabilité des imines a toujours été incertaine, ce qui représente une entrave à leur développement. Il est possible de greffer un aldéhyde sur des cycles aromatiques[38] et en particulier les thiophènes[39]. C'est tout le contraire avec les amines. Il est difficile de retrouver des structures aromatiques comportant un ou des amines qui s'avèrent stables à l'air libre et qui résistent à l'hydrolyse. C'est ce qui limite principalement l'attrait des liens imines pour la production de matériaux conducteurs. Notre laboratoire a exploré différentes avenues possibles pour la synthèse d'amine sur des cycles aromatiques et principalement le

thiophène. Le thiophène a été le choix de prédilection au départ étant donné qu'il arbore une bande de conduction accrue.

Il faudra alors se pencher sur les propriétés engendrées par la formation du lien imine. Quelques exemples utilisant le *p*-phénylènediamine (molécule 0-1, figure 0-6) ont déjà été décrits brièvement dans la littérature, mais seulement du côté synthèse et de la spectroscopie UV-visible, sans jamais chercher plus loin[40]. Les composés étaient difficilement solubles et présentaient des potentiels d'oxydation élevés. Compte tenu des limitations de 0-1, l'idéal aurait été d'utiliser un diaminothiophène comme 0-2. Il aurait été un parfait candidat pour former un analogue au polythiophène et exploiter ses propriétés. Malheureusement, cette molécule est instable vue qu'elle s'oxyde très facilement à l'air libre[41].

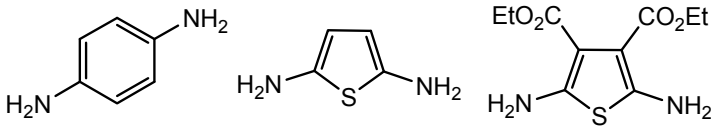

0-1 0-2 0-3

Figure 0-6. Diamino hétérocycles.

En incorporant des groupements électroattracteurs en position 3 et 4, la déficience en électron des amines rend celles-ci moins réactives sous des conditions atmosphériques normales. La stabilité de cette molécule vient aussi de son état solide à température

ambiante. La littérature montre l'existence du diaminothiophène 0-3[42]. Même si cette molécule est utilisée dans la synthèse de dérivés pharmaceutiques[43] depuis 40 ans, elle n'a jamais attiré les chercheurs pour des applications électroniques. Cette synthèse est faite à température de la pièce à partir de réactifs peu coûteux. Le rendement de la réaction n'est pas très considérable, mais une optimisation des conditions permet d'obtenir facilement des quantités appréciables de produit avec des précipitations relativement simples.

Après avoir réussi à synthétiser un thiophène diamine stable, il sera possible de synthétiser des composés conjugués modèles comportant un lien imine. On espère prouver que les défauts évoqués au sujet des imines ne sont pas valides dans les composés conjugués. Il faudra donc démontrer la stabilité et la synthèse des composés. Notre but sera alors d'explorer ces propriétés de manière électrochimique et spectroscopique étant donné que celles-ci seront identiques chaque fois qu'elles seront synthétisées. Ce n'est pas tant les propriétés des nouveaux composés formés qui importent, mais plutôt ce qu'il sera possible de ressortir comme avantages des liens imines ou du moins des caractéristiques intéressantes. Pour ce faire, il était évident de commencer par l'analyse des oligomères pour bien comprendre les propriétés spectroscopiques et électrochimiques des molécules composées de liens imine. Ces modèles reflèteront très bien les propriétés de ce type de composés et seront plus faciles à analyser que des polymères équivalents. Ils seront aussi propices à vérifier la compatibilité de leurs propriétés opto-électroniques avec des applications électroniques. Étant donné la rareté des composés imine à base de thiophène

trouvés dans la littérature, une étude détaillée est nécessaire. Les divers points à investiguer sont la validité de la synthèse, la formation de composés stables, leurs structures, les propriétés spectroscopiques et électrochimiques ainsi que leurs caractéristiques photophysiques. Des études systématiques propriétés/structures ont été effectuées à cet effet.

L'approche utilisée sera davantage structurale, même si elle semblera être combinatoire compte tenu du nombre de composés analysés. Les vérifications seront effectuées en vue de découvrir s'il est possible d'obtenir des matériaux conjugués et des propriétés comparables aux matériaux conjugués traditionnels. Les composés seront comparés à leurs analogues carbonés et aux analogues préparés à partir de 0-1 et enfin, l'analyse des propriétés en fonction des structures sera effectuée.

DESCRIPTION DES CHAPITRES

C'est dans cette optique que nous proposons une étude des liaisons imine divisées en cinq différents chapitres qui répondront aux différentes questions quant aux liens imines et leurs dérivés thiophène conjugués. Les cinq chapitres constitueront cinq articles intégraux dans lesquels l'auteur de cette thèse a considérablement contribué. Ceux-ci ont été spécialement choisis parmi la quinzaine de nos travaux publiés sur les imines. Toutes les sections de ce manuscrit sont séparées par chapitre. Ainsi, les informations supplémentaires de ces articles se retrouvent en annexe toujours séparées par chapitre. Un

résumé des sujets des publications choisies et leur apport dans le contexte de cette recherche sont décrits ci-dessous:

Dans le premier chapitre (chapitre I), la stratégie de synthèse de thiophènes conjugués avec l'utilisation des liens imine avec des exemples comportant des groupes électrodonneurs et électroaccepteurs est expliquée. La synthèse de ces liens s'effectue très facilement. La stabilité s'avère le point le plus avantageux des imines conjuguées contrairement à la croyance populaire en chimie organique. Il est donc possible d'utiliser les liens imine pour la construction de matériaux conjugués. Les propriétés spectroscopiques et électrochimiques de ces nouvelles molécules sont brièvement discutées. Les molécules conjuguées ont été confirmées et, ce, peu importe la position de l'amine dans le lien imine ou la position des groupes électroniques.

L'article II va plus en profondeur sur l'effet des liaisons imine sur les propriétés des molécules conjuguées, notamment la fluorescence. Les exemples illustrés y démontrent les concepts généraux de leurs propriétés spectroscopiques. On travaille alors avec des molécules à base de fluorènes, un peu plus actives spectroscopiquement pour faciliter les observations. Les effets du lien imine réduit considérablement la fluorescence qui se désactive de manière non-radiative. La position de ce lien ne semble pas être ce qui importe le plus. On voit apparaître une certaine réversibilité dans l'oxydation de ce type de composé.

Au chapitre III, on explore plus en profondeur les propriétés spectroscopiques des composés et même leurs stabilités. Des études sont alors faites concernant le cation radicalaire formé lors d'une oxydation. Dans cet article, les molécules ont des groupements terminaux qui leur confèrent une oxydation réversible. Des changements de couleurs sont observés par oxydation chimique ou électrochimique. Les composés conjugués synthétisés à partir d'imines résistent à ces stress.

Ainsi, au chapitre IV, la synthèse de différentes molécules contenant différents hétérocycles conjugués et l'utilisation de ces molécules pour la polymérisation menant à des polymères comonomères ont été démontrées. On note la facilité de créer un comonomère contenant différents hétérocycles dans le but de préparer des composés non symétriques. Il est alors possible de parvenir à des propriétés spécifiques en choisissant les bonnes unités à inclure dans la structure. Des essais de polymérisation sont effectués. Ils seront davantage explorés dans le prochain chapitre.

Dans le dernier chapitre (V), les difficultés entourant l'utilisation de comonomères pour la polymérisation seront explorées. C'est un peu la suite du chapitre précédent, mais on pousse davantage les recherches. Pour ce faire, l'utilisation d'oligomères comportant des unités thiophène, pyrrole et furane comme étant nos trois blocs de construction modulaire semble bienvenue pour préparer des composés symétriques et non symétriques à base d'imines conjugués. Cet article se veut très complet et la synthèse, les propriétés

spectroscopiques et électrochimiques, l'électropolymérisation et la régiorégularité obtenue de ces molécules modèles seront décrites. On y verra comment contrôler les propriétés d'un comonomère en utilisant notre stratégie bien connue. Des essais de polymérisation seront présentés de même que le contrôle de la régiorégularité avec ces comonomères. Les polymères produits seront caractérisés davantage dans cet article que dans le précédent.

RÉFÉRENCES DES ARTICLES

Les références complètes des différents articles constituant cette thèse sont présentées ci-dessous. La situation des articles au moment du dépôt est énoncée de même que l'apport des différents coauteurs :

I. J. Mater. Chem., 2007, 17, 1166-1177.

Tunable spectroscopic and electrochemical properties of conjugated push-push, push-pull and pull-pull thiopheno azomethines. Stéphane Dufresne, Marie Bourgeaux et W. G. Skene. Journal of Materials Chemistry, article complet, publié. J'ai effectué toutes les manipulations de synthèse et de caractérisations physiques sauf pour deux molécules sur la vingtaine de molécules présentées. J'ai participé à la rédaction d'une première ébauche de l'article avec Marie Bourgeaux. Elle a synthétisé et caractérisé deux molécules dans cet article.

II. J. Phys. Chem. C, 2010, 114, 13106-13112.

Insights into the effect of the ketylminine group on the fluorescence deactivation of oligofluorenes. Stéphane Dufresne, Ivan Ulliel Roche, Thomas Skalski et W. G. Skene. Journal of Physical Chemistry C, article complet, publié. La synthèse et la caractérisation ont été faites en majeure partie par moi-même. J'ai écrit les principales conclusions de ces expériences. Ivan Ulliel Roche et Thomas Skalski ont respectivement complété ou corroboré certains résultats et fait les essais préliminaires de synthèse.

III. J. Mater. Chem., 2010, 20, 4861-4866.

Towards materials with reversible oxidation and the tuneable colours using heterocyclic conjugated azomethines. Stéphane Dufresne, Andréanne Bolduc et W. G. Skene. Journal of Materials Chemistry, article complet, publié. J'ai effectué toutes les manipulations de synthèse et de caractérisations physiques contenus dans cet article. J'ai participé à la rédaction de la discussion principalement. Andréanne Bolduc a fait des mesures complémentaires concernant deux composés sur huit.

IV. J. Org. Chem., 2008, 73, 3859-3866.

Unsymmetric pyrrole, thiophene, and furan-conjugated comonomers prepared using azomethine connections: potential new monomers for alternating homocoupled products. Stéphane Dufresne et W. G. Skene. Journal of Organic Chemistry, article complet, publié.

La synthèse et la caractérisation de toutes les données mentionnées dans cet article sont le fruit de mon travail. J'ai résumé les éléments essentiels à la rédaction de l'article.

V. Opto-Electronic Property Tailoring of Conjugated Heterocyclic Azomethines – The effect of Pyrrole, Thiophene and Furans. Stéphane Dufresne et W. G. Skene. Journal of Physical Organic Chemistry, article complet, accepté pour publication. Les diverses manipulations en laboratoire ont été effectuées par l'auteur de ces lignes. J'ai rassemblé toutes les données et écrit les grandes lignes de cet article.

BIBLIOGRAPHIE

1. Letheby, H., *J. Chem. Soc.* **1862,** *15*, 161-163.

2. Inzelt, G., Historical Background (Or: There Is Nothing New Under the Sun). In *Conducting Polymers*, Springer Berlin Heidelberg: Leipzig, Germany, 2008; pp 265-269.

3. Chiang, C. K.; Druy, M. A.; Gau, S. C.; Heeger, A. J.; Louis, E. J.; MacDiarmid, A. G.; Park, Y. W.; Shirakawa, H., *J. Am. Chem. Soc.* **1978,** *100* (3), 1013-1015.

4. (a) Heeger, A. J., *Angew. Chem. Int. Ed.* **2001,** *40* (14), 2591-2611; (b) MacDiarmid, A. G., *Angew. Chem. Int. Ed.* **2001,** *40* (14), 2581-2590; (c) Shirakawa, H., *Angew. Chem. Int. Ed.* **2001,** *40* (14), 2574-2580.

5. Burroughes, J. H.; Bradley, D. D. C.; Brown, A. R.; Marks, R. N.; Mackay, K.; Friend, R. H.; Burns, P. L.; Holmes, A. B., *Nature* **1990,** *347* (6293), 539-541.

6. Horowitz, G.; Fichou, D.; Peng, X.; Xu, Z.; Garnier, F., *Solid State Commun.* **1989,** *72* (4), 381-384.

7. (a) Perepichka, I. F.; Perepichka, D. F., *Handbook of Thiophene-based Materials: Applications in Organic Electronics and Photonics*. John Wiley & Sons: Chichester, UK, 2009; Vol. 1, p 417; (b) Perepichka, I. F.; Perepichka, D. F., *Handbook of Thiophene-based Materials: Applications in Organic Electronics and Photonics*. John Wiley & Sons: Chichester, UK, 2009; Vol. 2, p 445; (c) Chen, J.; Cao, Y., *Acc. Chem. Res.* **2009,** *42* (11), 1709-1718; (d) Cheng, Y.-J.; Yang, S.-H.; Hsu, C.-S., *Chem. Rev.* **2009,** *109* (11), 5868-5923.

8. Skotheim, T. A.; Elsenbaumer, R. L.; Reynolds, J. R., *Handbook of Conducting Polymers*. 3rd ed.; CRC Press: Boca Raton, FL, 2007; Vol. 1, p 727.

9. Roncali, J., *Chem. Rev.* **1992,** *92* (4), 711-738.

10. (a) Bu, H.-B.; Götz, G.; Reinold, E.; Vogt, A.; Schmid, S.; Blanco, R.; Segura, J. L.; Bäuerle, P., *Chem. Commun.* **2008**, 1320-1322; (b) Grisorio, R.; Piliego, C.; Cosma, P.; Fini, P.; Mastrorilli, P.; Gigli, G.; Suranna, G. P.; Nobile, C. F., **2008,** *64* (37), 8738-8745.

11. Gal, Y.-S.; Jin, S.-H.; Park, J.-W.; Lim, K.-T.; Kim, S. Y., *Mol. Cryst. Liq. Cryst.* **2010,** *530*, 56 - 63.

12. Ashraf, R. S.; Gilot, J.; Janssen, R. A. J., *Sol. Energ. Mat. Sol. Cells.* **2010,** *94* (10), 1759-1766.

13. Lin, H.-y.; Liou, G.-S., *J. Polym. Sci. A* **2009,** *47* (1), 285-294.

14. (a) Maior, R. M. S.; Hinkelmann, K.; Eckert, H.; Wudl, F., *Macromolecules* **1990,** *23* (5), 1268-1279; (b) McCullough, R. D., *Adv. Mater.* **1998,** *10* (2), 93-116; (c) Demeter, D.; Allain, M.; Leriche, P.; Grosu, I.; Roncali, J., *Tetrahedron Lett.* **2010,** *51* (31), 4117-4120.

15. Demadrille, R.; Rannou, P.; Bleuse, J.; Oddou, J.-L.; Pron, A.; Zagorska, M., *Macromolecules* **2003,** *36* (19), 7045-7054.

16. (a) Miyaura, N.; Yamada, K.; Suzuki, A., *Tetrahedron Lett.* **1979,** *20* (36), 3437-3440; (b) Miyaura, N.; Suzuki, A., *J. Chem. Soc., Chem. Comm.* **1979,** (19), 866-867.

17. (a) Milstein, D.; Stille, J. K., *J. Am. Chem. Soc.* **1978,** *100* (11), 3636-3638; (b) Stille, J. K., *Angew. Chem. Int. Ed.* **1986,** *25* (6), 508-524.

18. (a) Tamao, K.; Sumitani, K.; Kumada, M., *J. Am. Chem. Soc.* **1972,** *94* (12), 4374-4376; (b) Kumada, M., *Pure Appl. Chem.* **1980,** *52* (3), 669-679.

19. Izumi, T.; Kobashi, S.; Takimiya, K.; Aso, Y.; Otsubo, T., *J. Am. Chem. Soc.* **2003,** *125* (18), 5286-5287.

20. Chujo, Y., *Conjugated Polymer Synthesis*. Wiley-VCH Verlag GmbH & Co. KGaA: Weinheim, Germany, 2010; p 313.

21. Gibson, V. C., *Adv. Mater.* **1994,** *6* (1), 37-42.

22. Goto, H.; Akagi, K.; Shirakawa, H.; Oh, S. Y.; Araya, K., *Synth. Met.* **1995,** *71* (1-3), 1899-1900.

23. Li, Z. a.; Ye, S.; Liu, Y.; Yu, G.; Wu, W.; Qin, J.; Li, Z., *J. Phys. Chem. B* **2010,** *114* (28), 9101-9108.

24. Shim, H.-K.; Ahn, T.; Song, S.-Y., *Thin Solid Films* **2002,** *417* (1-2), 7-13.

25. Sugimoto, R. T., Shinji; Gu, Hal Bon; Yoshino, Katsumi, *Chem. Express* **1986,** *1* (11), 635-638.

26. Heeger, A. J.; Kivelson, S.; Schrieffer, J. R.; Su, W. P., *Rev. Mod. Phys.* **1988,** *60* (3), 781.

27. (a) Kaiser, A. B., *Adv. Mater.* **2001,** *13* (12-13), 927-941; (b) Kaiser, A. B., *Rep. Prog. Phys.* **2001,** *64* (1), 1.

28. (a) Sirringhaus, H.; Brown, P. J.; Friend, R. H.; Nielsen, M. M.; Bechgaard, K.; Langeveld-Voss, B. M. W.; Spiering, A. J. H.; Janssen, R. A. J.; Meijer, E. W.; Herwig, P.;

de Leeuw, D. M., *Nature* **1999,** *401* (6754), 685-688; (b) Osaka, I.; McCullough, R. D., *Acc. Chem. Res.* **2008,** *41* (9), 1202-1214.

29. Roncali, J.; Garreau, R.; Delabouglise, D.; Garnier, F.; Lemaire, M., *J. Chem. Soc., Chem. Comm.* **1989,** (11), 679-681.

30. Taka, T., *Synth. Met.* **1991,** *41* (3), 1177-1180.

31. Sariciftci, N. S., *Mater. Today* **2004,** *7* (9), 36-40.

32. (a) Moses, D., *Appl. Phys. Lett.* **1992,** *60* (26), 3215-3216; (b) Gaal, M.; Gadermaier, C.; Plank, H.; Moderegger, E.; Pogantsch, A.; Leising, G.; List, E. J. W., *Adv. Mater.* **2003,** *15* (14), 1165-1167; (c) Samuel, I. D. W.; Turnbull, G. A., *Mater. Today* **2004,** *7* (9), 28-35.

33. (a) Barlow, S.; Odom, S. A.; Lancaster, K.; Getmanenko, Y. A.; Mason, R.; Coropceanu, V.; Brédas, J.-L.; Marder, S. R., *J. Phys. Chem. B* **2010,** *114* (45), 14397-14407; (b) Kulhánek, J.; Bures, F.; Pytela, O.; Mikysek, T.; Ludvík, J.; Ruzicka, A., *Dyes Pigm.* **2010,** *85* (1-2), 57-65; (c) Li, X.; Kim, S.-H.; Son, Y.-A., *Dyes Pigm.* **2009,** *82* (3), 293-298.

34. Pruneanu, S.; Veress, E.; Marian, I.; Oniciu, L., *J. Mater. Sci.* **1999,** *34* (11), 2733-2739.

35. Brédas, J.-L.; Beljonne, D.; Coropceanu, V.; Cornil, J., *Chem. Rev.* **2004,** *104* (11), 4971-5004.

36. (a) Pina, J.; Seixas de Melo, J.; Burrows, H. D.; Bilge, A.; Farrell, T.; Forster, M.; Scherf, U., *J. Phys. Chem. B.* **2006,** *110* (31), 15100-15106; (b) Zhang, X.; Johnson, J. P.; Kampf, J. W.; Matzger, A. J., *Chem. Mater.* **2006,** *18* (15), 3470-3476.

37. (a) Baylis, E. K.; Campbell, C. D.; Dingwall, J. G., *J. Chem. Soc., Perkin Trans. 1* **1984**, 2845-2853; (b) Corey, E. J.; Grogan, M. J., *Org. Lett.* **1999,** *1* (1), 157-160; (c) Sampson, P. B.; Honek, J. F., *Org. Lett.* **1999,** *1* (9), 1395-1397.

38. (a) Chardonnens, L.; Noël, F., *Helv. Chim. Acta* **1973,** *56* (1), 280-284; (b) Downie, I. M.; Earle, M. J.; Heaney, H.; Shuhaibar, K. F., *Tetrahedron* **1993,** *49* (19), 4015-4034.

39. (a) Mitsumori, T.; Inoue, K.; Koga, N.; Iwamura, H., *J. Am. Chem. Soc.* **1995,** *117* (9), 2467-2478; (b) Wei, Y.; Yang, Y.; Yeh, J.-M., *Chem. Mater.* **1996,** *8* (11), 2659-2666.

40. (a) Destri, S.; Porzio, W.; Dubitsky, Y., *Synth. Met.* **1995,** *75* (1), 25-36; (b) Dubitsky, Y. A.; Catellani, M.; Bolognesi, A.; Destri, S.; Porzio, W., *Synth. Met.* **1993,** *55* (2-3), 1266-1271; (c) Simionescu, C. I.; Grovu-Ivanoiu, M.; Cianga, I.; Grigoras, M.; Duca, A.; Cocârla, I., *Angew. Makromol. Chem.* **1996,** *239* (1), 1-12; (d) Simionescu, C. I.; Cianga, I.; Ivanoiu, M.; Airinei, A.; Grigoras, M.; Radu, I., *Eur. Polym. J.* **1999,** *35* (10), 1895-1905; (e) Simionescu, C. I.; Cianga, I.; Ivanoiu, M.; Duca, A.; Cocarla, I.; Grigoras, M., *Eur. Polym. J.* **1999,** *35* (4), 587-599; (f) Ng, S. C.; Chan, H. S. O.; Wong, P. M. L.; Tan, K. L.; Tan, B. T. G., *Polymer* **1998,** *39* (20), 4963-4968.

41. Bourgeaux, M.; Vomscheid, S.; Skene, W. G., *Synth. Commun.* **2007,** *37* (20), 3551-3558.

42. (a) Gewald, K., *Chem. Ber.* **1965,** *98* (11), 3571-3577; (b) Gewald, V. K.; Kleinert, M.; Thiele, B.; Hentschel, M., *J. Prak. Chem.* **1972,** *314* (2), 303-314.

43. (a) Sabnis, R. W.; Rangnekar, D. W.; Sonawane, N. D., *J. Heterocycl. Chem.* **1999,** *36* (2), 333-345; (b) Huang, Y.; Dömling, A., *Chem. Biol. Drug Des.* **2010,** *76* (2), 130-141.

I. CHAPITRE I

Tunable spectroscopic and electrochemical properties of conjugated push-push, push-pull and pull-pull thiopheno azomethines

*Stéphane Dufresne, Marie Bourgeaux, and W. G. Skene**

Département de Chimie, Pavillon JA Bombardier, Université de Montréal, CP 6128, succ. Centre-ville, Montréal, Québec, CANADA, H3C 3J7,

Received 9th November 2006, Accepted 22nd December 2006

First published as an Advance Article on the web 23rd January 2007

DOI : 10.1039/b616379c

J. Mater. Chem. **2007**, *17*, 1166-1177.

ABSTRACT:

Novel azomethines consisting uniquely of thiophene units were examined. The highly conjugated compounds were prepared by condensing air stable aminothiophenes with 2-thiophene aldehydes, which were substituted with various electronic groups. The resulting azomethines are highly conjugated and are both reductively and hydrolytically resistant. Various electron donating and accepting groups placed in the 2-position of 5-thiophenecarboxaldehyde lead to electronically delocalized *push-push, pull-pull*, and *push-pull* azomethines. These electronic groups affect both the HOMO and the LUMO levels, which influence the absorption and emission spectra. Colors spanning the entire visible spectrum ranging from yellow to blue are possible with these nitrogen containing conjugated compounds. Excited state deactivation of the singlet excited state occurs predominately by internal conversion while only a small amount of energy is dissipated by intersystem crossing to the triplet state and by fluorescence. The ensuing fluorescence and phosphorescence of the thiopheno azomethines are similar to their thiophene analogues currently used in functional devices, but with the advantage of a low triplet state and tunable HOMO-LUMO energy levels extending from 3.0 to 1.9 eV. Quasi-reversible electrochemical radical cation formation is possible while the oxidation potential is dependent of the nature of the electronic group appended to the thiophene. The crystallographic data of the electronic *push-push* system show the azomethine bonds are planar and linear and they adopt the *E* isomer.

KEYWORDS: diamino thiophene, azomethines, fluorescence, triplet, internal conversion, intersystem crossing, conjugated materials, cyclic voltammetry, HOMO-LUMO energy gaps.

Introduction

Conjugated materials have received much attention as they offer many new possibilities for devices combining unique optical, electrical, and mechanical properties.[1] Particular interest is found with thiophene based materials because of their low oxidation potentials[2] and their equally low band-gap properties,[3] which make them useful for many electronic devices. Moreover, these compounds show such versatility because of their semiconductor like property obtained with chemical doping that further makes them suitable for commercial applications. As a result of the diverse emissive and conductive properties and various synthetic means to their formation, conjugated thiophene materials have found many applications including uses as hole injection layers in OLED/PLEDs, in flexible light displays, solar cells, flat panel displays, field effect transistors, non-linear optical materials, sensors, and/or low power consumption products, to name but a few.[4, 5]

As attractive as these conjugated materials are for their physical properties, their synthesis is however challenging. Typical synthetic methods such as Suzuki[6] and Wittig[7] strategies or electropolymerization[8] used to obtain conjugated thiophenes are often quite stringent. Alternating π-conjugated units with various electron donor and acceptor groups cannot be readily obtained by these normal coupling means. Standard synthetic means furthermore do not easily promote the selective one-pot addition of monomer units in high yields to afford unsymmetric electronic π-conjugated *push-pull* systems. Such conjugated compounds along with their electronic *pull-pull* and *push-push* analogues offer a viable

means for spectroscopic property tuning and they provide a new realm of easily synthesized functional materials for enhanced emitting devices or non-linear optical materials.[9]

Azomethines (-N=CH-) are appealing alternatives for conjugated materials because of the mild reaction conditions required for their synthesis. They have the advantage of increased yields and selective addition through the condensation reaction between an amine and an aldehyde, requiring less difficult purifications. The result of the easy reaction between the two complementary groups is a robust azomethine connection that is conjugated and exhibits a high stability towards hydrolysis and reduction when aryl precursors are employed.[10-13] Research progress regarding functional azomethine materials has unfortunately not been as prolific as their carbon analogues because of the limited number of available stable aryl diamino precursors. Such precursors often undergo undesired oxidative decomposition while the resulting azomethine products do not have suitable properties for functional applications and suffer from problematic irreversible oxidation.[14, 15] Only recently have efforts focused on taking advantage of these robust bonds to end cap oligomers using thiophene aldehyde precursors.[16] The recent introduction of stable aminothiophenes (**I-1** and **I-3**) has further helped to develop azomethine research leading to conjugated azomethines consisting uniquely of thiophene units.[17, 18] These extremely stable compounds do not suffer from the limitations of previous azomethines.[19] Furthermore, they have the added advantage of being isoelectronic to their carbon analogues,[20] making them suitable replacements for conventional thiophene materials.

Recently, we developed a route to synthesize oligothiopheno azomethines by selective reagent addition.[21, 22] The potential advantages of azomethine-based materials concomitant with our previous success with such compounds[13] have prompted us to develop new symmetric and unsymmetric thiopheno azomethines. The main objective is to examine the physical properties, among which are the spectroscopic and photophysical properties including the cyclic voltammetry of these new compounds. These are of particular interest, given the limited number of the photophysical and electrochemical studies regarding azomethines, especially their thiophene derivatives. Herein, we present the preparation and the characterization of conjugated thiopheno azomethines containing terminal electron donating and accepting groups. The sequential assembly of these electronic *push-push*, *pull-pull* and *push-pull* π-conjugated compounds is presented. The steady-state and time-resolved photophysics, electrochemical properties, HOMO-LUMO energy gaps, and crystal structure of these unique thiopheno azomethines are also investigated.

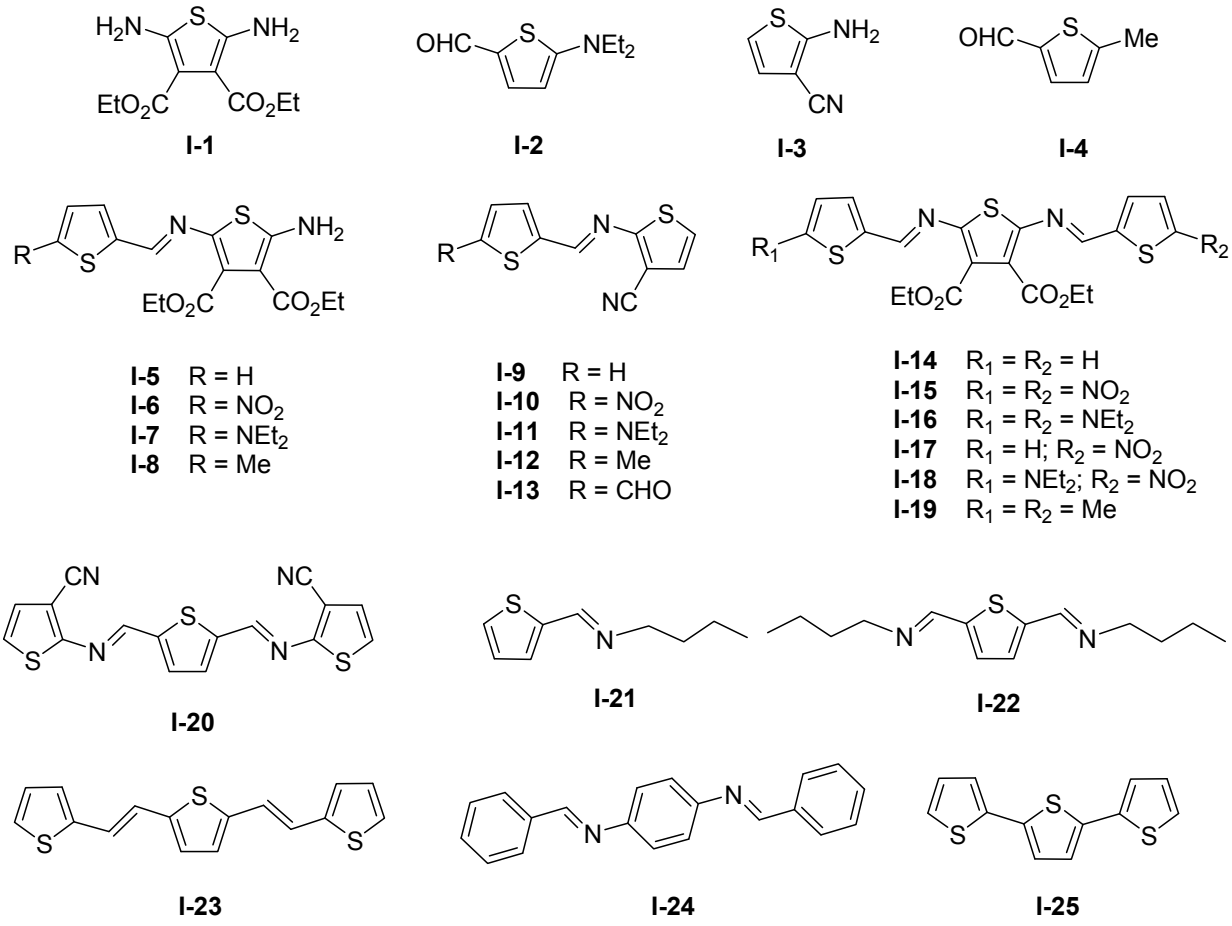

Chart I-1. Conjugated azomethines examined, their precursors, and some representative carbon analogues.

Results and Discussion

Synthesis

The reaction conditions to afford the azomethines involve shifting the equilibrium by simple dehydration via hygroscopic solvents (i.e., absolute ethanol and anhydrous toluene and THF) or mild drying agents (i.e., molecular sieves and alkali sulfates). These parameters concomitant with the formation of the thermodynamically favorable conjugated products displace the equilibrium in favor of the products without the need of stringent conditions, unlike standard carbon coupling methods. The versatile reaction supports a wide variety of common organic solvents with selective product formation (Scheme I-1) through the judicious choice of solvent, temperature and reagent stoichiometry. This selectivity is courtesy of the different reactivity of the amino groups of **I-1** in its pristine form relative to its monoazomethine form. Selective monoaddition to yield the amino monoazomethines is done with one equivalent of the corresponding aldehyde by condensing it with **I-1** at room temperature or by refluxing in ethanol. Both instances lead exclusively to the monoadducts, owning to the deactivation by the electron withdrawing ester group. The deactivating group is further responsible for the increased stability of **I-1** relative to its unsubstituted 2,5-diamino thiophene analogue, which spontaneously undergoes oxidative decomposition under ambient conditions and cannot be isolated. The electron withdrawing group is also responsible for decreasing the amine nucleophilicity. As a result, only mild reaction conditions are required for the condensation of monoazomethines. The electron withdrawing effect of the azomethine bond in the

monoazomethine further reduces the amine reactivity. More stringent reaction conditions are therefore required to push the second condensation to form the bisazomethine. This provides a means to tailor product formation by changing either the reagent stoichiometry or the solvents used. The resulting azomethine bond is sufficiently robust that it resists reduction with common reducing agents such as $NaBH_4$ and resists even strong reductants including DIBAL and H_2/Pd using standard protocols. Only in the case of refluxing with DIBAL for 10 hours did reduction of the azomethine occur. Azomethine hydrolysis occurs only with prolonged heating with concentrated acid in water saturated organic solvents. No product decomposition was observed even after eighteen months in solution under normal conditions.

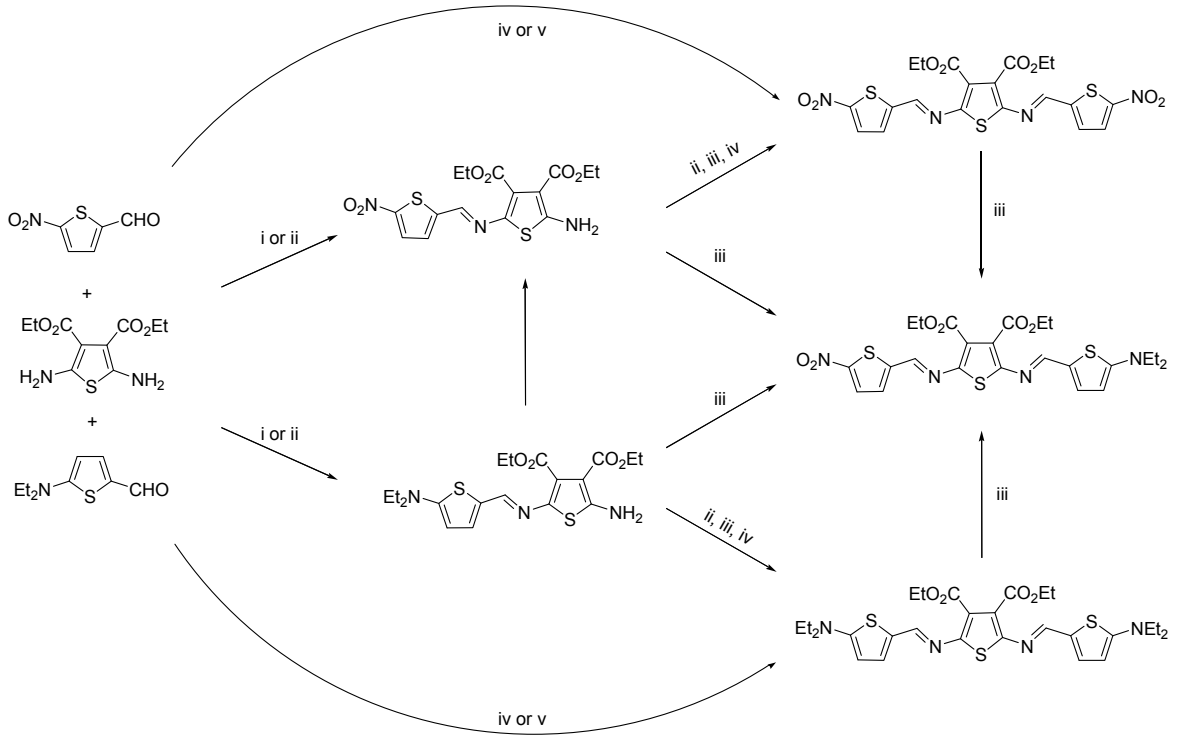

Scheme I-1. Conjugated thiophene assembly by complementary precursors leading to tunable properties. Experimental conditions: i) EtOH, Δ, ii) *i*-PrOH, Δ, iii) $TiCl_4$, DABCO, toluene, Δ, iv) *n*-BuOH, Δ.

The monoazomethines **I-5**-**I-8** are formed exclusively in ethanol regardless of the aldehyde used and the stoichiometry employed. By simply changing the solvent polarity and using different boiling point solvents, such as isopropanol or *n*-butanol, the reaction can be pushed to afford the corresponding bisazomethines in most cases (*vide infra*). Condensation can be done sequentially in a one-pot fashion directly from **I-1** with two equivalents of the corresponding aldehyde. Alternatively, an additional equivalent of aldehyde can be added to **I-5** to afford **I-14**. In all cases in which controlled addition was

possible, the condensation reaction was optimally catalyzed with ca. 5 mole % of trifluoroacetic acid. The controlled addition methodology is amenable to any aldehyde combination with **I-1** and provides a useful method for preparing new conjugated thiophenes. The reduced amine reactivity arising from the electron withdrawing ethyl ester group is evident with monomer **I-1** in which **I-14** can be obtained only by using high boiling point solvents, such as *n*-butanol.

Unlike **I-1**, selective product formation was not observed with the monoamine precursor **I-3**. The addition of one equivalent of **I-3** to 2,5-thiophene dicarboxaldehyde afforded a mixture of monoadduct **I-13** with a predominate amount of bisazomethine **I-20**. Product control with **I-3** was not possible even in ethanol at room temperature that otherwise led to product control with **I-1**. Unlike previous examples that exploited solubility differences to afford selective product formation,[13, 23] such selectivity was not observed with **I-3**. The lack of selectivity is attributed to the electron withdrawing cyano group that deactivates the amine and results in reduced reactivity towards the aldehyde. The cyano electron withdrawing effect of **I-13** increases the aldehyde reactivity towards nucleophilic addition. The unreacted amount of **I-3** therefore condenses preferentially with **I-13** immediately upon its formation resulting in the observed abundance of **I-20** relative to **I-13**.

Synthesis of the substituted bisazomethines is not straightforward owing to the different reactivity of the amino group of **I-1** towards the various aldehydes. The

bisazomethines are obtained with mild dehydration methods only with prolonged reaction times that result in significant aldehyde decomposition. The strong electron donating character of the diethylamino group of **I-2** deactivates the aldehyde such that nucleophilic addition of **I-1** cannot be done under mild conditions. Alternatively, its reactivity can be increased with a Lewis acid such as $TiCl_4$.[24] This route significantly decreases the reaction time while improving the yields of the coupling reaction to afford conjugated monoazomethines (**I-7** and **I-11**) and bisazomethines (**I-16** and **I-18**). Conversely, the electron withdrawing nitro group of 5-nitrothiophene-2-carboxaldehyde allowed for easy azomethine formation by simple heating with an acid catalyst in isopropanol only with the amino precursors **I-1** and **I-3**. The strong electron withdrawing nature of the nitro group, the high degree of conjugation, concomitant with the ester withdrawing capacity of **I-6**, further reduces the amine's nucleophilic character and prevents bisazomethine formation. This explains the difficulty in forming **I-15**, which could be obtained only by the Lewis acid method from **I-1** or **I-6**. Since these compounds are highly conjugated, the electronic withdrawing/donating groups exert their influence throughout the entire molecule. The reactivity of the terminal amine in the monoazomethines is therefore influenced by these electronic effects.

The synthesis of the unsymmetric compounds was further challenging because of their dynamic covalent character resulting in Lewis acid induced component exchange illustrated in Scheme I-2.[25, 26] Under our coupling conditions, attempts to obtain the

unsymmetric **I-17** from **I-5**, resulted quantitatively in **I-6**. Instead of undergoing the second condensation to form a bisazomethine, the terminal thiophene was exchanged with 2-nitrothiophenecarboxaldehyde, according to Scheme I-2. The resulting product is the thermodynamically stable **I-6** and its formation is consistent with previous examples of Lewis acid catalyzed component exchange.[26, 27] Consequently, the synthesis of **I-17** was achieved by exploiting the dynamic component reaction to exchange the thiophenes under stoichiometric conditions from **I-14**. The 2-diethylaminothiophene can also sustain a dynamic component exchange and be replaced either by thiophenecarboxaldehyde or by 2-nitrothiophenecarboxaldehyde component in the conjugated bisazomethines. Thus, as predicted by the thermodynamic stability and the reactivity of each compound, the nitrothiophene preferentially exchanges with the thiophene compound, which in turn, can displace the diethylamino thiophene unit according to Scheme I-2. The advantage of this dynamic behavior is a tunable synthesis for each compound. The observed dynamic behavior assures formation of the most thermodynamically stable product, further supporting the conjugated character of the azomethine compounds. A diverse library of electronic *push-push*, *pull-pull* and *push-pull* conjugated compounds is therefore possible via the step-wise pathways and opens a new synthetic means of tunable materials.

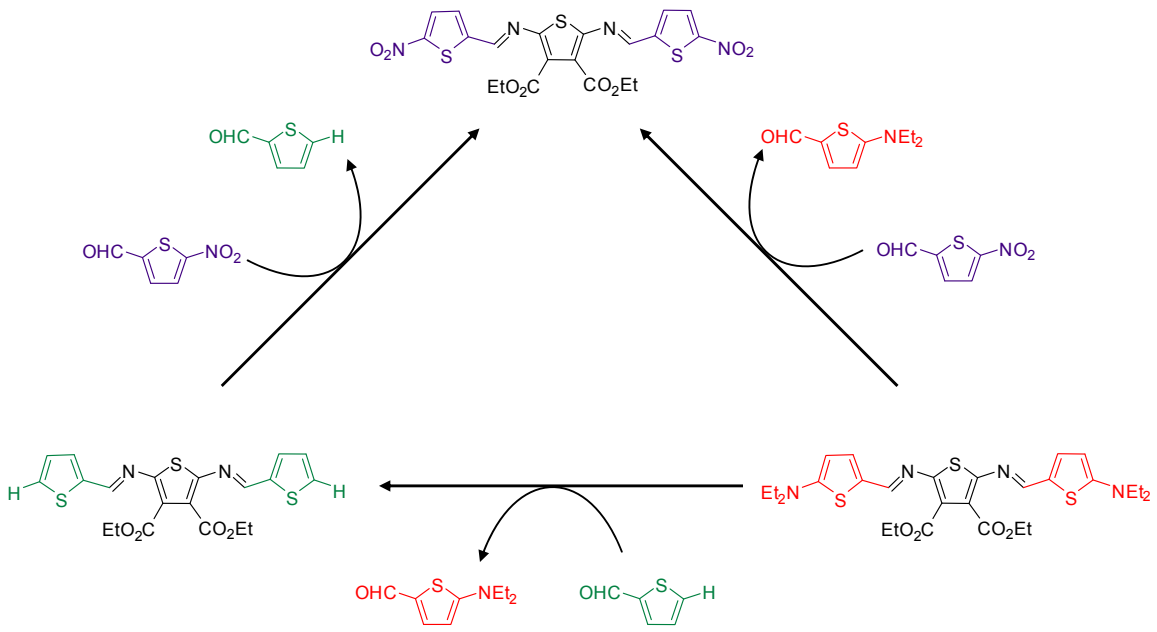

Scheme I-2. Possible Lewis acid promoted dynamic component exchange of different monomers.

Spectroscopic Properties

The extent of oligomerization can visually be followed by the intense color change from yellow (**I-1**) to orange (**I-5)** and to deep red (**I-14)** with the unsubstituted compounds. Their pronounced bathochromic change (Figure I-1 and Table I-1) is indicative of the conjugation degree arising from azomethine bond formation. The observed transitions are dominated by lowering of the excited electronic π-π^* levels owing to the stabilization from increasing the degree of conjugation. The molar extension coefficients are substantially high for all the azomethines because of the highly allowed π-π^* transitions. The linear bathochromic shift with the reciprocal number of unsubstituted thiophene units observed (inset Figure I-1) further supports the conjugated nature of the azomethine bond. The

bathochromic shift is consistent with a planar rigid π-conjugation of the compounds. Moreover, extrapolation of the curve gives the potential absorption maximum for an azomethine polymer consisting entirely of thiophene units, being ca. 500 nm.

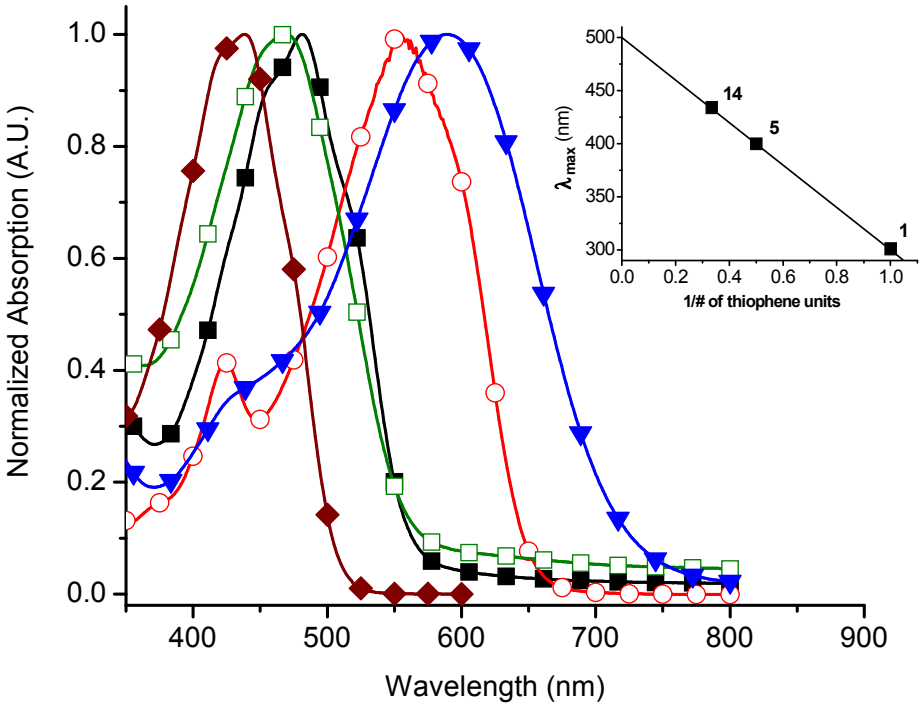

Figure I-1. Influence of terminal electronic groups on the absorption spectra of **I-14** (closed diamonds), **I-15** (closed squares), **I-16** (open circles), **I-17** (open squares), **I-18** (closed triangles). Inset: reciprocal number of thiophene units versus the change in absorption maximum for the unsubstituted thiophenes.

Table I-1. Spectroscopic values for the various reagents and azomethines measured in anhydrous acetonitrile.

	Module	Abs.[a] (nm)	$\varepsilon_{\lambda max}$ ($M^{-1}\,cm^{-1}$)	Em.[b] (nm)	Φ_{fl}[c] (10^{-3})	Φ_{fl}(77K)[d]	τ_{fl}[e] (ns)	ΔE[f] (eV)	E_g[g] (eV)	k_r[h] (μs^{-1})	k_{nr}[i] (ns^{-1})	Phos.[j] (nm)
Reagents	**I-1**	305	37,000	335	2.5	0.0089	13.5	3.7	3.0	0.19	0.08	479
	I-2	371	32,000	408	0.5	0.0058	0.3	3.2	3.0	1.67	3.34	543
	I-3	279	15,000	304	3E-3	7.7E-6	3.9	4.2	3.9	8E-4	0.27	493
	I-4	295	10,000	323	0.2	0.00058	4.6	4.0	3.3	0.04	0.20	500
Amino-mono-azomethine	**I-5**	400	19,000	480	2.9	0.97	14.0	2.9	2.6	0.21	0.07	525
	I-6	490	29,000	637	1.2	0.89	16.7	2.3	2.0	0.07	0.06	698
	I-7	452	42,000	542	2.7	0.96	13.5	2.5	2.3	0.93	0.07	549
	I-8	404	16,000	516	2.3	0.94	1.0	2.7	2.3	2.30	1.00	530
Mono-azomethine	**I-9**	370	14,000	439	3.9	0.79	5.4	3.2	2.7	0.72	0.18	479
	I-10	400	36,000	454	2.6	0.68	5.8	2.9	2.5	0.45	0.17	536
	I-11	473	49,000	545	8.7	0.82	11.1	2.4	2.3	0.78	0.09	578
	I-12	379	17,000	451	1.3	0.68	0.5	2.9	2.7	2.60	2.00	520
	I-13	385	22,000	426	1.5	0.72	1.5	3.0	2.6	1.00	0.67	481
Bis-azomethine	**I-14**	440	64,000	534	2.8	0.71	13.2	2.6	2.3	0.21	0.07	560
	I-15	481	37,000	589	1.6	0.15	11.9	2.4	2.1	0.13	0.08	600
	I-16	555	34,000	659	1.9	0.95	16.6	2.0	2.0	0.11	0.06	751
	I-17	470	30,000	614	5.6	0.70	14.1	2.3	2.1	0.40	0.07	695
	I-18	588	45,000	660	2.1	0.51	9.3	1.9	1.6	0.23	0.11	686
	I-19	427	46,000	559	1.3	0.90	1.9	2.5	2.2	0.68	0.52	598
	I-20	451	65,000	500	1.4	0.56	2.1	2.6	2.3	0.67	0.48	575
Model Compounds	**I-21**	277	24,000	306	0.2	0.76	4.3	4.2	3.8	0.05	0.25	481
	I-22	312	27,000	344	0.6	0.50	1.6	3.7	3.5	0.38	0.63	490
	I-23[k]	423	-	-	-	-	-	2.5	2.4			-
	I-24	376[l]	28,400[l]	-	-	-	-	-	-			-
	I-25	351[m]	24,000[o]	422[m]	56[o]	-	0.2[o]	3.2[p]	3.1[p]	280	4.72	-

[a]Absorption maximum. [b]Emission maximum. [c]Fluorescence quantum yields at λ_{ex} = 303 nm, relative to bithiophene.[30] [d]Fluorescence quantum yields at 77 K relative to room temperature. [e]Monoexponential fluorescence lifetime measured at λ_{em} max. [f]Absolute HOMO-LUMO spectral difference. [g]Spectroscopic band-gap. [h]$k_R = \Phi_{fl}/\tilde{\tau}_{fl}^{i} k_{NR} = k_R(1-\Phi_{fl})/\Phi_{fl}$. [j]Phosphorescence measured in 1:4 methanol/ethanol matrix at 77 K. [k]From Roncali and Frère.[57] [l]From Gawinecki[58] and Neuse.[59] [m]From Seixas de Melo.[30-32, 35] [o]From Roncali.[57] [p]From Ratner and Marks.[60]

The combined spectroscopic results for the various thiopheno azomethines are reported in Table I-1. The absorption and emission spectra intercept provides the relative energy difference between the ground and the excited states.[28] From the combined normalized absorption-emission spectra, the relative HOMO-LUMO transition can be calculated from the spectral overlap. The absorption method further provides an estimate for the band-gap that can be derived from the absorption onset in the red region of the spectrum. This method applies to our compounds since only a slight bathochromic shift of ca. 20 nm between solution and thin film was observed. The measured values by this method show the azomethines possess lower band-gaps relative to their carbon analogues such as **I-23** and **I-25**. The similarity of the azomethines to structurally comparable nitrogen free thiophenes is evident from the photophysical data presented in Table I-1. The electronic groups chosen are known to influence both the HOMO and LUMO levels, which is evident from the spectroscopic data. In general, the electron donating and the electron

withdrawing groups are known to decrease the HOMO and increase the LUMO levels, respectively. Such perturbations translate into apparent energy gap differences and intense absorption and emission spectral variations.

The monoazomethines **I-9**-**I-13** serve as reference compounds to illustrate the effect of the electronic groups. The amine group greatly affects both the absorption and the emission compared to the nitro group. This is supported by the pronounced spectral shifts of 100 nm for the donor group and only slight shifts of 30 nm for the acceptor group, relative to the reference compound **I-9**. The similar spectroscopic properties of the methylated analogue **I-9** and **I-12** confirm the pronounced spectroscopic change is a result of the electronic groups. The same tendency is observed also with the amino monoazomethines (**I-5**-**I-8**) whose terminal -NH_2 further influences the properties via its donating character. The electronic terminal groups can collectively influence the resulting properties courtesy of the highly conjugated azomethine bond. The withdrawing -NO_2 and donating -NH_2 of **I-6** jointly stabilize the ground and excited states, respectively, leading to an electronic *push-pull* system. This results in pronounced bathochromic absorption and emission shifts relative to **I-5**. Only slight bathochromic shifts are observed with **I-7** because of the two amino groups that work in opposition leading to an electronic *push-push* system.

The bisazomethines exhibit the same spectroscopic trend as the monoazomethines. Both the absorption and the emission spectra of the bisazomethine undergo large bathochromic shifts relative to the monoazomethines because of the increased conjugation. The pronounced stabilization implies a high degree of delocalization and planarity throughout the azomethines. The electronic group cooperativity is more pronounced for the bisazomethines than for the monoazomethines, supported by the spectral differences observed for **I-15**-**I-18** relative to the unsubstituted **I-14**. The *push-push* compounds **I-15** and **I-17** exhibit slight spectral shifts of 40 nm while the corresponding amino substituted *pull-pull* compound undergoes a large bathochromic shift around 70 nm, relative to **I-14**. The electronic *push-pull* system (**I-18**), combining both a donor and an acceptor group, exhibits the most pronounced absorption and emission bathochromic shifts. The *push-pull* effect greatly perturbs the electronic transitions and reduces the HOMO-LUMO energy gap between the ground and excited states. The net outcome is an intense visible blue color for **I-18** in addition to an extremely low HOMO-LUMO energy gap of 1.9 eV. From these observations, it can be concluded that the donating group has a greater effect on the electronic transitions than the nitro group, supported by the pronounced bathochromic shifts. This is concomitant with the ester groups on the thiophene central ring that also influence the spectroscopic properties through their withdrawing character. Thus, depending on the substituent chosen, it is possible to tailor the electronic properties of a given bisazomethine by perturbing either the HOMO or LUMO energy levels.

The influence of the nitrogen placement within the azomethine bond upon the resulting spectroscopic properties was examined with model compounds **I-14** and **I-20**. The spectroscopic properties, including HOMO-LUMO energy gap and molar extinction coefficients, of these two compounds are very similar, which confirms the comparable withdrawing effect of the cyano and the ester groups upon the electronic transitions. This is further supported by the similar spectroscopic results for the analogues **I-9** versus **I-12** and **I-14** versus **I-19**. The placement of the nitrogen within the azomethine bond does not perturb the electronic transitions given the comparable spectroscopic results among the studied compounds. Conversely, the nature and the number of substituents in the 5 and 5' positions (Figure I-2) greatly affect the electronic transitions, which in turn, influence the absorption and emission spectra in addition to the HOMO-LUMO energy gap.

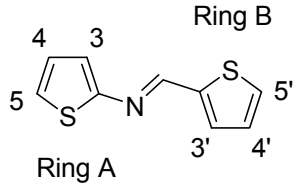

Figure I-2. Numbering scheme of thiopheno azomethines.

Steady-state and time-resolved fluorescence measurements further provide valuable insight into the excited state deactivation pathways of these compounds. Both the similar ns fluorescence lifetimes and the calculated radiative rate constants (k_f) for all the azomethines imply similar deactivation modes of the singlet excited state for all the compounds. The monoexponential lifetimes suggest unimolecular deactivation which is

further supported by the dilute experimental conditions, which preclude bimolecular self-quenching. The low fluorescence quantum yields are indicative of nonradiative quenching deactivation processes such as intersystem crossing (ISC) to the triplet state or by internal conversion (IC). Photoisomerization between the *E* and the *Z* isomers is also a possible deactivation mode.[29] However, no such photoproducts were observed. The low fluorescence quantum yield for the thiopheno azomethines is however not surprising since thiophenes are known to weakly fluoresce because of efficient ISC to the triplet state. This is understood to occur by heavy atom induced spin orbit coupling by the sulfur atoms.[30-35] This behavior is expected to be enhanced further by the azomethine nitrogen that contributes to the heavy atom effect concomitant with the increased degree of conjugation, which favors ISC by narrowing the singlet-triplet gap. Population of the triplet manifold is supported by the phosphorescence measurements at 77 K that show a bathochromic emission relative to the fluorescence and a monoexponential emission decay (Figure I-3). The phosphorescence quantum yields at this low temperature can be calculated by relative actinometry with fluorenone.[36] The phosphorescence quantum yields measured for all the studied compounds are approximately the same, $\Phi_{phos} \leq 0.1$. The triplet energies can be calculated from the E(0,0) transition from the phosphorescence spectra and these values are comparable to those of **I-23** and **I-25**.[33, 37]

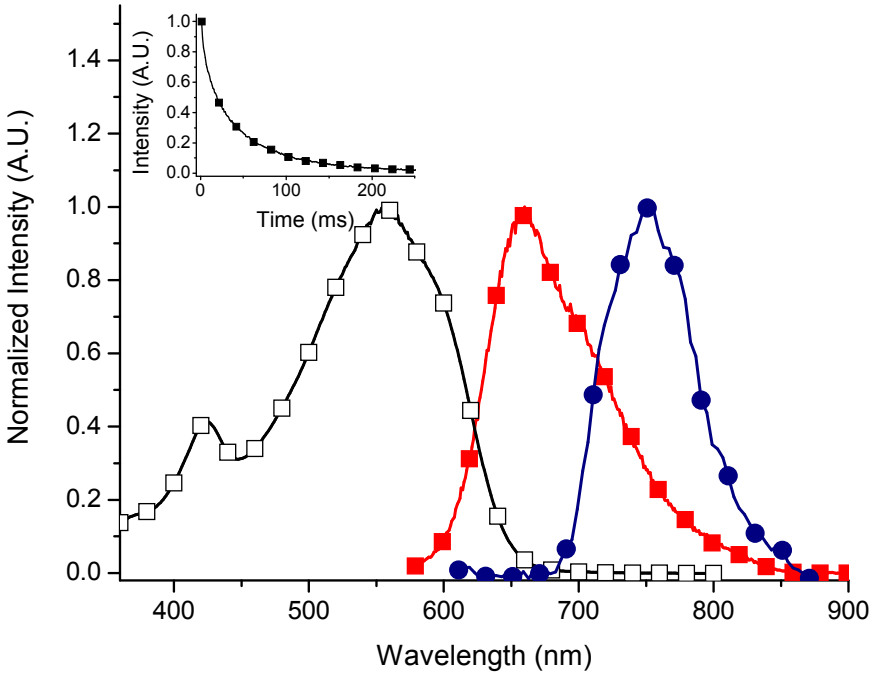

Figure I-3. Normalized absorption (open squares) and fluorescence (closed squares) spectra of **I-16** in acetonitrile. Phosphorescence (closed circles) spectrum measured in 4:1 ethanol:methanol matrix at 77 K. Inset: Phosphorescence decay monitored at 760 nm.

Further evidence of the triplet state is provided by ns-laser flash photolysis (LFP) from the weakly absorbing transients observed at 280 and 370 nm for the monoazomethine and bisazomethine, respectively (Figure I-4). The transients produced by the intense laser pulse are assigned to the triplets owing to their monoexponential decay kinetics that are similar to benzophenone (inset Figure I-4) in addition to being quenched with standard triplet quenchers such as oxygen, 1,4-cyclohexadiene, β-carotene, and methylnaphthalene.[38] Also apparent in the transient absorption spectra are negative absorptions resulting from the

strong ground state bleaching of the azomethines. These are mirror images of the ground state absorption spectra and confirm the transient absorption is much weaker than the ground state absorption. Even though there is direct evidence for the triplet state by LFP, this manifold is not preferentially formed and therefore it is not responsible for deactivating the singlet state. This is derived from the surprisingly weak azomethine transient signal. Large triplet extinction coefficients (ε_T) $\geq$ 10 000 M^{-1} cm $^{-1}$ are assumed for the azomethines because of their high degree of conjugation.[39] Owing to the intense ε_T, a transient signal of equal intensity to benzophenone (ε_T = 8 400 M^{-1} cm^{-1}, Φ_T = 1) is expected if the azomethine triplet was produced in significant amount. Since both Φ_T and ε_T contribute to the LFP signal, the weak azomethine signal obtained under identical experiment conditions as benzophenone (Figure I-4), confirms the azomethine triplet formation is inefficient. An upper limit of $\Phi_T \approx 0.05$ is derived from the LFP signal relative to benzophenone and is in agreement with the phosphorescence quantum yields. Evidence for the low triplet efficiency of the azomethines is further supported by the calculated nonradiative rate constants (k_{nr}) that are greater than **I-25**, which is known to efficiently populate its triplet state.[31] The faster k_{nr} values taken together with the weak LFP signal implies that deactivation of the singlet state occurs predominately by nonradiative IC and not by a manifold shift to the triplet state as with conventional thiophenes.

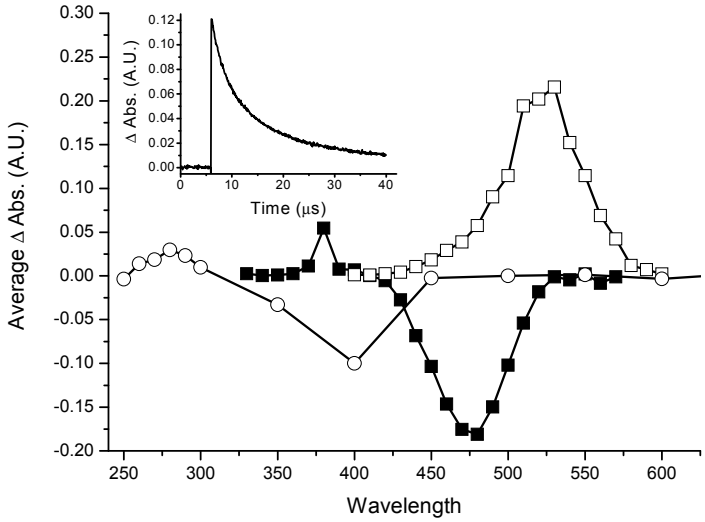

Figure I-4. Transient absorption spectra of benzophenone (open squares), **I-6** (open circles), and **I-17** (closed squares) recorded 100 μs after the laser pulse at 266 nm in deaerated acetonitrile. Inset: The decay of triplet benzophenone recorded at 525 nm.

Evidence for the IC deactivation mode is confirmed by the relative fluorescence at 77 K that is two and half orders of magnitude greater than that at room temperature (Figure I-5). All modes of excited state deactivation involving bond rotation and diffusion controlled quenching processes are suppressed at this low temperature leading to Φ_{fl} (77 K) ranging between 0.53 and 0.97 for the compounds studied. Accurate values for the low temperature fluorescence yields cannot be derived because of experimental errors associated with calculating the weak fluorescence signal at room temperature relative to the intense one at 77 K. Nonetheless, the observed fluorescence signal decrease at room temperature is from efficient nonradiative deactivation of the singlet excited state by IC

according to Φ_{fl} (77 K) - Φ_{fl} (RT) ≈ Φ_{IC}. This is in contrast to conventional oligothiophenes, such as **I-25**, that efficiently populate their triplet state by ISC with $\Phi_T \geq 0.8$.[30-32] Even though the major deactivation pathway is by IC, a certain amount of the excited state energy remains unaccounted according to the following energy conservation equation: $\Phi_{fl} + \Phi_{ISC} + \Phi_{IC} \approx 1$. The residual excited state energy must be dissipated by ISC to the triplet. Since only a weak signal is seen by LFP, the imine bond must therefore be a good triplet deactivator leading to rapid and efficient intramolecular self-quenching of this excited state.

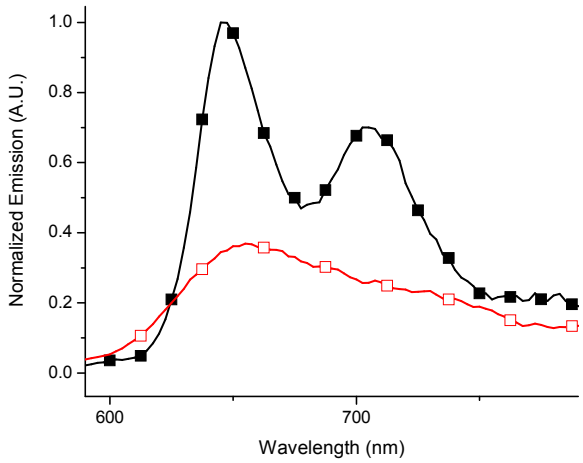

Figure I-5. Fluorescence of **I-15** at 77 K (closed squares) relative to room temperature (open squares, magnified 50 times).

Cyclic Voltammetry

Thiophene azomethines undergo two detectable step-wise oxidations by cyclic voltammetry. The first oxidation corresponds to a one electron process from the thiophene to form a radical cation. This is followed by removal of an additional electron to form a

dication. Even through the specific thiophene unit that undergoes oxidation cannot be unambiguously assigned, the first oxidation process consistently occurs between 0.4 and 1.6 V and is greatly affected by the electronic groups. Furthermore, the first oxidation step is quasi-reversible (Figure I-6) unlike homologous aryl azomethines that exhibit irreversible behavior regardless of the scan rate and experimental conditions.

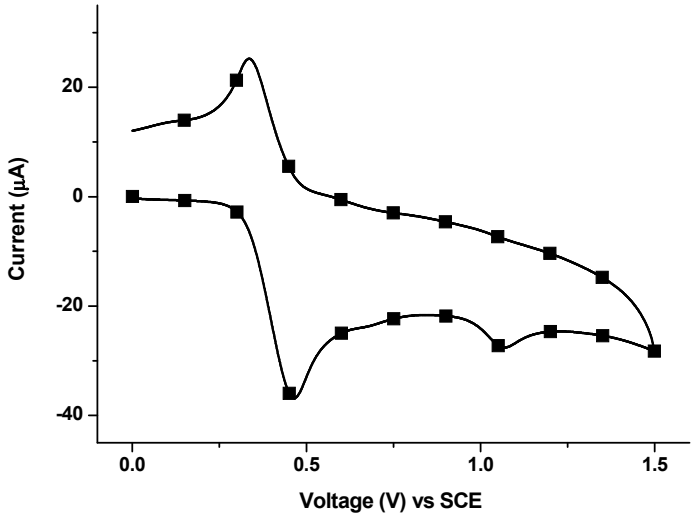

Figure I-6. Typical cyclic voltammogram of **I-16** in anhydrous dichloromethane at 100 mV/s with 0.1 M NBu_4PF_6 as an electrolyte.

In addition to an oxidation process, the azomethine bond can potentially be reduced. This process normally involves two rapid and undistinguishable sequential steps each involving one electron transfer[40, 41] However, no such processes were observed for any of the studied azomethines either in dichloromethane or at large negative potentials in DMF. This is in accordance with other reductive imine studies[42, 43] and supports the observed

robustness of the conjugated azomethine bond towards chemical reductants. A reversible six electron reduction was however observed for **I-15**, **I-17**, and **I-18,** which is assigned to the reduction of the nitro group. Conversely, an irreversible reduction was observed at low potentials only for **I-9** and **I-20**. Chemical reduction of these two compounds was also possible with $NaBH_4$. The irreversible process is most likely from cyanide ion formation followed by complete thiophene decomposition.[44] NMR product studies support this in which no thiophene or azomethine is detectable after the chemical reduction of **I-9** and **I-20** with $NaBH_4$ in methanol and room temperature.

The ability of the electronic groups to modify the HOMO/LUMO levels is apparent from the measured oxidation potentials. The donating amino group increases the HOMO level, resulting in a decrease in the oxidation potential. On average, a 500 mV reduction in the oxidation potential was observed for the amino containing compounds relative to their unsubstituted analogues. A pronounced reduction in the oxidation potential is apparent with the *push-push* system **I-16** where the two amino groups combine to increase the HOMO level. Unfortunately, the ability of the withdrawing group to decrease the LUMO level is not apparent since the reduction potentials cannot be measured. This notwithstanding, an increase in the oxidation potential was observed for the nitro containing thiophenes and suggests a destabilization of the HOMO level. The measured HOMO/LUMO values and their influence by the electronic groups are consistent with the spectroscopic measurements.

The oxidation onset provides the ionization potential (IP) according to $IP = E^{ox}_{onset}(SCE) + 4.4$, where $E^{ox}_{onset}(SCE)$ is the oxidation potential onset in volts versus the SCE electrode.[45] The ionization potentials are obtained from the measured oxidation potentials by applying a 0.39 V correction factor. Similarly, the LUMO values are calculated from the electron affinity (EA) given by the reduction onset potential (E^{red}_{onset}) according to $EA = E^{red}_{onset}(SCE) + 4.4$. Since no apparent azomethine electrochemical reduction was observed under our experimental conditions, the electrochemical oxidation onset and the spectroscopically measured HOMO-LUMO energy gaps can be combined to calculate the LUMO energy level according to $LUMO = HOMO - E_g$. The resulting values are reported in Table I-2. The oxidation potential taken together with the spectroscopic E_g data provide an accurate representation of the HOMO-LUMO energy levels. The resulting energy diagram shown in Figure I-7 illustrates the perturbation effect of the various electronic groups upon the HOMO and LUMO energy levels. Since the oxidation potential for quasi-irreversible processes is dependent upon the scan rate and hence the calculated HOMO energy level, the cyclic voltammetry measurements of all the compounds were performed under identical scan rates. In general, the azomethine oxidation potentials and their HOMO-LUMO energy gaps can be modulated such that they are similar to their carbon analogues (**I-23** and **I-25**)[46] and lower than their aryl azomethine homologues (**I-24**), making them compatible for use in functional devices. Moreover, the HOMO level can be tailored courtesy of the electronic groups such that the energy levels

are compatible with that of ITO in OLEDs, thus making these compounds potential hole injection layers in working devices.

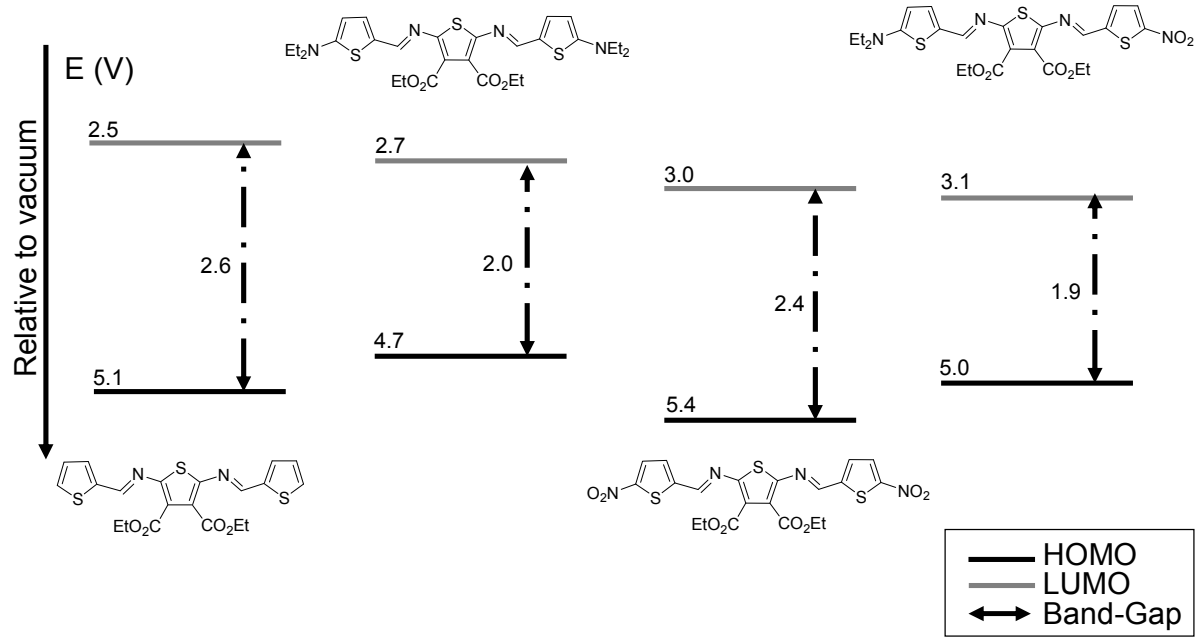

Figure I-7. Schematic representation of the relative HOMO-LUMO energy gaps influenced by different terminal electronic groups.

Table I-2. Cyclic voltammetry[a] values for the various thiopheno azomethines measured in anhydrous acetonitrile.

	Module	E_{pa}^{1}[b] (V)	E_{pa}^{2} (V)	E_{pc}^{1} (V)	E_{pc}^{2} (V)	$E_{pa(poly)}$ (V)	HOMO (-eV)	LUMO (-eV)
	I-1	0.6	1.1	-	-	-	4.9	1.2
	I-2	1.0	-	-	-	1.6	5.3	2.1
Reagents	**I-3**	1.3	-	-	-	-	5.7	1.5
	I-4	1.2	1.7	-0.7	-	-	5.6	1.6
	I-5	1.0	1.4	-	-	1.6	5.4	2.5
Amino-	**I-6**	1.1	-	-0.7	-1.1	-	5.5	3.2
mono-	**I-7**	0.4	1.0	-	-	-	4.7	2.2
Azomethine	**I-8**	0.8	-	-	-	-	5.1	2.4
	I-9	0.9	-	-	-	1.7	5.2	2.0
	I-10	1.3	-	-0.6	-0.9	-	5.6	2.7
Mono-	**I-11**	0.7	1.7	-	-	-	5.0	2.6
Azomethine	**I-12**	1.2	-	-	-	-	5.5	2.6
	I-13	1.2	-	-1.0	-1.3	-	5.5	2.5
	I-14	1.0	1.3	-	-	0.7	5.1	2.5
	I-15	1.1	1.6	-0.5	-1.0	-	5.4	3.0
Bis-	**I-16**	0.4	1.1	-	-	-	4.7	2.7
Azomethine	**I-17**	1.0	1.4	-0.6	-1.2	-	5.3	3.0
	I-18	0.7	1.4	-0.7	-1.1	2.1	5.0	3.1
	I-19	0.9	1.1	-	-	-	5.2	3.0
	I-20	1.2	-	-0.9	-1.2	-	5.5	2.9
	I-21	1.0	-	-	-	1.4	5.3	1.1
Model	**I-22**	1.0	-	-	-	-	5.3	1.6
Compounds	**I-23**[c]	0.9	-	-	-	-	-	-
	I-24	1.5[d]	-	-	-	-	-	-
	I-25	1.1[e]	-	-	-	-	-	-

[a]Values reported are against a Ag/AgCl (sat'd) reference electrode.. [b]Voltammetry measurements done in CH_2Cl_2 and a scan rate of 100 mV/sec. [c]From Roncali and Frère.[57] [d]From Rao.[41] [e]From Roncali.[57]

Compounds **I-21** and **I-22** were synthesized as models to systematically assign the effect of the simple azomethine and the electronic groups on the oxidation potentials. These model compounds also help to deconvolute the azomethine oxidation processes, which have only been partially examined to date.[10, 43, 47] The oxidation potentials of **I-21** and **I-22** are mutually identical and they are similar to the other thiopheno azomethines. This implies the simple azomethine bond exerts little effect on the oxidation potential of the thiophenes.[2, 3, 5, 48] Rather, the oxidation potentials are influenced uniquely by the electronic groups and the degree of conjugation. Unlike with other thiopheno azomethines, **I-21** undergoes irreversible oxidation resulting from radical cation coupling to form a dimer. The product eventually is deposited as a thin film on the working electrode upon prolonged oxidation times. Conversely, the one electron oxidation to generate the radical cation is quasi-reversible for **I-22** and represents one of only a few examples of azomethine quasi-reversible oxidation. The reversible-like behavior is a result of substitution in the 5 and 5' position (Figure I-2) that prevents coupling between radical cations. This suggests that product formation occurs predominately via these two positions. The quasi-reversible radical cation formation is in contrast to other azomethines that undergo irreversible oxidation regardless of substitution, scan speeds, and experimental conditions because of

the extremely reactive radical cation.[49] Dimer formation by oxidative coupling was observed only for the compounds that possess one substitution in either the 5 or 5' positions.[2, 50] Conversely, electrochemically induced polymerization was possible only with **I-14** owing to its unsubstituted 5,5' positions.[22]

To further verify the observed irreversible oxidation was a result of radical cation coupling via the α,α positions, compounds **I-8**, **I-12** and **I-19** were examined. The terminal methyl groups of these model compounds suppress α-α oxidative coupling via the 5,5' positions, but do not prevent any β-β coupling defects via the 3', 4, and 4' positions. No electrochemically induced oxidative product coupling was observed for these compounds, while exhibiting reversible one electron oxidation. The lack of coupling products for **I-8** and **I-12** suggest coupling of the radical cations occurs exclusively on the thiophene Ring B (Figure I-2) and not on Ring A, to which the amine is directly bound. This may be from the electron withdrawing ester that increases the oxidation potential of thiophene A such that the oxidation occurs preferentially on Ring B. Furthermore, no significant difference was observed for the oxidation potentials of **I-8**, **I-12**, and **I-19** relative to their unalkylated analogues **I-5**, **I-9**, and **I-14**, respectively. This suggests that simple alkylation does not affect the oxidation potential. The absence of significant difference in the oxidation potentials validates the irreversible process for azomethine oxidation and confirms that the coupling of intermediates occurs preferentially by α-α coupling via the 5, 5' positions. This

is further supported by the lack of coupling products with monoazomethines **I-10-I-13** along with the previous electrochemical polymerization of an alkylated derivative of **I-14**.[22]

Crystal Structure

Similar to the carbon analogues, two geometric azomethine isomers are possible; *E* and *Z*. Unlike their carbon analogues, differentiation between the two azomethine isomers is difficult by ^{1}H-NMR. The NMR spectra of all the azomethines studied showed exclusively one imine peak in the 8-9 ppm region confirming the exclusive formation of one isomer, which is assumed to be the more thermodynamically stable *E* isomer. The crystal structures obtained for **I-5**,[51] **I-14**[52] and **I-16** are all consistent and confirm that both azomethine bonds in these structures adopt the *E* configuration. To confirm the *E* isomer did not preferentially crystallize, NMR spectra of the crystals used for x-ray diffraction and the mother liquor were both measured and they yielded identical ^{1}H-NMR spectra. This is further corroborated by repeated crystallization of various compounds from Chart I-1 that consistently yielded the same crystal structure. Accurate correlation between the solid state and solution structures can be assumed because similar absorption spectra were observed for samples both in solution and in thin film. The latter are known to increase the planarity of twisted molecules leading to increased conjugation resulting in bathochromic shifts in the absorption spectra.

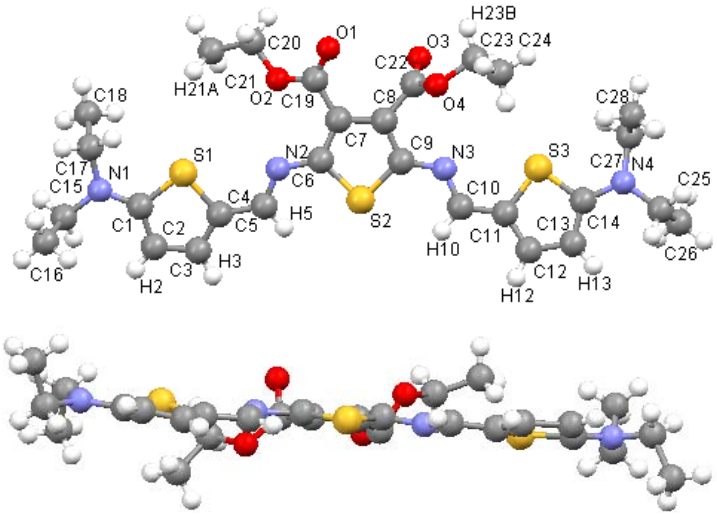

Figure I-8. Schematic representation of crystal structure **I-16**, top view (top) and seen along the *a* crystal axis parallel to the thiophene units (bottom).

The crystal structure of **I-16**, represented in Figure I-8, clearly shows the heteroatom units adopt an anti-parallel arrangement. The same anti-parallel arrangement of the sulfur atoms was also observed with other monoazomethines and bisazomethines.[17, 51, 53] The added advantage of the anti-parallel conformation and the resulting linearity confers a high degree of conjugation and validates the spectroscopic results. This arrangement is also ideal for providing high conductivities that are expected with doping.[17] The average mean planes of the terminal thiophenes were found to be twisted 5.8^{o} and 10.6^{o} from the mean plane of the central thiophene and its two azomethine bonds. The low twisting angle provides a planar and linear configuration to the molecule. The measured mean plane angles for **I-14** and **I-16** are in contrast to homoaryl azomethines that have twisted mean planes varying between 55^{o} and 65^{o} from the central

thiophene.[12, 14, 54] A 45^{o} angle between the two thiophene mean planes is also apparent with azomethines derived from thiophene dicarboxaldehyde such as **I-25**.[13, 23, 55] The deviation from planarity is required for the homoaryl azomethines to avoid steric hindrance between the ortho hydrogen on the homoaryl ring and the azomethine hydrogen, which are separated only by 2.16 Å.[13, 55] A high degree of intramolecular hydrogen bonding and intermolecular π-stacking further contribute to the observed planar structures. This is evident from the four contacts present for **I-16** involving H5···S2, H10···S2, H27A···S3, and H17A···S1. There exists also a CH···O intermolecular hydrogen bond between C17H-17···O1 *i* = (-x, -y, -z). The geometric parameters of this arrangement are H···O 2.34 Å, C···O 3.198 (12) Å, C-H···O 141^{o} and the pairs are linked by an inversion-center to form dimers. The crystallographic data furthermore shows the azomethine bond distances to be shorter than its carbon analogue (Table I-3), which are in part responsible for the increased planarity and high degree of conjugation.[56]

Table I-3. Selected crystallographic data of thiophene azomethines and a carbon analogue.

	I-5[a]	**I-14**[b]		**I-16**		**I-23**[c]	
		side A	side B	side A	side A	side A	Side B
plane angle[d]	7.3°	9.1°	25.3°	10.6°	5.8°	0°	6°
-C=N-[e]	1.283 Å	1.277 Å	1.286 Å	1.296 Å	1.282 Å	1.278 Å	1.439 Å
=N-Aryl-[e]	1.351 Å	1.381 Å	1.393 Å	1.363 Å	1.374 Å	1.585 Å	1.312 Å
=CH-Aryl-	1.426 Å	1.443 Å	1.435 Å	1.432 Å	1.418 Å	1.614 Å	1.430 Å

[a] From Skene.[51] [b] From Dufresne.[52] [c] From Zobel.[57] [d] Refers to the mean plane angle between the central thiophene and the terminal thiophene units. [e] For **I-23**, the value refers to –C=C- bond distance. [e] Values taken from Skene[21].

Conclusion

The first examples of electronic *push-push*, *pull-pull* and *push-pull* conjugated thiophene azomethines were presented. The formation of the highly conjugated azomethine bond is responsible for displacing the equilibrium in favor of reductively and hydrolytically resistant new materials. Through the selective synthesis, different substituents and electronic groups can be incorporated into the conjugated framework leading to symmetric and unsymmetric compounds. These electronic groups provide a means to control the physical properties such as HOMO-LUMO energy gap, absorption, and color emission because of the inherent conjugation of the azomethine bond that allows perturbation of the HOMO and LUMO energy levels. The spectroscopic and electrochemical properties can

be tailored by varying the number of thiophene units and the nature of the electronic groups substituted on the thiophenes. Reversible-like oxidation behavior and low potentials make these azomethines suitable for p-type doping while their linear and planar conformations impart a high degree of conjugation. Such properties are particularly useful because they permit fine-tuning of the various properties of the products formed. This, in turn, allows for a myriad of possibilities in the application of these compounds to meet the needs of the electronics industry, which is not easily achieved using conventional materials.

Acknowledgments

The authors acknowledge financial support from the Natural Sciences and Engineering Research Council Canada, Fonds de Recherche sur la Nature et les Technologies, the Centre for Self-Assembled Chemical Structures, and Canada Foundation for Innovation. Gratitude is extended to Dr. M. Simard for assistance with the crystal structure analyses and to Prof. D. Zargarian for helpful suggestions. M.B. thanks the Université de Montréal for a graduate scholarship.

References

1. (a) Dimitrakopoulos, C. D.; Malenfant, P. R. L. *Adv. Mater.* **2002**, *14*, 99-117. (b) Rupprecht, L. *Conductive Polymers and Plastics in Industrial Applications*, Society of Plastics Engineers/Plastics Design Library, Brookfield, Conn., 1999.

2. Hansford, K. A.; Guarin, S. A. P.; Skene, W. G.; Lubell, W. D. *J. Org. Chem.* **2005**, *70*, 7996 -8000.

3. Roncali, J.; Blanchard, P.; Frère, P. *J. Mater. Chem.* **2005**, *16*, 1589-1610.

4. (a) Toal, S. J.; Magde, D.; Trogler, W. C. *Chem. Commun.* **2005**, *43*, 5465-5467. (b) Rogers, J. A.; Bao, Z.; Baldwin, K.; Dodabalapur, A.; Crone, B.; Raju, V. R.; Kuck, V.; Katz, H.; Amundson, K.; Ewing J.; Drzaic, P. *Proc. Natl. Acad. Sci. U.S.A.* **2001**, *98*, 4835-4840. (c) Kelley, T. W.; Baude, P. F.; Gerlach, C.; Ender, D. E.; Muyres, D.; Haase, M. A.; Vogel, D. E.; Theiss, S. D. *Chem. Mater.* **2004**, *16*, 4413-4422.

5. Perepichka, I. F.; Perepichka, D. F.; Meng, H.; Wudl, F. *Adv. Mater.* **2005**, *17*, 2281-2305.

6. Beaupré, S.; Leclerc, M. *Macromolecules* **2003**, *36*, 8986-8991.

7. Drury, A.; Maier, S.; Rüther M.; Blau, W. J. *J. Mater. Chem.* **2003**, *13*, 485-490.

8. Lima, A.; Schottland, P.; Sadki, S.; Chevrot, C. *Synth. Met.* **1998**, *93*, 33-41.

9. (a) Lamère, J. F.; Lacroix, P. G.; Rivera, N. F. J. M.; Santillan R.; Nakatani, K. *J. Mater. Chem.* **2006**, *16*, 2913-2920. (b) Casado, J. Delgado, M. C. R.; Merchán, M. C. R.; Hernández, V.; Navarrete, J. T. L.; Pappenfus, T. M.; Williams, N.; Stegner, W. J.; Johnson, J. C.; Edlund, B. A.; Janzen, D. E.; Mann, K. R.; Orduna, J.; Villacampa, B. *Chem. Eur. J.* **2006**, *12*, 5485-5470. (c) Oliva, M. M. C.; M. M. M. Raposo, J.; Fonseca, A. M. C.; Hartmann, H.; Hernandez, V.; Lopez Navarrete, J. T. *J. Org. Chem.* **2006**, *71*, 7509-7520.

10. Thomas, O.; Inganäs, O.; Andersson, M. R. *Macromolecules* **1998**, *31*, 2676-2678.

11. Ng, S. C.; Chan, H. S. O.; Wong, P. M. L.; Tan, K. L.; Tan, B. T. G. *Polymer* **1998**, *39*, 4963-4968.

12. Yang, C.-J.; Jenekhe, S. A. *Macromolecules* **1995**, *28*, 1180-1196.

13. Skene, W. G.; Dufresne, S. *Org. Lett.* **2004**, *6*, 2949-2952.

14. Tsai, F.-C.; Chang, C.-C.; Liu, C.-L.; Chen, W.-C.; Jenekhe, S. A. *Macromolecules* **2005**, *38*, 1958-1966.

15. Yang, C.-J.; Jenekhe, S. A. *Macromolecules* **1995**, *28*, 1180-1196.

16. Kiriy, N.; Bocharova, V.; Kiriy, A.; Stamm, M.; Krebs, F. C.; Adler, H.-J. *Chem. Mater.* **2004**, *16*, 4765-4771.

17. Skene, W. G. *Polym. Prepr.* **2004**, *45*, 252-253.

18. (a) Dufresne, S.; Skene, W. G. *PMSE Prepr.* **2005**, *92*, 16-17. (b) Skene, W. G. *World Pat.* WO 2005073265, 2005.

19. Huang, C.-H.; McClenaghan, N. D.; Kuhn, A.; Hofstraat, J. W.; Bassani, D. M. *Org. Lett.* **2005**, *7*, 3409-3412.

20. (a) Wang, C.; Shieh, S.; LeGoff, E.; Kanatzidis, M. G. *Macromolecules* **1996**, *29*, 3147-3156. (b) Yang, C.-J.; Jenekhe, S. A. *Chem. Mater.* **1991**, *3*, 878-887.

21. Skene, W. G.; Trefz, T. *Polym. Prepr.* **2004**, *45*, 563-564.

22. Bourgeaux, M.; Perez Guarìn, S. A.; Skene, W. G. *J. Mater. Chem.* **2007**, *17*, 972-979.

23. Skene, W. G.; Dufresne, S. *Polym. Prepr.* **2004**, *45*, 728-729.

24. Boone, H. W.; Bryce, J.; Lindgren, T.; Padias, A. B.; Hall, H. K. J. *Macromolecules* **1997**, *30*, 2797-2799.

25. (a) Rowan, S. J.; Cantrill, S. J.; Cousins, G. R. L.; Sanders, J. K. M.; Stoddart, J. F. *Angew. Chem. Int. Ed.* **2002**, *41*, 898-952. (b) Godoy-Alcántar, C.; Yatsimirsky A. K.; Lehn, J.-M. *J. Phys. Org. Chem.*, **2005**, *18*, 979-985. (c) Lehn, J.-M. *Prog. Polym. Sci.* **2005**, *30*, 814. (d) Zhao, D.; Moore, J. S. *Macromolecules* **2003**, *36*, 2712-2720. (d) Giuseppone N.; Lehn, J.-M. *PMSE Prepr.* **2004**, *90*, 725.

26. Giuseppone, N.; Schmitt, J.-L.; Schwartz, E.; Lehn, J.-M. *J. Am. Chem. Soc.* **2005**, *127*, 5528-5539.

27. (a) Giuseppone, N.; Lehn, J.-M. *Chem. Eur. J.* **2006**, *12*, 1723-1735. (b) Giuseppone, N.; Lehn, J.-M. *Chem. Eur. J.* **2006**, *12*, 1715-1722.

28. Van Der Looy, J. F. A.; Thys, G. J. H.; Dieltiens, P. E. M.; De Schrijver, D.; Van Alsenoy, C.; Geise, H. J. *Tetrahedron* **1997**, *53*, 15069-15084.

29. Lehn, J.-M. *Chem. Eur. J.* **2006**, *12*, 5910-5915.

30. Seixas de Melo, J.; Elisei, F.; Gartner, C.; Aloisi, G. G.; Becker, R. S. *J. Phys. Chem. A* **2000**, *104*, 6907-6911.

31. Seixas de Melo, J.; Elisei, F.; Becker, R. S. *J. Chem. Phys.* **2002**, *117*, 4428-4435.

32. Becker, R. S.; Seixas de Melo, J.; Maçanita, A. L.; Elisei, F. *J. Phys. Chem.* **1996**, *100*, 18683-18695.

33. Wasserberg, D.; Marsal, P.; Meskers, S. C. J.; Janssen, R. A. J.; Beljonne, D. *J. Phys. Chem. B* **2005**, *109*, 4410-4415.

34. (a) Paa, W.; Yang, J.-P.; Rentsch, S. *Appl. Phys. B.* **2000**, *71*, 443-449. (b) Burrows, H. D.; Arnaut, L. G.; Pina, J.; Seixas de Melo, J.; Chattopadhyay, N.; Alcacer, L.; Charas, A.; Morgado, J. *Chem. Phys. Lett.* **2005**, *402*, 197-201.

35. (a) Seixas de Melo, J.; Silva, L. M.; Arnaut, L. G.; Becker, R. S. *J. Chem. Phys.* **1999**, *111*, 5427-5433. (b) Seixas de Melo, J.; Burrows, H. D.; Svensson, M.; Andersson, M. R.; Monkman, A. P. *J. Chem. Phys.* **2003**, *118*, 1550-1556.

36. (a) Andrews, L. J.; Deroulede, A.; Linschltz, H. *J. Phys. Chem.* **1978**, *82*, 2304-2309. (b) Murphy, R. S.; Moorlag, C. P.; Green, W. H.; Bohne, C. *J. Photochem. Photobiol. A* **1997**, *110*, 123-129.

37. Wasserberg, D.; Dudek, S. P.; Meskers, S. C. J.; Janssen, R. A. J. *Chem. Phys. Lett.* **2005**, *411*, 273-277.

38. Scaiano, J. C. *CRC Handbook of Organic Photochemistry*, CRC Press, Boca Raton, 1989.

39. (a) Carmichael, I.; Hug, G. L. *J. Phys. Chem. Ref. Data* **1986**, *15*, 1-250. (b) Carmichael, I.; Helman, W. P.; Hug, G. L. *J. Phys. Chem. Ref. Data* **1987**, *16*, 239-260. (c) Carmichael, I.; Hug, G. L. *Handbook of Organic Photochemistry*, ed. J. C. Scaiano, CRC Press, Boca Raton, Florida, 1989, pp. 369-403.

40. Lund, H.; Hammerich, O. *Organic Electrochemistry* Marcel Dekker, New York, 2001.

41. Rao, T. V. D. P.; Veerabhadram, G.; Sastry, K. S. *J. Electrochem. Soc. India* 2001, **50**, 68-71.

42. (a) Koch, R. W.; Dessy, R. E. *J. Org. Chem.* **1982**, *47*, 4452-4459. (b) Soucaze-Guillous, B.; Lund, H. *J. Electroanal. Chem.* **1997**, *423*, 109-114.

43. Baizer, M. M.; Lund, H. *Organic Electrochemistry: An Introduction and A Guide*, Marcel Dekker, Inc., New York, 1983.

44. Gavar, R. A.; Stradyn, Y. P.; Fleisher, M. B.; Kadysh, V. P.; Slavinskaya, V. A. *Theor. Exp. Chem.* **1981**, *16*, 267-270.

45. Agrawal, A. K.; Jenekhe, S. A. *Chem. Mater.* **1996**, *8*, 579-589.

46. Even though a suitable analogue for spectroscopic and electrochemical data comparison should contain an electron withdrawing group similar to **1**, there are no literature examples for such derivatives of **23**.

47. (a) Simionescu, C. I.; Cianga, I.; Ivanoiu, M.; Duca, A.; Cocarla, I.; Grigoras, M. *Eur. Polym. J.* **1999**, *35*, 587-599. (b) Diaz, F. R.; del Valle, M. A.; Brovelli, F.; Tagle, L. H.; Bernede, J. C. *J. Appl. Polym. Sci.* **2003**, *89*, 1614-1621.

48. Roncali, J. *Chem. Rev.* **1992**, *92*, 711-738.

49. (a) Caballero, A.; Tárraga, A.; Velasco, M. D.; Molina, P. *Dalton Trans.* **2006**, *11*, 1390-1398. (b) Higuchi, M.; Yamamoto, K. *Polym. Adv. Tech.* **2002**, *13*, 765-770. (c) Catanescu, O.; Grigoras, M.; Colotin, G.; Dobreanu, A.; Hurduc, N.; Simionescu, C. I. *Eur. Polym. J.* **2001**, *37*, 2213-2216. (d) Grigoras, M.; Catanescu, C. O.; Colotin, G. *Macromol. Chem. Phys.* **2001**, *202*, 2262-2266.

50. (a) Jérôme, C.; Maertens, C.; Mertens, M.; Jérôme, R.; Quattrocchi, C.; Lazzaroni, R.; Brédas, J. L. *Synth. Met.*, **1996**, *83*, 103-109. (b) Jérôme, C.; Maertens, C.; Mertens, M.;

Jérôme, R.; Quattrocchi, C.; Lazzaroni, R.; Brédas, J. L. *Synth. Met.* **1997**, *84*, 163-164. (c) v. Haare, J. A. E. H.; Havinga, E. E.; v. Dongen, J. L. J.; Janssen, R. A. J.; Cornil, J.; Brédas, J.-L. *Chem. Eur. J.* **1998**, *4*, 1509-1522.

51. Skene, W. G.; Dufresne, S.; Trefz, T.; Simard, M. *Acta Cryst.* **2006**, *E62*, o2382–o2384.

52. Dufresne, S.; Bourgeaux, M.; Skene, W. G. *Acta Cryst.* **2006**, *E62*, o5602-o5604.

53. Skene, W. G.; Trefz, T. *PMSE Prepr.* **2004**, *91*, 326-327.

54. Grigoras, M.; Catanescu, C. O. *J. Macromol. Sci. Polym. Rev.* **2004**, *C44*, 131-173.

55. Skene, W. G.; Dufresne, S. *Acta Cryst.* **2006**, *E62*, o1116-o1117.

56. (a) Blanchard, P.; Brisset, H.; Illien, B.; Riou, A.; Roncali, J. *J. Org. Chem.* **1997**, *62*, 2401-2408. (b) Ruban, G.; Zobel, D. *Acta Cryst.* **1975**, *B31*, 2632-2634.

57. (a) Elandaloussi, E. H.; Frère, P.; Richomme, P.; Orduna, J.; Garin, J.; Roncali, J. *J. Am. Chem. Soc.* **1997**, *119*, 10774-10784. (b) Jestin, I.; Frère, P.; Blanchard, P.; Roncali, J. *Angew. Chem. Int. Ed.* **1998**, *37*, 942-945.

58. Gawinecki, R.; Muzalewski, F. *Polish J. Chem.* **1984**, *58*, 1091-1098.

59. Coville, N. J.; Neuse, E. W. *J. Org. Chem.* **1977**, *42*, 3485-3491.

60. Facchetti, A.; Yoon, M.-H.; Stern, C. L.; Hutchison, G. R.; Ratner, M. A.; Marks, T. J. *J. Am. Chem. Soc.* **2004**, *126*, 13480-13501.

II. CHAPITRE II

Insights into the Effect of the Ketylimine Group on the Fluorescence Deactivation of Oligo-Fluorenes

Stéphane Dufresne,[1] Ivan Ulliel Roche,[1,2] Thomas Skalski,[1,3] and W. G. Skene[1]*

[1]Centre for Self-Assembled Chemical Structures, Département de Chimie, Université de Montréal, CP 6128, Centre-ville, Montreal, QC

[2]Current Address: Ecole Nationale Supérieure de Chimie et Physique de Bordeaux (ENSCPB) 16 avenue Pey Berland, 33600 Pessac, France

[3]Current Address: Université d'Artois, Unité de Catalyse et de Chimie du Solide, UMR CNRS n°8181 Faculté Jean Perrin, rue Jean Souvraz, S.P.18, 62307, Lens Cédex, France

Received : May 3, 2010; Revised Manuscript Received June 29, 2010

Published on Web 07/14/2010

DOI : 10.1021/jp104026y

J. Phys Chem C. **2010**, *114(30)*, 13106-13112.

Abstract

A series of oligofluorenes containing arylketylimines in the 9-position ranging between 1 and 3 fluorene segments was prepared. The conjugated ketylimines were prepared using dehydration and Lewis acid protocols from the corresponding oligofluorenones. These heteroconjugated oligomers were prepared for examining the effect of the ketylimine moiety on the photophysical properties relative to their ketone counterparts. Both the ketylimine and fluorenone containing oligofluorenes exhibited reduced fluorescence relative to their corresponding all-fluorene analogues. Temperature dependent emission measurements and steady-state fluorescence quenching confirmed that fluorescence deactivation of the ketylimines occurred predominately by intramolecular photoinduced electron transfer (PET). This is in contrast to their oligofluorenone counterparts that dissipated their singlet excited state energy via nonradiative internal conversion. The measured diffusion controlled fluorescence quenching rate constants (3×10^{10} M^{-1} s^{-1}) combined with the calculated exergonic energetics ranging from -10 to -116 kJ/mol derived from the Rehm-Weller equation for the oligofluorenyl ketylimines corroborate that the ketylimines fluorescence deactivation occurs by intramolecular PET.

Introduction

Conjugated materials have received much attention because of their optoelectronic properties that are suitable for plastic electronics including light emitting diodes and photovoltaics, to name but a few. Polyfluorenes and its derivatives have been extensively studied owing to their intrinsic high emission making them ideal materials for use in emitting devices.[1] The added benefit of polyfluorene and its derivatives is that they are thermally and chemically robust, and as such, they can withstand the harsh oxidative and reductive environment present within an emitting device. Unfortunately, random oxidative decomposition can take place along the polymer chain. The resulting ketyl defects have detrimental effects on the device efficiency and are responsible for both contaminating the pristine emission with a green component and reducing the emission yields.[2-5]

The exact mode by which the fluorenone defect (**II-1**) deactivates the emission and the origins of undesired green emission in polyfluorenes remain contentious.[4] Nonetheless, the ketone group is interesting because it provides a reactive point at which functionality can be introduced into the conjugated fluorene polymer. As result, the polymer's properties can be adjusted by incorporating different groups at the ketyl centre.[6-9] For example, simple condensation of the ketyl group with amines leads to stable ketylimines. By judiciously choosing the amine used for ketylimine formation, the properties of the polyfluorenes such as solubility, electronic effects, color, and emission yields, to name but a few, can potentially be tailored. [10,11]

Although, fluorene ketylimines such as **II-8** can potentially be prepared by using simple condensation methods, few examples of these compounds are known.[12-14] Even fewer reports investigated their photophysical properties, and to date, no extensive photophysical property investigations have been undertaken. Such studies are extremely beneficial for understanding the excited state deactivation modes, and in turn, for designing future generations of highly fluorescent compounds with desired properties. By comparing the photophysical properties of ketylimines to their carbon counterparts, the effect of the heteroatomic bond on the properties can be had. This is beneficial for determining whether the imine bond is isoelectronic to its vinylene analogues.[15,16] We were therefore incited to examine the fluorescence deactivation of oligofluorene ketylimine derivatives in order to understand their structure-fluorescence properties. In particular, the effect of the heteroatomic bond and the number of fluorene units on the singlet excited state properties was investigated. Herein, we present the preparation and the photophysical properties of novel oligo-fluorenyl ketylimines in order to understand their singlet excited state deactivation modes.

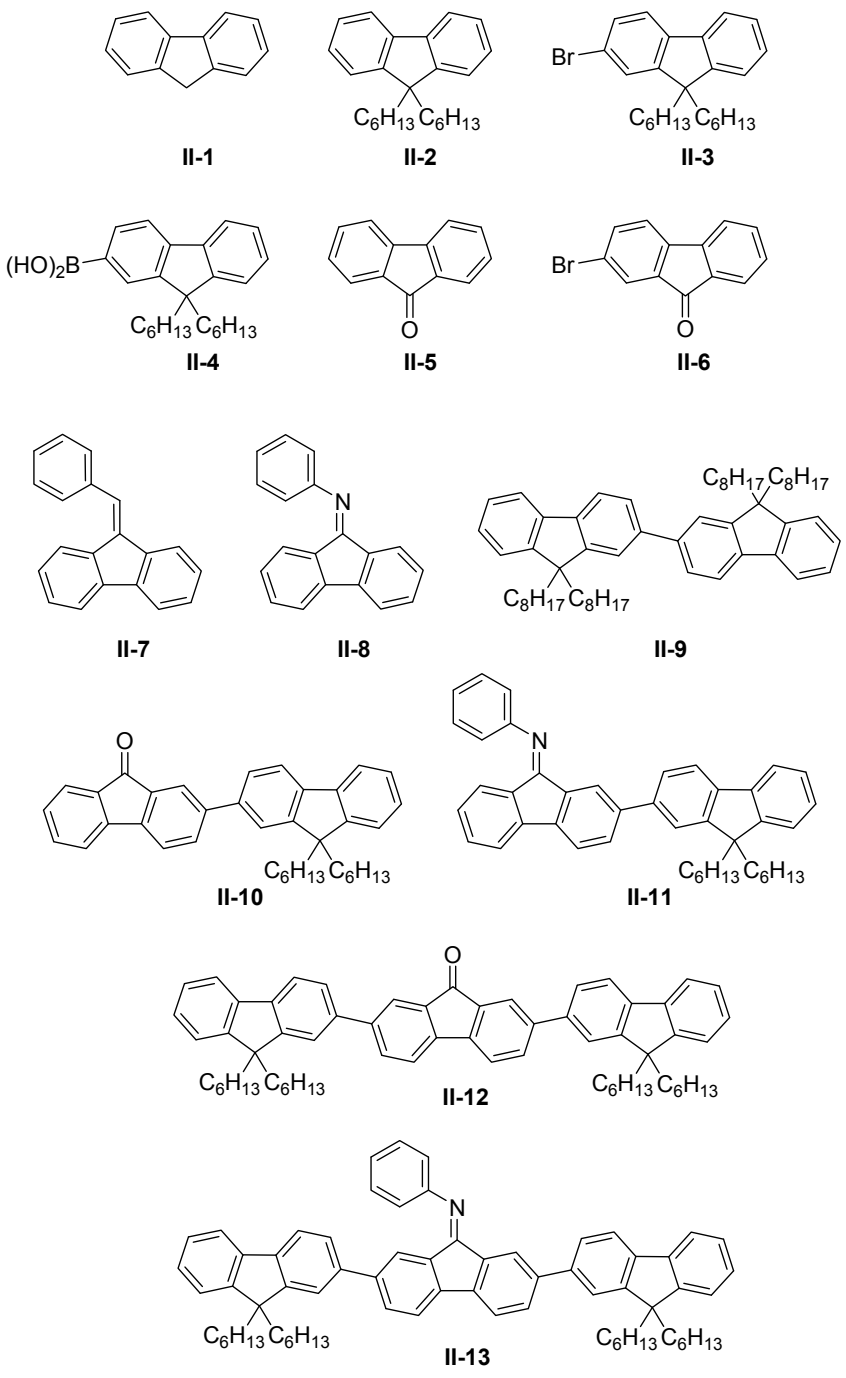

Figure II-1. Ketylimines prepared and investigated and their representative analogues and precursors.

Experimental

Materials and general methods

All chemicals including **II-1, II-5, II-6** and **II-7** were commercially available from Aldrich and were used as received unless otherwise stated. Anhydrous and deaerated solvents were obtained with a Glass Contour solvent purification system. ^{1}H-NMR and ^{13}C-NMR spectra were recorded on a Bruker 400 MHz spectrometer with the appropriate deuterated solvents.

Spectroscopic methods

The absorption measurements were done on a Cary-500 spectrometer while the fluorescence studies were performed on an Edinburgh Instruments FLS-920 fluorimeter after deaerating the samples thoroughly with nitrogen for 20 minutes. Fluorescence absolute quantum yields were measured at 10^{-5} M by exciting the compounds of study at the corresponding maximum absorption in spectroscopic grade dichloromethane at room temperature in an integrating sphere.

Electrochemical methods

Cyclic voltammetric measurements were performed on a Bio Analytical Systems EC Epsilon potentiostat. Compounds were dissolved in anhydrous and deaerated dichloromethane at 10^{-4} M with NBu_4PF_6 in sufficient concentration in order to achieve

highly conductive solutions. A platinum electrode was used as auxiliary and working electrodes, while and a saturated Ag/AgCl electrode was used as the reference electrode.

Highest-occupied molecular orbital (HOMO) and lowest-unoccupied molecular orbital (LUMO) energy levels and spin densities were calculated semi-empirically using DFT calculation methods available in Spartan 06 with 6-31g* basis set. The bond angles, distances, torsions, and other parameters were experimentally derived from the X-ray data for **II-12** from the data deposited in the CCDC, corresponding to no. 698740.

Laser Flash Photolysis Measurements.

Laser flash photolysis experiments were done with a Luzchem mini-LFP system exciting at 355 nm with the third harmonic of a Continuum Surelite Nd:YAG laser with 10 ns pulses. Solutions were prepared in dichloromethane with absorbances between 0.3 and 0.5 at the excitation wavelength and deaerated for 20 min with nitrogen prior to analyses. The transient absorption spectrum was generated by monitoring the change between the pre- and postlaser flash signals as a function of monitoring wavelength. 1,4-Cyclohexadiene was used as a triplet quencher for assigning the transient signal.[17]

Synthesis

2-Bromo-9,9-dihexyl-9H-fluorene (II-3). In a round bottom flask was dissolved NaOH (47.5 g) in distilled water (50 mL). To this solution was added 2-bromofluorene (5 g, 30.4 mmol) with a catalytic amount of benzyltriethylammonium bromide in DMSO (100 mL) to which was added 1-bromohexane (29 g, 176 mmol) drop-wise. The mixture was then kept under nitrogen and allowed to react for 96 hours during which time the mixture changed colors. The crude product was then extracted with ether (60 mL) and washed with 4 x 100 mL water. The organic layer was dried with $MgSO_4$, filtered, and concentrated. The compound was then separated by flash chromatography using hexanes/AcOEt (85/15%) to give the product as a light yellow viscous oil (7.4 g, 88 %). ^{1}H-NMR (acetone-d_6): δ = 7.76 (s, 1H), 7.70 (d, 1H, J = 8.0 Hz), 7.60 (d, 1H, J = 1.6 Hz)), 7.47 (dd, 1H, J = 8.0 Hz and J = 1.8 Hz), 7.41 (m, 1H), 7.31 (m, 2H), 2.05 (d, 4H), 1.05 (m, 12H) 0.71 (t, 6H, J = 6.7 Hz), 0.54 (m, 4H). ^{13}C-NMR (acetone-d_6): δ = 154.9, 152.0, 142.3, 141.9, 131.8, 129.5, 128.9, 128.0, 124.7, 123.2, 122.5, 121.7, 57.2, 41.7, 33.2, 30.8, 25.5, 24.1, 15.2.

9,9-Dihexyl-9H-fluoren-2-yl-2-boronic acid (II-4). To **II-3** (929 mg, 2.25 mmol) dissolved in anhydrous THF (30 m) was added *n*-BuLi (2.2 M in hexanes, 1.33 mL, 2.93 mmol) at -78^{o}C and the reaction mixture was allowed to react for 1 hour before adding triisopropylborate (1.56 mL, 6.76 mmol). The crude product was extracted with ether and

then concentrated after reaction completion overnight. The product was recrystallised from dichloromethane/hexanes (752 mg, 88%). The compound was used without any further purification.

2-Bromo-9H-fluoren-9-one (II-6). 2-Bromofluorene (1 g, 4 mmol) was dissolved in DMSO (15 mL) with cesium carbonate (6.65 g, 20 mmol) and the reaction mixture was vigorously stirred at room temperature for 3 days. Sufficient water (80 mL) was then added to precipitate the product, which was filtered and isolated as a yellow solid (0.96 g, 91%). M.p.: 145-147 °C. ^{1}H-NMR (acetone-d_6): δ = 7.78 (m, 4H) 7.65 (m, 2H), 7.46 (dd, 1H, J = 8.3 Hz and J = 0.9 Hz). HRMS(+) calculated for $[C_{25}H_{33}Br]^{+}$: 258.9753 found 258.97492.

2-(9,9-Dihexyl-9H-fluoren-7-yl)-9H-fluoren-9-one (II-10). In anhydrous toluene (20 mL) was dissolved **II-6** (274 mg, 1.05 mmol) and **II-4** (400 mg, 1.05 mmol). Aqueous Na_2CO_3 (2 M, 10 mL) was then added before the addition of tetrakistriphenylphosphine palladium (0.175 mg, 0.16 mmol). The mixture was refluxed overnight under nitrogen while protected from light. The crude product was extracted with ethyl acetate/water and the organic layers were concentrated. A gravity column with basic alumina using dichloromethane/hexanes (50:50) was used to afford the product as an orange viscous oil (304 mg, 55 %). ^{1}H-NMR (acetone-d_6): δ = 8.00- 7.37 (m, 14H), 2.15 (m, 4H), 1.08 (m, 12H), 0.75 (t, 6H, J = 6.7 Hz), 0.67 (m, 4H). ^{13}C-NMR (acetone-d_6): δ = 193.3, 152.0, 151.3, 144.7, 143.4, 143.0, 141.7, 141.1, 139.0, 137.7, 135.5, 134.7, 133.7, 129.6, 127.8,

127.4, 126.1, 124.2, 123.3, 122.5, 121.7, 121.6, 121.3, 120.6, 120.3, 55.6, 40.4, 31.7, 29.8, 24.1, 22.7, 13.7. HRMS(+) calculated for $[C_{38}H_{41}O]^+$: 513.31519 found 513.31363.

N-(2-(9,9-Dihexyl-9H-fluoren-7-yl)-9H-fluoren-9-ylidene)benzenamine (II-11). **II-10** (60 mg, 0.117 mmol) and DABCO (60 mg, 1.17 mmol) were mixed in anhydrous toluene (25 mL) under nitrogen. Titanium chloride 1M in toluene (0.87 mL, 0.351 mmol) was added to the mixture at 0^oC. Aniline (68 mg, 0.663 mmol) was then added and the reaction was refluxed for 3-4 hours after which the mixture was concentrated and redissolved in acetone. The titanium salts were removed and the title compound was isolated as a yellow-orange oil (45 mg, 65%) after flash chromatography on alumina with hexanes and increasing the solvent polarity ethyl acetate. ^{1}H-NMR (acetone-d_6): δ = 7.98-7.37 (m, 19H), 2.18 (m, 4H), 0.89 (m, 12H), 0.74 (t, 6H, J = 7.6 Hz), 0.67 (m, 4H). ^{13}C-NMR (acetone-d_6): δ = 193.2, 152.0, 151.3, 144.7, 143.3, 143.0, 141.7, 141.1, 139.0, 135.5, 135.2, 134.7, 133.7, 132.6, 129.7, 129.6, 127.8, 127.4, 126.1, 125.6, 125.5, 124.2, 123.3, 122.5, 121.7, 121.6, 121.3, 120.6, 120.3, 120.2, 118.6, 55.6, 40.4, 31.7, 29.8, 24.1, 22.7, 13.7. HRMS(+) calculated for $[C_{44}H_{46}N]^+$: 588.36248 found 588.36186.

2-(9,9-Dihexyl-9H-fluoren-2-yl)-7-(9,9-dihexyl-9H-fluoren-7-yl)-9H-fluoren-9-one (II-12). 2,7-Dibromo-9H-fluoren-9-one (60 mg, 0.181 mmol) and **II-4** (137 mg, 0.362 mmol) were mixed in aqueous Na_2CO_3 (2 M, 10 mL) and isopropanol (20 mL). The mixture was deaerated for 20 minutes after which tetrakistriphenylphosphine palladium

(40 mg, 0.036 mmol) was added. The mixture was refluxed overnight while protecting from light. The crude product was extracted with ethyl acetate and then isolated as a yellow solid (107 mg, 70%) after flash chromatography. M.p.: 133-135 °C. ^{1}H-NMR (acetone-d_6): δ = 8.03-7.37 (m, 20H), 2.14 (m, 8H), 1.10 (m, 24H), 0.76 (t, 6H, J = 7.6 Hz), 0.67 (m, 8H). ^{13}C-NMR (acetone-d_6): δ = 193.2, 152.0, 151.3, 143.3, 142.9, 141.7, 141.1, 139.0, 135.5, 133.8, 127.8, 127.4, 126.1, 123.3, 122.6, 121.8, 121.6, 120.6, 120.3, 55.7, 55.5, 40.4, 31.7, 24.1, 22.7, 13.7. HRMS(+) calculated for $[C_{63}H_{73}O]^{+}$: 920.61288 found 920.61061.

N-(2-(9,9-Dihexyl-9H-fluoren-2-yl)-7-(9,9-dihexyl-9H-fluoren-7-yl)-9H-fluoren-9-ylidene)benzenamine (II-13). DABCO (133 mg, 1.19 mmol) and **II-12** (100 mg, 0.12 mmol) were mixed in anhydrous toluene (25 mL) under nitrogen. Titanium chloride 1M in toluene (354 μL, 0.35 mmol) and aniline (55 mg, 0.59 mmol) were then added and the mixture was refluxed for 3-4 hours. The solvent was then evaporated and the solids were taken up in acetone. The insoluble precipitate was filtered off and the organic solution was concentrated. The produced was isolated as a yellow powder after flash chromatography on alumina using hexanes and a very little amount of ethyl acetate. (86 mg, 80%) M.p.: 160-162 °C. ^{1}H-NMR (acetone-d_6): δ = 8.27 (s, 1H), 7.98-7.78 (m, 10H), 7.59 (t, 2H), 7.51-7.35 (m, 8H), 7.28 (s, 1H), 7.16 (d, 2H, J = 7.3 Hz), 7.00 (s, 1H), 2.17 (m, 8H), 1.08 (m, 24H), 0.76 (t, 6H, J = 6.8 Hz), 0.75 (t, 6H, J = 6.8 Hz), 0.59 (m, 8H). ^{13}C-NMR (acetone-d_6): δ = 163.0, 152.9, 151.9, 151.7, 151.3, 151.1, 142.8, 142.2, 141.4, 141.2, 141.1, 141.0, 139.7, 138.9, 138.8, 132.5, 131.3, 130.8, 129.8, 127.7, 127.4, 126.2,

125.6, 125.6, 124.6, 123.3, 121.7, 121.6, 121.6, 121.1, 120.7, 120.6, 120.5, 120.2, 118.7, 55.7, 55.5, 40.6, 40.5, 31.8, 31.8, 29.8, 24.1, 22.7, 22.7, 13.7. HRMS(+) calculated for $[C_{69}H_{78}N]^+$: 920.61288 found 920.61061.

Results and Discussion

Synthesis

Given our previous successful syntheses of aldimines using mild condensation protocols such as refluxing absolute ethanol, we originally used this approach to prepare the ketylimine analogues **II-8**, **II-11**, and **II-13**.[17-24] The ketylimines derived from aniline were chosen as desired targets because they were expected to be inherently more stable than their alkyl analogues, therefore allowing for photophysical investigation without signal contamination from hydrolysis or decomposition products. The required precursors were prepared according to known methods starting from commercially available reagents.[25, 26, 27] The required fluorenones for Suzuki coupling were prepared by oxidizing the corresponding fluorenes with cesium carbonate under ambient conditions.[25] These fluorenone derivatives were successfully coupled using Suzuki protocols with the corresponding alkylated fluorenes to afford the desired fluorene-fluorenone diad (**II-10**) and triad (**II-12**) precursors. The latter were then reacted with aniline to yield the ketylimines **II-11** and **II-13**, respectively. Unfortunately, the ketylimines could not be prepared using our previously successful mild dehydration protocols. The ketone is sterically hindered requiring stringent dehydration conditions using anhydrous toluene and

ketone activation with $TiCl_4$. Although imines are acid sensitive and decompose on acid silica, **II-8**, **II-11**, and **II-13**, were nonetheless isolated as pure compounds in reasonable yields via column chromatography.[13, 28-30] Most importantly, the desired ketylimines were isolated in sufficient purity required for spectroscopic and electrochemical studies.

Spectroscopic Properties

The photophysics of fluorenone (**II-5**) are known to be highly dependent on solvent polarity, which perturb the n, π^* and π, π^* energy levels.[31] The solvent polarity effects the lowest lying singlet energy relative to the highest triplet energy level resulting in a n, π^* character in apolar solvents and π, π^* character in polar solvents. The fluorescence quantum yield of **II-5** and its derivatives are therefore highly dependent on solvent polarity. Unfortunately, the limited solubility of **II-7**-**II-13** precludes extensive photophysical characterization in various solvents, especially those of polarity. Nonetheless, the spectroscopic properties of the ketylimines, their fluorenone analogues and their precursors were examined in dichloromethane as a result of their high solubility in this solvent. All the compounds reported in Figure II-1 exhibited two absorbance bands; a strong n, π^* in the UV and a bathochromically shifted weak π, π^* absorbance. This is evident in Figure II-2 for **II-12**. The long wavelength absorbance in conjunction with the fluorescence spectra was used to calculate the absolute energy gaps (ΔE) between the HOMO and LUMO energy levels according to known means.[32] It is evident from the data in Table II-1 that the ketylimines exhibit the same spectroscopic trends with increasing degree of conjugation as

their ketone precursors. Both the absorbance and fluorescence maximum are bathochromically shifted with increasing number of fluorenes. The ΔE values also decrease with increasing number of fluorenes, consistent with increasing degree of conjugation of the oligomers.

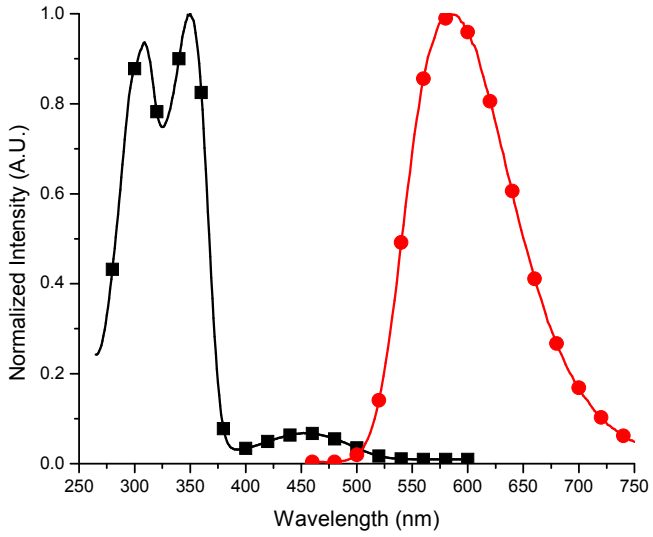

Figure II-2. Normalized absorbance (black squares) and fluorescence (red circles) spectra of **II-12** measured in anhydrous and deaerated dichloromethane.

Table II-1. Various spectroscopic properties.

	Compound	Abs. (nm)[a,b]	fl. (nm)[a]	ΔE (ev)	E_g spec	Φ_{fl}[c]		
						CH_2Cl_2	MeOH	77 K/RT[d]
Precursors	**II-1**	261	302	4.4	3.9	0.50	0.14	4
	II-2	267 (304)	319	4.0	3.9	0.40	0	-
	II-3	276	323	3.9	3.8	0.04	0.02	80
	II-5	258 (377)	505	2.9	3.6	0.02	0	7
Monomers	**II-7**	259 (328)	402	3.4	3.1	0.00	0.01	2
	II-8	258, 298 (388)	478	2.8	2.6	0.04	0.03	15
Diads	**II-9**[e]	(327)	380	2.9	3.4	0.67	-	-
	II-10	296 (332, 421)	559	2.5	2.4	0.11	0.02	113
	II-11	296 (332, 429)	559	2.5	2.4	0.06	0.01	47
Triads	**II-12**	308 (349, 454)	584	2.4	2.3	0.04	0	11
	II-13	297 (349, 421)	566	2.6	2.5	0.0	0	6

[a]Measured in CH_2Cl_2. [b]Values in parentheses denote most bathochromically shifted absorption maximum. [c]Absolute fluorescence quantum yield measured using an integrating sphere. [d]Fluorescence quantum yield ratio measured at 77 K in 1:4 methanol/ethanol matrix and room temperature in methanol. The change in refractive index is minimal for the two temperatures, therefore no temperature dependent fluorescence correction is required. [e]Ref.[33]

As seen in Table II-1, the fluorescence quantum yields of the oligo-ketylimines are consistently lower than the corresponding oligofluorenones. The reported values are absolute quantum yields and are therefore accurate values. This is in contrast to quantum yields obtained by relative actinometry where the accuracy of the values derived by such methods is highly dependent on the references and solvents. Nonetheless, the measured values are extremely low. Temperature dependent fluorescence measurements were done in order to assign the origins of the reduced fluorescence. At 77 K, all internal conversion (IC) deactivation modes by bond rotation are suppressed. Increased fluorescence should therefore be observed if nonradiative IC deactivation by bond rotation is an efficient deactivation mode. Some temperature dependence fluorescence is expected since deactivation by bond rotation around the fluorene-fluorenone is a known efficient mode for singlet excited state quenching.[34] Homogeneous glass matrices suitable for low temperature measurements are possible only with 4:1 ethanol/methanol solvent mixtures. The absolute fluorescence quantum yields were therefore measured at room temperature in this solvent in order to evaluate the emission yields for direct comparison to those at 77 K. As seen in Table II-1, the absolute room temperature fluorescence in the methanol/ethanol mixture is lower than the fluorescence in dichloromethane. This is not surprising given the solvent dependent fluorescence of substituted fluorenes (vide supra). The fluorescence yields of both the oligo-ketones and ketylimines increased at 77 K relative to the room temperature fluorescence. However, the increase in emission yield was more pronounced for **II-9** and **II-12** than for their corresponding ketylimines at 77 K. This implies that the

ketylimines deactivate by means other than by simple IC. This is in contrast to the fluorenones. Although accurate 77 K/room temperature fluorescence ratios are not possible owing to the extremely weak and noisy room temperature fluorescence, the temperature dependent fluorescence nonetheless confirm that the fluorescence of oligofluorenones is much more affected by temperature than their ketylimines counterparts.

Additional evidence for different deactivation modes of the ketone and ketylimines is had from the HOMO-LUMO energy levels. The optimized structures for calculating the molecular orbitals were taken from the crystal structure data of both **II-12** and **II-8**.[4] Although a better model for comparing the HOMO/LUMOs of **II-12** would be **II-13**, we were unable to obtain suitable crystals for X-ray analysis of this compound. Crystal structure data is desired for inputting the optimized geometry and coordinates for the semi-empirical calculations, resulting in accurate energy level calculations. Suitable crystals for XRD analysis was possible with **II-8** and whose coordinates were subsequently used for calculating the energy levels using the DFT methods of 6-31g* basis set. As seen in Figure II-3, the HOMOs are distributed evenly across the oligofluorene **II-12** while the corresponding LUMOs are located exclusively on the central fluorenone moiety. The HOMO and LUMOs for the ketylimine **II-8** are inverted relative to its ketone counterpart. This is evident in Figure II-4 where the HOMO is concentrated on the ketylimine moiety and the LUMO is found on the fluorene segment. The different orbital configurations for the highest and lowest molecular orbitals between **II-12** and **II-8** imply that both

compounds exhibit different photophysical properties, and hence, different singlet excited state deactivation processes.

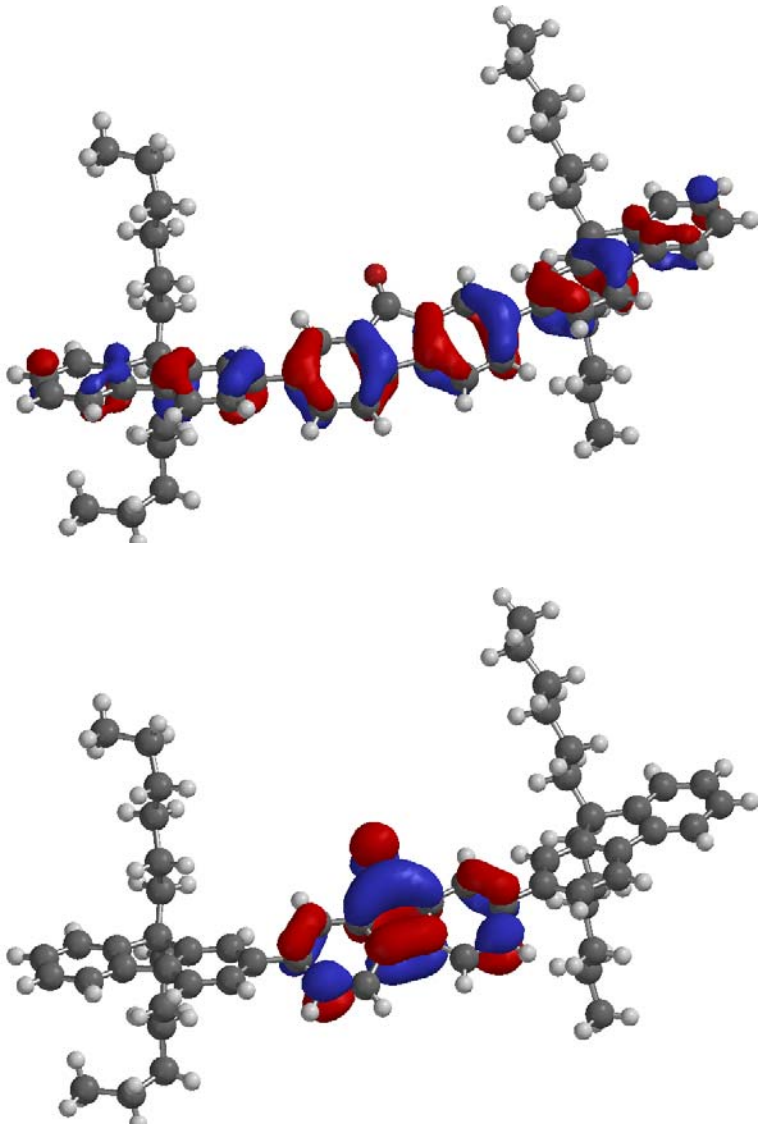

Figure II-3. Calculated highest occupied (top) and lowest unoccupied molecular orbitals (bottom) for **II-12**.

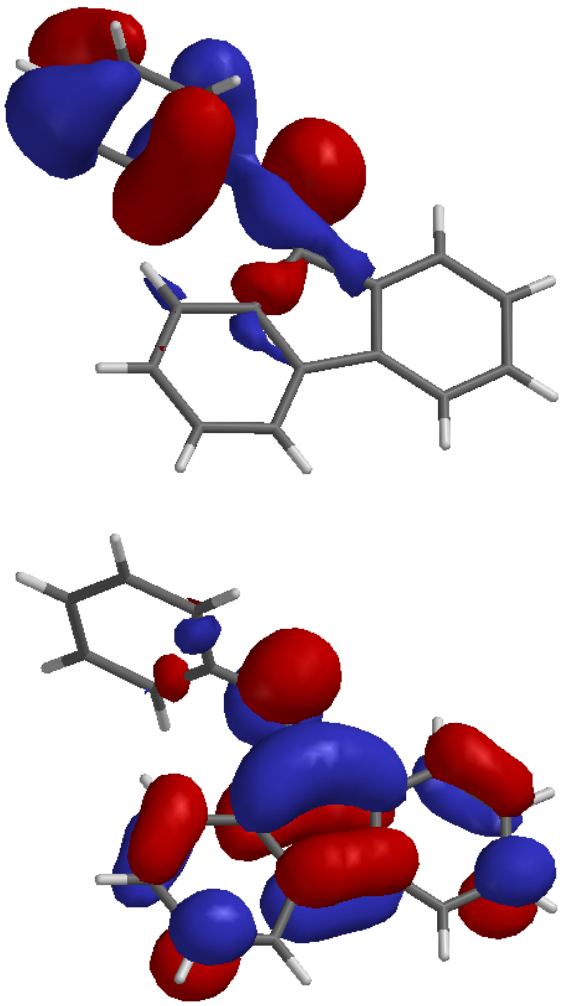

Figure II-4. Calculated highest occupied (top) and lowest unoccupied molecular orbitals (bottom) for **II-8**.

The presence of an excited state deactivation mode unique to ketylimines is evident from the fluorescence yield of **II-8**, which is consistently lower than **II-1**, **II-2**, and **II-9**. The singlet excited state quenching was further investigated in order to assign the origins of the suppressed ketylimine fluorescence. Although fluorescence deactivation studies using

the ketylimines (**II-8**, **II-11**, and **II-13**) with various quenchers is ideal for probing the deactivation modes, their weak fluorescence precludes their direct fluorescence investigation. As a result, **II-1, II-5** and **II-9** were used as the fluorophores for quenching studies because of their inherent fluorescence. Stern-Volmer analyses of these fluorophores were done using **II-5**, **II-7**, and **II-8** as quenchers and by examining the change in fluorescence as a function of quencher concentration according to: $\Phi_0/\Phi = 1 + k_q\tau[\text{quencher}]$, where Φ_0 is the fluorescence in the absence of quencher, Φ the fluorescence with quencher, k_q the second order fluorescence quenching rate constant, and τ the fluorophore fluorescence lifetime in the absence of quencher. A representative fluorescence quenching of **II-1** with **II-7** is seen in Figure II-5. The inherent fluorophores' fluorescence is quenched with the addition of the ketylimines, similar to Stern-Volmer analysis shown in the inset of Figure II-5. From the measured fluorophore lifetimes and Stern-Volmer constants, the bimolecular quenching rate constant (k_q) for fluorescence deactivation by the ketylimines was calculated. The calculated k_q for deactivation of **II-1**, **II-5**, and **II-9** with **II-5**, **II-7**, and **II-8** in dichloromethane were all diffusion controlled (3×10^{10} M^{-1} s^{-1}).[32]

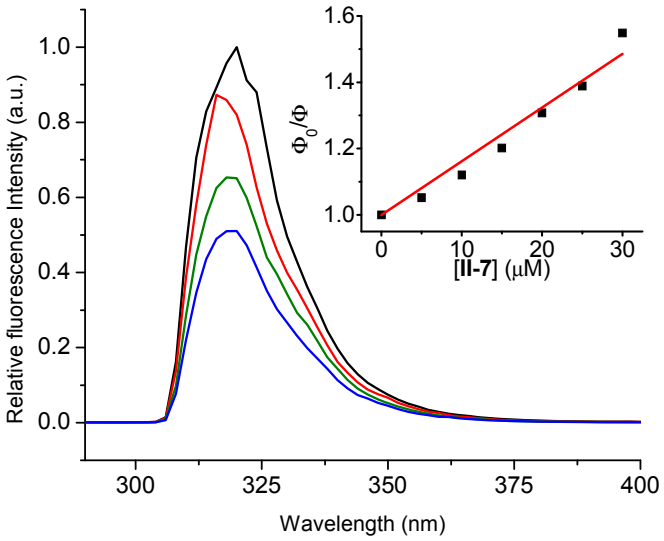

Figure II-5. Fluorescence quenching of **II-1** in dichloromethane with the addition of 0 μL (black), 40 μL (red), 180 μL (green), 260 μL (blue) **II-7**. Inset: Stern-Volmer quenching of **II-1** with **II-7**.

The measured diffusion controlled quenching rate constants imply that deactivation occurs by efficient photoinduced electron transfer from the fluorophore's excited singlet state to the ketylimine acceptor. The quencher amount required for deactivating 95 % of the produced singlets can be calculated according to: 20 x k_o / k_q, where k_o is the inherent fluorophore lifetime and k_q is the quenching rate constant derived from the Stern-Volmer quenching experiments. From the fluorescence quenching data, it can be calculated that 0.4 mM of **II-8** is required to quench the fluorescence **II-1** and **II-9** by intermolecular PET. For **II-11** and **II-13**, the fluorophore and ketylimine quencher are covalently linked leading to intramolecular PET. The excited state fluorophore concentration produced under such

conditions is ca. μM while the effective quencher ground state concentration is ca. 3 M.[35] The ground state ketylimine concentration of **II-8**, **II-11**, and **II-13** under such conditions is 20 times greater than what is required to quench 95 % of the excited fluorophore. This leads to rapid and efficient fluorescence quenching by intramolecular PET from the fluorene moiety to the ketylimine bond. The excess inherent ketylimine concentration in the ground state concomitant with rapid k_q and lack of significant temperature dependent fluorescence confirm that the reduced ketylimine fluorescence is a result of efficient intramolecular PET.[36, 37] This efficient quenching mode is also responsible for the lack of room temperature fluorescence for the ketylimines.

Table II-2. Electrochemical properties measured in anhydrous and deaerated dichloromethane relative to saturated Ag/Ag^+ electrode.

Compound	E_{pa}^1 (eV)	E_{pa}^2 (eV)	E_{pc} (eV)	E_g (eV)
II-1	0.9	-	-1.3	2.6
II-2	1.4	1.8	-0.4 and -1.0	2.3
II-3	1.5	1.9	-0.5 and -1.0	2.4
II-5	0.9	1.8	-1.0	2.3
II-7	1.7	-	-1.9	4.0
II-8	1.5	-	-1.4	3.3
II-9	1.5	-	-2.3	3.5
II-10	1.4	1.8	-1.6	3.4
II-11	1.4	1.8	-1.6	3.4
II-12	1.3	1.5	-1.6	3.3
II-13	1.2	1.5	-1.8	3.4

Further evidence for PET quenching is had from the complementarity of the electron donor and acceptor energy levels. The fluorophore donor and the ketylimine acceptor's suitability of undergoing PET can empirically be calculated according to the Rehm-Weller equation: $\Delta G°_{eT} = E_{pa}^{onset}$ (fluorophore) - E_{pc}^{onset} (quencher) - $\Delta E_{0,0}$ - λ.[38] The relationship takes into account the fluorophore's oxidation potential (E_{pa}), the ketylimine's capacity to accept the electron from the fluorophore (E_{pc}), and the solvent reorganization energy (λ). The E_{pa} and E_p^t correspond to the oxidation and reduction potentials of the fluorophore and ketylimine, respectively. The energy gap ($\Delta E_{0,0}$) between the ground and excited singlet states of the fluorophore must also be taken into account

since PET involves electron transfer from its excited state. This is calculated from the normalized absorption and fluorescence spectra of the fluorophores. The required electrochemical values for the Rehm-Weller equation can be measured by cyclic voltammetry (Figure II-6) from the oxidation and reduction potentials for the electron donor and acceptor, respectively. The corresponding redox potentials measured are reported in Table II-2. Although the reduction potential of an aliphatic ketylimine would be ideal for calculating the PET $\Delta G°_{eT}$, the capacity of the ketylimine moiety to capture the excited electron can nevertheless be taken from the E_{pc} of **II-8**. The calculated energetics of intramolecular PET for **II-11** and **II-13** are -16 and -45 kJ/mol, respectively. Similarly, the intermolecular PET energetics for quenching of **II-2** and **II-9** by **II-8** are -116 and -10 kJ/mol, respectively. The exergonic values confirm that the PET is favourable and corroborate the fluorescence quenching data. In contrast, the calculated ΔG_{eT} for intramolecular PET from the fluorenyl moiety to the ketone are endergonic. This confirms that singlet excited state deactivation of oligofluorenes does not occur by PET, unlike their ketylimine counterparts. Further evidence for the different excited stated deactivation modes for the ketones and ketylimines is had from the transient absorption spectroscopy. A transient assigned to the triplet was observed at 430 nm for **II-10** by laser flash photolysis while no signal was detected for the ketylimines. This implies that singlet excited state deactivation occurs by intersystem crossing in the case of the oligofluorenyl ketones while the absence of signal observed with the ketylimines confirms that their suppressed fluorescence is not a result of triplet formation.

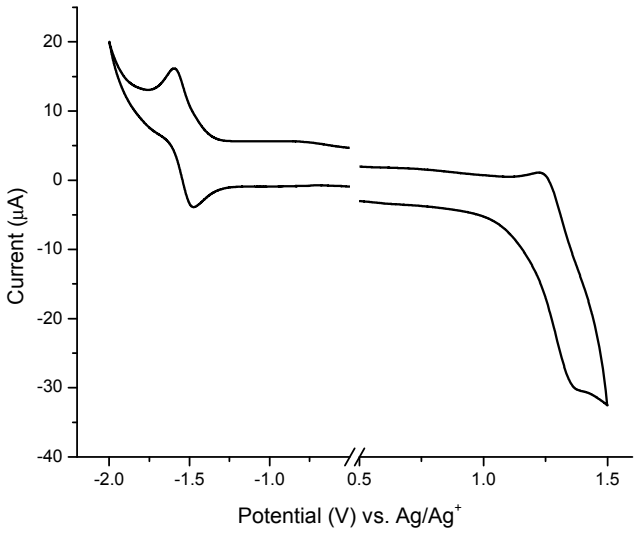

Figure II-6. Cyclic voltammogram of **II-11** obtained in anhydrous and deaerated dichloromethane with 0.1 M $TBAPF_6$.

As seen in Figure II-6, the anodic and cathodic processes of **II-11** are dissimilar in that the oxidation process is irreversible while the reduction process is reversible. This behavior is not reserved exclusively for the ketylimines, but also occurs with the oligofluorenes. To understand the origin of the different electrochemical behavior between the reduction and oxidation processes, **II-13** was investigated by theoretical means. Given that the anodic and cathodic processes correspond to the radical cation and anion formation, respectively, these two intermediates were theoretically calculated. The resulting spin densities calculations are represented in Figure II-7. It is clear that the spin densities of these two radical ions are different. The spin densities of the radical cation is evenly

distributed across all the fluorene segments while that of the radical anion is located exclusively on the central fluorene unit. Consequently, the radical anion cannot undergo radical coupling as a result of steric hindrance resulting in a reversible cathodic behaviour. Conversely, the radical cation can cross-couple via conventional anodic polymerization resulting in the irreversible oxidation of this intermediate.[39] Therefore, the fluorene substitution structure plays an important role in reversible electrochemical behavior. The observed reversible cathodic behaviour further confirms that the heteroatomic bond is robust and does not undergo electrochemical reduction at the potentials investigated.

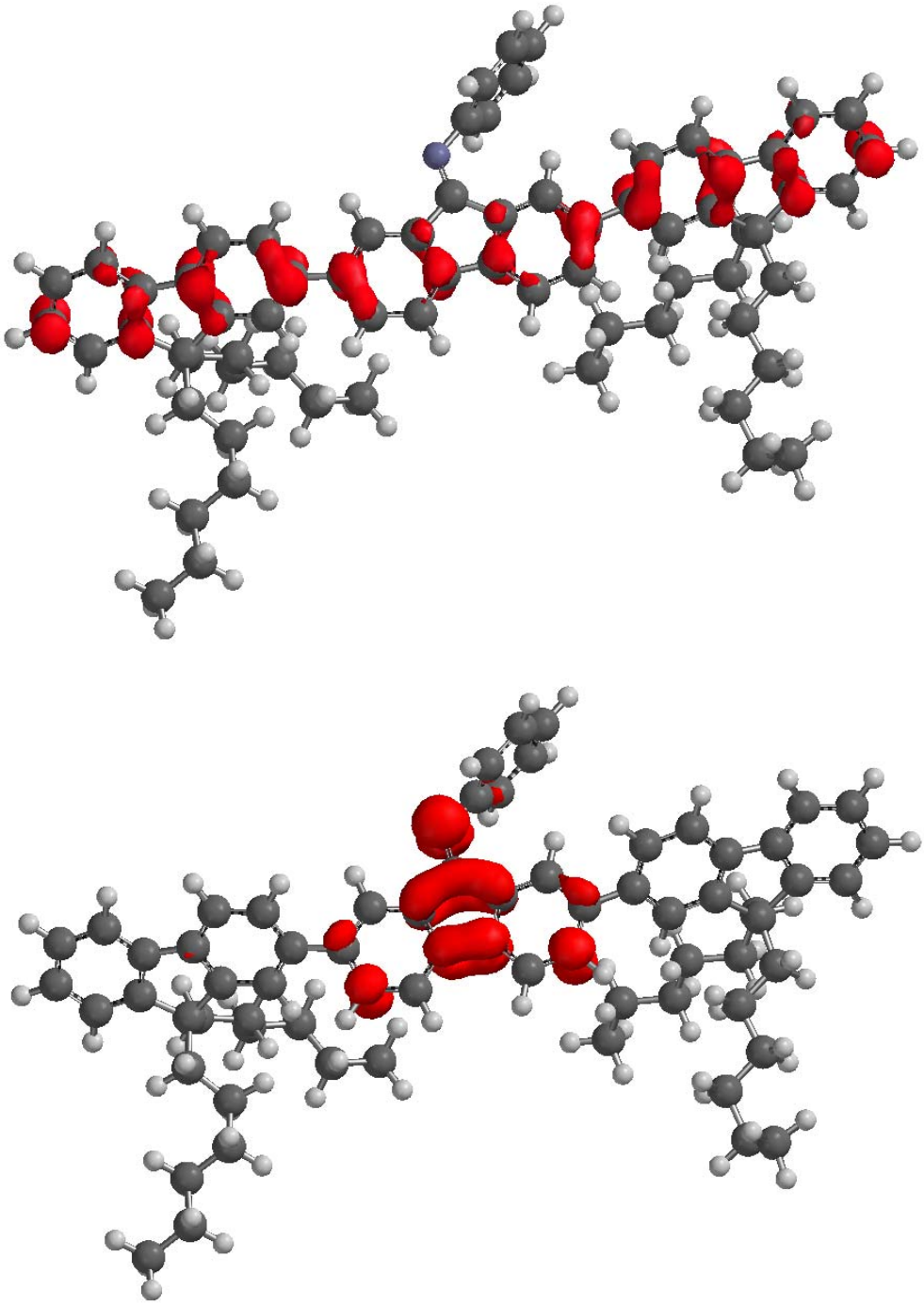

Figure II-7. Calculated electron density of the radical cation (top) and radical anion (bottom) for **II-13**.

Additional evidence for the different excited-state deactivation modes for the ketones and the ketylimines is had from the transient absorption spectroscopy. A transient assigned to the triplet was observed at 430 nm for **II-10** and 440 nm for **II-12** by laser flash photolysis (**Figure II-8**) while no signal was detected for the ketylimines. This implies that singlet excited state deactivation occurs by intersystem crossing in the case of the oligofluorenyl ketones while the absence of signal observed with the ketylimines confirms that their suppressed fluorescence is not a result of triplet formation.

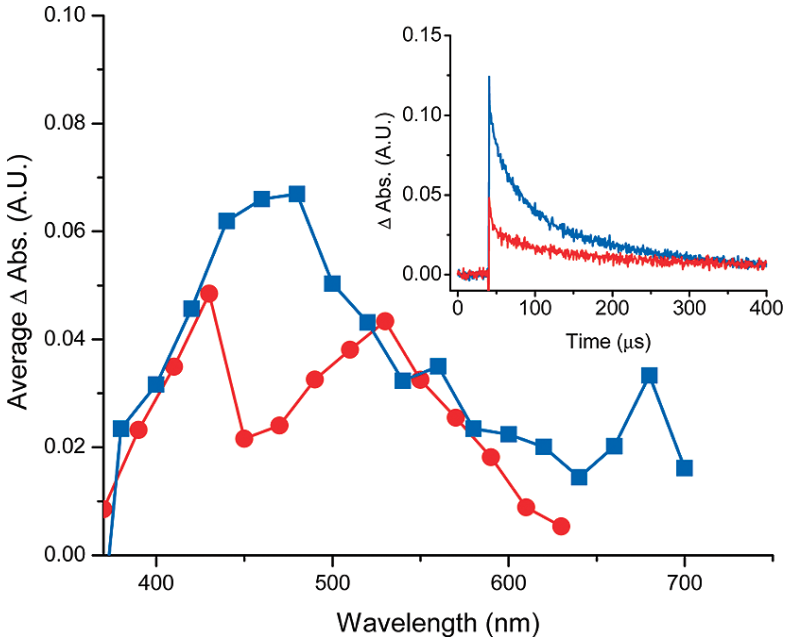

Figure II-8. Transient absorption spectra of **II-10** (■) and **II-12** (●) after exciting at 355 nm at 72 μs after the laser pulse in deaerated dichloromethane. Inset: decay of triplet **II-10** (blue) and **II-12** (red) monitored at 420 and 440 nm, respectively.

Conclusion

It was demonstrated that fluorenyl ketylimines exhibit fluorescence quantum yields well below that of their ketone counterparts. Although the heteroatomic fluorene derivatives exhibited slight fluorescence increase at reduced temperature, internal conversion involving fluorenyl-fluorene bond rotation was not found to play a major role in quenching the ketylimine fluorescence, unlike its ketone analogues. Deactivation of the fluoroenyl ketylimine singlet excited states occurred predominately by intramolecular PET from the fluorenyl moiety to the heteroconjugated portion. The PET mechanism was energetically corroborated according to the Rehm-Weller equation in addition to singlet excited state deactivation with diffusion controlled rates. This is in contrast to the oligofluorenes whose deactivation by PET was found to be endergonic and deactivation involves intersystem crossing to the triplet state. Although, the heteroatomic bond quenches the fluorescence, suppressing this deactivation mode would result in desired high fluorescence, resulting in on/off fluorescence not possible with its ketone counterpart.

Acknowledgements

NSERC Canada is thanked for DG, SRG, and RTI grants allowing this work to be performed in addition to CFI for additional equipment funding. WGS also thanks both the Humboldt Foundation and the RSC for a JWT Jones Travelling Fellowship, allowing this manuscript to be completed. SD, IUR, and TS thank NSERC, conseil régional d'Aquitaine

and the CROUS de Bordeaux and Le conseil général du Nord Pas de Calais and Le conseil municipal de Vaulx Vraucourt for graduate scholarships, respectively.

References

1. Grimsdale, A. C.; Leok Chan, K.; Martin, R. E.; Jokisz, P. G.; Holmes, A. B. *Chem. Rev.* **2009**, *109*, 897-1091.

2. Montilla, F.; Mallavia, R. *Adv. Funct. Mater.* **2007**, *17*, 71-78.

3. Romaner, L.; Pogantsch, A.; Freitas, P. S. d.; Scherf, U.; Gaal, M.; Zojer, E.; List, E. J. W. *Adv. Funct. Mater.* **2003**, *13*, 597-601.

4. Chan, K. L.; Sims, M.; Pascu, S. I.; Ariu, M.; Holmes, A. B.; Bradley, D. D. C. *Adv. Funct. Mater.* **2009**, *19*, NA.

5. Wu, Y.-S.; Li, J.; Ai, X.-C.; Fu, L.-M.; Zhang, J.-P.; Fu, Y.-Q.; Zhou, J.-J.; Li, L.; Bo, Z.-S. *J. Phys. Chem. A* **2007**, *111*, 11473-11479.

6. Becker, K.; Lupton, J. M.; Feldmann, J.; Nehls, B. S.; Galbrecht, F.; Gao, D. Q.; Scherf, U. *Adv. Funct. Mater.* **2006**, *16*, 364-370.

7. Pijper, T. C.; Pijper, D.; Pollard, M. M.; Dumur, F. d. r.; Davey, S. G.; Meetsma, A.; Feringa, B. L. *J. Org. Chem.* **2010**, *75*, 825-838.

8. Jo, J.; Vak, D.; Noh, Y.-Y.; Kim, S.-S.; Lim, B.; Kim, D.-Y. *J. Mater. Chem.* **2008**, *18*, 654-659.

9. Kappaun, S.; Scheiber, H.; Trattnig, R.; Zojer, E.; List, E. J. W.; Slugovc, C. *Chem. Commun.* **2008**, 5170-5172.

10. Hayashi, S.; Inagi, S.; Fuchigami, T. *Macromolecules* **2009**, *42*, 3755-3760.

11. Lincker, F.; Delbosc, N.; Bailly, S.; Bettignies, R. D.; Billon, M.; Pron, A.; Demadrille, R. *Adv. Funct. Mater.* **2008**, *18*, 3444-3453.

12. Meng, Q.; Thibblin, A. *J. Am. Chem. Soc.* **1997**, *119*, 1224-1229.

13. Suzuki, K.; Matsu-Ura, N.; Horii, H.; Sugita, Y.; Sanda, F.; Endo, T. *J. Appl. Polym. Sci.* **2002**, *83*, 1744-1749.

14. Dai, W.; Srinivasan, R.; Katzenellenbogen, J. A. *J. Org. Chem* **1989**, *54*, 2204-2208.

15. Yang, C.-J.; Jenekhe, S. A. *Chem. Mater.* **1991**, *3*, 878-887.

16. Kuder, J. E.; Gibson, H. W.; Wychick, D. *J. Org. Chem.* **1975**, *40*, 875-879.

17. Scaiano, J. C. *CRC Handbook of Organic Photochemistry*; CRC Press: Boca Raton, 1989.

18. Dufresne, S.; Bolduc, A.; Skene, W. G. *J. Mater. Chem.* **2010**, *20*, 4861-4866.

19. Bolduc, A.; Dufresne, S.; Skene, W. G. *J. Mater. Chem.* **2010**, *20*, 4820-4826.

20. Dufresne, S.; Guarìn, S. A. P.; Bolduc, A.; Bourque, A. N.; Skene, W. G. *Photochem. Photobiol. Sci.* **2009**, *8*, 796-804.

21. Dufresne, S.; Callaghan, L.; Skene, W. G. *J. Phys. Chem. B* **2009**, *13*, 15541-15549.

22. Bourque, A. N.; Dufresne, S.; Skene, W. G. *J. Phys. Chem. C* **2009**, *113*, 19677–19685.

23. Dufresne, S.; Skene, W. G. *J. Org. Chem.* **2008**, *73*, 3859-3866.

24. Tsang, D.; Bourgeaux, M.; Skene, W. G. *J. Photochem. Photobiol. A* **2007**, *192*, 122-129.

25. Skene, W. G.; Pérez Guarìn, S. A. *J. Fluores.* **2007**, *17*, 540-546

26. Park, K. K.; Tsou, L. K.; Hamilton, A. D. *Synthesis* **2006**, *21*, 3617–3620.

27. Li, X.; Xiao, Y.; Qian, X. *Org. Lett.* **2008**, *10*, 2885-2888.

28. Kanibolotsky, A. L.; Berridge, R.; Skabara, P. J.; Perepichka, I. F.; Bradley, D. D. C.; Koeberg, M. *J. Am. Chem. Soc* **2004**, *126*, 13695-13702.

29. O'Donnell, M. J.; Polt, R. L. *J. Org. Chem.* **1982**, *47*, 2663-2666.

30. Saroja, G.; Pingzhu, Z.; Ernsting, N. P.; Liebscher, J. *J. Org. Chem* **2004**, *69*, 987-990.

31. Meng, Q.; Thibblin, A. *J. Am. Chem. Soc.* **1997**, *119*, 1224-1229.

32. Murphy, R. S.; Moorlag, C. P.; Green, W. H.; Bohne, C. *J. Photochem. Photobiol. A* **1997**, *110*, 123-129.

33. Turro, N. J.; Ramamurthy, V.; Scaiano, J. C. *Principles of Molecular Photochemistry: An Introduction*; University Science Books: Sausalito, 2009.

34. Dufresne, S.; Bourgeaux, M.; Skene, W. G. *J. Mater. Chem.* **2007**, *17*, 1166-1177.

35. Belletete, M.; Beaupre, S.; Bouchard, J.; Blondin, P.; Leclerc, M.; Durocher, G. *J. Phys. Chem. B* **2000**, *104*, 9118-9125.

36. Assuming the density of the thiophenoazomethines to be ca. 0.8 g/ml.

37. Kavarnos, G. J.; Turro, N. J. *Chem. Rev.* **2002**, *86*, 401-449.

38. Sarker, A. M.; Kaneko, Y.; Nikolaitchik, A. V.; Neckers, D. C. *J. Phys. Chem. A* **1998**, *102*, 5375-5382.

39. Gilbert, A.; Baggott, J. *Essentials of Molecular Photochemistry*; CRC Press: Boca Raton, 1991.

40. Roncali, J. *Chem. Rev.* **1992**, *92*, 711-738.

III. CHAPITRE III

Towards materials with reversible oxidation and tuneable colours using heterocyclic conjugated azomethines

*Stéphane Dufresne, Andréanne Bolduc, and W. G. Skene**

Laboratoire de caractérisation photophysique des matériaux conjugués, Département de Chimie, Pavillon JA Bombardier, Université de Montréal, CP 6128, succ. Centre-ville, Montréal, Québec, CANADA, H3C 3J7,

Received 1st March 2010, Accepted 1st April 2010

First published as an Advance Article on the web 5th May 2010

DOI : 10.1039/c0jjm00557f

J. Mater. Chem. **2010**, **20**, 4861-4866.

ABSTRACT:

The spectroelectrochemical behaviour of heterocyclic azomethines prepared by condensing complementary aldehydes and amines was observed as intense colour changes of the oxidized products relative to the neutral form. The tuneable colours and reversible oxidation were contingent on the heterocycles.

Introduction

Thiophene based conjugated materials have gained a wide importance because of their spectroscopic and electrochemical properties.[1-6] This is in part a result of their doped intermediates that are stable. These oxidized intermediates additionally are of particular interest owing to their colour that is significantly different from the neutral form.[7, 8] As a result, polythiophene derivatives have found uses in electrochromic devices, taking advantage of both their stable intermediates and contrasting colours between the neutral and oxidized forms.[9]

Functional materials with multiple colour states capable of displaying a large palette of colours are required to meet the demands of consumer electronics. In addition to incorporating electron donor and acceptor segments, materials with desired electrochromic properties to meet these stringent demands are possible by using vinylene linkages.[10-13] The preparation of vinylenes using Gilch and Horner-Emmons protocols however requires rigorous reaction conditions such as anhydrous solvents and inert atmospheres.[14, 15] These coupling methods also produce significant by-products requiring product purification in order not to compromise the materials' colour and performance. Alternate straightforward coupling methods not requiring stringent protocols with simple- to no-product purification are therefore desired for preparing new functional materials with potential electrochromic applications.

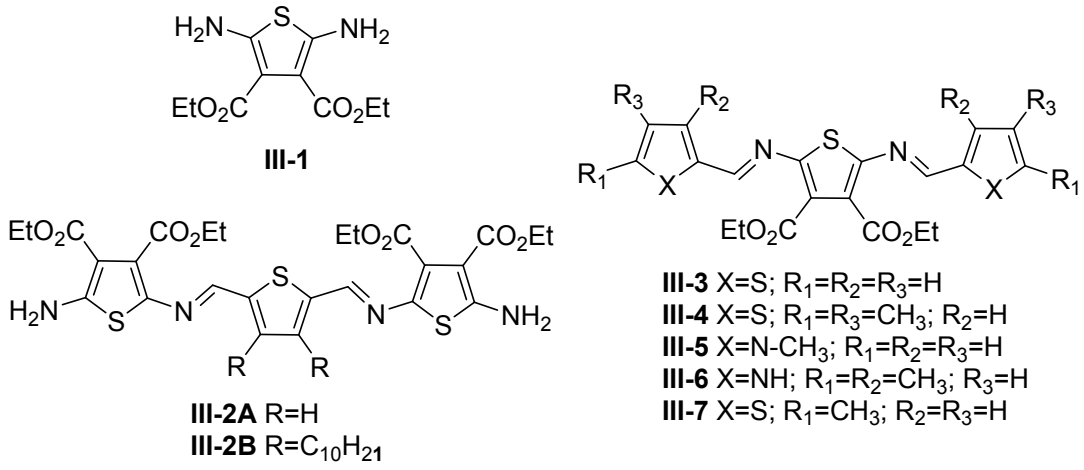

Chart III-1. Heterocyclic azomethines examined.

Azomethines (-N=C-) are highly attractive alternatives to vinylene linkages in part because they are isoelectronic to their carbon counterparts.[16, 17] They are further advantageous because of their straightforward synthesis involving simple condensation of the complementary aldehyde and amine precursors without the use of stringent reaction conditions such as anhydrous solvents, metal catalysts, and inert atmospheres. Their synthesis is additionally environmentally friendly with water being the unique by-product produced. Azomethines also exhibit high hydrolytic, oxidative, and reductive resistance.[18-20] Despite these benefits, azomethines have not been fully exploited as functional materials. This is a result of previously investigated homoaryl azomethines that are oxidatively and hydrolytically unstable and decompose while exhibiting high oxidation potentials (E_{pa}).[21-25] Therefore, stable azomethines that can be reversibly oxidized and exhibit large spectral changes between their neutral and oxidized intermediates are required for demonstrating the suitability of azomethines as functional

materials. Herein, we present the first reported examples of stable azomethines that exhibit tuneable color changes of both the neutral and oxidized forms contingent upon structure. Property tuning including colour tweaking of the neutral and oxidized intermediates and low E_{pa} are also presented for these stable azomethines contingent on the heterocycles used for their preparation. Reversible oxidation and electrochromic properties dependent on structure and heterocycles are also presented in order to demonstrate the suitability of azomethines as functional materials.

Experimental

Electrochemical measurements

Cyclic voltammetry measurements were performed on a Bio Analytical Systems EC Epsilon potentiostat. Compounds were dissolved in anhydrous and deaerated dichloromethane at 10^{-4} M along with sufficient NBu_4PF_6 supporting electrolyte for satisfactory conductivity. A platinum button electrode was used as the working electrode while platinum wire and saturated Ag/AgCl electrodes were employed as auxiliary and reference electrodes, respectively. The measured electrochemical potentials can be converted to universal SCE values by applying a 45 mV correction factor.[26] ITO glass slides for electropolymerization studies were obtained from Delta Technologies Ltd. Single sided coated ITO boro-aluminosilicate glass slides (25 x 25 x 0.7 mm) of sheet resistance 4-10 Ω were cut to afford working electrodes for polymerization of 1 x 2.5 cm in size. The

electrochemical band-gaps (E_g) were calculated by known means from the measured oxidation (E_{pa}) and reduction potentials (E_{pc}) according to $E_{pa} - E_{pc} + 0.4$.[27, 28]

Spectrochemical measurements

Spectroelectrochemical measurements were done combining a Bio Analytical Systems EC Epsilon potentiostat with a Cary-500 spectrometer using a thin optical path length cuvette with a platinum gauze wire as the working electrode, a platinum counter electrode, and saturated Ag/AgCl reference electrode by applying a potential greater than the E_{pa} of the given compound. The spectroelectrochemical cell was provided by CH Instruments Japan (CHI140A) with a spectroscopic height of 6.5 mm and an optical pathlength of 1 mm.

Synthesis

The synthesis of **III-1**,[29] **III-2B**,[30] and **III-3**[19] were done according to previous reports. Meanwhile, the reported yields of the new compounds are unoptimized.

A representative synthetic procedure for the azomethines is (5-(diethyl 5-amino-thiophen-3,4-dicarboxylate-2-ylimino)methyl)thiophen-2-yl)methylene)-diethyl thiophene-3,4-dicarboxylate-2,5-diamine (**III-2A**) as follows: In a small vial was added diethyl 2,5-diaminothiophene-3,4-dicarboxylate (138 mg, 0.53 mmol) and 2,5-thiophenedicarboxaldehyde (25 mg, 0.18 mmol). A few drops of TFA diluted in ethanol

were added and the reaction completion was determined by TLC (ca. 15 minutes). The resulting solid was precipitated from acetone/hexanes to give the title compound as a red solid (90 mg, 82 %) M.p.: 244-246 °C. ^{1}H-NMR (acetone-d_6): δ = 8.20 (s, 2H), 7.58 (s, 4H), 7.50 (s, 2H), 4.37 (q, 4H, *J* = 7.2 Hz), 4.23 (q, 4H, *J* = 7.2 Hz), 1.43 (t, 6H, *J* = 7.2 Hz), 1.30 (t, 6H, *J* = 7.2 Hz). ^{13}C-NMR (acetone-d_6): δ = 164.9, 164.3, 161.6, 155.6, 153.0, 146.2, 145.3, 132.4, 131.7, 61.1, 60.0, 14.4, 14.0.

Diethyl 2,5-bis((4,5-dimethylthiophen-2-yl)methyleneamino)thiophene-3,4-dicarboxylate (III-4). In a 50 mL round bottom flask was added 4,5-dimethylthiophene-2-carboxaldehyde (192 mg, 1.37 mmol) dissolved in 25 mL of anhydrous toluene to which was subsequently added DABCO (461 mg, 4.11 mmol), $TiCl_4$ 1.0 M solution in toluene (1.51 mL, 1.51 mmol) at 0 ^{o}C and then **III-1** (100 mg, 0.39 mmol). The mixture was then refluxed for three hours and the solvent was then evaporated in vacuo. Precipitation in hexanes/ethylacetate (50/50) yielded the title product as a red solid (52 mg, 27 %). M.p.: 169-171 °C. ^{1}H-NMR (acetone-d_6): δ = 8.55 (s, 2H), 7.45 (s, 2H), 4.30 (q, 4H, *J* = 7.2 Hz), 2.44 (s, 6H), 2.18 (s, 6H), 1.36 (t, 6H, *J* = 7.2 Hz). ^{13}C-NMR (acetone-d_6): δ = 163.1, 152.9, 149.2, 142.5, 138.1, 137.6, 135.6, 127.0, 61.0, 14.1, 13.4, 13.0. HRMS(+) calculated for $[C_{24}H_{26}N_2O_4S_3+H]^+$: 503.11275, found: 503.11255.

Diethyl 2,5-bis((1-methyl-1H-pyrrol-2-yl)methyleneamino)thiophene-3,4-dicarboxylate (III-5). 1-Methyl-2-pyrrole-carboxaldehyde (200 mg, 1.83 mmol) was

dissolved with DABCO (200 mg, 1.83 mmol) in anhydrous toluene at 0 ^{o}C followed by the slow addition of $TiCl_4$ 1.0 M solution in toluene (1.83 mL, 1.83 mmol). **III-1** (90 mg, 0.35 mmol) was then added followed by refluxing for 3-4 hours. The solvent was evaporated in vacuo and the product isolated as a red solid (57 mg, 37 %) after purification by flash chromatography starting with hexanes with 1% triethylamine and increasing the polarity to hexanes/ethylacetate (50%/50% v/v). M.p.: 134-136 °C. ^{1}H-NMR (acetone-d_6): δ = 8.33 (s, 2H), 7.11 (d, 2H, J = 2.0 Hz), 6.85 (dd, 2H, ^{3}J = 4.0 and ^{5}J = 1.8 Hz), 6.24 (dd, 2H, J = 4.0 Hz and 2.5 Hz), 4.29 (q, 4H, J = 7.1 Hz), 4.07 (s, 6H), 1.33 (t, 6H, J = 7.1Hz). ^{13}C-NMR (acetone-d_6): δ = 163.5, 149.5, 149.3, 132.2, 129.9, 126.1, 121.8, 109.9, 60.9, 36.9, 14.1. HRMS(+) calculated for $[C_{22}H_{24}N_4O_4S+H]^{+}$: 441.15910 found 441.15811.

Diethyl 2,5-bis((3,5-dimethyl-1H-pyrrol-2-yl)methyleneamino)thiophene-3,4-dicarboxylate (III-6). In a 50 mL round bottom flask was added 3,5-dimethylpyrrole-2-carboxaldehyde (86 mg, 0.70 mmol) dissolved in 25 mL of anhydrous toluene to which was subsequently added DABCO (260 mg, 2.32 mmol), $TiCl_4$ 1.0 M solution in toluene (0.93 mL, 0.93 mmol) at 0 ^{o}C followed by the addition of **III-1** (60 mg, 0.23 mmol). The mixture was refluxed for three hours afterwhich the solvent was then removed. The product was obtained as a orange-red powder (35 mg, 32 %) after purification by flash chromatography eluted with hexanes/ethylacetate (90 % / 10 % v/v) up to hexanes/ethylacetate (50 % / 50 % v/v). M. decomp.: 99 °C. ^{1}H-NMR (acetone-d_6): δ = 11.18 (s, 2H) 8.11 (s, 2H), 5.87 (s, 2H), 4.20 (q, 4H, J = 7.1 Hz), 2.23 (s, 6H), 1.24 (t, 6H,

J = 7.1 Hz). ^{13}C-NMR (acetone-d_6): δ = 163.7, 150.3, 147.8 137.3, 130.8, 125.9, 122.6, 118.8, 112.4, 60.9, 14.5, 13.5, 11.8. HRMS(+) calculated for $[C_{24}H_{28}N_4O_4S+H]^+$: 469.19040, found: 469.18978.

Diethyl 2,5-bis((5-methylthiophen-2-yl)methyleneamino)thiophene-3,4-dicarboxylate (III-7). In a 50 mL round bottom flask was added 5-methylthiophene-2-carboxaldehyde (173 mg, 1.37 mmol) dissolved in 25 mL of anhydrous toluene to which was subsequently added DABCO (461 mg, 4.11 mmol), $TiCl_4$ 1.0 M solution in toluene (1.51 mL, 1.51 mmol) at 0 ^oC followed by **III-1** (100 mg, 0.39 mmol). The mixture was then refluxed for three hours and the solvent was then removed. Precipitation from hexanes/ethylacetate (50%/50% v/v) yielded the title product as a red solid (39 mg, 21 %). M.p.: 110-112 °C. 1H-NMR (acetone-d_6): δ = 8.60 (s, 2H), 7.55 (d, 2H, J = 3.5 Hz), 6.95 (d, 2H, J = 3.6 Hz), 4.30 (q, 4H, J = 7.2 Hz), 2.56 (s, 6H), 1.36 (t, 6H, J = 7.2 Hz). ^{13}C-NMR (acetone-d_6): δ = 163.1, 153.2, 149.2, 148.8, 140.4, 135.7, 127.6, 127.1, 61.1, 15.5, 14.1. HRMS(+) calculated for $[C_{22}H_{22}N_2O_4S_3+H]^+$: 475.08145, found: 475.08065.

Crystal data: **III-5**: M_r = 440.51, monoclinic, space group P21/c, a = 13.7006(3), b = 16.7642(4), c = 20.2638(5) Å, β = 101.8690(10)^o, V = 4554.68(19) Å^3, Z = 8, ρ = 1.285 gcm^{-3}, μ = 1.558 mm^{-1}, F(000) = 1856, GOF = 1.075, A total of 49416 reflections were collected in the range θ 3.30-71.98^o, 8910 of which were unique

(R_{int} = 0.0475). R1(wR2) = 0.0536(0.1410) for 567 parameters and 7601 reflections (I>2s(I)).

Results and discussion

The novel triads reported in Chart III-1 were prepared as model compounds for investigating the effect of structure on the azomethines' properties including spectroelectrochemistry, oxidation potentials, and reversibility of oxidation. Meanwhile, **III-2B** was used a model compound for comparing to **III-2A** for investigating the influence of the alkyl chains on the electrochemical and the radical cation spectroscopic properties. Azomethines derived from the diaminothiophene **III-1** and heterocyclic aldehydes were prepared since electrochromic properties suitable for functioning devices were expected. The advantage of these heterocycles is that the corresponding azomethines are oxidatively and reductively robust.[20, 30] The influence of the different heterocycles, placement of the azomethine, and the placement of **III-1** (central *vs* terminal) on both the oxidation potential and the electrochromic properties could also be investigated. Although the azomethine analyses were performed in dichloromethane, the compounds exhibit high solubility in all organic solvents, except aliphatic hydrocarbons and acetone.

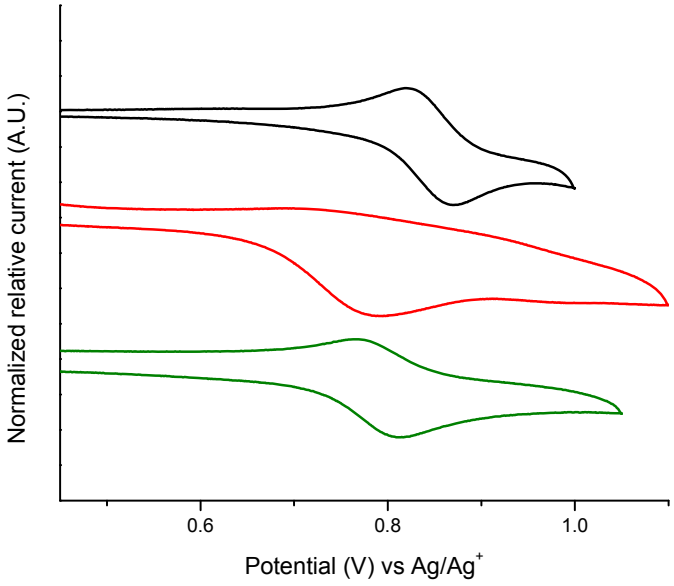

Figure III-1. Cyclic voltammograms of **III-2A** (black), **III-5** (red) and **III-6** (green) recorded in dichloromethane at 100 mV/sec with a saturated Ag/AgCl electrode. Inset: absorption of **III-5** (red) and its anodically prepared polymer deposited (black) on ITO.

As seen in Figure III-1, **III-2A** exhibits reversible oxidation. Similarly, **III-4** and **III-6** are also reversibly oxidized. This is in contrast to other azomethines that undergo irreversible oxidation as a result of imine decomposition.[31-34] The reversible anodic behaviour observed for **III-2A**, **III-4**, **III-6**, and **III-7** confirms that the imine bond is oxidatively resistant. Substitution in the α,α' position of the triad structure plays an important role in whether reversible oxidation is possible. This is evidenced by the irreversible oxidation of **III-3** and **III-5**, which differ from **III-4** and **III-6**, respectively, only by the absence of methyl groups in the α-α' terminal positions. Substitution in

these 2-positions α to the sulphur atom of these triads prevents homo-coupling of the radical cations, which otherwise yield polymers by standard anodic polymerization.[35, 36] Moreover, the reversible oxidation observed for **III-2A**, implies that that the generated radical cation is preferentially located on either of the trimer's terminal thiophenes and is most likely located on the carbon α to the sulphur atom.[4] The terminal amines of **III-2A** prevent cross-coupling of the radical cations generated in the 2-position, resulting in the observed reversible anodic behaviour. Conversely, an irreversible oxidation for **III-2A** would be observed if the radical cation was located on the trimer's central thiophene and would undergo radical cation cross-coupling at either the 3 or 4 positions. This would be particularly possible given the inherent reactivity of the radical cation that is capable of overcoming any steric effects leading to radical cation cross-coupling. The reversible anodic behaviour observed for **III-2A**, **III-2B, III-4**, and **III-6** nonetheless demonstrate that the terminal groups are responsible for suppressing the reactivity of the radical cation leading to reversible oxidation.

To confirm that reversible oxidation is contingent on substitution at the α position to the sulphur of the terminal heterocycles, **III-5** was anodically polymerized on ITO by repeated cycling between 0 and 1.1 V. As seen in Figure III-2, both the anodic and cathodic peaks are shifted to less positive values with repeated cycling. This confirms that the product produced has a higher degree of conjugation than the monomer. The anodic cycling using an ITO electrode instead of the button Pt electrode

results in the polymer being deposited on the ITO as a film, similarly to the anodic polymerization of **III-3**.[36, 37] The broad absorption measured on ITO vs. the monomer (Inset Figure III-2) confirms a highly conjugated polymer immobilized on the ITO was obtained.[38] The polymer nature is further evidenced by the insolubility of the immobilized material in various organic solvents compared to the triad. Reversible one-electron oxidation of azomethines is nonetheless possible by adjusting the triad structure and by incorporating terminal groups that prevent radical cation cross-coupling via the terminal positions. Moreover, the reversible oxidation demonstrates that the imine linkage is anodically resistant, which is in contrast to homoaryl imines and other previously reported imines.[24, 31, 39-42]

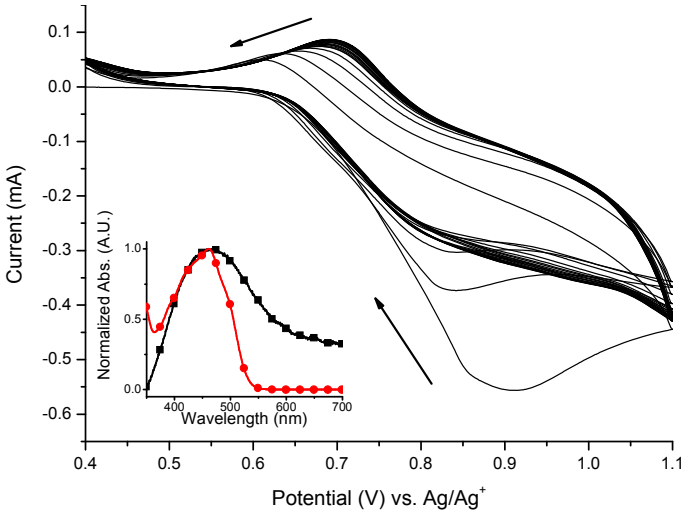

Figure III-2. Cyclic voltammogram of **III-5** cycled 40 times between 0.4 and 1.1 V. The arrows indicate the direction of the anodic and cathodic peak shifts with increasing cycling. Inset: normalized absorption of **III-5** (red) and its anodically prepared polymer deposited (black) on ITO.

The E_{pa} of previously investigated azomethines occurred at high E_{pa}, precluding their use as functional materials.[34, 43-46] This is the case of **III-3** whose E_{pa} is 1.16 V (Table III-1) as a result of the electron withdrawing esters, required for rendering the compound air stable.[20, 30, 47] High E_{pa} further results in oxidative decomposition and unwanted over oxidized by-products when anodically polymerized. The E_{pa} can be tailored as a function of structure. This is evidenced by the 350 mV decrease in the E_{pa} possible by placing the strong electron donating amine groups in the terminal positions for **III-2A** vs. **III-3**. Modification of the E_{pa} via electronic effects is further seen by comparing **III-2A** vs. **III-2B** (Table III-1). These trimers differ only via the alkyl substitution on the central thiophene. The E_{pa} of **III-2B** is 100 mV less positive than **III-2A** as a result of the weak donating effect of the alkyl groups.[28] Similar lowering of the E_{pa} is also possible by exchanging the terminal thiophene units for pyrroles, as seen with **III-5** and **III-6**. Chemical oxidation of the triads is possible owing to their low oxidation potentials (*vide infra*), while both the neutral and oxidized forms are air stable. This is supported by the lack of decomposition products detected either spectroscopically or by ^{1}H-NMR for both the neutral and oxidized forms.

The azomethines are highly conjugated as evidenced by their intense absorbances in the visible (Table III-1, Figure III-3). Absorbance tuning is possible as a function of structure. For example, a 50 nm bathochromic shift arising from electronic effects occurs when **III-1** is placed in the terminal positions (**III-2**) vs. the central core (**III-3**). A similar

bathochromic shift occurs by exchanging the terminal thiophenes for pyrroles, as seen with **III-3** vs. **III-4**. It should be noted that the colours observed for the neutral azomethines are usually difficult to obtain with their all-carbon counterparts. Moreover, pronounced colour changes between the neutral and oxidized forms of the heterocyclic azomethines are possible. This is illustrated in the inset of Figure III-3 (top and bottom) showing the stark colour transitions from red to green for **III-2A** and orange to purple for **III-6**. It should be noted that the observed colors are challenging to obtain with their vinylene derivatives, especially those of similar molecular weight. Moreover, the imines presented are the first examples of such compounds that not only undergo reversible color changes, but also exhibit stark color changes between their neutral and oxidized forms. The reversible oxidation is further confirmed from the electrochromism shown in Figure III-3. The clear isobestic point observed at 560 nm for **III-2A** and 505 nm for **III-6** confirms that only two species are present; the neutral and oxidized forms and it further confirms that no decomposition occurs. This is evidenced by the same absorption intensity being obtained upon reducing the oxidized form to the neutral state. This further confirms that the azomethines can be reversibly oxidized. The effect of heterocycles and the structure on the spectroscopic properties of the generated radical cation are evident from Table III-1. It should be noted that the spectroscopic properties of the radical cations are influenced by subtle structural modifications as evidenced by comparing **III-2A** *vs*. **III-2B**. The alkyl groups of **III-2B** stabilize the radical cation resulting in a 7 nm bathochromic shift relative to the radical cation of **III-2A**. Nonetheless, reversible electrochromic behaviour of

azomethines is possible contingent on structure and the color of both the neutral azomethines and their radical cations can also be tailored contingent on structure. The stark color changes between the neutral and oxidized forms in addition to the reversible anodic process imply that azomethines are viable materials for electrochromic applications.

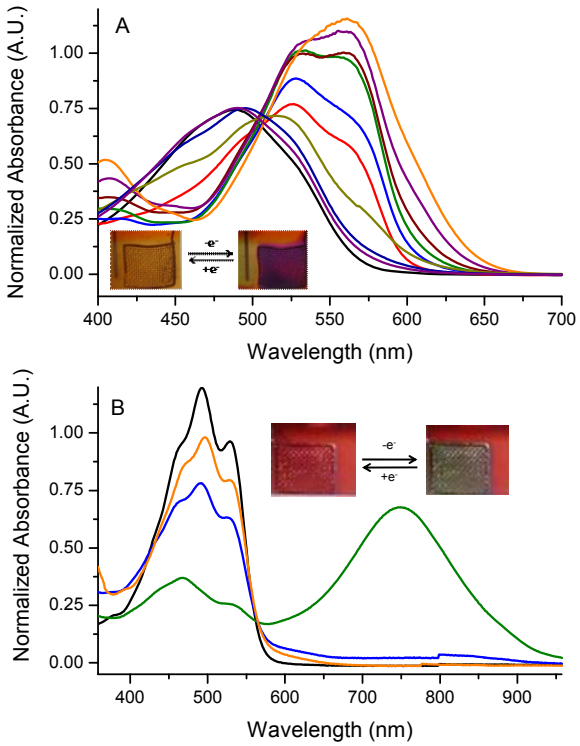

Figure III-3. Spectroelectrochemistry of **III-6** recorded in anhydrous and deaerated dichloromethane with 0.1 M $TBAPF_6$ at 1000 mV for 0 (black), 2 (red), 5 (blue), 8 (green), 11 (brown), 14 (purple), 17 (orange) minutes, and –100 mV for 2 (dark yellow), 5 (navy blue), 8 (purple) minutes. B) Spectroelectrochemistry of **III-2A** recorded in anhydrous and deaerated dichloromethane with 0.1 M $TBAPF_6$ at 1000 mV for 0 (black), 4 (green) minutes and –100 mV for 1 (blue), 10 (orange) minutes. Inset: Colour observed for the neutral (left) and oxidized (right) azomethine at the platinum mesh electrode.

The high degree of conjugation observed spectroscopically is further confirmed by the crystal structure of **III-5** shown in Figure III-4. Crystals of **III-5**, suitable quality for X-ray diffraction analysis, were grown from the slow evaporation acetone to give red blocks. Two different molecules per lattice were found to crystallize within the monoclinic $P2_1/c$ lattice. Neither solvent nor counter-ions were found in the closed-packed stacking. It can be seen that the mean plane angles of the terminal pyrroles are slightly twisted from the mean plane of the central thiophene to which they are connected. The mean plane angle of the terminal N-methylpyrrole including N11 is twisted by 14.44 (4)^o from the central thiophene by 27.30 (7)^o for the heterocycle with N14. The second molecule located within the crystal lattice was found to have smaller mean plane angles: 7.22 (3)^o for N21 and 11.60 (4)^o for N24. The small mean plane angles imply the aryl groups of **III-5** are nearly coplanar. This is similar to its all-thiophene analogue whose analogous mean plane angles are 9.04 (4)^o and 25.07 (6)^o. The small mean plane angle twisting between the heterocycles and the imines, obvious when looking along the *c*-axis of the compound, as seen in the bottom of Figure III-4, confers a high degree of conjugation to the trimer. This is in contrast to homoaryl containing azomethines whose mean plane angles are twisted by up to 65^o, resulting in reduced conjugation and limited colors in the visible absorption spectrum.

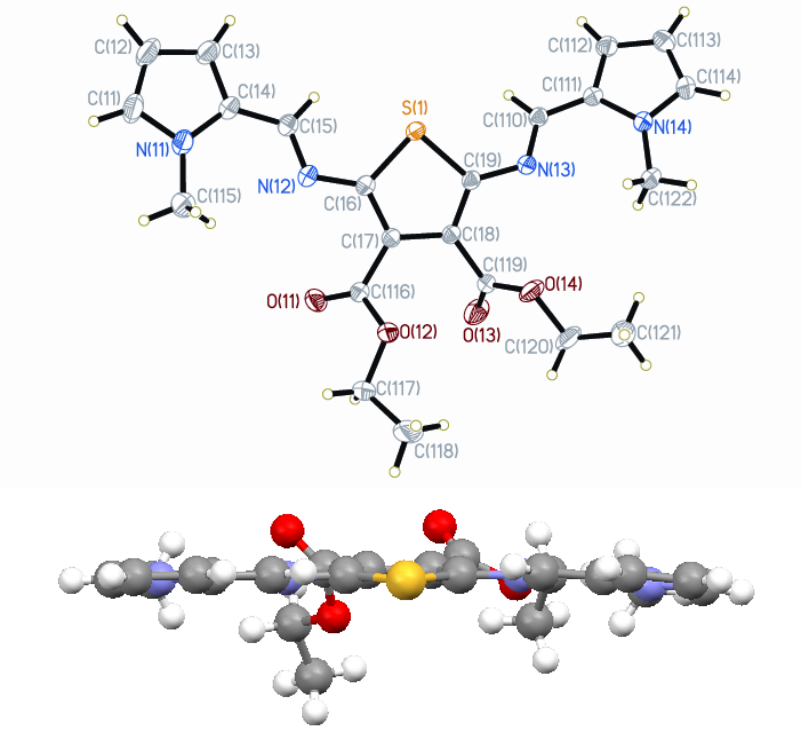

Figure III-4. X-ray crystallographic structure of **III-5** and the corresponding numbering (top) and seen along the *c*-axis (bottom).

The compounds were additionally oxidized chemically with $FeCl_3$ to confirm their stability. As seen in Figure III-5, the azomethines undergo significant colour changes similar to those obtained anodically. No decomposition of the compounds upon oxidation was observed as evidenced by the absence of colour fading of the oxidized intermediates. The oxidized products were subsequently reduced to the neutral form with hydrazine without any colour fading compared to the original neutral state (Figure III-5). More than five chemical oxidation-reduction cycles were possible without significant product

decomposition. It should be noted that no special precautions, such as deaerating the samples or anhydrous solvents were required, confirming that the oxidized intermediates are stable. This is in contrast to other azomethines that decompose under similar conditions or are hydrolyzed.[40, 48, 49] The examples shown in Figure III-5 combined with the absorption spectra collectively demonstrate that an array of colours of both the neutral and oxidized azomethines is possible by judicious choice of heterocycles and electronic groups and that the azomethine linkage is robust. Although many compounds undergo colour changes when oxidized, the heterocyclic azomethines shown are among the first reported examples of stable azomethines that can sustain repeated oxidation while exhibiting stark colour changes and tuning of both the neutral and oxidized forms. The collective electrochemical and chemical oxidation results additionally confirm that imines can be reversible oxidized and further demonstrate that these compounds are hydrolytically and oxidatively robust. This is contrary to what is generally accepted of imines that are incorrectly assumed to be highly unstable, easily hydrolyzed, anodically unstable, and exhibit no functional materials properties.

Table III-1. Various properties of the azomethine triads measured in anhydrous and deaerated dichloromethane.

Triad	λ_{abs} (nm)	$R^{\bullet+}$ (nm)[a]	E_{pa} (V)[b]	E_{pc} (V)[b]	E_g (eV)[c]	Reversibility [d]
III-2A	492	749	0.9	-1.2	2.5	Yes
III-2B[d]	505	792	0.8	-0.9	1.7	Yes
III-3[f]	440	-	1.2	-1.3	2.6	No
III-4	465	541	1.1	-1.3	2.8	Yes
III-5	457	-	0.8	-1.4	2.6	No
III-6	492	560	0.9	-1.2	2.7	Yes
III-7	427	-	0.9	-1.2	2.5	No

[a]Intermediate produced anodically with applied potential slightly greater than E_{pa} and chemically with $FeCl_3$. [b]Values reported are against a saturated Ag^+/AgCl electrode and can be corrected to SCE by applying a 45 mV correction factor.[26] [b]Electrochemical band-gaps derived from the measured E_{pa} and E_{pc} according to E_{pa}-E_{pc} + 0.4. [d]Refers to oxidized intermediate. [e]From reference 30. [f]From references [20, 30, 47]

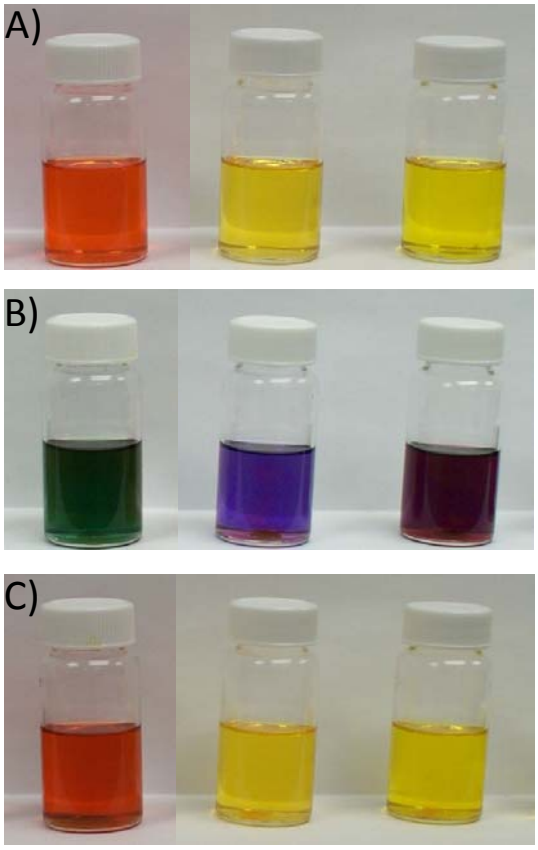

Figure III-5. Solutions of **III-2A** (left panels), **III-7** (middle panels), and **III-4** (right panels in dichloromethane (A), (B) the addition of $FeCl_3$, (C) followed by the addition of hydrazine after standing with $FeCl_3$ for 10 minutes.

Conclusions

In summary, the first examples of reversible oxidation and spectroelectrochemical properties of azomethines contingent on structure were demonstrated. It was shown that the E_{pa} of the heterocyclic azomethines is lower than previously reported examples and that

reversibility of the oxidation process could be tailored as a function of structure. Colour tuning of the neutral and stable oxidized intermediate is contingent on the heterocycles and electronic groups. Although, the azomethines presented exhibited comparable electrochemical and spectroelectrochemical properties to their carbon analogues, the latter have benefitted from over 20 years of property optimization. With similar optimization, electrochromic, electrochemical and colour properties surpassing vinylene derivatives are expected. Nonetheless, the heterocyclic examples presented are suitable as functional materials in part as a result of their unprecedented reversible anodic behaviour concomitant with the colour tuning of both the neutral and oxidized states. Taking into account their similar properties compared to their carbon counterparts together with their ease of synthesis and purification, and tuneable colors of both the neutral and oxidized forms, the azomethine examples are attractive alternatives to current vinylene compounds.

Acknowledgements

The authors acknowledge financial support from the Natural Sciences and Engineering Research Council Canada and additional equipment funding from the Canada Foundation for Innovation and the Centre for Self-Assembled Chemical Structures. Both S.D. and A.B. thank NSERC Canada for graduate scholarships. WGS also thanks the RSC for a JWT Jones Travelling Fellowship, allowing the completion of this manuscript.

References

1. Sonmez, G.; Schottland, P.; Reynolds, J. R. *Synth. Met.* **2006**, *156*, 130-137.

2. Roncali, J.; Blanchard, P.; Frère, P. *J. Mater. Chem.* **2005**, *16*, 1589-1610.

3. Perepichka, I. F.; Perepichka, D. F.; Meng, H.; Wudl, F. *Adv. Mater.* **2005**, ***17***, 2281-2305.

4. Roncali, J. *Chem. Rev.* **1992**, *92*, 711-738.

5. Garnier, F.; Tourillon, G.; Gazard, M.; Dubois, J. C. *J. Electroanal. Chem.* **1983**, *148*, 299-303.

6. Tourillon, G.; Garnier, F. *J. Electroanal. Chem.* **1984**, *161*, 51-58.

7. Walczak, R. M.; Reynolds, J. R. *Adv. Mater.* **2006**, *18*, 1121-1131.

8. Monk, P. M. S.; Mortimer, R. J.; Rosseinsky, D. R. *Electrochromism and Electrochromic Devices*, Cambridge University Press, Cambridge, 2007.

9. Skotheim, T. A.; Reynolds, J. R. *Handbook of Conducting Polymers*, CRC Press, Boca Raton, FL, 2007.

10. Mei, J.; Heston, N. C.; Vasilyeva, S. V.; Reynolds, J. R. Macromolecules **2009**, *42*, 1482-1487.

11. Beaujuge, P. M.; Vasilyeva, S. V.; Ellinger, S.; McCarley, T. D.; Reynolds, J. R. Macromolecules **2009**, *42*, 3694-3706.

12. Steckler, T. T.; Zhang, X.; Hwang, J.; Honeyager, R.; Ohira, S.; Zhang, X.-H.; Grant, A.; Ellinger, S.; Odom, S. A.; Sweat, D.; Tanner, D. B.; Rinzler, A. G.; Barlow, S.; Brédas,

J.-L.; Kippelen, B.; Marder, S. R.; Reynolds, J. R. *J. Am. Chem. Soc.* **2009**, *131*, 2824–2826.

13. Beaujuge, P. M.; Ellinger, S.; Reynolds, J. R. *Nat. Mater.* **2008**, *7*, 795-799.

14. Yu, N.; Zhu, R.; Peng, B.; Huang, W.; Wei, W. *J. Appl. Polym. Sci.* **2008**, *108*, 2438-2445.

15. Morin, J.-F.; Drolet, N.; Tao, Y.; Leclerc, M. *Chem. Mater.* **2004**, *16*, 4619-4626.

16. Wang, C.; Shieh, S.; LeGoff, E.; Kanatzidis, M. G. *Macromolecules* **1996**, *29*, 3147-3156.

17. Yang, C.-J.; Jenekhe, S. A. *Chem. Mater.* **1991**, *3*, 878-887.

18. Bourgeaux, M.; Skene, W. G. *Macromolecules* **2007**, *40*, 1792-1795.

19. Bourgeaux, M.; Pérez Guarin, S. A.; Skene, W. G. *J. Mater. Chem.* **2007**, *17*, 972-979.

20. Pérez Guarìn, S. A.; Bourgeaux, M.; Dufresne, S.; Skene, W. G. *J. Org. Chem.* **2007**, *72*, 2631-2643.

21. Suematsu, K.; Nakamura, K.; Takeda, J. *Colloid. Polym. Sci.* **1983**, *261*, 493-501.

22. Morgan, P. W.; Kwolek, S. L.; Pletcher, T. C. *Macromolecules* **1987**, *20*, 729-739.

23. Destri, S.; Pasini, M.; Pelizzi, C.; Porzio, W.; Predieri, G.; Vignali, C. *Macromolecules* **1998**, *32*, 353-360.

24. Zotti, G.; Randi, A.; Destri, S.; Porzio, W.; Schiavon, G. *Chem. Mater.* **2002**, *14*, 4550-4557.

25. Kiriy, N.; Bocharova, V.; Kiriy, A.; Stamm, M.; Krebs, F. C.; Adler, H.-J. *Chem. Mater.* **2004**, *16*, 4765-4771.

26. Zoski, C. A. ed., *Handbook of Electrochemistry*, Elsevier Science, Radarweg, 2007.

27. Jérôme, C.; Maertens, C.; Mertens, M.; Jérôme, R.; Quattrocchi, C.; Lazzaroni, R.; Brédas, J. L. *Synth. Met.* **1996**, *83*, 103-109.

28. Bard, A. J.; Faulkner, L. R.; *Electrochemical Methods: Fundamentals and Applications*, John Wiley & Sons, 2001.

29. Bourgeaux, M.; Vomscheid, S.; Skene, W. G. *Synth. Commun.* **2007**, *37*, 3551-3558.

30. Bourgeaux, M.; Skene, W. G. *J. Org. Chem.* **2007**, *72*, 8882-8892.

31. Al-Yusufy, F. A.; Bruckenstein, S.; Schlindwein, W. S. *J. Sol. Stat. Electrochem.* **2007**, *11*, 1263–1268.

32. Destri, S.; Khotina, I. A.; Porzio, W.; Botta, C. *Opt. Mater.* **1998**, *9*, 411-415.

33. Brooker, S.; Iremonger, S. S.; Plieger, P. G. *Polyhedron* **2003**, *22*, 665-671.

34. Brovelli, F.; Valle, M. A. D.; Fernando, Y.; Díaz, R.; Bernède, J. C. *J. Bol. Soc. Chil. Quim.* **2001**, *46*, 219-337.

35. Tang, S.; Liu, M.; Lu, P.; Cheng, G.; Zeng, M.; Xie, Z.; Xu, H.; Wang, H.; Yang, B.; Ma, Y.; Yan, D. *Org. Elect.* **2008**, *9*, 241-252.

36. Pérez Guarìn, S. A.; Skene, W. G. *Mater. Lett.* **2007**, *61*, 5102-5106.

37. Pérez Guarìn, S. A.; Dufresne, S.; Tsang, D.; Sylla, A.; Skene, W. G. *J. Mater. Chem.* **2007**, *17*, 2801-2811.

38. The anodically produced polymer is currently being characterized and is outside the scope of the current report.

39. Amari, C.; Pelizzi, C.; Predieri, G.; Destri, S.; Porzio, W.; Einsiedel, H.; Menges, B.; Mittler-Neher, S. *J. Mater. Chem.* **1996**, *6*, 1319-1324.

40. Destri, S.; Porzio, W. *Synth. Met.* **1995**, *75*, 25-36.

41. Yang, C.-J.; Jenekhe, S. A. *Macromolecules* **1995**, *28*, 1180-1196.

42. Yen, H.-J.; Liou, G.-S. *Org. Electr.* **2010**, *11*, 299-310.

43. Diaz, F. R.; Moreno, J.; Tagle, L. H.; East, G. A.; Radic, D. *Synth. Met.* **1999**, *100*, 187-193.

44. Higuchi, M. Y.; Yamamoto, K. *Polym. Adv. Tech.* **2002**, *13*, 765-770.

45. Skopalová, J.; Lemr, K.; Kotouèek, M.; Èáp, L.; Barták, P. *Fresenius J. Anal. Chem.* **2001**, *370*, 963-969.

46. Rao, T. V. D. P.; Veerabhadram, G.; Sastry, K. S. *J. Electrochem. Soc. India* **2001**, *50*, 68-71.

47. Dufresne, S.; Skene, W. G. *J. Org. Chem.* **2008**, *73*, 3859-3866.

48. Grigoras, M.; Catanescu, C. O. *J. Macromol. Sci. Polym. Rev.* **2004**, *C44*, 131-173.

49. Amari, C.; Pelizzi, C.; Predieri, G.; Destri, S.; Porzio, W. *Synth. Met.* **1995**, *72*, 7-12.

IV. CHAPITRE IV

Unsymmetric Pyrrole, Thiophene, and Furan Conjugated Comonomers Prepared Using Azomethine Connections: Potential New Monomers for Alternating Homo-Coupled Products

*Stéphane Dufresne and W. G. Skene**

Département de Chimie, Pavillon J. A. Bombardier, Université de Montréal, CP 6128, succ. Centre-ville, Montréal, Québec, CANADA, H3C 3J7.

* corresponding author

Received January 30, 2008

Published on Web 04/15/2008

J. Org. Chem. **2008**, *73*, 3859-3866

Graphical Abstract

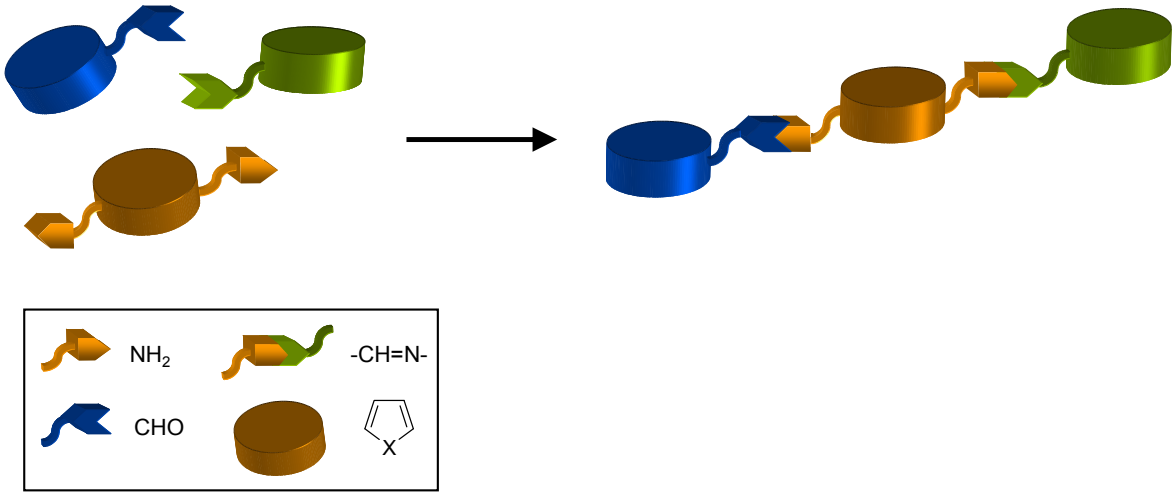

Abstract

Unsymmetric comonomers consisting of thiophene, pyrrole, and furan heterocycles were prepared using azomethine bonds. Photophysical investigation of the novel π-donor-donor-donor segmented compounds revealed that their singlet excited state is only partially deactivated by internal conversion unlike their all-thiophene azomethine analogues. Temperature dependent steady-state and time-resolved emission studies demonstrated that the unsymmetric compounds deactivated efficiently their singlet excited state by intersystem crossing to populate the triplet manifold. This lower energy state is rapidly deactivated by nonradiative self-quenching. The comonomers and their anodically prepared conjugated homo-coupled products are both electrochemically active, resulting in new compounds that can be mutually oxidized and reduced. Meanwhile, the oxidation potentials of the coupled products are shifted by up to 400 mV to more cathodic potentials relative to their corresponding comonomers, confirming their increased degree of conjugation.

Introduction

Conjugated materials such as phenylvinylenes have found many applications as functional materials because of their interesting photophysical and electrochemical properties. Many potential applications for such materials include light emitting diodes,[1-8] solar cells,[9-11] field effect transistors,[12-14] and molecular sensors.[15] Even though π-conjugated materials are successfully prepared by well established protocols, including Wittig coupling,[16, 17] the products must be extensively purified in order to remove undesired by-products. For example with Wittig coupling, triphenylphosphine oxide accounts for a considerable amount of the product obtained and it also leads to inconsistent properties in the final products if it is not thoroughly removed. Similar inconsistent properties occur with anodically prepared polymers[18-20] owing to uncontrollable competing side reactions such as α–β-coupling, over oxidation, and cross-linking defects. Comparable defects can also occur with the electrochemical preparation of alternating copolymers owing to mismatched oxidation potentials of the different monomers. Consequently, the oxidation potentials of the two monomers to be copolymerized must be similar in order to suppress homopolymerization and other undesired defects. An appropriate solution to these problematic electrochemical shortcomings involves the use of comonomers. These are monomers containing the elements of the copolymer structure consisting of a central aromatic core sandwiched between external aryl groups. Such an arrangement offers the possibility to suppress polymer defects that would otherwise limit the degree of conjugation leading to incompatible properties for uses as functional materials.[21-23]

Despite the synthetic advantages of using comonomers for the anodic preparation of conjugated polymers, their synthesis involves challenging coupling reactions and they also suffer from problematic purifications. Additionally, unsymmetric π-rich or π-poor comonomers desired for controlling the spectroscopic and electrochemical properties are difficult to prepare in high yields by these protocols (*vide infra*).[24, 25] Given the potential enhanced property tailoring that is possible with unsymmetric comonomers, new and efficient methods for the synthesis of such comonomers are therefore required.

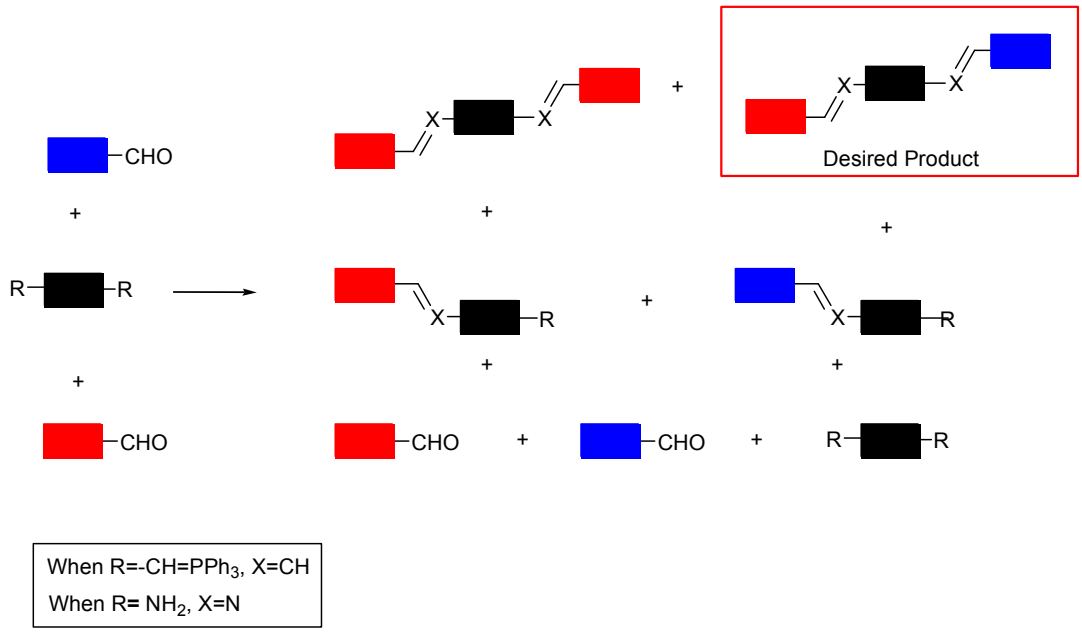

Scheme IV-1. Schematic representation of potential product distribution for a three-component reaction of vinylene and azomethine formation prepared by Wittig and azomethine condensation reactions, respectively.

Coupling of complementary aryl aldehydes and amines affording azomethines (-N=CH-) is an ideal alternative for the synthesis of conjugated comonomers. Not only are azomethines isoelectronic to their C=C vinylene analogues, but mild reaction conditions are required for their synthesis involving simple purifications when necessary. Unlike conventional coupling techniques that give a mixture of products when using a three component reaction depicted in Scheme IV-1, selective product formation affording unsymmetric products is possible with azomethines by controlling the reagent stoichiometry and solvents.[26, 27] The result of the self-assembly between the two complementary aryl groups is a robust bond exhibiting high hydrolytic, oxidative, and reductive resistance.[26-28]

To address the synthetic challenge of unsymmetric conjugated comonomers consisting of various heterocycles, we used the stable diaminothiophene **IV-1** for preparing the novel azomethines reported in Scheme IV-2. This heterocycle is an ideal compound to use as a core for comonomer synthesis because it possesses a low oxidation potential, which when incorporated into a comonomer is ideal for anodic coupling. This eliminates the risk of undesired decomposition products that are otherwise produced with monomers possessing high oxidation potentials. Additionally, **IV-1** is air-stable, and condensation with aryl aldehydes is achieved easily affording stable conjugated comonomers, which are capable of sustaining anodic polymerization. Our previous successful comonomer synthesis[26-31] and our ongoing conjugated azomethines research have prompted us to

prepare a new series of unsymmetric π-rich heterocyclic comonomers consisting of thiophenes, pyrroles, and furans and to investigate their physical properties. These new π-donor-donor-donor compounds and their anodically produced polymers are of particular interest because they are expected to exhibit enhanced properties relative to homoaryl azomethines. For example, mutual oxidation and reduction leading to p- and n-doping of the azomethine comonomers is expected contrary to their oligothiophene and thiophene vinylene analogues that can be only p-doped.

Even though **IV-1** has been known since the early 70's,[32, 33] its challenging preparation and low yields preclude it as a suitable precursor for the preparation of azomethines. Subsequently, diamino precursors required for azomethine preparation have been limited to phenylene diamine and its derivatives. Such homoaryl precursors are problematic because they decompose under ambient conditions while their azomethine products are highly insoluble.[22, 34-36] Moreover, they suffer from unwanted oxidative decomposition and conjugated polymers produced anodically by α-α homo-coupling are rarely obtained.[21, 37] The properties of the homoaryl azomethine are also incompatible with functional materials, and as a result, azomethines have attracted little attention.[23, 38, 39] Our recent simple scale-up preparation of **IV-1**[26-29, 40] concomitant with its optimized condensation for the preparation of novel azomethines consisting uniquely of thiophenes has renewed the interest in azomethines as functional materials. Given the importance of assessing the compatibility of these new compounds as functional materials, we examined

the structure-property relationship of novel unsymmetric heterocyclic conjugated azomethines. Herein, we present the preparation of novel π-rich comonomers along with their photophysics and redox properties including their anodically coupled products.

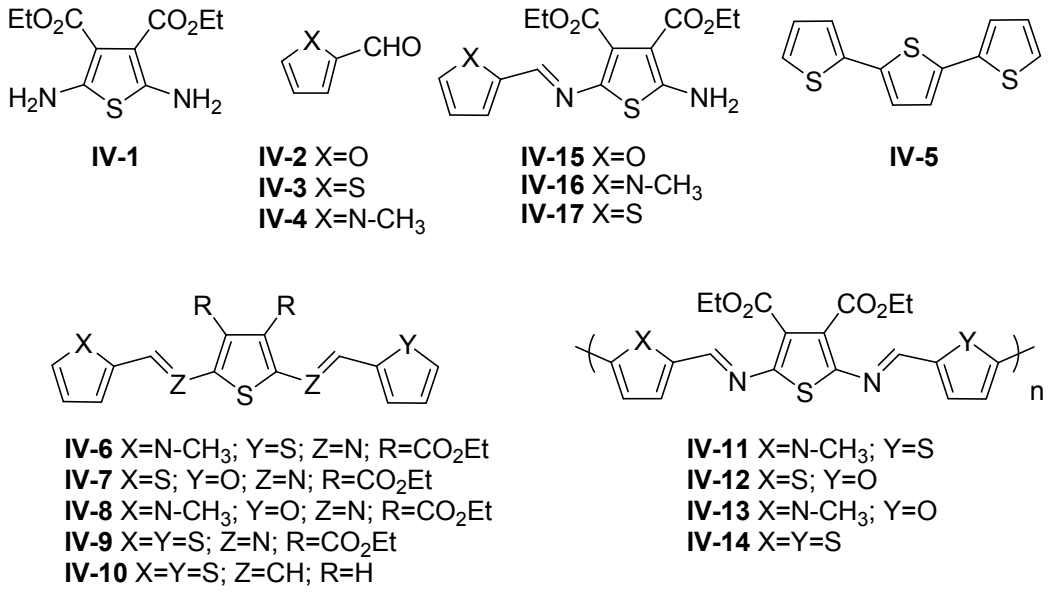

Scheme IV-2. Azomethines examined, their precursors and their corresponding products obtained by anodic coupling. For simplicity, **IV-11**-**IV-14** are illustrated as *head-to-tail* products even though a mixture of *head-to-tail* and *head-to-head* regioregular products are expected.

Results and Discussion

Preparation

The diaminothiophene core (**IV-1**) required for the condensation with heteroaldehydes **IV-2**-**IV-4** was obtained in large quantities by a modified one-pot Gewald[32, 40] batch reaction using inexpensive ethylcyanoacetate and elemental sulfur. The electron withdrawing ester in the 3 and 4 positions deactivate the electron rich amines conferring a high degree of stability to **IV-1** under ambient conditions. In contrast, its electron rich unsubstituted analogue cannot be isolated and it spontaneously decomposes under ambient conditions. The azomethine formed when condensing an arylaldehyde with **IV-1** is also electron withdrawing and it further reduces the reactivity of the remaining terminal amine in monoazomethine compounds such as **IV-15**-**IV-17**. More stringent reaction conditions are therefore required to induce the second condensation for the preparation of bisazomethines such as the unsymmetric comonomers reported in Scheme IV-2. The change in amine reactivity provides a versatile means to prepare **IV-6**-**IV-8** in a step-wise manner from the corresponding monoazomethine, **IV-15**-**IV-17**. The required monoazomethines were obtained by refluxing 1 equivalent of the arylaldehyde with **IV-1**. The selectivity for monoaddition to afford uniquely the corresponding monoazomethines is apparent from the reaction yields. An unselective reaction affording a mixture of monoazomethine and symmetric bisazomethines would otherwise lead to low product yields. The unsymmetric bisazomethines were prepared with 1 equivalent of the corresponding aldehyde which was activated with $TiCl_4$ and then combined with either

IV-15-IV-17 in refluxing toluene. The bisazomethine products obtained in good yields confirm the robustness of the azomethine while weak azomethine linkages would decompose under the reaction conditions used. The stability of the comonomers is further evidenced by the absence of exchange products involving Lewis acid mediated aldehyde exchange.[28, 41, 42] The differential reactivity notwithstanding, the order in which the aldehydes must be reacted in order to obtain the final comonomers had to be carefully chosen. For example, **IV-7** and **IV-8** could only be prepared from the furan azomethine **IV-15** while **IV-6** could be obtained only from **IV-17**. No bisazomethine product was obtained with **IV-16**.

In spite of having to purify the products by column chromatography, the compounds were isolated in reasonable yields. Given the Lewis acid reaction conditions concomitant with the inherent acidic and hydroscopic nature of silica gel that would otherwise hydrolyze labile azomethines, the moderate yields of the comonomers concomitant with the absence of hydrolysis products confirm that the azomethines are robust and stable. The stability of the azomethine bond is evidenced by the lack of reduction with common reducing reagents including $NaBH_4$ and DIBAL. In addition, no decomposition products were observed when exposing the compounds to ambient conditions for prolonged periods of time, which would otherwise hydrolyze moisture and oxygen sensitive azomethines.[43]

Spectroscopy

The properties of the azomethine derivatives relative to their vinylene carbon analogue (**IV-10**) are seen in Table IV-1 where a 50 nm bathrochromic shift in both the absorption and fluorescence maximum occurred as a result of the heteroconjugated bond.[44, 45] Similarly, a 150 nm absorption bathochromic shift was observed for the comonomers relative to **IV-1**. The same trend was also observed for the fluorescence that is bathochromically shifted by ca. 200 nm relative to **IV-1**. The large spectroscopic shifts are consistent with a highly co-planar π-conjugated structure (*vide infra*) across which the excited state energy can delocalize efficiently. This is in contrast to homoaryl azomethines whose azomethine mean plane angles are twisted,[46] limiting severely their degree of conjugation.

Table IV-1. Comonomer spectroscopic data measured in anhydrous acetonitrile.

Compound	Abs. (nm)[a]	Em. (nm)[b]	Φ_{fl} (10^{-3})[c]	$\Phi_{fl\ (77K)}$[d]	Φ_{ISC}[e]	E_g (eV)[f]	k_r (μs^{-1})[g]	k_{nr} (ns^{-1})[h]	Phos. (nm)[i]
IV-1	305	335	2.5	0.009	0.99	3.0	0.19	0.08	479
IV-5[j]	351	422	50.0	-	0.90	3.2	250	4.8	682
IV-6	457	540	0.38	0.39	0.61	2.2	0.12	0.32	566
IV-7	420	525	0.65	0.21	0.79	2.3	0.31	0.48	552
IV-8	452	535	1.2	0.43	0.57	2.3	0.92	0.77	550
IV-9[k]	440	534	2.8	0.71	0.29	2.3	0.21	0.07	560
IV-10	407[l]	495[m]	27[m]	≈ 0.3[m]	0.15[n]	2.7[o]	20	13	530[n]

[a] Absorption maximum. [b] Emission maximum. [c] Fluorescence quantum yields at λ_{ex} = 303 nm, relative to bithiophene.[28] [d] Fluorescence quantum yields at 77 K relative to room temperature. [e] Φ_{ISC} = 1- Φ_{fl} (77K). [f] Spectroscopic HOMO-LUMO energy gap. [g] $k_r = \Phi_{fl}/\tau_f$. [h] $k_{nr} = k_r(1-\Phi_{fl})/\Phi_{fl}$. [i] Phosphorescence measured in 4:1 ethanol/methanol glass matrix at 77 K. [j] From Seixas de Melo *et al.* and Wasserberg *et al*.[47, 48] [k] From Dufresne *et al*.[28] [l] From Jérôme *et al*.[49] [m] From Apperloo *et al*.[50] [n] From Ginocchietti *et al*.[51] [o] From Frère *et al*.[52]

The absorption and fluorescence spectra provide further information relative to the energy differences between the excited and ground states of the comonomers.[26-28, 30] The spectroscopically derived HOMO-LUMO energy gap (E_g) taken from the absorption edge reported in Table 1 for the comonomers is lower than their oligothiophene analogue **IV-5** as well as the vinylene analogue **IV-10**. This is a result of the energy levels being affected by the heteroconjugated bond and the electron-withdrawing ester groups. The narrower energy gap and the lower energy levels of the azomethine comonomers imply the easy condensation method is a suitable means for obtaining conjugated materials with enhanced properties.

Not only do the spectroscopic data provide valuable information regarding the effect of the heteroconjugated bond on the physical properties relative to **IV-10**, they also illustrate the donor strength of the different heterocycles. The effect of the different

π-donor groups is seen from the absorption maximum of the comonomers relative to the symmetric all-thiopheno azomethine **IV-9**. Both **IV-6** and **IV-8** are shifted bathochromically by 25 nm relative to **IV-9**. The observed absorption and fluorescence shifts result from the strong π-donor property of the N-methyl pyrrole. The azomethines consisting of N-methyl pyrrole undergo increased delocalization resulting in an electronic push-pull system with the electron withdrawing esters. The resulting π-donor-donor-acceptor type arrangement promotes intramolecular charge transfer (ICT). The subsequent increased delocalization of the pyrrole azomethine derivatives is evidenced by the absorption bathochromic shifts. Conversely, the poor π-donor properties of the furan heterocycle prevent ICT. This results in a decreased delocalization as evidenced by the 20 nm hypsochromic shift for the absorption and fluorescence spectra of **IV-7** versus **IV-9**.

The weak fluorescence observed from the steady-state emission analyses confirms the comonomers do not dissipate efficiently their singlet excited state by radiative means. This is not surprising since heterocycles such as thiophene and pyrrole are known to deactivate preferentially their singlet excited state by intersystem crossing (ISC) to the triplet state. However, the nonemissive mode of singlet excited state energy dissipation of the azomethine comonomers proceeds differently via internal conversion (IC). This is supported by the 3 orders of magnitude difference between the fluorescence observed in a glass matrix at 77 K relative to that at room temperature (rt; Figure IV-1). Energy dissipating modes responsible for deactivating the singlet excited state by IC such as bond

rotation cannot occur in the low temperature solid matrix. The energy dissipated by IC can therefore be calculated from the fluorescence at different temperatures according to: $\Phi_{IC} \approx \Phi_{fl}$ (77 K) – Φ_{fl} (rt). The large difference between the nonradiative rate (k_{nr}) and the radiative (k_r) rate constants further corroborates singlet excited state deactivation by IC. It is worthy to note that vinylenes such as **IV-10** also undergo IC; however, their room temperature fluorescence is greater than the analogous azomethine derivatives.[50] This implies that deactivation of the excited state by rotation around the aryl–CH- and aryl–N= bonds is more efficient for the azomethines than for their corresponding vinylene analogues. The azomethine fluorescence can therefore be modulated by decreasing the temperature, which reduces the modes of deactivation by bond rotation leading to high emission. Similarly, an increase in fluorescence is also expected from the azomethines in the solid state because emission quenching by bond rotation is equally suppressed in this state. The controllable fluorescence is in contrast to oligothiophenes such as **IV-5** that are inherently weak emitters owing to uncontrollable ISC. Consequently, their fluorescence cannot be modulated to obtain high emissions such as with the azomethines. [53]

Even though the low temperature measurements confirm IC is responsible for the reduced azomethine fluorescence, this deactivation mode does not account entirely for the nonradiative deactivation. This is apparent from summing the Φ_{IC}, calculated from the low temperature fluorescence, and the Φ_{fl} reported in Table IV-1, which gives less than the expected unity. By substituting the calculated values into the standard energy conservation

equation: $\Phi_{fl} + \Phi_{ISC} + \Phi_{IC} \approx 1$, it becomes evident that Φ_{ISC} to the triplet state occurs significantly (0.45) for **IV-6**-**IV-8**. Even though precise measurements of Φ_{IC} are not possible because of the extremely weak fluorescence observed at rt, ISC nonetheless occurs to a higher degree with the different heteroaryl azomethines than for **IV-9**. This is surprising because the reduced number of thiophenes in addition to the preferred azomethine deactivation by IC[47] were expected to decrease the amount of ISC. Although, photoisomerization is an additional possible deactivation mode of the singlet excited state, this quenching pathway can be eliminated since no photoisomerization products were observed. The absence of photoisomers is further consistent with the extremely low photoisomerization quantum yield of **IV-10**.[51] Despite the shift in the deactivation mode from IC to ISC, the amount of triplet produced for the π-donor-donor-donor azomethines is consistent with analogous ter-oligo furans and pyrroles consisting of at least one thiophene, whose Φ_{ISC} are ca. 0.7.[47] The heterocyclic azomethines therefore exhibit triplet properties that are more closely related to their aryl-aryl analogues than their vinylene analogues as a result of lowering of the singlet excited state favoring a $S_1 \rightarrow T_1$ transition.

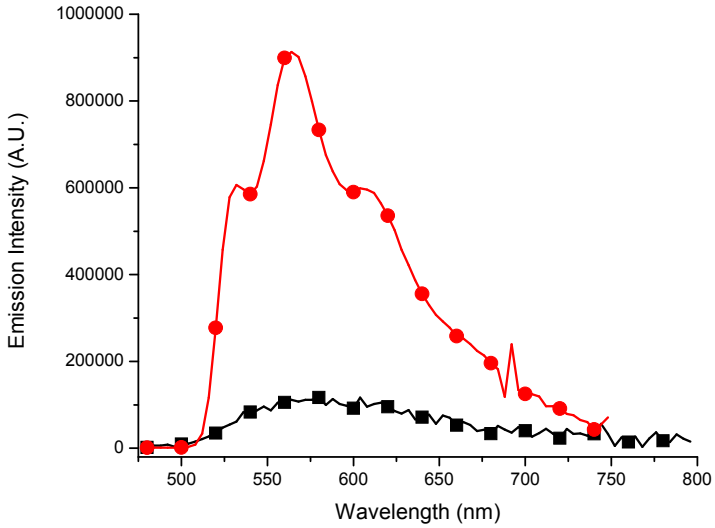

Figure IV-1. Fluorescence of **IV-6** measured at RT (■) and magnified 100 times relative to the fluorescence at 77 K measured in a 4:1 ethanol/methanol glass matrix (●).

Phosphorescence measurements were done at 77 K (Figure IV-2) in order to confirm ISC. The μs acquisition times used for these low temperature measurements ensure that the acquired emission spectra are free from fluorescence occurring on the ns timescale. Confirmation of the triplet state formation is further had from the low temperature emissions that are bathochromically shifted relative to the fluorescence. To ensure the observed emissions were assigned correctly to the phosphorescence, the emissions were recorded under the same experimental conditions, but at room temperature instead of a frozen matrix at 77 K. Since the triplet state is rapidly deactivated with diffusion controlled kinetics at room temperature, the absence of any observable signal at

room temperature with the μs acquisition confirms the emission at 77 K is from the triplet. The triplet energies can thus be derived from the 0,0 band where the measured azomethine values are lower than **IV-10**. The lower triplet energy of **IV-6**-**IV-8** vs. **IV-10** concomitant with the lower singlet excited state are most likely responsible for the shift in the azomethine deactivation from IC to ISC arising from matching of symmetry allowed $S_1 \rightarrow T_1$ transitions.

Even though the triplet energy can be confirmed by the low temperature measurements, accurate quantification of the triplet state by this simple steady-state method is difficult and is only possible by the time resolved method of laser flash photolysis (LFP). However, no transient signal was detected by this technique. Given the LFP time resolution is < 100 ns concomitant with the triplet formation confirmed by steady-state studies at 77 K, the absence of transient signal by LFP confirms the triplet states of **IV-6**-**IV-8** are self-quenched rapidly leading to nonradiative emission.[26-28, 30, 54] It is well established that the electrochemically produced amount of triplet vs. singlet states is 3:1.[55] The azomethine triplets that would be produced electrochemically in emitting would therefore be efficiently self-quenched resulting in pristine emission and no delayed emission. The self-quenching concomitant with an expected high fluorescence quantum yields possible by suppressing bond rotation deactivation modes possible in the solid-state would make the comonomers suitable for functional materials relative to their oligomeric analogues.

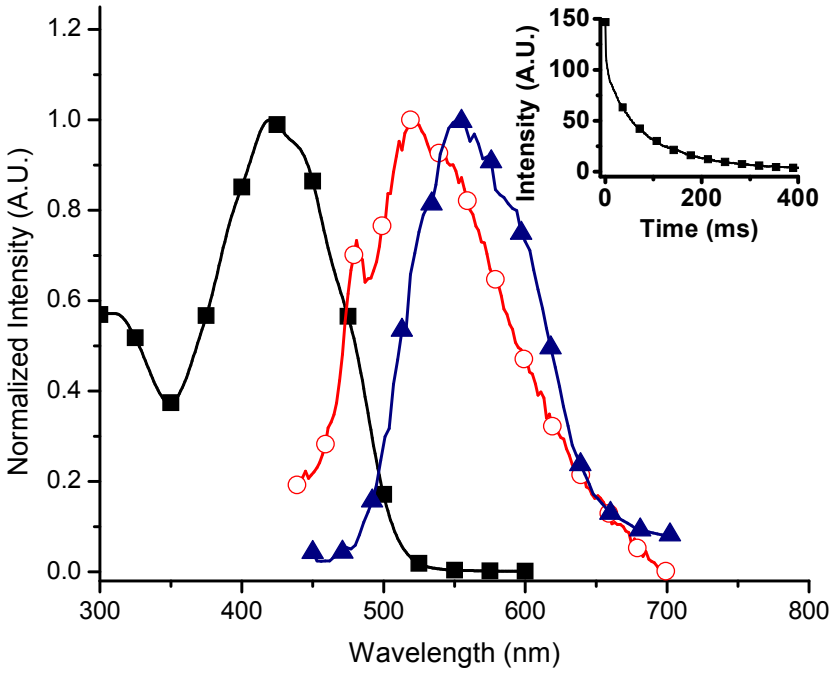

Figure IV-2. Normalized absorption (■) and fluorescence (o) spectra of **IV-7** in acetonitrile. Phosphorescence (▲) spectrum measured in 4:1 ethanol-methanol glass matrix at 77 K. Inset: phosphorescence decay monitored at 552 nm at 77 K.

X-ray Crystallography

Even though only one isomer was confirmed by ^{1}H NMR for **IV-6-IV-8**, absolute assignment to either the *E* or *Z* isomer is not possible by NMR, unlike its carbon analogue. However, the crystal structures obtained for **IV-7-IV-9** confirmed that they adopt the *E* isomer. The crystal data also proved that **IV-8** is co-planar with the heteroatoms orientating themselves in an anti-parallel arrangement (Figure IV-3), which is consistent with other azomethines.[56, 57] The mean planes described by the terminal heterocycles are only twisted slightly from the mean plane described by the central thiophene and the two azomethine bonds to which they are connected (Table IV-2).[26-28] The observed mean plane angles are in agreement with other heterocyclic azomethines and are in contrast to homoaryl azomethines whose mean planes are highly twisted by 65^{o}.[58] Although **IV-7** and **IV-8** are not entirely co-planar, the compounds are still conjugated through the central thiophene and the two azomethine bonds. Moreover, the spectroscopic data suggest the compounds are highly conjugated and therefore are co-planar in solution. Despite the differences of the mean plane angles between the aryl groups and the azomethine bonds, the C=N, N-aryl, and CH-aryl bond distances for **IV-6-IV-8** are the same with experimental error. Although the bisazomethines are unsymmetric, the similar bond lengths measured for the two heterocycles in the structure confirm the compounds are geometrically symmetric. Additionally, the observed co-planarity of the aryl groups and the azomethine bonds validate the high degree of π-conjugation derived from the spectroscopic data.

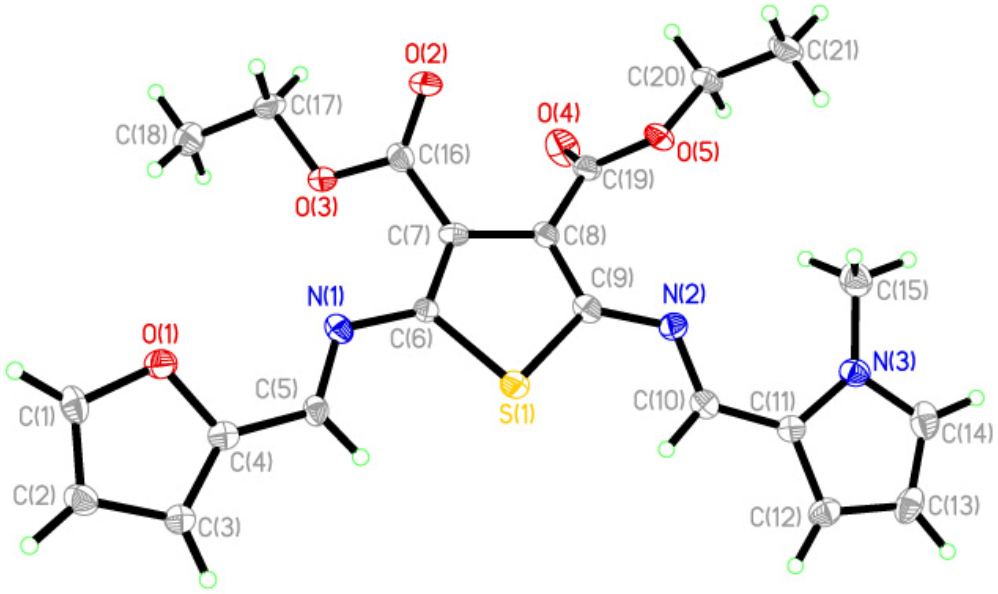

Figure IV-3. ORTEP representation of **IV-8** with the ellipsoids drawn at 30% probability level.

The crystallographic data also show that intermolecular interactions take place between the comonomers in the solid-state. For example, π-stacking occurs between the central thiophene and its complementary terminal pyrrole involving two molecules in different parallel planes that are separated by 3.431 (3) Å for **IV-8**. Such interactions contribute to the linear and co-planar configurations adopted by the comonomers. The inherent co-planar and anti-parallel configurations of the azomethines are opposite to oligothiophenes, such as **IV-5**, which require steric elements such as long alkyl chains incorporated into their backbone in order to achieve such regioregularity configurations.[59-62] Given this configuration is partially responsible for the high

conductivities and mobilities for oligothiophenes,[63] the inherent co-planarity of the comonomers is expected to also confer similar electrical properties upon doping.

Table IV-2. Selected comonomer crystallographic data.

	IV-6[a,b]		**IV-7**[b]		**IV-8**[b]	
	N-methyl pyrrole	thiophene	thiophene	furan	N-methyl pyrrole	furan
plane angle (°)[c]	4.1(1)	4.3(1)	33.6(7)	7.9(2)	18.0(4)	18.7(4)
-C=N- (Å)	1.296(9)	1.279(2)	1.286(4)	1.286(4)	1.287(5)	1.287(5)
=N-Aryl- (Å)	1.373(2)	1.377(2)	1.381(3)	1.385(3)	1.374(4)	1.374(4)
=CH-Aryl- (Å)	1.434(9)	1.436(9)	1.435(4)	1.418(4)	1.419(5)	1.419(5)

[a] Dufresne *et al*.[64] [b] Refers to parameters measured between the terminal heterocycle and the central thiophene. [c] Refers to the mean plane angle between the central thiophene and the terminal heterocycle. Values in parentheses refer to uncertainty of measured values.

Electrochemistry

Consistent with the oxidation of similar heterocycles, the comonomers underwent an irreversible oxidation corresponding to a one-electron oxidation and formation of the radical cation. In addition to the oxidation process, a reduction process was also observed as seen in Figure IV-4. Given the low potential at which the cathodic process occurred

combined with the absence of reduced products with standard reductants such as $NaBH_4$ and DIBAL, the electrochemical reduction corresponds to the radical anion formation. To ensure the observed reduction process was not from residual oxygen, the samples were thoroughly deaerated with nitrogen. Meanwhile, oxygen reduction with control experiments in air saturated solutions occurred at potentials different from those observed in the absence of oxygen. Given the absence of oxygen reduction at -1.43 V (Ag/Ag^+),[65] combined with the 300 mV fluctuation of the reduction potential (E_{pc}) as a function of azomethine structure, the observed cathodic processes are due uniquely to radical anion formation of the comonomers and not to oxygen reduction. The oxidation and reduction onsets can therefore be used to calculate accurately the HOMO and LUMO energy levels, respectively, reported in Table IV-3 in addition to the energy gaps (E_g) according to standard methods. The consistency between the electrochemically derived E_g and the spectroscopic values validates the electrochemical results. Both methods confirm that the azomethine E_g are smaller than **IV-10** confirming the heteroaryl azomethines are more conjugated than their carbon analogues.

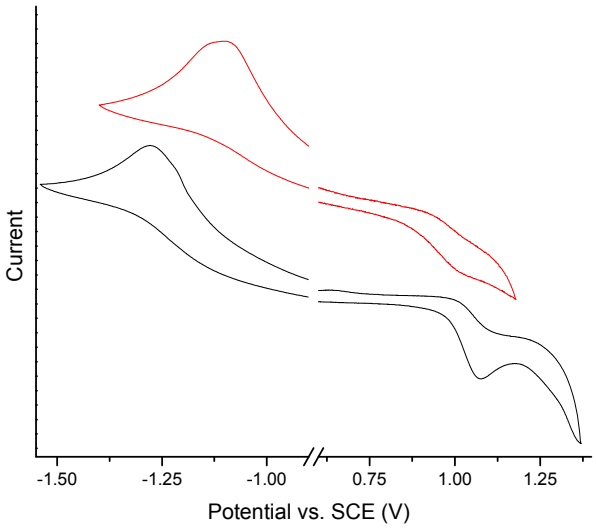

Figure IV-4. Cyclic voltammogram of **IV-8** (black) and **IV-13** (red) measured in anhydrous and deaerated dichloromethane at a scan rate of 100 mV/sec with 0.1 M Bu_4NPF_6 of supporting electrolyte.

Similar to other aryl azomethines and heterocycles, the comonomers studied were oxidized irreversibly owing to the high reactivity of the produced radical cation. The reactivity was exploited for radical cation homo-coupling analogous to other heterocycles, resulting in anodically produced films deposited on an ITO electrode. In comparison, homoaryl azomethine comonomers and their corresponding polymers decompose under similar anodic conditions. The bathochromic absorptions of the deposited film relative to the corresponding comonomers (Table IV-3) confirm the anodically produced product is more conjugated arising from α-α homo-coupling. The conjugated nature of the deposited

material is supported further by the measured oxidation potentials of the deposited films that are cathodically shifted by ca. 300 mV relative to the corresponding comonomers as seen in Figure IV-4. Even though substantially lower oxidation potentials (E_{pa}) of the coupled products relative to their monomers are expected, the increased number of ester electron withdrawing groups found in the homo-coupled products counteract any lowering of the E_{pa} that would otherwise be gained from an increase in the degree of conjugation.[66] Furthermore, radical cation formation of the polymer films derived from **IV-6**-**IV-8** occurs at much lower desired values ($\leq$ 800 mV) while that for **IV-9** and other polyazomethines occurs at $\geq$ 1.0 V. The unsymmetric comonomers are therefore advantageous because their anodically coupled products can be oxidized at lower potentials than their analogues.

Given the unsymmetric nature of the compounds, both *head-to-head* and *head-to-tail* homo-coupled products are expected. The spectroscopic and electrochemical data nonetheless provide evidence of anodic coupling of the azomethine derived comonomers. These represent the first examples of homo-coupled azomethine co-monomers consisting of various heterocycles. The different sequence of heterocycles in the comonomers additionally offers the means to tailor not only the E_{pa}, but also the E_g that can be modulated by 50 kJ/mol. The spectroscopic data also confirm that **IV-6** and **IV-7** have an average degree of polymerization of 6 and 3, respectively, derived from the absorption shifts as a function of the reciprocal degree of conjugation.[31] The low degree of polymerization is responsible for the irreversible oxidation of the anodically produced films

while reversible radical cation is expected with higher molecular weight products. This notwithstanding, the E_{pa} at which the radical cation occurs can be modulated by the heterocycle sequence in the comonomer while more cathodic potentials are possible with the anodically coupled products relative to their corresponding comonomers. Meanwhile the electrochemical data confirm that both the comonomers and the resulting coupled products can be mutually oxidized and reduced conferring upon them n- and p-doping properties. This implies the coupled products and their corresponding comonomers can act as mutual charge injectors and acceptors. This is in contrast to their analogues **IV-5** and **IV-10** that can be exclusively oxidized at low potentials and therefore can only be used as hole injection materials.

Table IV-3. Spectroscopic and cyclic voltammetry values for comonomers and their corresponding polymers.

Compound	Abs (nm)[a]	E_{pa}^{1} (V)[b]	E_{pc}^{1} (V)[c]	HOMO (eV)[d]	LUMO (eV)[d]	E_g[e]
IV-6	457	1.1	-1.3	5.4	3.1	2.3
IV-7	420	1.0	-1.2	5.3	3.2	2.1
IV-8	452	1.1	-1.3	5.4	3.1	2.3
IV-9	440	1.0	-1.3	5.3	3.1	2.2
IV-10[f]	407	0.9	-	5.2	2.6	2.6
IV-11	483	0.7	-1.1	5.0	3.3	1.7
IV-12	455	0.8	-1.3	5.1	3.1	2.0
IV-13	477	1.0	-1.1	5.3	3.3	2.0
IV-14[g]	466	0.9	-1.0	5.2	3.4	1.8

[a] Absorbance on ITO electrode except for **IV-6**-**IV-8** measured in acetonitrile. [b] Oxidation potential. [c] Reduction potential. [d] Relative to vacuum level. [e] Electrochemical HOMO-LUMO energy gap. [f] From Jérôme *et al*.[49, 67] [g] From Bourgeaux *et al*.[26, 27]

Conclusion

In conclusion, we presented the first examples of unsymmetric π-rich conjugated comonomers consisting of thiophene, pyrrole, and furan heterocycles. The versatility of the diaminothiophene **IV-1** to condense selectively with a variety of heteroaryl aldehydes leading to unsymmetric comonomers consisting of different heteroaryl units was possible.

This provides a general coupling route for innovative conjugated analogues with tunable photophysical and electrochemical properties. The simple azomethine connections formed during the preparation of these compounds are hydrolytically and reductively robust. The azomethines however can be oxidized and reduced to their radical ion intermediates leading to mutual p- and n-dopable functional materials. The anodically coupled products exhibited more cathodic E_{pa} confirming their increased degree of conjugation compared to their corresponding comonomers. Furthermore, tunability of the E_{pa} in the anodically produced products is possible via different heterocycles. Despite undergoing a shift from IC to ISC, the rapid and efficient self-quenching of the triplet state afford pristine emission while the fluorescence yield can be controlled by external parameters such as temperature.

Experimental Section

Synthesis

2,5-Diamino-thiophene-3,4-dicarboxylic acid diethyl ester (IV-1). The synthesis was done according to previous reports.[40]

Diethyl 2-((furan-2-yl)methyleneamino)-5-aminothiophene-3,4-dicarboxylate (IV-15). **IV-2** (37 mg, 0.39 mmol) and **IV-1** (100 mg, 0.39 mmol) were mixed in anhydrous isopropanol with a catalytic amount of TFA and refluxed for 12 hours. The reaction was then purified by flash chromatography (SiO_2) eluted with hexanes/ethylacetate (90/10) up to hexanes/ethylacetate (60/40) to afford 110 mg (85%) of a brownish yellow

solid. M.p.: 151-153 °C. ^{1}H-NMR (acetone-d_6): δ = 7.92 (s, 1H), 7.75 (d, 1H, J = 1.3 Hz), 7.50 (s, NH_2), 6.97 (d, 1H, J = 3.4 Hz), 6.63 (dd, 1H, ^{3}J = 3.4 Hz and 1.6 Hz). ^{13}C-NMR (acetone-d_6): δ = 165.0, 164.3, 161.1, 152.6, 146.1, 140.7, 133.3, 130.8, 115.3, 112.8, 102.0, 61.0, 60.0, 14.1, 14.1. HRMS(+) calculated for $[C_{15}H_{16}N_2O_5S+H]^+$: 337.08527 found 337.08535.

Diethyl 2-((thiophen-2-yl)methyleneamino)-5-aminothiophene-3,4-dicarboxylate (IV-17). In a 50 mL round bottom flask was added **IV-1** (50 mg, 0.19 mmol) in absolute ethanol (20 mL) to which was added **IV-3** (24 mg, 0.21 mmol) and a catalytic amount of trifluoroacetic acid (TFA). The mixture was refluxed for 20 hours under normal atmosphere. Complete removal of the solvent led to an orange solid which was purified by flash chromatography (SiO_2) and eluted with hexanes/ethylacetate (80 % / 20 %). The product was isolated as an orange solid (81 %). M.p.: 114-116 °C. ^{1}H-NMR (acetone-d_6): δ = 8.24 (s, 1H), 7.63 (d, 1H, J = 5.0Hz), 7.52 (dd, 1H, J = 3.7 Hz and J = 0.7 Hz), 7.48 (s, 2H), 7.14 (dd, 1H, J = 5.0 Hz and 3.7 Hz), 4.32 (q, 2H, J = 7.2 Hz), 4.19 (q, 2H, J = 7.1 Hz), 1.37 (t, 3H, J = 7.1 Hz), 1.26 (t, 3H, J = 7.1 Hz). ^{13}C-NMR (acetone-d_6): δ = 165.0, 164.3, 161.1, 161.0, 146.1, 143.2, 132.8, 132.1, 130.5, 128.4, 101.8, 61.0, 60.0, 14.3, 14.1. HRMS(+) calculated for $[C_{15}H_{16}O_4N_2S_2+H]^+$: 353.06242, found: 353.06251.

Diethyl 2-((1-methyl-1H-pyrrol-2-yl)methyleneamino)-5-((thiophen-2-yl)methyleneamino)thiophene-3,4-dicarboxylate (IV-6). In a 50 mL round bottom flask was added **IV-4** (40 mg, 0.37 mmol) dissolved in anhydrous toluene (25 mL) to which was subsequently added DABCO (159 mg, 1.42 mmol), $TiCl_4$ 1.0 M solution in toluene (0.28 mL, 0.28 mmol) at 0 ^oC and then **IV-17** (100 mg, 0.28 mmol) was added. The mixture was then refluxed for 4 hours after which the solvent was removed. Purification by flash chromatography (SiO_2) with ether/hexanes (30/70), switched to hexanes/ethylacetate (70/30) and then increased up to hexanes/ethylacetate (50/50) to yield the title product as a red solid (63 mg, 50%). M.p.: 112-114 °C. ^{1}H-NMR (acetone-d_6): δ = 8.68 (s, 1H), 8.35 (s,1H), 7.80 (d, 1H, *J* = 4.9 Hz), 7.72 (d, 1H, *J* = 3.7 Hz), 7.23 (dd, 1H, *J* = 4.9 Hz and 3.7 Hz), 7.14 (m, 1H), 6.87 (q, 1H, *J* = 4.0 Hz and 1.8 Hz), 6.24 (q, 1H, *J* = 4.0 Hz and 2.5 Hz), 4.32 (q, 2H, *J* = 7.0 Hz), 4.28 (q, 2H, *J* = 7.2 Hz), 4.07 (s, 3H), 1.37 (t, 3H, *J* = 7.1 Hz), 1.31 (t, 3H, *J* = 7.0 Hz). ^{13}C-NMR (acetone-d_6): δ = 163.5, 163.0, 152.2, 152.2, 150.3, 146.6, 142.6, 134.5, 132.6, 132.6, 129.9, 128.9, 128.8, 124.9, 122.4, 110.1, 61.1, 61.0, 37.0, 14.2, 14.0. HRMS(+) calculated for $[C_{21}H_{21}N_3O_4S_2+H]^+$: 444.10462 found 444.10396.

Diethyl 2-((furan-2-yl)methyleneamino)-5-((thiophen-2-yl)methyleneamino) thiophene-3,4-dicarboxylate (IV-7). In a 50 mL round bottom flask was added **IV-3** (27 μL, 0.29 mmol) dissolved in anhydrous toluene (25 mL) to which was subsequently added DABCO (125 mg, 1.11 mmol), $TiCl_4$ 1.0 M solution in toluene (0.29 mL,

0.29 mmol) at 0 ^{o}C and then **IV-15** (75 mg, 0.22 mmol) was added. The mixture was then refluxed for 4 hours after which the solvent was then removed. Purification by flash chromatography (SiO_2) with ether/hexanes (50/50) and 1% triethylamine, switched to hexanes/ethylacetate (70/30) and then increased up to hexanes/ethylacetate (50/50) with 1% NEt_3 to yield the title product as a red solid (79 mg, 83%). M.p.: 133-135 °C. ^{1}H-NMR (acetone-d_6): δ = 8.75 (s, 1H), 8.38 (s,1H), 7.89 (d, 1H, J = 1.4 Hz), 7.85 (d, 1H, J = 5.0 Hz), 7.77 (dd, 1H, J = 3.8 Hz and 0.8 Hz), 7.25 (q, 1H, J = 5.0 Hz and 3.7 Hz), 7.24 (d, 1H, J = 3.6 Hz), 6.73 (dd, 1H, J = 3.5 Hz and 1.8 Hz), 4.32 (q, 2H, J = 7.1 Hz), 4.30 (q, 2H, J = 7.1 Hz), 1.36 (t, 3H, J = 7.2 Hz), 1.33 (t, 3H, J = 7.2 Hz). ^{13}C-NMR (acetone-d_6): δ = 163.0, 153.7, 152.1, 149.5, 147.9, 147.7, 146.1, 142.4, 140.6, 135.1, 133.2, 128.9, 127.8, 127.3, 119.0, 113.4, 61.2, 61.2, 14.2, 14.0. HRMS(+) calculated for $[C_{20}H_{18}N_2O_5S_2+H]^{+}$: 431.07299 found 431.07201.

Diethyl 2-((1-methyl-1H-pyrrol-2-yl)methyleneamino)-5-((furan-2-yl) methyleneamino)thiophene-3,4-dicarboxylate (IV-8). In a 50 mL round bottom flask was added **IV-4** (32 mg, 0.29 mmol) dissolved in anhydrous toluene (25 mL) to which was subsequently added DABCO (125 mg, 1.11 mmol), $TiCl_4$ 1.0 M solution in toluene (0.29 mL, 0.29 mmol) at 0 ^{o}C and then **IV-15** (75 mg, 0.22 mmol) was added. The mixture was then refluxed for 4 hours after which the solvent was removed. Purification by flash chromatography (SiO_2) with ether/hexanes (30/70) and 1% triethylamine, switched to hexanes/ethylacetate (70/30) and then increased up to hexanes/ethylacetate (50/50) with

1 % NEt_3 to yield the title product as a red solid (45 mg, 47%). M.p.: 110-114 °C. ^{1}H-NMR (acetone-d_6): δ = 8.36 (s, 1H), 8.33 (s,1H), 7.86 (d, 1H, *J* = 1.5 Hz), 7.20 (d, 1H, *J* = 3.5 Hz), 7.14 (m, 1H), 6.88 (q, 1H, *J* = 3.9 Hz and 1.5 Hz), 6.71 (q, 1H, *J* = 3.6 Hz and 1.8 Hz), 6.25 (q, 1H, *J* = 3.9 Hz and 2.6 Hz), 4.31 (q, 2H, *J* = 7.1 Hz), 4.28 (q, 2H, *J* = 7.2 Hz), 4.09 (s, 3H), 1.34 (t, 3H, *J* = 7.0 Hz), 1.31 (t, 3H, *J* = 7.0 Hz). ^{13}C-NMR (acetone-d_6): δ = 163.5, 163.0, 152.5, 152.3, 150.4, 147.6, 146.9, 146.3, 132.7, 129.9, 129.2, 124.9, 122.4, 118.3, 113.3, 110.1, 61.1, 61.0, 37.0, 14.1, 14.0. HRMS(+) calculated for $[C_{21}H_{21}N_3O_5S+H]^+$: 428.12747 found 428.12668.

Crystal Structure Determination

Diffraction data for **IV-6** was collected on a diffractometer using graphite-monochromatized CuK\α radiation with 1.54178 Å. The structures were solved by direct methods (SHELXS97). All non-hydrogen atoms were refined based on Fobs2 (SHELXS97), while hydrogen atoms were refined on calculated positions with fixed isotropic U, using riding model techniques.

Diffraction data for **IV-8** was collected on a Bruker FR591 diffractometer using graphite-monochromatized CuK\α radiation with 1.54178 Å. The structures were solved by direct methods (SHELXS97). All non-hydrogen atoms were refined based on Fobs2 (SHELXS97), while hydrogen atoms were refined on calculated positions with fixed isotropic U, using riding model techniques.

Table IV-4. Details of crystal structure determination for **IV-8**.

Formula	$C_{21}H_{21}N_3O_5S$
Mw (g/mol); F(000)	427.47 g/mol ; 896
Crystal color and form	Red plate
Crystal size (mm)	0.15 x 0.09 x 0.05
T (K); $d_{calcd.}$ (g/cm^3)	150 (2) ; 1.407
Crystal System	Monoclinic
Space Group	$P2_1/c$
Unit Cell: a (Å)	15.041 (3)
b (Å)	7.5421 (15)
c (Å)	18.827 (4)
α (°)	90.000
β (°)	109.17 (3)
γ (°)	90.000
V (Å^3); Z	2017.4 (8) ; 4
θ range (°); completeness	3.11 – 72.07 ; 0.960
Reflections: collected / independent; R_{int}	19643 / 3816 ; 0.147
μ (mm^{-1}) Abs. Corr.	1.767 Semi-empirical
R1(F); wR(F^2) [$I > 2\sigma(I)$]	0.0775; 0.1560
R1(F); wR(F^2) (all data)	0.1529; 0.1875
GoF(F^2)	0.955
Max. residual e^- density	-0.504 $e^-\cdot$Å^{-3}

Acknowledgements

The authors acknowledge financial support from the Natural Sciences and Engineering Research Council Canada, and the Centre for Self-Assembled Chemical Structures. Appreciation is extended Prof. D. Zargarian for helpful discussions and to Joao-Nicolas Blair-Pereira. S.D. thanks the Université de Montréal for a graduate scholarship.

Supporting Information Available

^{1}H and ^{13}C spectra of **IV-6-IV-8**, **IV-15**, and **IV-17**, absorption and emission spectra of **IV-6-IV-8**, cyclic voltammograms of **IV-6-IV-8** and **IV-11-IV-13**, and CIF for **IV-7** and **IV-8**. This material is available free of charge via the Internet at http://pubs.acs.org.

References

1. Veinot, J. G. C.; Marks, T. J. *Acc. Chem. Res.* **2005**, *38*, 632-643.

2. Perepichka, I. F.; Perepichka, D. F.; Meng, H.; Wudl, F. *Adv. Mater.* **2005**, *17*, 2281-2305.

3. Leclerc, M. *J. Polym. Sci. Part A: Polym. Chem.* **2001**, *17*, 2867-2873.

4. Williams, E. L.; Haavisto, K.; Li, J.; Jabbour, G. E. *Adv. Mater.* **2007**, *19*, 197-202.

5. Parthasarathy, G.; Liu, J.; Duggal, A. R. *Electrochem. Soc. Interface* **2003**, *12*, 42-47.

6. Mitschke, U.; Bauerle, P. *J. Mater. Chem.* **2000**, *10*, 1471-1507.

7. Kraft, A.; Grimsdale, A. C.; Holmes, A. B. *Angew. Chem. Int. Ed.* **1998**, *37*, 402-428.

8. Ton-That, C.; Stockton, G.; Phillips, M. R.; Nguyen, T.-P.; Huang, C. H.; Cojocaru, A. *Polym. Int.* **2008**, *57*, 496-501.

9. Gratzel, M. M., Jacques-E. *Electr. Transf. Chem.* **2001**, 589-644.

10. Segura, J. L.; Martín, N.; Guldi, D. M. *Chem. Soc. Rev.* **2005**, *34*, 31-47.

11. Smith, G. B. *Sol. Energy Mater. Sol. Cells* **2004**, *84*, 395-409.

12. Horowitz, G. *Adv. Mater.* **1998**, *10*, 365-377.

13. Katz, H. E.; Dodabalapur, A.; Bao, Z. In *Handbook of Oligo- and Polythiophenes*; Fichou, D., Ed.; Wiley-VCH Verlag GmbH: Weinheim, Germany, 1999, p 459-489.

14. Kraft, A. *Chem. Phys. Chem.* **2001**, *2*, 163-165.

15. Mikroyannidis, J. A.; Barberis, V. P. *J. Polym. Chem. A Polym. Chem.* **2007**, *45*, 1481-1491.

16. Hu, Z.-Y.; Fort, A.; Barzoukas, M.; Jen, A. K. Y.; Barlow, S.; Marder, S. R. *J. Phys. Chem. B* **2004**, *108*, 8626-8630.

17. Turbiez, M.; Frere, P.; Roncali, J. *Tetrahedron* **2005**, *61*, 3045-3053.

18. Jenkins, I. H.; Rees, N. G.; Pickup, P. G. *Chem. Mater.* **1997**, *9*, 1213-1216.

19. Hughes, G.; Bryce, M. R. *J. Mater. Chem.* **2005**, *15*, 94-107.

20. Moliton, A.; Hiorns, R. C. *Polym. Int.* **2004**, *53*, 1397-1412.

21. Ng, S. C.; Chan, H. S. O.; Wong, P. M. L.; Tan, K. L.; Tan, B. T. G. *Polymer* **1998**, *39*, 4963-4968.

22. Yang, C.-J.; Jenekhe, S. A. *Macromolecules* **1995**, *28*, 1180-1196.

23. Thomas, O.; Inganäs, O.; Andersson, M. R. *Macromolecules* **1998**, *31*, 2676-2678.

24. Hansford, K. A.; Guarin, S. A. P.; Skene, W. G.; Lubell, W. D. *J. Org. Chem.* **2005**, *70*, 7996 -8000.

25. Dufresne, S.; Hanan, G. S.; Skene, W. G. *J. Phys. Chem. B* **2007**, *111*, 11407-11418.

26. Bourgeaux, M.; Perez Guarin, S. A.; Skene, W. G. *J. Mater. Chem.* **2007**, *17*, 972-979.

27. Pérez Guarìn, S. A.; Bourgeaux, M.; Dufresne, S.; Skene, W. G. *J. Org. Chem.* **2007**, *72*, 2631-2643.

28. Dufresne, S.; Bourgeaux, M.; Skene, W. G. *J. Mater. Chem.* **2007**, *17*, 1166-1177.

29. Bourgeaux, M.; Skene, W. G. *Macromolecules* **2007**, *40*, 1792-1795.

30. Pérez Guarìn, S. A.; Dufresne, S.; Tsang, D.; Sylla, A.; Skene, W. G. *J. Mater. Chem.* **2007**, *17*, 2801-2811.

31. Pérez Guarìn, S. A.; Skene, W. G. *Mater. Lett.* **2007**, *61*, 5102-5106.

32. Gewald, V. K.; Kleinert, M.; Thiele, B.; Hentschel, M. *J. Prak. Chem.* **1972**, *314*, 303-314.

33. Gewald, K.; Gruner, M.; Hain, U.; Süptitz, G. *Monats. Chem.* **1988**, *119*, 985-992.

34. Yang, C.-J.; Jenekhe, S. A. *Chem. Mater.* **1991**, *3*, 878-887.

35. Suematsu, K.; Nakamura, K.; Takeda, J. *Colloid. Polym. Sci.* **1983**, *261*, 493-501.

36. Morgan, P. W.; Kwolek, S. L.; Pletcher, T. C. *Macromolecules* **1987**, *20*, 729-739.

37. Brovelli, F.; Rivas, B. L.; Bernede, J. C. *J. Chilean Chem. Soc.* **2005**, *50*, 597-602.

38. Tsai, F.-C.; Chang, C.-C.; Liu, C.-L.; Chen, W.-C.; Jenekhe, S. A. *Macromolecules* **2005**, *38*, 1958-1966.

39. Kiriy, N.; Bocharova, V.; Kiriy, A.; Stamm, M.; Krebs, F. C.; Adler, H.-J. *Chem. Mater.* **2004**, *16*, 4765-4771.

40. Bourgeaux, M.; Vomscheid, S.; Skene, W. G. *Synth. Commun.* **2007**, *37*, 3551-3558.

41. Ono, T.; Fujii, S.; Nobori, T.; Lehn, J.-M. *Chem. Commun.* **2007**, 4360-4362.

42. Giuseppone, N.; Lehn, J.-M. *Chem. Eur. J.* **2006**, *12*, 1723-1735.

43. Wuts, P. G. M.; Greene, T. W. *Greene's Protective Groups in Organic Synthesis*; 4th ed.; Wiley-Interscience, 2007.

44. Van Der Looy, J. F. A.; Thys, G. J. H.; Dieltiens, P. E. M.; De Schrijver, D.; Van Alsenoy, C.; Geise, H. J. *Tetrahedron* **1997**, *53*, 15069-15084.

45. An appropriate analogue for directly comparison would be diethyl ester substituted in position 3 and 4. However, no examples of such a compound are reported.

46. Skene, W. G.; Dufresne, S. *Org. Lett.* **2004**, *6*, 2949-2952.

47. Seixas de Melo, J. E., Fausto; Becker, Ralph S. *J. Chem. Phys.* **2002**, *117*, 4428-4435.

48. Wasserberg, D.; Marsal, P.; Meskers, S. C. J.; Janssen, R. A. J.; Beljonne, D. *J. Phys. Chem. B* **2005**, *109*, 4410-4415.

49. Jérôme, C.; Maertens, C.; Mertens, M.; Jérôme, R.; Quattrocchi, C.; Lazzaroni, R.; Brédas, J. L. *Synth. Met.* **1996**, *83*, 103-109.

50. Apperloo, J. J.; Martineau, C.; Hal, P. A. v.; Roncali, J.; Janssen, R. A. J. *J. Phys. Chem. A* **2002**, *106*, 21-31.

51. Ginocchietti, G.; Galiazzo, G.; Mazzucato, U.; Spalletti, A. *Photochem. Photobiol. Sci.* **2005**, *4*, 547-553.

52. Frère, P.; Raimundo, J.-M.; Blanchard, P.; Delaunay, J.; Richomme, P.; Sauvajol, J.-L.; Orduna, J.; Garin, J.; Roncali, J. *J. Org. Chem.* **2003**, *68*, 7254-7265.

53. Becker, R. S.; Seixas de Melo, J.; Maçanita, A. L.; Elisei, F. *J. Phys. Chem.* **1996**, *100*, 18683-18695.

54. Tsang, D.; Bourgeaux, M.; Skene, W. G. *J. Photochem. Photobiol. A* **2007**, *192*, 122-129.

55. Kobrak, M. N.; Bittner, E. R. *Phys. Rev. B* **2000**, *62*, 11473-11486.

56. Dufresne, S.; Bourgeaux, M.; Skene, W. G. *Acta Cryst.* **2006**, *E62*, o5602-o5604.

57. Skene, W. G.; Dufresne, S.; Trefz, T.; Simard, M. *Acta Cryst.* **2006**, *E62*, o2382–o2384.

58. Skene, W. G.; Dufresne, S. *Acta Cryst.* **2006**, *E62*, o1116-o1117.

59. Iovu, M. C.; Jeffries-El, M.; Zhang, R.; Kowalewski, T.; McCullough, R. D. *J. Macromol. Sci. A Pure Appl. Chem.* **2006**, *43*, 1991-2000.

60. Iovu, M. C.; Jeffries-El, M.; Sheina, E. E.; Cooper, J. R.; McCullough, R. D. *Polymer* **2005**, *46*, 8582-8586.

61. Sheina, E. E.; Khersonsky, S. M.; Jones, E. G.; McCullough, R. D. *Chem. Mater.* **2005**, *17*, 3317-3319.

62. Pan, H.; Liu, P.; Li, Y.; Wu, Y.; Ong, B. S.; Zhu, S.; Xu, G. *Adv. Mater.* **2007**, *19*, 3240-3243.

63. Roncali, J.; Thobie-Gautier, C. *Adv. Mater.* **1994**, *6*, 846-848.

64. Dufresne, S.; Skene, W. G. *Acta Cryst.* **2008**, *E64*, 1.

65. Lide, D. R. *Handbook of Chemistry & Physics*; 88 ed.; Taylor & Francis CRC, 2007.

66. We demonstrated previously with 3,4-dialkylated comonomers that α-α coupling is produced exclusively. See ref. 31.

67. Jérôme, C.; Maertens, C.; Mertens, M.; Jérôme, R.; Quattrocchi, C.; Lazzaroni, R.; Brédas, J. L. *Synth. Met.* **1997**, *84*, 163-164.

V. CHAPITRE V

Opto-Electronic Property of Conjugated Heterocyclic Azomethines – The effect of Pyrrole, Thiophene and Furans

*Stéphane Dufresne and W. G. Skene**

Département de Chimie, Pavillon J. A. Bombardier, Université de Montréal, CP 6128, succ. Centre-ville, Montréal, Québec, CANADA, H3C 3J7.

* corresponding author

Accepted May 10, 2011 in J. Phys. Org. Chem.

Abstract

A series of *de novo* symmetric and unsymmetric heterocyclic azomethine dyads and triads consisting of furans, thiophenes, pyrroles, and methyl-pyrroles were prepared. These were for investigating the effect of various heterocycles and the degree of conjugation on the spectroscopic and electrochemical properties. It was found that for a similar series, bathochromic absorbance and fluorescence shifts occurred when progressing in the order of furan < thiophene < pyrrole ≈ methyl-pyrrole. Meanwhile the spectroscopic properties of the heterocyclic azomethines were bathochromically shifted relative to their homoaryl analogues as a result of increased degree of conjugation and electronic effects. The former was confirmed by crystallographic studies showing the heterocycles adopted co-planar and anti-parallel arrangements. Although all the compounds studied showed no fluorescence at room temperature, their fluorescence could be restored at low temperatures, implying deactivation of the singlet excited manifold by bond rotation. Meanwhile, irreversible oxidation was observed for all the azomethines studied and their oxidation potentials were contingent on the heterocycle and number of azomethines, ranging between 0.8 and 1.4 V. The irreversible oxidation was due to radical cation cross-coupling resulting in products with higher degrees of conjugation. Anodic product formation was confirmed both electrochemically and spectroscopically in addition to by mass spectrometry.

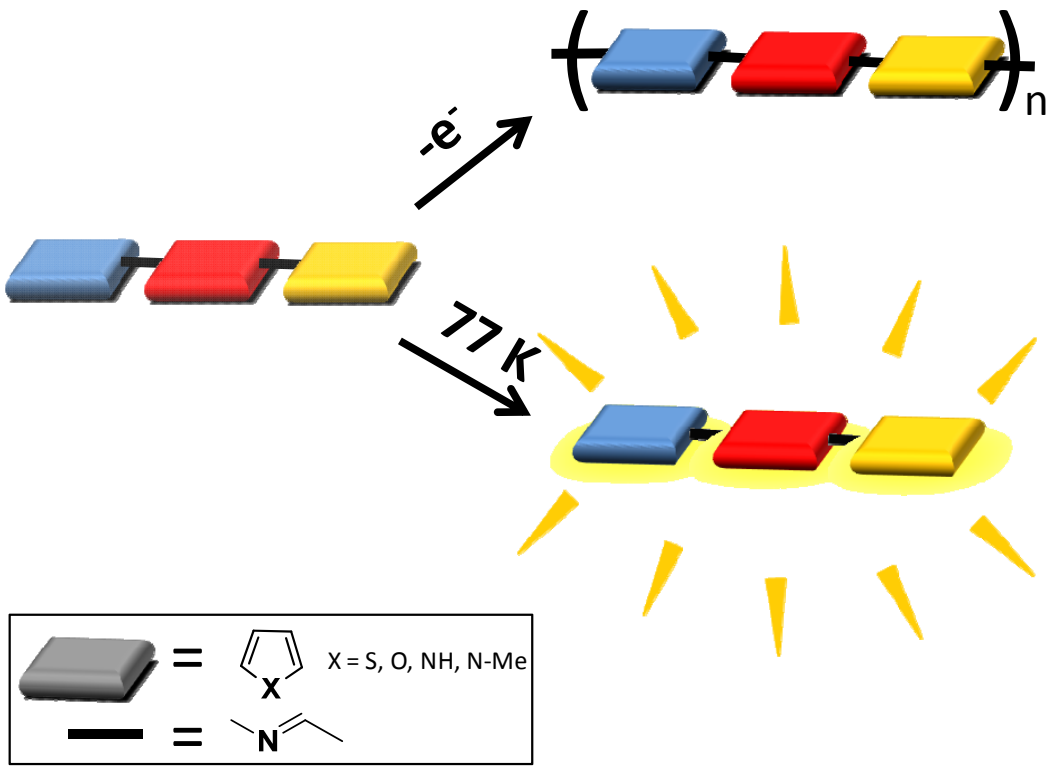
-é
n
77 K
X = S, O, NH, N-Me
X
N

Introduction

Conjugated materials have found uses in organic devices including light emitting diodes, photovoltaics, and field effect transistors.[1-3] This is in part owing to their opto-electronic properties that are compatible with such devices. While these materials are prepared from aryl-aryl coupling protocols, property enhancements resulting in increased device efficiencies are possible by incorporating vinylene linkages.[4, 5] These unsaturated connection units are understood to prevent rotation around the aryl-aryl axis leading to increased planarity. Despite the enhanced opto-electronic properties possible with vinylene derivatives, their preparation requires stringent reaction conditions.[6-8] They additionally produce substantial mass amounts of unwanted by-products relative to the desired products, requiring extensive purification for achieving optimal properties and device performance.

Azomethines (-N=CH-) are attractive alternatives to vinylene linkages in part owing to their straightforward preparation that does not requiring stringent reaction conditions.[9] Moreover, they are isoelectronic to their carbon counterparts.[10] Even though azomethines are synthetically more attractive than their vinylene counterparts, they have not been pursued as replacement functional materials for their carbon counterparts. This is a result of previously studied materials that exhibited limited properties.[11-14] It is also generally accepted that azomethines are hydrolytically, oxidatively, and reductively unstable in addition to being acid sensitive, precluding their use as functional materials in working devices.[15-17] Some property improvements are possible with homoarylazomethines.[11, 18] However, their opto-electronic properties are not comparable to their vinylene analogues. This is a results of inherent twisting around the aryl-azomethine bonds that limits their

degree of conjugation.[10, 19-27] Enhanced azomethine opto-electronic properties comparable to their vinylene analogues are however possible with thiophene derivatives.[6, 7, 28] This is in part a result of coplanarization of the thiophene-azomethine moieties. This leads to higher degrees of conjugation relative to the homoaryl azomethines, resulting in delocalization of the heterocyclic electronic effects across the entire conjugated framework.

Although enhanced properties are possible with azomethines prepared exclusively with thiophenes, the resulting opto-electronic properties with other heterocycles have not been assessed beyond our seminal investigation of unsymmetric systems.[29] We were therefore incited to investigate the effect of different heterocycles on the electrochemical and photophysical properties of symmetric and unsymmetric heterocyclic azomethines. This is of particular interest for gaining important understanding of azomethine structure/property relationships and for the design and preparation of new functional materials with enhanced properties for potential use in devices. To this means, dyad and triad model compounds (Chart V-1) consisting of one and two azomethines, respectively, were prepared consisting uniquely of furans, pyrroles, and thiophenes and a central thiophene. Both symmetric and unsymmetric derivatives of these model compounds were prepared in addition to their corresponding homoraryl counterparts for further understanding the heterocyclic effects on the opto-electronic properties. In particular, the absorbance, fluorescence and fluorescence quantum yields contingent on structure were examined. These were complemented by examining the anodic behaviour of the azomethines and for gaining insight into their oxidation processes for preparing anodically coupled products. The preparation, photophysical, crystallographic, and electrochemical properties of the *de novo* conjugated heterocyclic azomethines are herein presented for

illustrating the robustness of heterocyclic azomethines and the enhanced properties possible with conjugated heteroatomic and heterocyclic compounds.

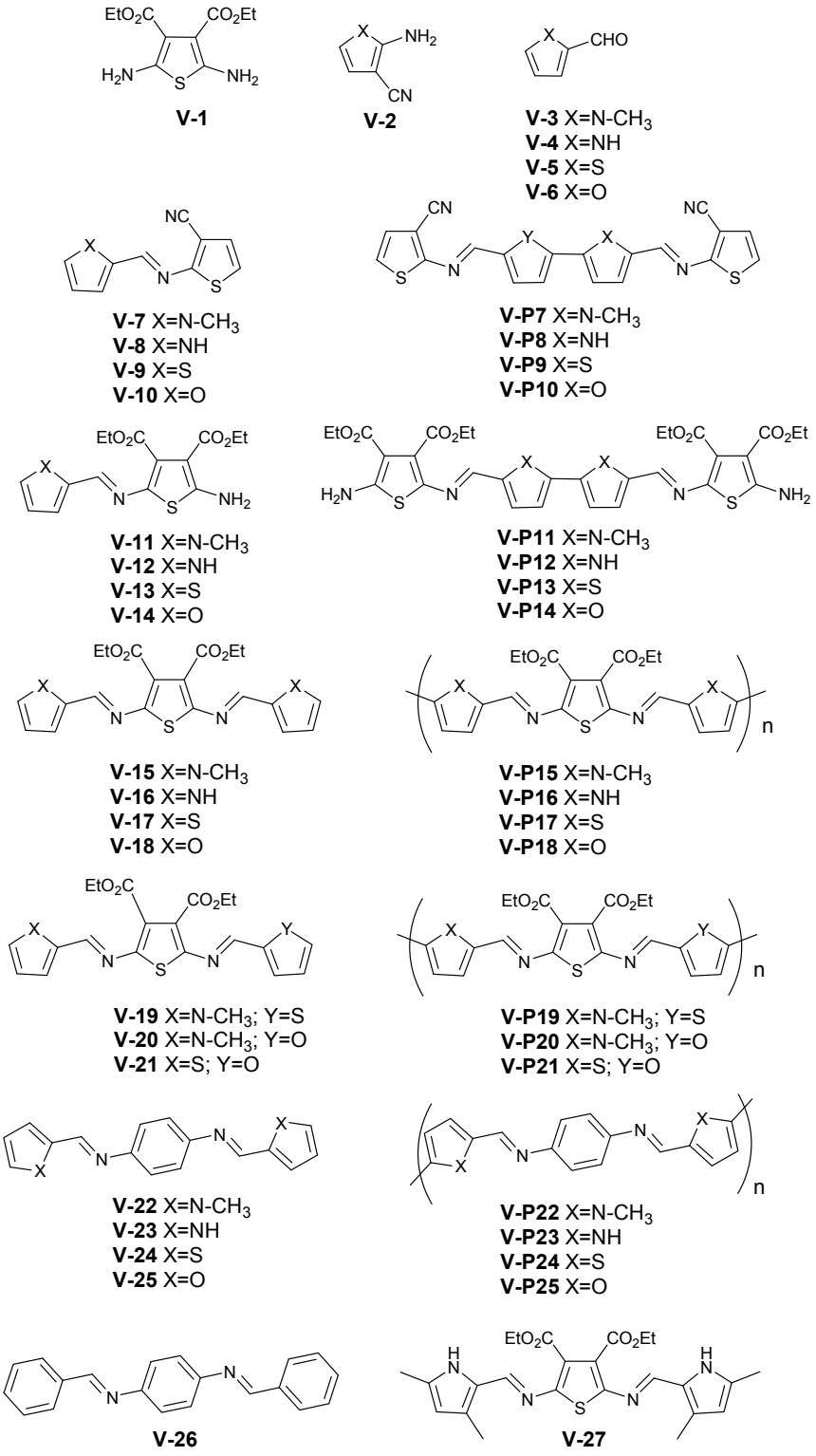

Chart V-1. Heterocyclic azomethines, representative homoaryl analogues and anodically coupled products prepared and investigated.

Experimental Section

Materials and general methods

All chemicals were commercially available from Aldrich including **V-3**-**V-6** and were used as received unless otherwise stated. Anhydrous and deaerated solvents were obtained with a Glass Contour solvent purification system. ^{1}H-NMR and ^{13}C-NMR spectra were recorded on a Bruker 400 MHz spectrometer with the appropriate deuterated solvents.

Spectroscopic methods

The absorption measurements were done on a Cary-500 spectrometer while the fluorescence studies were performed on an Edinburgh Instruments FLS-920 fluorimeter after deaerating the samples thoroughly with nitrogen for 20 minutes. Fluorescence quantum yields were measured with samples of low sample concentration (10^{-5} M) in dichloromethane excited close to their maximum absorption wavelength relative to bithiophene (ϕ_f = 0.013). Phosphorescence measurements were done on a Cary Eclipse at 77 K in a 4:1 ethanol/methanol solvent. The same matrix was used for low temperature fluorescence measurements.

Electrochemical methods

Cyclic voltammetric measurements were performed on a Bio Analytical Systems EC Epsilon potentiostat. Compounds were dissolved in anhydrous and deaerated dichloromethane at 10^{-4} M with NBu_4PF_6 in sufficient concentration in order to achieve

highly conductive solutions. A platinum electrode was used as auxiliary and working electrodes, while a saturated Ag/AgCl electrode was used as the reference electrode.

Crystal Structure Determination

Diffraction data for **V-20** were collected on a Bruker FR591 diffractometer using graphite-monochromatized CuK\α radiation with 1.54178 Å. The structures were solved by direct methods (SHELXS97). All non-hydrogen atoms were refined based on Fobs2 (SHELXS97), while hydrogen atoms were refined on calculated positions with fixed isotropic U, using riding model techniques.

Experimental for polymers

Single sided ITO coated plates were purchased from Delta Technologies (R_S = 5-10 Ω. These were cut into rectangular shapes and were used as the working electrode. The substrates were used after cleaning with standard washing protocols with water, acetone and dichloromethane for 20 minutes followed by ultrasonication. The cross-coupled products were electrochemically deposited onto the ITO Corning 1737 plates by 50 repeated anodic scans ranging from 0 to 1.4 V at 100 mV/sec. Alternatively, the anodic coupling was done by applying an anodic potential 100 mV greater than the corresponding radical cation and held at the potential for 10 minutes. A final potential of -100 mV was applied for 2 minutes for ensuring the resulting products were in the neutral form.

Sufficient material of the anodically coupled product for standard polymer characterization methods was obtained according to the experimental procedures described

above with the exception of the working electrode. The button platinum working electrode was replaced by a large area platinum mesh gauze. Several mg of **19** were dissolved in anhydrous dichloromethane (75 mL) and a potential 100 mV greater than its first E_{pa} (i.e. 1.2 V) was applied for 20 minutes under a blanket of nitrogen followed. The precipitated products were neutralized for 2 minutes by applying a potential of -100 mV. The solvent was removed under reduced pressure and the resulting polymer was dissolved in a mixture of ethyl acetate/diethyl ether (50:50) and the residual NBu_4PF_6 was removed by filtration.

Synthesis

The preparation of **V-1-V-2**, **V-13-V-14, V-17** and **V-19-V-21** were done according to previously reported methods.[9, 29, 30]

2-((1-Methyl-1H-pyrrol-2-yl)methyleneamino)thiophene-3-carbonitrile (V-7). **V-3** (53 mg, 0.48 mmol) and **V-1** (60 mg, 0.48 mmol) were mixed in anhydrous isopropanol (20 mL) with a catalytic amount of trifluoroacetic acid (TFA) and then refluxed for 12 hours. The reaction mixture was concentrated in vacuo and the crude mixture was purified by flash chromatography eluted with hexanes/ethyl acetate (90/10) up to hexanes/ethyl acetate (60/40) to afford the product as a yellow solid (30 mg, 60%). M.p.: 116-118 °C. ^{1}H-NMR (acetone-d_6): δ = 8.47 (s, 1H), 7.28 (d, 1H, ^{3}J = 5.7 Hz), 7.21 (d, 1H, ^{3}J = 5.7 Hz), 7.19 (dd, 1H, ^{3}J = 2.0 Hz and ^{5}J = 1.8 Hz), 6.95 (dd, 1H, ^{3}J = 4.0 Hz and ^{5}J = 1.7), 6.27 (dd, 1H, ^{3}J = 4.0 Hz and ^{3}J = 2.1 Hz), 4.12 (s, 3Hz). ^{13}C-NMR (acetone-d_6): δ = 165.7, 151.6, 133.1, 129.5, 127.5, 122.9, 120.5, 115.1, 110.2, 104.0, 37.0. HRMS(+) calculated for $[C_{11}H_9N_3S+H]^+$: 216.05955 found 216.05889.

2-((1H-Pyrrol-2-yl)methyleneamino)thiophene-3-carbonitrile (V-8). In a 50 mL round bottom flask, **V-1** (60 mg, 0.48 mmol) was dissolved in isopropanol (20 mL). To this, was added with vigorous stirring, **V-4** (46 mg, 0.48 mmol) and a catalytic amount of TFA followed by refluxing for 12 hours. The title compound was isolated as a yellow powder (68 %) after purification by flash chromatography (SiO_2) eluted with hexanes/ethyl acetate (90/10) up to hexane/ethyl acetate (50/50). M.p.: 77-79 °C. ^{1}H-NMR (acetone-d_6): δ = 11.35 (s, NH), 8.45 (s, 1H), 7.29 (s, 1H, J = 1.8 Hz), 7.26 (d, 1H, J = 5.7 Hz), 7.19 (d, 1H, J = 5.7 Hz), 6.96 (t, 1H, J = 1.8 Hz), 6.37 (m, 1H, J = 1.8 Hz). ^{13}C-NMR (acetone-d_6): δ =

165.4, 151.2, 130.2, 127.8, 127.0, 120.6, 120.4, 115.1, 111.6, 103.5. HRMS(+) calculated for $[C_{10}H_7N_3S+H]^+$: 202.04334 found 202.04380.

2-[(Thiophen-2-ylmethylene)-amino]-thiophene-3-carbonitrile (V-9). **V-2** (50 mg, 0.40 mmol) and **V-5** (54 mg, 0.48 mmol) were mixed in anhydrous isopropanol (20 mL) with a catalytic amount of TFA and then refluxed for 20 hours. The reaction mixture was concentrated and then purified by flash chromatography eluted with hexanes/ethyl acetate (90 % / 10 % v/v) up to hexanes/ethyl acetate (60 % / 40 % v/v) to afford the product as an orange solid (61 mg, 70 %). M.p.: 58-60 °C. ^{1}H-NMR (acetone-d_6): δ = 8.49 (s, 1H), 7.90 (d, 1H, J = 5.0 Hz), 7.82 (dd, 1H, ^3J = 3.7 Hz and 1.0 Hz), 7.42 (d, 1H, J = 5.7 Hz), 7.26 (d, 1H, J = 5.6 Hz), 7.26 (dd, 1H, J = 4.8 Hz and J = 3.5 Hz). ^{13}C-NMR (acetone-d_6): δ = 163.4, 155.4, 141.8, 136.2, 133.9, 129.0, 128.1, 122.5, 114.6, 105.8. HRMS(+) calculated for $[C_{10}H_6N_2S_2+H]^+$: 219.00452, found: 219.00514.

2-((Furan-2-yl)methyleneamino)thiophene-3-carbonitrile (V-10). **V-6** (54 mg, 0.56 mmol) and **V-1** (70 mg, 0.56 mmol) were refluxed in anhydrous isopropanol (20 mL) in a 50 mL flask where the solution turned orange after 12h of stirring under nitrogen. The solution was then concentrated under vacuum to near dryness. The crude product was loaded onto a silica column and eluted with hexanes/ethyl acetate (90/10) up to hexanes/ethyl acetate (75/25) to give the product as a yellow-orange solid (95 mg, 83 %). M.p.: 86-88 °C. ^{1}H-NMR (acetone-d_6): δ = 8.55 (s, 1H), 7.95 (d, 1H, J = 1.5 Hz), 7.45 (d, 1H, J = 5.7 Hz), 7.35 (d, 1H, J = 3.4 Hz), 7.30 (d, 1H, J = 5.7 Hz), 6.77 (dd, 1H, ^3J = 3.5 Hz and 1.7 Hz). ^{13}C-NMR (acetone-d_6): δ = 163.8, 151.7, 149.1, 148.4, 128.2, 122.6, 120.5,

114.6, 113.5, 106.0. HRMS(+) calculated for $[C_{10}H_6N_2OS+Na]^+$: 225.00930 found 225.00885.

Diethyl 2-((1-methyl-1H-pyrrol-2-yl)methyleneamino)-5-aminothiophene-3,4-dicarboxylate (V-11). **V-3** (32 mg, 0.29 mmol) and **V-2** (75 mg, 0.29 mmol) were mixed in anhydrous isopropanol (20 mL) with a catalytic amount of TFA and then refluxed for 12 hours. The reaction mixture was concentrated and then purified by flash chromatography eluted with hexanes/ethyl acetate (50/50) to afford the product as a yellow solid (81 mg, 80 %). M.p.: 130-132 °C. ^{1}H-NMR (acetone-d_6): δ = 7.94 (s, 1H), 7.35 (s, NH_2), 6.96 (dd, 1H, ^3J = 4.1 Hz and ^5J = 2.0 Hz), 6.64 (dd, 1H, ^3J = 3.9 Hz and ^5J = 1.8 Hz), 6.14 (dd, 1H, ^3J = 3.8 Hz and 2.5 Hz), 4.29 (q, 2H, J = 7.1 Hz), 4.21 (q, 2H, J = 7.1 Hz), 3.95 (s, 3H), 1.34 (t, 3H, J = 7.1 Hz), 1.28 (t, 3H, J = 7.1 Hz). ^{13}C-NMR (acetone-d_6): δ = 165.5, 164.4, 160.1, 144.3, 134.6, 130.2, 130.0, 128.0, 119.0, 109.1, 101.7, 61.0, 59.8, 36.7, 14.1, 14.1. HRMS(+) calculated for $[C_{16}H_{19}N_3O_4S+H]^+$: 350.11690 found 350.11781.

Diethyl 2-((1H-pyrrol-2-yl)methyleneamino)-5-aminothiophene-3,4-dicarboxylate (V-12). **V-4** (28 mg, 0.29 mmol) and **V-2** (75 mg, 0.29 mmol) were mixed in anhydrous isopropanol (20 mL) with a catalytic amount of TFA and followed by refluxing for 12h. The reaction was concentrated and then purified by flash chromatography eluted with hexanes/ether (50/50) up to diethyl ether (100 %) only to afford the product as of an orange powder (74 mg, 76 %). M.p.: 161-163 ^{o}C. ^{1}H-NMR (acetone-d_6): δ = 10.68 (s, NH), 7.92 (s, 1H), 7.34 (s, NH_2), 7.04 (dd, 1H, ^3J = 3.6 and ^5J = 2.4 Hz), 6.65 (dd, 1H, ^3J = 3.6 and ^5J = 2.2 Hz), 6.23 (dd, 1H, ^3J = 3.6 and 2.4 Hz). ^{13}C-NMR (acetone-d_6): δ = 165.3,

164.4, 160.0, 143.8, 134.5, 130.7, 127.6, 124.1, 116.3, 110.5, 101.8, 60.9, 59.8, 14.1, 14.0. HRMS(+) calculated for $[C_{15}H_{17}N_3O_4S+H]^+$: 336.10125 found 336.10208.

Diethyl 2,5-bis((1-methyl-1H-pyrrol-2-yl)methyleneamino)thiophene-3,4-dicarboxylate (V-15). **V-3** (200 mg, 1.83 mmol) and DABCO (200 mg, 1.83 mmol) were dissolved in anhydrous toluene (20 mL) at 0 ^oC followed by the slow addition of $TiCl_4$ (1.0 M, 1.83 mL, 1.83 mmol). **V-2** (90 mg, 0.35 mmol) was subsequently added and the reaction mixture was refluxed for 3-4 h. The solvent was evaporated and the product isolated as a red solid after purification by flash chromatography with 1% triethylamine in hexanes up to hexanes/ethyl acetate (50/50) (57 mg, 37 %). M.p.: 134-136 °C. ^{1}H-NMR (acetone-d_6): δ = 8.33 (s, 2H), 7.11 (d, 2H, J = 2.0 Hz), 6.85 (dd, 2H, ^3J = 4.0 and ^5J = 1.8 Hz), 6.24 (dd, 2H, J = 4.0 Hz and 2.5 Hz), 4.29 (q, 4H, J = 7.1 Hz), 4.07 (s, 6H), 1.33 (t, 6H, J = 7.1Hz). ^{13}C-NMR (acetone-d_6): δ = 163.5, 149.5, 149.3, 132.2, 129.9, 126.1, 121.8, 109.9, 60.9, 36.9, 14.1. HRMS(+) calculated for $[C_{22}H_{24}N_4O_4S+H]^+$: 441.15910 found 441.15811.

Diethyl 2,5-bis((1H-pyrrol-2-yl)methyleneamino)thiophene-3,4-dicarboxylate (V-16). **V-4** (173 mg, 1.74 mmol) and DABCO (195 mg, 1.74 mmol) were dissolved in anhydrous toluene (20 mL) at 0 ^oC followed by the slow addition of $TiCl_4$ (1.0 M, 1.74 mL, 1.74 mmol). **V-2** (90 mg, 0.35 mmol) was then added and the mixture was refluxed for 30 minutes. The title compound was isolated as a red solid (64 mg, 44%) after flash chromatography with hexanes/ether (34/66) with 1% triethylamine and up to diethyl ether (100%). M.p.: 185-187 °C. ^{1}H-NMR (acetone-d_6): δ = 10.98 (s, NH), 8.31 (s, 2H), 7.20 (d,

2H, *J* = 0.4 Hz), 6.87 (d, 2H, *J* = 1.2 and 2.0 Hz), 6.33 (d, 2H, *J* = 2.2 Hz), 4.26 (q, 4H, *J* = 7.1 Hz), 1.30 (t, 6H, *J* = 7.1 Hz). ^{13}C-NMR (acetone-d_6): δ = 163.4, 149.7, 149.4, 130.6, 126.0, 125.2, 119.0, 111.2, 60.9, 14.0. HRMS(+) calculated for $[C_{20}H_{20}N_4O_4S+H]^+$: 413.12780 found 413.12778.

Diethyl 2,5-bis((furan-2-yl)methyleneamino)thiophene-3,4-dicarboxylate (V-18). In a 50 mL round bottom flask was added **V-6** (112 mg, 1.16 mmol) dissolved in anhydrous toluene (25 mL) to which was subsequently added DABCO (434 mg, 3.87 mmol) and $TiCl_4$ (1.0 M , 1.55 mL, 1.55 mmol) at 0 ^oC. **V-2** (100 mg, 0.39 mmol) was then added and the mixture was refluxed for 2 h after which the solvent was then evaporated. Purification by flash chromatography (SiO_2) with hexanes and increased up to hexanes/ethyl acetate (50/50) yielded the title product as a red solid (30 mg, 19 %). M.p.: 145-147 °C. ^{1}H-NMR (acetone-d_6): δ = 8.40 (s, 2H), 7.91 (d, 2H, *J* = 1.2 Hz), 7.26 (d, 2H, *J* = 3.5 Hz), 6.74 (dd, 2H, *J* = 3.5 Hz and 1.8 Hz), 4.31 (q, 4H, *J* = 7.1 Hz), 1.34 (t, 6H, *J* = 7.1 Hz). ^{13}C-NMR (acetone-d_6): δ = 162.9, 152.2, 149.8, 147.9, 147.8, 127.5, 119.0, 113.4, 61.2, 14.0. HRMS(+) calculated for $[C_{20}H_{18}N_2O_6S+H]^+$: 415.09583 found 415.09530.

N^1,N^4-Bis((1-methyl-1H-pyrrol-2-yl)methylene)benzene-1,4-diamine (V-22). In a 50 mL round bottom flask, 1,4-phenylenediamine (70 mg, 0.65 mmol) was dissolved in isopropanol (20 mL). To this, was added **V-3** (139 μL, 1.36 mmol) and a catalytic amount of TFA with vigorous stirring followed by refluxing for 12 hours. The title compound was isolated as a yellow solid (120 mg, 64 %) by precipitation in ethyl acetate/hexanes (5/95). M.p.: 127-129 °C. ^{1}H-NMR (acetone-d_6): δ = 8.46 (s, 2H), 7.24 (s, 4H), 6.98 (t, 2H, *J* =

1.9 Hz), 6.73 (dd, 2H, ^{3}J = 3.8 Hz and ^{5}J =1.7 Hz), 6.18 (dd, 2H, J = 3.8 Hz and 2.6 Hz). ^{13}C-NMR (acetone-d_6): δ = 150.4, 150.3, 130.9, 129.6, 121.9, 118.6, 108.9, 36.4. HRMS(+) calculated for $[C_{18}H_{18}N_4+H]^+$: 291.16042 found 291.16030.

N^1,N^4-Bis((1H-pyrrol-2-yl)methylene)benzene-1,4-diamine (V-23). In a 50 mL round bottom flask, 1,4-phenylenediamine (70 mg, 0.65 mmol) was dissolved in isopropanol (20 mL). To this was added **V-4** (129 mg, 1.36 mmol) with vigorous stirring along with a catalytic amount of TFA followed by refluxing for 12 hours. The title compound was isolated as a yellow powder (147 mg, 86 %) by precipitation in ethyl acetate/hexanes (5/95). M.p.: 205-207 °C. ^{1}H-NMR (acetone-d_6): δ = 10.93 (s, NH), 8.40 (s, 2H), 7.23 (s, 4H), 7.10 (s, 2H), 6.71 (dd, 2H, ^{3}J = 3.5 Hz and ^{5}J =1.3 Hz), 6.27 (dd, 2H, J = 3.4 Hz and 2.7 Hz). ^{13}C-NMR (acetone-d_6): δ = 150.0, 149.2, 131.7, 123.5, 122.0, 116.3, 110.1. HRMS(+) calculated for $[C_{16}H_{14}N_4+H]^+$: 263.12912 found 263.12930.

N^1,N^4-Bis((thiophen-2-yl)methylene)benzene-1,4-diamine (V-24). In a 50 mL round bottom flask, 1,4-phenylenediamine (70 mg, 0.65 mmol) was dissolved in isopropanol (20 mL). To this, was added **V-5** (124 μL, 1.36 mmol) with vigorous stirring and a catalytic amount of TFA followed by refluxing for 12 hours. The title compound was isolated as a yellow solid (163 mg, 85 %) by precipitation in ethyl acetate/hexanes (5/95). M.p.: 171-173 °C. ^{1}H-NMR (acetone-d_6): δ = 8.84 (s, 2H), 7.74 (d, 2H, J = 5.0 Hz), 7.67 (d, 2H, J = 3.5 Hz), 7.35 (s, 4H), 7.23 (dd, 2H, J = 4.5 Hz and 3.8 Hz). ^{13}C-NMR (acetone-d_6): δ = 153.0, 149.8, 143.7, 133.2, 130.8, 128.3, 122.4. HRMS(+) calculated for $[C_{16}H_{12}N_2S_2+H]^+$: 297.05147 found 297.05132.

N^1,N^4-Bis((furan-2-yl)methylene)benzene-1,4-diamine (V-25). In a 50 mL round bottom flask, 1,4-phenylenediamine (70 mg, 0.65 mmol) was dissolved in isopropanol (20 mL). To this, was added **V-6** (113 μL, 1.36 mmol) with vigorous stirring and a catalytic amount of TFA followed by refluxing for 12 h. The title compound was isolated as a yellow powder (115 mg, 67 %) by precipitation in ethyl acetate/hexanes (5/95). M.p.: 144-146 °C. ^{1}H-NMR (acetone-d_6): δ = 8.49 (s, 2H), 7.83 (d, 2H, J = 1.4 Hz), 7.34 (s, 4H), 7.12 (d, 2H, J = 3.4 Hz), 6.69 (dd, 2H, J = 3.4 Hz and 1.8 Hz). ^{13}C-NMR (acetone-d_6): δ = 153.8, 150.7, 148.2, 146.8, 122.8, 116.5, 113.1. HRMS(+) calculated for $[C_{16}H_{12}N_2O_2+H]^+$: 265.09715 found 265.09747.

Results and Discussion

The series of compounds reported in Chart V-1 were prepared for investigating the effect of the heterocycles in addition to the degree of conjugation on the electrochemical and photophysical properties. Important information can be had by comparing the heterocyclic derivatives (**V-15**-**V-21**) to the homoaryl benchmark (**V-26**). Although an unsubstituted amino derivative of **V-1** would be advantageous for direct comparison of the properties with **V-26**, this is not possible owing to the instability of such a precursor. As a result, **V-1** was used in lieu for preparing the targeted compounds because of its stability under ambient conditions. Given **V-1** and **V-2** were used for preparing all the heterocyclic azomethines, the effect of their electron withdrawing group on the observed properties is consistent for all the azomethine derivatives.

Additional property effects contingent on structure can be had from the compounds reported in Chart V-1. For example, the effect of incorporating a heterocycle in the terminal position is also possible with derivatives **V-22**-**V-25**. Additional information can be had from the symmetric (**V-15**-**V-18**) and unsymmetric (**V-19**-**V-21**) dyads. The effect by the number of azomethines and hence the degree of conjugation on the properties is also possible by comparing dyads **V-7**-**V-10** with their corresponding triads **V-15**-**V-18**. Meanwhile, the effect of the terminal amine (**V-11**-**V-14**) on the properties is additionally derived by comparing the measured properties to **V-7**-**V-10**. The added advantage of **V-11**-**V-14** is that anodic coupling is possible and the resulting products can be spectroscopically and electrochemically analyzed (vide infra).

Spectroscopy

The photophysical properties including absorbance, fluorescence, fluorescence quantum yields, phosphorescence, and fluorescence lifetimes of the various azomethines were investigated for deciphering the contributions of the above mentioned effects. The measured results are collectively tabulated in Table V-1 and in the Supporting Information. Upon comparing the similar heterocyclic compounds for example, **V-7**, **V-11**, **V-15**, and **V-22**, the effect of the degree of conjugation on the spectroscopic properties can be had. In all cases, the absorbance and fluorescence maxima were both bathochromically shifted by ca. 70 nm upon progressing from the dyads to the triads. Meanwhile the homoaryl derivatives **V-22**-**V-25** exhibited absorbance and fluorescence maxima comparable to their corresponding dyads. This is in contrast to the homoaryl benchmark **V-26**, whose absorbance and fluorescence maxima are hypsochromically shifted relative to the triads. The spectroscopic data confirm that extended degrees of conjugation are possible with the heterocyclic derivatives relative to their homoaryl azomethines.

Table V-1. Spectroscopic[a] and electrochemical[b] data for the different azomethines.

	Compound	Abs[c] (nm)	Fluo[d] (nm)	Φ_{fl}[e] ($\Phi_{77\,K}$)[f]	ΔE[g] (eV)	E_g[h] (eV)	E_{pa} (V)	E_{pc} (V)	E_g[i] (eV)	HOMO (-eV)	LUMO (-eV)	$E_{pa(polymer)}$ (V)[j]	$E_{pc(polymer)}$ (V)[j]	abs_{ITO} (nm)[j]
	V-1	305	335	2.5×10^{-3} (8.9×10^{-3})	3.7	3.0	0.6	-	-	4.9	1.2	-	-	-
	V-2	279	304	3×10^{-6} (7.7×10^{-6})	4.2	3.9	1.3	-	-	5.6	1.5	-	-	-
Dyads	V-7	382	473	9.4×10^{-5} (0.76)	2.9	2.7	1.4	-1.6	2.9	5.7	2.8	1.3	-1.1	439
	V-8	380	472	1.1×10^{-4} (0.42)	3.0	2.7	1.4	-1.6	2.9	5.7	2.8	1.3	-1.1	433
	V-9	370	439	3.9×10^{-3} (0.79)	3.2	2.7	1.7	-1.4	3.0	6.0	3.0	1.3	-1.2	433
	V-10	363	429	2.3×10^{-4} (0.56)	3.1	2.8	1.7	-1.4	3.0	6.0	3.0	1.4	-1.1	412
	V-11	390	472	4.3×10^{-4} (0.59)	2.9	2.7	0.8	-1.9	2.6	5.1	2.5	0.6	-1.3	424
	V-12	391	474	2.6×10^{-4} (0.48)	2.9	2.7	0.8	-1.9	2.6	5.1	2.5	0.6	-1.4	430
	V-13	400	480	2.9×10^{-3} (0.97)	2.9	2.6	1.0	-1.4	2.3	5.3	3.0	0.7	-1.2	434
	V-14	390	469	7.7×10^{-4} (0.88)	2.9	2.7	1.0	-1.3	2.2	5.3	3.1	0.7	-1.4	431
Triads	V-15	457	538	5.1×10^{-3} (0.82)	2.5	2.3	0.8	-1.4	2.1	5.1	3.0	0.8	-1.1	486
	V-16	452	504	2.5×10^{-3} (0.88)	2.6	2.3	1.0	-1.4	2.3	5.3	3.0	0.8	-1.2	483
	V-17	440	534	2.8×10^{-3} (0.74)	2.6	2.3	0.9	-1.3	2.1	5.2	3.1	0.7		485
	V-18	430	494	9.6×10^{-4} (0.81)	2.8	2.4	1.0	-1.2	2.1	5.3	3.2	0.8	-1.3	480
	V-19	457	531	3.8×10^{-4} (0.39)	2.4	2.2	1.0	-1.3	2.2	5.3	3.1	0.7	-1.2	483
	V-20	452	531	1.2×10^{-3} (0.43)	2.5	2.3	1.1	-1.3	2.3	5.4	3.1	1.0	-1.1	477
	V-21	420	519	6.5×10^{-4} (0.21)	2.6	2.3	1.1	-1.2	2.2	5.4	3.2	0.8	-1.3	455
Analogues	V-22	367	419	1.2×10^{-3} (0.71)	3.2	2.8	1.0	-2.2	3.1	5.3	2.2	0.8	-1.3	404
	V-23	365	404	3.3×10^{-3} (0.69)	3.1	2.7	1.0	-2.2	3.1	5.3	2.2	0.8	-1.2	397
	V-24	366	416	3.7×10^{-4} (0.63)	3.1	2.9	1.4	-1.8	3.1	5.7	2.6	1.3	-1.2	420
	V-25	360	422	4.6×10^{-4} (0.59)	3.2	2.9	1.3	-1.8	3.0	5.6	2.6	1.0	-1.4	448
	V-26[k]	354	410	0.68-0.99	-	2.7	-	-	-	-	-	-	-	-

[a]In anhydrous acetonitrile [b]Values reported against Ag/AgCl (sat'd) in CH_2Cl_2. [c]Absorption maximum. [d]Emission maximum. [e]Fluorescence quantum yields at λ_{ex} = 303 nm, relative to bithiophene.[31] [f]Fluorescence quantum yields at 77 K relative to room temperature. [g]Absolute HOMO-LUMO spectral difference. [h]Spectroscopic energy-gap. [i]Electrochemical energy-gap. [j]Data for anodically coupled products immobilized on ITO electrodes. [k]Literature values.[32-34]

Although the azomethine bond is electron withdrawing, its electronic effect is insufficient to offset any gain achieved with increasing the degree of conjugation. This is corroborated by the spectral bathochromic shifts observed for **V-15**-**V-18** relative to their dyad analogues **V-7**-**V-10**. This is further supported by **V-11**-**V-14** whose absorption spectra are shifted by only 10 nm relative to **V-7**-**V-10**, while the fluorescence spectra are relatively similar. The collective spectroscopic data confirm that the heterocyclic azomethines are more conjugated that the homoaryl derivatives, which is further supported by the molar absorptivity coefficients that were found to be between 25 000 and 40 000 $cm^{-1}M^{-1}$ (see supporting information). Meanwhile, the steady-state spectroscopic data suggest that the degree of conjugation for the homoaryl derivatives **V-22**-**V-25** is confined to the heterocycle-azomethine moiety and that delocalization across the entire molecule is reduced. The spectroscopic data further confirm that the heterocyclic derivatives are more conjugated than their homoaryl counterparts, most likely owing in part to the high degree of coplanarity (vide infra) of the heterocyclic azomethines combined with the electronic effects of the π-rich heterocycles.

The general trend of the various heterocycles on the spectroscopic properties is represented in Figure V-1. It is evident that the absorbance is bathochromically shifted by ca. 30 nm for each heterocycle upon progressing in the order of furane < thiophene < pyrrole < methyl pyrrole. The same trend was observed for all the azomethines studied and is consistent with the increasing electron richness of the heterocycle. Moreover, the combined electronic effects on the spectral data are seen with the unsymmetric **V-19**-**V-21** whose spectra are bathochromically shifted relative to their symmetric counterparts.

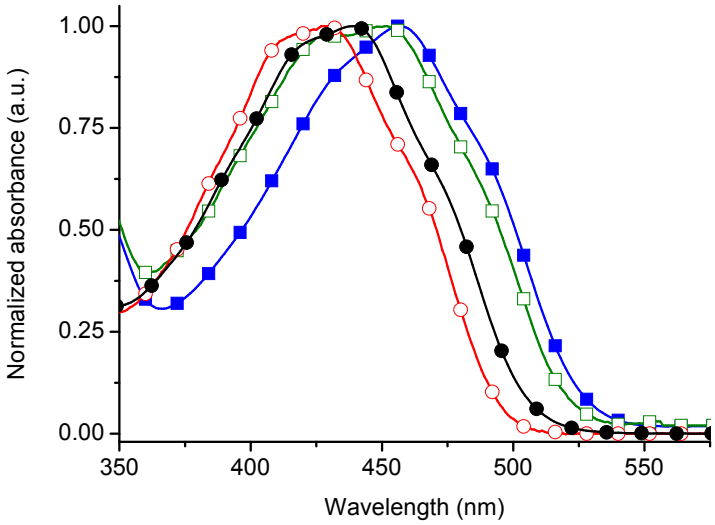

Figure V-1. Effect of different heterocycles on the absorbance spectra: **V-15** (■), **V-16** (□), **V-17** (●), **V-18** (○).

All the compounds studied exhibited weak fluorescence quantum yields (Φ_f) on the order of < 10^{-3}. This is in contrast to their vinylene analogues such as **V-26** that fluoresce with Φ_f ranging between 0.68 and 0.99.[35, 36] Although many assumptions are made for deriving quantum yields relative to standards such as bithiophene (Φ_f = 0.013), the fluorescence for all the compounds is nonetheless extremely low. We verified the accuracy of the fluorescence measurements using the integrating sphere method. This provides absolute fluorescence yields regardless of excitation and emission wavelengths and emission yields.[37] The fluorescence yields for the azomethines were all below the detection limit (Φ_f < 0.01), confirming the quenched fluorescence regardless of the degree of conjugation and the type of heterocycle.

Low temperature fluorescence measurements were subsequently undertaken in order to gain insight into the origins of the fluorescence quenching and deactivation modes of the azomethines. At 77 K, internal conversion (IC) deactivation modes by either simple bond rotation or intramolecular processes requiring geometric alignment involving bond rotations are suppressed. Increased fluorescence should therefore be observed if nonradiative IC deactivation by either of these rotation modes is an efficient deactivation manifold. Homogeneous glass matrices suitable for low temperature measurements were done with a 4:1 ethanol/methanol matrix.

As seen in Table V-1, the low temperature fluorescence is several orders of magnitude greater than that at room temperature. The measured values suggest that the fluorescence can be restored to near quantitative values at low temperature. The azomethines therefore have temperature sensor-like properties such that the fluorescence can be *turned-on* and *turned-off* with temperature. Although, the temperature dependent fluorescence confirms that the singlet excited state of the azomethines is deactivated by internal conversion, the quantum yield of this process cannot be accurately measured. This is a result of the large error associated in comparing the intense fluorescence signal at 77 K to the extremely noisy and weak room temperature signal (Figure V-2). The temperature dependent fluorescence nonetheless confirms that the azomethine fluorescence is temperature dependent. It further confirms that deactivation by internal conversion involving bond rotation/alignment is a major deactivation mode of azomethine singlet excited state deactivation. Meanwhile, deactivation of the singlet manifold is consistent for all the azomethines and is independent of the type of heterocycle and degree of conjugation. It is noteworthy that weak fluorescence was observed regardless of solvent polarity and

proticity implying that simple polar effects and perturbation of the singlet-triplet manifolds are not the reason for the quenched fluorescence.

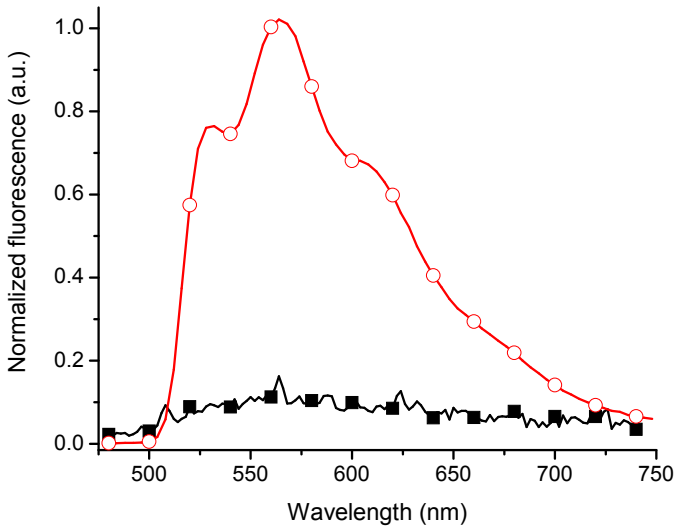

Figure V-2. Fluorescence of **V-20** at room temperature magnified 100 times (■) and 77 K (o).

Laser flash photolysis (LFP) was used to further investigate the excited state deactivation modes of the azomethines. Short-lived transients on the order of μs can be spectroscopically detected and assigned by this time resolved method. No transient was detected for any of the azomethines, implying that intramolecular deactivation involving radical or radical ion formation does not occur. Although no signal was measured by LFP, triplet formation by intersystem crossing (ISC) cannot be unequivocally dismissed. This is because the shortest transient lifetime detectable by the system is ≈ 100 ns and triplet quenching by intramolecular energy transfer would occur on a shorter timescale. Phosphorescence measurements were subsequently done in a glass matrix at 77 K. At this

low temperature, collisional deactivation processes that would otherwise thermally deactivate the triplet are eliminated. Weak phosphorescence should subsequently be seen if the triplet state is formed. Even though phosphorescence (Figure V-3) was observed for all the azomethines studied, only qualitative information regarding the triplet state can be obtained given that $\Phi_{phos} < \Phi_{ISC}$. Azomethine phosphorescence confirms that the triplet is produced at 77 K, but that it is efficiently deactivated at room temperature.

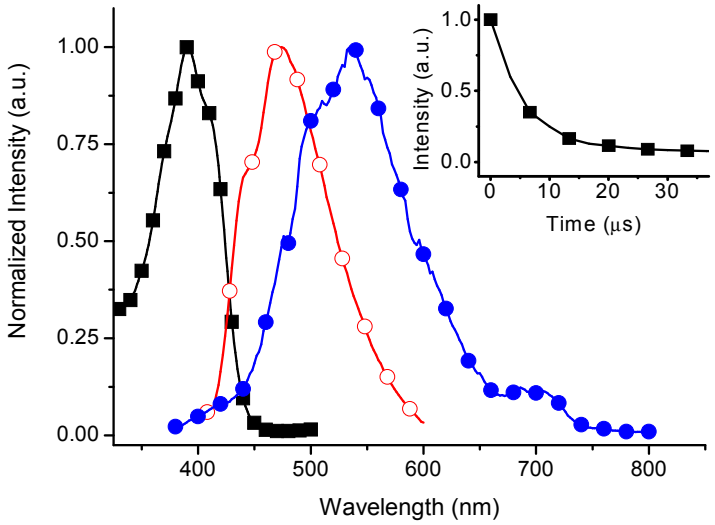

Figure V-3. Normalized absorption (■) and fluorescence (o) spectra of **V-12** in acetonitrile. Phosphorescence spectrum of **V-12** (●) measured in 4:1 ethanol/methanol matrix at 77 K. Inset : phosphorescence decay monitored at 538 nm.

In light of the high fluorescence yields measured at low temperatures, deactivation by intersystem crossing is not a major deactivation mode. The collective steady-state and time-resolved spectroscopic data confirm that the suppressed fluorescence is predominately

a result of deactivation of the singlet excited state by internal conversion means involving bond rotation. The fluorescence can therefore be restored at low temperatures by suppressing these energy wasting modes. Meanwhile, the steady-state spectroscopic data confirm that both the absorbance and fluorescent spectra are contingent on not only the nature of the heterocycle, but also on the number of azomethine bonds.

Crystallographic data

Single crystal X-ray diffraction analysis of **V-20** was investigated for determining the twisting between the aryl-azomethine planes and for investigating its impact on the degree of conjugation. The X-ray crystallography data shown in Figure V-4 confirm that **V-20** is unsymmetric and that it consists of a central thiophene sandwiched between a furan and pyrrole. The figure also shows the heterocycles adopt an anti-parallel arrangement. It is further evident that the two connecting azomethine bonds both adopt the *E* isomer and that the compound is linear. Most importantly, the mean plane angles between the terminal heterocycles and the central thiophene are ca 18^{o}.

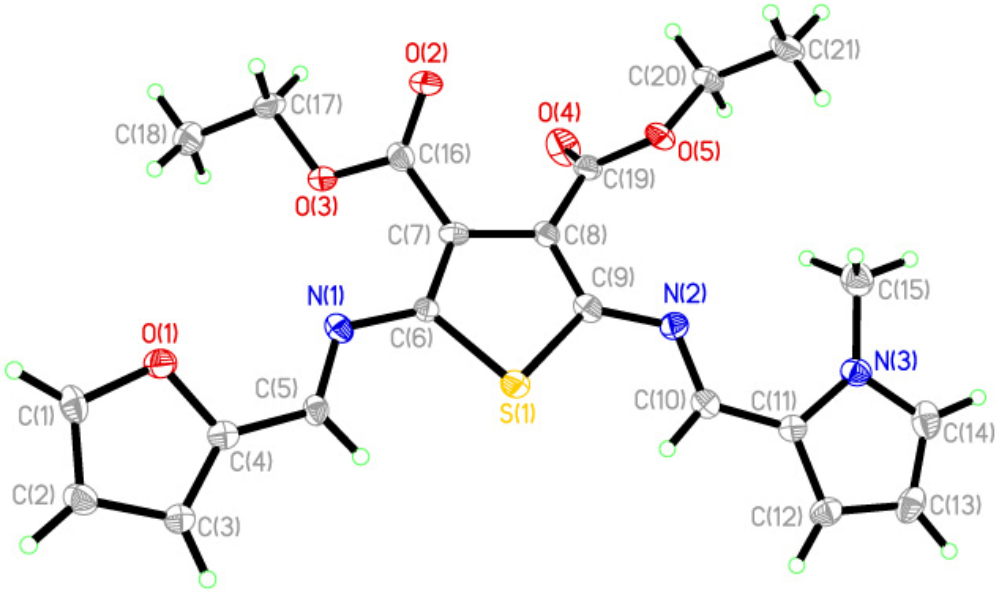

Figure V-4. ORTEP representation of **V-20** with the ellipsoids drawn at 30% probability.

The crystallographic data for **V-11**-**V-21**[6, 29, 38-42] were compared for examining the effect of the various heterocycles on the molecular arrangement and for correlating with the spectroscopic data. The data are collectively summarized in Table V-2. It can be seen that the mean plane angles between the terminal heterocycles and the central thiophene range between 2.5 – 34°. This is in contrast to their homoaryl derivative **V-23** whose analogous mean planes are twisted between 32.9 and 56.4°.[43] The increased twisting of the homoaryl derivatives corroborates the spectroscopic data that the heterocyclic azomethines have an increased degree of conjugation. This is in part responsible for the observed bathochromic spectral shifts. It should be noted that the heterocycles of **V-11**-**V-21** all adopt anti-parallel arrangements and are coplanar. This arrangement contributes to their linearity and extended degree of conjugation. The latter allows delocalization of the electron rich heterocycles

across of the entire molecule. The azomethine and azomethine-aryl bonds were found to be shorter than the corresponding CH-aryl bonds.

Table V-2. Selected crystallographic data of **V-11**-**V-21**.

	V-11	**V-12**	**V-13**	**V-14**	**V-15**[a]		**V-16**		**V-17**		**V-18**[a]		**V-19**		**V-20**		**V-21**[a]	
	side N	side N	side S	side O	side N1	side N2	side N1	Side N2	side S1	side S2	side O1	side O2	side N	side S	side N	side O	side S	side O
plane angle (°)[b]	17.06(4)	10.2(1)	9.0(1)	2.51(4)	10.8(2)	19.5(2)	18.90(5)	10.31(4)	9.04(4)	25.07(6)	7.1(2)	30.8(2)	3.5(2)	3.5(1)	18.0(2)	18.8(2)	33.6(4)	7.9(5)
-C=N- (Å)	1.292(2)	1.275(2)	1.283(3)	1.289(2)	1.288(4)	1.286(4)	1.292(2)	1.384(2)	1.277(3)	1.286(3)	1.284(4)	1.285(4)	1.30(2)	1.279(9)	1.287(5)	1.287(4)	1.286(4)	1.286(4)
=N-Aryl- (Å)	1.372(2)	1.376(2)	1.381(3)	1.382(2)	1.378(4)	1.374(4)	1.383(2)	1.297(2)	1.381(3)	1.393(3)	1.377(4)	1.379(4)	1.373(2)	1.377(2)	1.374(5)	1.374(5)	1.381(4)	1.385(4)
=CH-Aryl- (Å)	1.424(2)	1.433(2)	1.426(3)	1.420(2)	1.425(4)	1.428(4)	1.441(2)	1.435(2)	1.443(3)	1.435(3)	1.427(4)	1.432(4)	1.434(9)	1.436(9)	1.419(5)	1.419(5)	1.435(4)	1.418(4)

a) The average of the two molecules present per unit cell was taken. b) Refers to the mean plane angle between the central thiophene and the terminal heterocycles.

According to Figure V-5, the crystal packing shows several interactions between the pyrrole-furan moieties. These are consistent with donor-acceptor type interactions between the two heterocycles. These interactions lead to regio-regular crystal packing involving alternating pyrrole-furan repeating motifs. Although hydrogen bonding is nonexistent for **V-20**, unlike other azomethines such as **V-11**-**V-14**, the heterocyclic donor-acceptor interactions are sufficiently strong as evidenced by the fact that X-ray quality crystals of this unsymmetric compound could be easily obtained. Nonetheless, the collective properties are responsible for the significantly different spectroscopic properties between the homo- and heterocyclic azomethines.

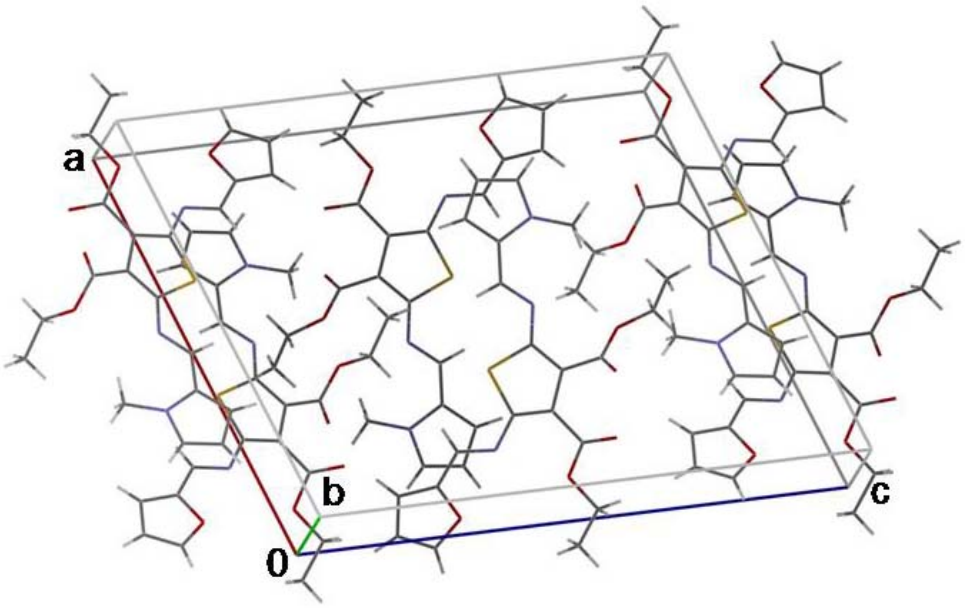

Figure V-5. Extended view along the *ac* axis of the crystal lattice of **V-20**.

Electrochemistry

Cyclic voltammetry was undertaken to further investigate the contribution of the various heterocycles and degree of conjugation on the oxidation (E_{pa}) and reduction potentials (E_{pc}). A typical voltammogram is seen in Figure 6. The effect of the different heterocycles is evident from the different E_{pa} for **V-7**-**V-10**. As seen in Table V-1, the E_{pa} for the furan and thiophene derivatives are between 100 and 300 mV more positive than their corresponding pyrrole analogues. Conversely, the E_{pc} of the furane and thiophene derivatives are less positive than their pyrroles counterparts. These trends are independent of the degree of conjugation and are consistent with the π-richness of the heterocycle.

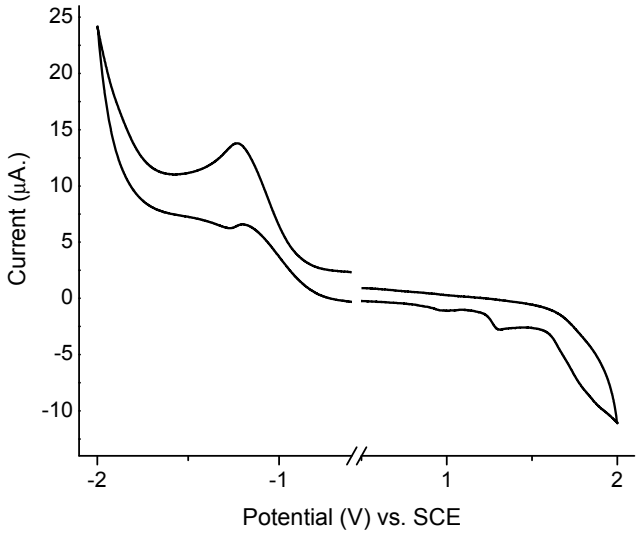

Figure V-6. Cyclic voltammogram of **V-18** measured in anhydrous and deaerated dichloromethane at a scan rate of 100 mV/sec.

The electronic effect on the oxidation potential is evident upon comparing the E_{pa} of **V-11**-**V-14** to their corresponding dyads. The electron donating terminal amine reduces the E_{pa} by ca. 600 mV. Meanwhile, the same reduction in E_{pa} occurs with the additional azomethine for the triads relative to the corresponding dyads. The reduced E_{pa} is a result of the increased degree of conjugation and confirms the extended delocalization of the azomethines. Both the increased E_{pa} and energy-gap (E_g) of the homoaryl derivatives **V-22**-**V-25** relative to their all-heterocylic counterparts corroborate the reduced degree of conjugation that was spectroscopically observed. The collective electrochemical data confirm that both the anodic and cathodic potentials can be tailored by incorporating different heterocycles into the azomethines and the number of azomethine bonds.

Anodic Coupling

As seen in Figure V-6, both the oxidation and reduction processes of **V-18** are irreversible. This behaviour is consistent for all the azomethines reported in Chart V-1. It can be argued that the irreversible processes are a result of azomethine decomposition and reduction of the heteroconjugated bond. The latter can be dismissed because the cathodic process was found to be a one-electron transfer. Conversely, azomethine reduction is a two-electron process. The anodic process is similarly a one-electron transfer process resulting in the radical cation. The irreversible oxidation is not from decomposition of the azomethines. Rather, the resulting radical cation undergoes cross-coupling according to

standard means.[44, 45] This was previously determined with terminally substituted derivatives such as **V-27** that were found to yield persistent radical cations.[6, 7, 46, 47]

In light of the unsubstituted 2, 2′-terminal positions of the heterocyclic azomethines, we investigated whether the radical cation could undergo standard cross-coupling to afford coupled products with increased degrees of conjugation. This was done both amperometrically and chronometrically by applying a potential slightly more positive than the E_{pa} of the azomethine of study. ITO coated glass electrodes were used for spectroscopically and electrochemically characterizing the anodically coupled products. A typical voltammogram for the anodic coupling is represented in Figure V-7 for **V-15**. The anodic wave shifts to less positive potentials with cycling between 1.1 and 0.4 V concomitant with a shift of the cathodic wave to more positive potentials. The former implies that the anodically coupled product is more conjugated than its corresponding monomer. Moreover, the resulting product adsorbed on the electrode exhibited a one-electron reversible oxidation. The increased degree of conjugation is further confirmed by a 30 nm bathochromic shift in the absorbance relative to the original **V-15**. To ensure that the measured properties were that of the neutral product and not its corresponding radical cation, a potential of 0 V was applied for two minutes prior to the measurements.

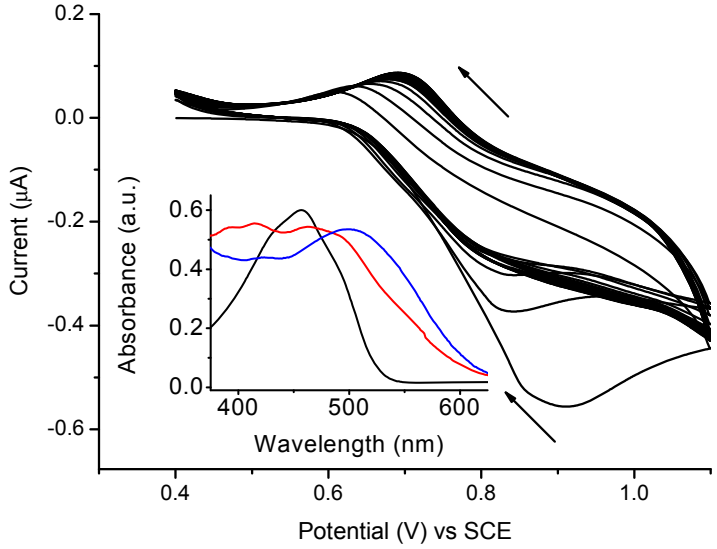

Figure V-7. Anodic coupling of **V-15** at 100 mV/s. Inset: absorbance of **V-15** deposited on ITO an electrode after applying E_{pa} = 1 V for 0 (black), 1 (red) and 5 min (blue).

E_{pa} shifts to less positive values and absorbance bathochromic shifts were observed for the anodically coupled products for all the azomethines studied. Given that the anodic coupling of **V-11**-**V-14** can only yield dimers, their similar absorbance shifts to the other anodically coupled products in Chart V-1 suggest that the anodically coupled products **V-P15**-**V-P25** are low molecular weight oligomers. The degree of oligomerization of the anodically coupled products can be spectroscopically estimated. This is possible with a calibration curve of absorbance as a function of the reciprocal number of atoms along the conjugated frame work. The estimated degree of oligomerization determined by this method from Figure V-8 for **V-15** is 12. Both the oxidation and absorbance shifts nonetheless provide

sound evidence that anodically coupled products with increased degrees of conjugation are formed. They further provide strong evidence that the azomethines are robust and that they do not decompose when oxidized.

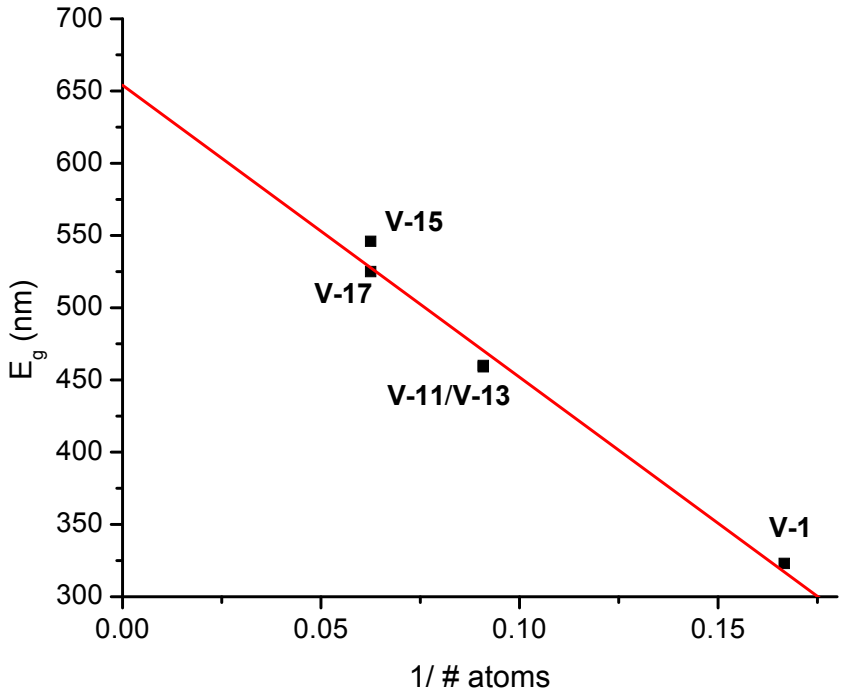

Figure V-8. Evolution of spectroscopic E_g as a function of the number of atoms along the conjugated framework for the methyl-pyrrole and thiophene containing dyads and triads.

To corroborate the qualitative data obtained from the anodically coupled products deposited on the ITO electrodes, absolute evidence for coupling product formation was further sought. **V-19** was therefore anodically coupled using a large surface area platinum

mesh gauze for obtaining sufficient material for standard characterization. Although an insufficient amount of soluble product was obtained for NMR characterization, a sufficiently soluble quantity was isolated for mass spectrometry. The resulting ESI mass spectrum is shown in Figure V-9. The major molecular ion peaks (m/z = 791 and 700) confirm that anodically coupled products are formed. The weaker molecular ion peaks (m/z = 457 and 545) suggest some azomethine hydrolysis, which most likely occurs during analysis/sample preparation. It should be noted that the MS data provide information relating to the lower molecular weight limit of the coupled products since higher ordered products are expected to be insoluble. The MS data further confirm that regio-regular anodic products are obtained and that homo-coupled (pyrrole-pyrrole/thiophene-thiophene) products are not formed.

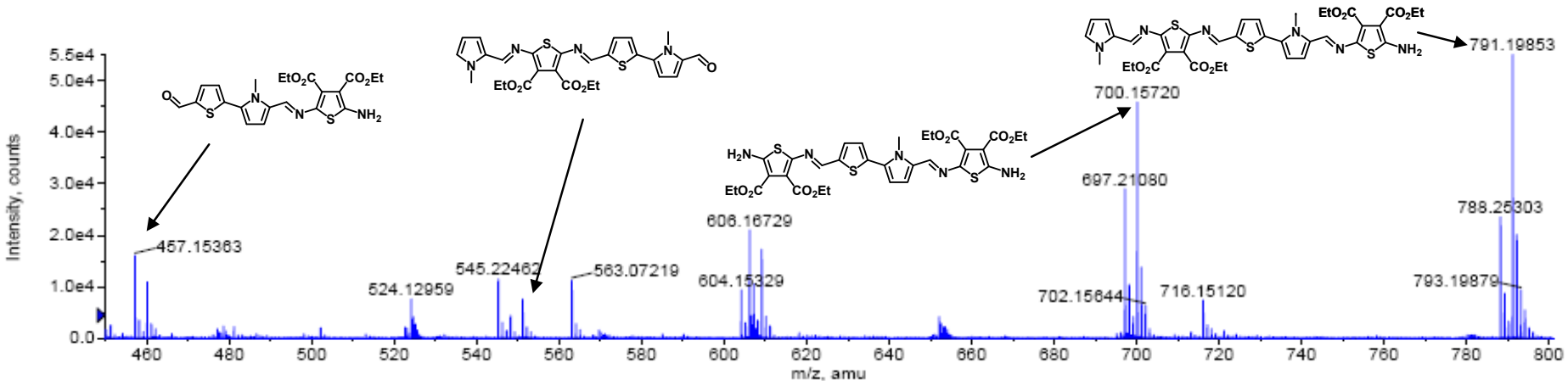

Figure V-9. Mass spectrum of **V-P19** in positive ESI mode.

Conclusion

It was found that both the spectroscopic and electrochemical properties of azomethines were contingent on the heterocycles and number of azomethine bonds. Although such behaviour is expected from chemical intuition, the first examples unequivocally confirming these properties with azomethines containing exclusively heterocycles were presented. It was also found that the suppressed fluorescence of azomethines could be restored at low temperatures. This opens the possibility of using conjugated azomethines as sensors. Meanwhile, anodic coupling was demonstrated with products of increased degree of conjugation being formed. The collective observed spectroscopic and electrochemical data confirm that azomethine property tailoring is possible by modifying the degree of conjugation, number of azomethines and type of heterocycle. The azomethines investigated illustrate that heterocyclic azomethines are robust and that functional materials-like properties are possible. Future generations of materials for a given application can therefore be prepared with the knowledge gained from the discovered fluorescence *turn-on* and *turn-off*, oxidation potentials, and property tailoring contingent on structure.

Acknowledgements

NSERC Canada is thanked for DG and RTI grants allowing this work to be performed in addition to CFI for additional equipment funding. S.D. also thanks NSERC for a graduate scholarship. W.G.S. also acknowledges both the Alexander von Humboldt

Foundation and the RSC for a JWT Jones Travelling fellowship, allowing the completion of this manuscript.

References

1. Ma, H.; Yip, H.-L.; Huang, F.; Jen, A. K. Y. *Adv. Funct. Mater.* **2010**, *20*, 1371.

2. Kamtekar, K. T.; Monkman, A. P.; Bryce, M. R. *Adv. Mater.* **2010**, *22*, 572.

3. Roncali, J. *Acc. Chem. Res.* **2009**, *42*, 1719.

4. Beaujuge, P. M.; Reynolds, J. R. *Chem. Rev.* **2010**, *110*, 268.

5. Mei, J.; Graham, K. R.; Stalder, R.; Reynolds, J. R. *Org. Lett.* **2010**, *ASAP*.

6. Dufresne, S.; Bolduc, A.; Skene, W. G. *J. Mater. Chem.* **2010**, *20*, 4861.

7. Bolduc, A.; Dufresne, S.; Skene, W. G. *J. Mater. Chem.* **2010**, *20*, 4820.

8. Sun, M.; Zhong, C.; Li, F.; Cao, Y.; Pei, Q. *Macromolecules* **2010**, *43*, 1714.

9. Bourgeaux, M.; Perez Guarin, S. A.; Skene, W. G. *J. Mater. Chem.* **2007**, *17*, 972.

10. Yang, C.-J.; Jenekhe, S. A. *Chem. Mater.* **1991**, *3*, 878.

11. Iwan, A.; Bilski, P.; Janeczek, H.; Jarzabek, B.; Domanski, M.; Rannou, P.; Sikora, A.; Pociecha, D.; Kaczmarczyk, B. *J. Molecul. Struc.* **2010**, *963*, 175.

12. Dufresne, S.; Guarìn, S. A. P.; Bolduc, A.; Bourque, A. N.; Skene, W. G. *Photochem. Photobiol. Sci.* **2009**, *8*, 796.

13. Dufresne, S.; Callaghan, L.; Skene, W. G. *J. Phys. Chem. B* **2009**, *13*, 15541.

14. Bourque, A. N.; Dufresne, S.; Skene, W. G. *J. Phys. Chem. C* **2009**, *113*, 19677.

15. Suematsu, K.; Nakamura, K.; Takeda, J. *Colloid. Polym. Sci.* **1983**, *261*, 493.

16. Rembaum, A. In *United States Patent Offce*; California Institute of Technology: United States, 1981, p 6.

17. Pont, D.; E.I. Du Pont De Nemours and Company: Great Britain, 1967, p 8.

18. Sek, D.; Jarzabek, B.; Grabiec, E.; Kaczmarczyk, B.; Janeczek, H.; Sikora, A.; Hreniak, A.; Palewicz, M.; Lapkowski, M.; Karon, K.; Iwan, A. *Synth. Met.* **2010**, *160*, 2065.

19. Sek, D.; Iwan, A.; Kaczmarczyk, B.; Jarzabek, B.; Kasperczyk, J.; Bednarski, H. *High Perf. Polym.* **2007**, *19*, 401.

20. Tsai, F.-C.; Chang, C.-C.; Liu, C.-L.; Chen, W.-C.; Jenekhe, S. A. *Macromolecules* **2005**, *38*, 1958.

21. Chang, C.-P.; Wang, C.-C.; Chao, C.-Y.; Lin, M.-S. *J. Polym. Res.* **2005**, *12*, 1.

22. Destri, S.; Pasini, M.; Pelizzi, C.; Porzio, W.; Predieri, G.; Vignali, C. *Macromolecules* **1998**, *32*, 353.

23. El-Shekeil, A. G.; Al-Yusufy, F. A.; Saknidy, S. *Polym. Int.* **1997**, *53*, 777.

24. Wang, C.; Shieh, S.; LeGoff, E.; Kanatzidis, M. G. *Macromolecules* **1996**, *29*, 3147.

25. Yang, C.-J.; Jenekhe, S. A. *Macromolecules* **1995**, *28*, 1180.

26. Amari, C.; Pelizzi, C.; Predieri, G.; Destri, S.; Porzio, W. *Synth. Met.* **1995**, *72*, 7.

27. Park, S. B.; Kim, H.; Zin, W. C.; Jung, J. C. *Macromolecules* **1993**, *26*, 1627.

28. Dufresne, S.; Roche, I. U.; Skalski, T.; Skene, W. G. *J. Phys. Chem.* **2010**, *114*, 13106.

29. Dufresne, S.; Skene, W. G. *J. Org. Chem.* **2008**, *73*, 3859.

30. Dufresne, S.; Bourgeaux, M.; Skene, W. G. *J. Mater. Chem.* **2007**, *17*, 1166.

31. Seixas de Melo, J.; Elisei, F.; Gartner, C.; Aloisi, G. G.; Becker, R. S. *J. Phys. Chem. A* **2000**, *104*, 6907.

32. Chaieb, A.; Vignau, L.; Brown, R.; Wantz, G.; Huby, N.; François, J.; Dagron-Lartigau, C. *Opt. Mater.* **2008**, *31*, 68.

33. Chaieb, A.; Khoukh, A.; Brown, R.; François, J.; Dagron-Lartigau, C. *Opt. Mater.* **2007**, *30*, 318.

34. Jiu, T.; Li, Y.; Gan, H.; Li, Y.; Liu, H.; Wang, S.; Zhou, W.; Wang, C.; Li, X.; Liu, X.; Zhu, D. *Tetrahedron* **2007**, *63*, 232.

35. Wu, C. C.; DeLong, M. C.; Vardeny, Z. V.; Ferraris, J. P. *Synth. Met.* **2003**, *137*, 939.

36. Bartholomew, G. P.; Bu, X.; Bazan, G. C. *Chem. Mater.* **2000**, *12*, 2311.

37. Bolduc, A.; Dufresne, S.; Hanan, G. S.; Skene, W. G. *Can. J. Chem.* **2010**, *88*, 236.

38. Dufresne, S.; Skene, W. G. *Acta Cryst.* **2008**, *E64*, o782.

39. Dufresne, S.; Skene, W. G. *Acta Cryst.* **2008**, *E64*, o710.

40. Dufresne, S.; Bourgeaux, M.; Skene, W. G. *Acta Cryst.* **2006**, *E62*, o5602.

41. Skene, W. G.; Dufresne, S.; Trefz, T.; Simard, M. *Acta Cryst.* **2006**, *E62*, o2382.

42. Dufresne, S.; Skene, W. G. *Acta Crystallographica Section E Structure Reports Online* **2010**, *66*, o3027.

43. Wang, Y.; Fu, H.; Peng, A.; Zhao, Y.; Ma, J.; Ma, Y.; Yao, J. *Chem. Comm.* **2007**, 1623.

44. Roncali, J. *Chem. Rev.* **1992**, *92*, 711.

45. Heinze, J. r.; Frontana-Uribe, B. A.; Ludwigs, S. *Chem. Rev.* **2010**, *110*, 4724.

46. Bourgeaux, M.; Skene, W. G. *J. Org. Chem.* **2007**, *72*, 8882.

47. Tshibaka, T.; Ulliel Roche, I.; Dufresne, S.; Lubell, W. D.; Skene, W. G. *J. Org. Chem.* **2009**, *74*, 9497.

Conclusion

Le domaine des matériaux conducteurs est au plus fort de son expansion. Il existe plus que jamais une nécessité de préparer des matériaux qui auront toujours les mêmes propriétés chaque fois qu'ils seront synthétisés, d'obtenir des matériaux avec des propriétés optoélectroniques intéressantes, de les fabriquer plus facilement que leurs analogues carbonés et même d'en espérer des propriétés meilleures que pour ces derniers. Ce travail avait pour but d'étudier une nouvelle classe de molécules faites d'imines pour tenter de répondre à toutes ces problématiques. On a vu au développement d'un protocole de synthèse de nouveaux comonomères menant à une étude fiable et méthodique des propriétés par rapport aux structures. Il y avait de nombreuses incertitudes à éclaircir étant donné la nature inconnue de la photophysique et l'électrochimie des composés imine. Notre étude se séparait en cinq chapitres menant à une meilleure compréhension de la conjugaison, du contrôle de la synthèse, de la fluorescence, de la stabilité et de l'oxydation anodique pour la polymérisation ou pour la formation du radical cation stable.

Le Chapitre 1 nous a éclairé sur la formation des liens imine entre unités thiophène. Sa synthèse peut être faite de plusieurs façons. Dans tous les cas, il a été possible d'affirmer que la liaison est stable. Le lien imine est favorable à une conjugaison accrue sur toute la molécule. Les premières structures par diffraction des rayons X confirment la formation du lien imine et la coplanarité de la molécule. Le lien se forme aussi en conformation *trans*.

Les groupements électrodonneurs et électroaccepteurs ont un effet prédéterminé sur les niveaux énergétiques de même que sur la longueur de la conjugaison. La voltampérométrie cyclique montre des oxydations, dans certains cas, réversibles et non-réversibles. Ainsi, les différentes propriétés spectroscopiques et électrochimiques sont sensiblement ce à quoi on pourrait s'attendre avec ce type de molécule conjuguée. Cependant, le rendement quantique de fluorescence est étrangement bas pour les oligothiophènes. Il fallait donc approfondir pour étudier comment l'énergie se dissipait de ces molécules.

Le second chapitre tente de répondre aux questions de la dissipation d'énergie avec des exemples d'imines sur des composés de fluorène. Le fluorène est une unité aromatique reconnu pour désactiver son excitation par une fluorescence intense. Ce type de composés sera plus spectroscopiquement actif, ce qui facilite les expérimentations. Les composés ont été synthétisés grâce à notre méthodologie déjà connue. Alternativement, l'article fait état de l'oxydation des fluorènes en fluorènone et comment on pourrait l'empêcher. Dans ce cas, le lien imine n'entre pas trop en jeu pour la conjugaison des molécules. Il permet alors d'obtenir des oxydations quasi-réversibles. On voit que le lien imine désactive l'état excité des composés fluorènes et, ce, près de la limite de la diffusion. Les mesures à 77 K restreignent les conversions internes par rotations ou vibrations. Cette désactivation est très certainement due au lien imine. Des calculs et différentes mesures spectroscopiques indiquent qu'un transfert d'électron photoinduit mène à la désactivation. Cette désactivation est non-radiative dans le cas des molécules comportant une liaison imine.

Le troisième chapitre réitère et prouve la synthèse facile en exploitant les différentes unités aromatiques thiophène, furane et pyrrole. Il est démontré qu'il est possible d'obtenir les molécules désirées symétriques ou non-symétriques aisément. De plus, on arrive à contrôler les propriétés spectroscopiques de ces molécules par le choix des unités incorporées dans la structure. L'état excité des molécules est désactivé par les liens imine. Les conclusions des précédents chapitres s'appliquent à nos oligo-hétérocycles. À ce moment, on apprend qu'ils semblent passer par un croisement intersystème. Les propriétés électrochimiques ne sont pas réversibles. Les potentiels d'oxydation des molécules imine sont modelables par l'utilisation de différents hétérocycles. L'oxydation de ces molécules mène vraisemblablement à la polymérisation par couplage oxydant.

Le chapitre suivant fait appel à des molécules où on a introduit des groupements pour rendre l'oxydation réversible. Les techniques de synthèse se veulent, comme à l'habitude, très facilement réalisables. En bloquant la position 5 des hétérocycles terminaux, il est impossible pour le cation radicalaire de réagir. La molécule s'étant faite enlever un électron est toujours stable mais les propriétés sont changées. Dans le cas où on remarque l'absence de tels groupements en position 5 et seulement à cette position, on assistera à un couplage anodique. La polymérisation de ces composés mène aussi à un système dopable réversible de type P. La formation d'un cation radicalaire provoque la formation de nouvelles bandes d'absorption. Ces différents changements se traduisent par un changement de couleur intense dans le domaine du visible. On peut l'observer par

oxydation chimique et par spectroélectrochimie. La stabilité du cation radicalaire permet de le réduire au composé neutre sans dégradation.

Le dernier article porte sur la synthèse de composés thiophène, pyrrole et furane. On veut comprendre la relation entre la structure et les propriétés de ces composés imines. La synthèse est faite suivant la méthodologie des articles précédents. L'effet des différents hétérocycles est bien présent sur les propriétés spectroscopiques bien que celles-ci soient comparables à celles trouvées dans les articles précédents. On a comparé celles-ci avec des molécules faites de 1,4-phénylènediamine pour prouver la conjugaison étendue. Les propriétés électrochimiques suivent la logique énoncée dans nos travaux antérieurs. On est alors capable d'ajuster les propriétés avec les différents hétérocycles impliqués. Le couplage anodique en position 5 est possible avec toutes ces molécules. Il est alors possible de polymériser ces molécules en solution ou sur plaque ITO. Des changements notables sont observés dans l'électrochimie ou la spectroscopie des matériaux produits. Des analyses plus poussées ont été faites sur les polymères pour établir leur conjugaison et leur régiospécificité. On a démontré le couplage entre unité de nature différente dans les molécules non-symétriques. Le polymère formé en est un régiorégulier dans ce cas (tête-à-queue).

Ces articles démontrent le travail qui était à faire pour approfondir les propriétés des molécules imine afin d'être utilisées comme matériaux conducteurs. La littérature n'avait

jusqu'alors pas exploité ce lien. Plusieurs séries de synthèses et de caractérisations ont été effectuées pour tenter de répondre aux grandes interrogations concernant le lien imine au sujet de la spectroscopie et de l'électrochimie. La stratégie utilisée a permis et permettra de prédire les propriétés des nouveaux composés synthétisés. Par la suite, la comparaison des caractéristiques physico-chimiques de nos composés avec leurs analogues carbonés et l'analyse des propriétés en fonction des structures a été possible. Quelques exemples de propriétés intéressantes ont été observés avec nos composés. Sans compter la facilité de synthèse et la reproductibilité de celle-ci, ce qui distingue particulièrement le travail sur les composés imine, contrairement aux autres techniques de synthèse, est la désactivation de la fluorescence par rotation/vibration. Différentes propriétés serviront dans différents types d'applications. Les imines trouveront bien leur niche dans le paysage des dispositifs électroniques.

Contrairement aux composés vinyliques ou phényliques, les composés imine n'ont pas bénéficié de 30 ans d'optimisation, de financement et de main d'œuvre. Il est fort à parier que l'on peut aspirer à un avenir tout aussi prometteur si on en faisait tout autant pour cette classe de composés.

Il sera toujours possible de parler de travaux futurs en pensant à différentes molécules à synthétiser car les possibilités sont infinies. De cette manière, on proposera d'ajouter des chaînes comme groupements permettant d'augmenter la solubilité. C'est une

méthode à préconiser pour éventuellement synthétiser des polymères d'une longueur notable. Naturellement, la synthèse des polymères correspondant au travail accompli ici et l'étude de leurs propriétés est envisageable. Il va de soi qu'une certaine recherche doit s'effectuer pour trouver les meilleures conditions pour la polymérisation.

Les propriétés mesurées démontrent que les imines hétérocycliques ont les propriétés désirées pour être utilisées dans les dispositifs électroniques. Néanmoins, il reste encore beaucoup de recherche à faire pour réaliser des dispositifs avec les imines. L'utilisation dans les dispositifs se fait surtout, pour ne pas dire exclusivement, à l'état solide. Les comportements à l'état solide sont parfois très différents de ceux en solution. De plus, les matériaux conducteurs sont souvent présentés sous forme de polymères. La polymérisation anodique ou par condensation et l'étude des propriétés du matériau résultant sont incontournables. On peut penser particulièrement à la conductivité ou la mobilité des charges.

La plupart des propriétés à l'état solide dépendent fortement des caractéristiques de la couche de matière tels que la méthode, l'épaisseur, l'alignement des composés et plus encore, de la cristallisation. Pour obtenir des performances maximales, il faut avoir un contrôle sur l'épaisseur des couches et la morphologie. La mobilité des chaînes polymériques est très limitée à l'état solide et c'est lorsque le polymère est déposé en

solution qu'il faut optimiser la morphologie hétérojonction. C'est justement le facteur déterminant des performances et de la stabilité des dispositifs.

Ces améliorations se situent à la frontière de la chimie, de la physique et de l'ingénierie. Elles nécessitent une expertise de chacun des domaines. Les collaborations sont ainsi devenues nécessaires pour la recherche dans ce domaine. Ce domaine multidisciplinaire apprend beaucoup aux étudiants qui relèvent le défi.

Au fil du temps, l'électronique organique donne l'impression qu'elle passera davantage par des systèmes 2D voire 3D plutôt que par des polymères conjugués considérés 1D. Les défauts de morphologie en utilisant des systèmes à plusieurs dimensions ne seront pas aussi fréquents si l'on contrôle bien la synthèse en premier lieu et la mise en œuvre du matériel par la suite. Les polymères et leurs chaînes solubilisantes auront toujours des problèmes reliés à leurs structures. Par contre, ils sont plus faciles à manipuler que les gros systèmes de type graphène.

La méthodologie, démontrée dans cette thèse, visant à assembler les molécules par liens imine peut être un bon moyen de contourner ces deux problèmes. Il va sans dire que le contrôle de la synthèse des imine est le point fort de celle-ci. Elle est facile à réaliser si on la compare à des méthodes traditionnelles.

Ainsi, cette thèse a mis principalement l'accent sur la synthèse facile et propre des liens imine, deux atouts majeurs qui démontraient la validité de ce projet. À la suite du présent manuscrit, nous pouvons conclure que la stabilité de ces liens a été démontrée. Il a été possible d'obtenir des résultats et des caractéristiques semblables aux matériaux utilisés actuellement. Il n'y a maintenant plus aucun doute sur la validité des liens imines dans les matériaux conjugués. Du point de vue de l'exploration des propriétés des composés imine conjugués, nous avons largement atteint notre but.

Il est évident que des matériaux organiques conducteurs concurrentiels doivent se montrer supérieurs à ce que l'on a développé jusqu'à maintenant. Cela devrait être la première étape de ce qui reste à accomplir, d'ailleurs de nombreux groupes de recherche s'y appliquent déjà. Beaucoup d'efforts sont déployés dans la synthèse de nouveaux composés révolutionnaires. D'autre part, on entreprend aussi d'améliorer la fabrication des dispositifs grâce à l'ingénierie à l'état solide de ces matériaux. Ces deux avenues sont maintenant en convergence quoique des difficultés soient rencontrées des deux côtés.

Il est nécessaire d'aborder la divergence des résultats des recherches sur les poly(thiophènes) pour illustrer la difficulté de fabrication de matériau. Pour une même structure, le poly(3-hexylthiophène) (P3HT), on peut observer des mobilités de l'ordre de 10^{-4} à 1 $cm^2V^{-1}s^{-1}$. Il en va de même pour la conductivité. Les divers facteurs influençant les résultats sont la régiorégularité du composé, le dopage, l'organisation dans le solide, l'axe

de prise de mesure, etc. Plusieurs problèmes restent à résoudre pour parvenir à des conductivités avoisinant les maximums théoriques. Ces valeurs s'avèreraient être la barre à atteindre pour la rentabilité de l'organique électronique.

Les difficultés rencontrées sont diverses. On peut nommer celles touchant le transfert efficace des électrons entre les couches. La chimie aux interfaces demeure un point névralgique des succès de l'électronique organique. Il faut d'ailleurs composer avec les phénomènes de recombinaison. Bien que cette chimie soit relativement nouvelle, nous pouvons entrevoir des solutions dans un proche futur.

La vision la plus réaliste de l'utilisation des imines est de les incorporer dans une recette déjà gagnante. Il sera possible d'appliquer nos connaissances des imines par la suite sur n'importe quelles stratégies qui triompheront dans cette course effrénée aux meilleurs matériaux. Pendant ce temps, notre projet s'attaque à d'autres priorités essentielles en ce qui a trait à la fabrication de nouveaux matériaux : la reproductibilité, les coûts et la pollution chimique. Sans prétention, il nous a été possible de travailler sur certains défauts des autres matériaux, notamment la synthèse, la régiorégularité, la stabilité, le dopage, etc. Ainsi, les imines offrent un choix alternatif dans la poursuite des recherches possibles pour la fabrication des matériaux conducteurs.

Des études supplémentaires sont à prévoir quant à la disposition de ces molécules dans le solide. Bien que des études de structures par diffraction des rayons X aient été réalisées, les conclusions sur des relations structure/organisation restent à faire. Des groupements pourront être ajoutés pour contrôler l'arrangement à l'état solide. La technique par liaison imine permet justement de combiner des blocs synthétiques très facilement.

Il est grand temps de tenter des mesures de mobilité et de conductivité avec les composés imines. Les essais de dispositifs vont de soi. Il est fort probable que des dispositifs prometteurs en milieu universitaire éveilleront l'attention des industries. Les applications peuvent être diverses dans le domaine de l'électronique organique.

Les composés imine pourront être synthétisés dans d'autre contexte d'utilisation. Les imines sont une fonction chimique parfaite pour la construction de molécules. De cette façon, il est possible de coupler n'importe quel bloc comportant une amine avec n'importe quel autre comportant un aldéhyde.

Nous pourrons utiliser le côté désactivant de l'imine comme senseur. L'imine est aussi sujet à complexer avec différents métaux. On peut donc envisager des polymères contenant des métaux.

Dans les avancés liées à ce projet, il ne faut pas oublier le côté personnel. J'ai beaucoup appris sur les différentes techniques de caractérisation. Il m'a été possible de superviser et de rencontrer beaucoup de gens exceptionnels. C'était l'occasion de faire une étude fondamentale en milieu universitaire et d'y apprécier son fonctionnement. Cette expérience inoubliable me permettra de continuer et d'approfondir le côté fabrication/application des dispositifs électroniques organiques dans les prochaines années.

AI. ANNEXE I - CHAPITRE I

Table of content

Experimental Section

Materials and general experimental

All reagents were commercially available from Aldrich and were used as received unless otherwise stated. Anhydrous and deareated solvents were obtained via a Glass Contour solvent purification system. Isopropanol was dried over activated molecular sieves and stored under nitrogen. ^{1}H-NMR spectra were recorded on a Bruker 400 spectrometer with the appropriate deuterated solvents.

Spectroscopic Measurements

Absorption measurements were done on a Cary-500 spectrometer and fluorescence studies were carried out on an Edinburgh Instruments FLS-920 fluorimeter after deareating the samples thoroughly with nitrogen for 20 minutes. Fluorescence quantum yields were measured at 10^{-5} M by exciting the corresponding compounds at 303 nm in anhydrous spectroscopic grade acetonitrile and compared to bithiophene ($\phi_{303nm} = 0.013$)[1] excited at the same wavelength. The actinometer absorbencies, and those of the compounds, were matched at the excitation wavelength to within 5%. The phosphorescence measurements were done on a Cary Eclipse in a 1:4 methanol/ethanol glass matrix at 77 K, exciting at the compound's absorption maximum. The triplet-triplet absorption spectra were measured in anhydrous acetonitrile using a Luzchem mini-LFP system excited at 266 nm from the forth harmonic of a Continuum YAG:Nd Sure-lite laser. The triplet quantum yields were measured by optically matching samples within 5 % at 266 nm with benzophenone, whose triplet growth was monitored at 525 nm ($\Phi_T = 1$) and was used the actinometer reference.[2]

Phosphorescence quantum yields were determined by comparing optically matched samples relative to fluorenone ($\Phi_{phosphorescence}$ = 0.06 in ethanol) at 77 K.[3]

Electrochemical Measurements

Cyclic voltammetric measurements were performed on a Bio Analytical Systems EC Epsilon potentiostat with a scan rate varying from 100 to 1000 mV/s. The compounds of study were dissolved in anhydrous and deareated dichloromethane at 10^{-5} M with 0.1 M NBu_4PF_6. A glassy carbon electrode and a platinum electrode were employed as working and auxiliary electrodes, respectively. A saturated Ag/AgCl electrode was used as the reference electrode. Ferrocene was added to the samples after the measurements and was used as an internal reference.

Synthetic Details

2,5-Diamino-thiophene-3,4-dicarboxylic acid diethyl ester (I-1). The optimized procedure is based on similar reports.[4] Sulfur (4.53 g, 0.14 mol) and triethylamine (7.09 mL, 0.05 mol) were stirred in DMF (15 mL) in a 250 mL three necked flask whereupon the solution turned red in color within 30 min of stirring at room temperature. Ethylcyanoacetate (20.4 mL, 0.19 mol) diluted in DMF (5 mL) was subsequently added drop-wise over 30 minutes resulting in the deepening of the color. The opaque solution was allowed to stir under ambient condition for three days after which the solvent was removed under vacuum leaving a brown solid. The solid was loaded onto a silica column and eluted with a hexanes gradient up to 35 % ethylacetate. The procedure was repeated a

second time to obtain 2.15 g (9 %) of the title compound as gold flaky crystals. M.p.: 155-156°C. ^{1}H-NMR (acetone-d^6): δ = 6.15 (s, 4H), 4.17 (q, 4H, J = 7.1 Hz), 1.25 (t, 6H, J = 7.0 Hz). ^{13}C-NMR (DMSO-d^6): δ = 165.6, 148.9, 104.5, 60.4, 14.8. EI-MS: m/z 258.1 ([M]+, 80 %), 212 ([M-C_2H_5O]+, 100%), Anal. calc. for $C_{10}H_{14}N_2O_4S$ (258.30): C 46.50, H 5.46, N 10.85, O 24.74, S 12.41, found: C 45.89, H 5.10, N 10.47, S 12.01.

5-Diethylaminothiophene-2-carbaldehyde (I-2). In a 100 mL round flask was added 5-bromothiophene-2-carboxaldehyde (1.37 mL, 11.5 mmol) in distilled water (15 mL). Diethylamine (12 mL, 11.5 mmol) was added slowly and then, the mixture was refluxed for 6 days. The resulting oil was extracted with ethyl acetate and was then purified by chromatography with hexanes/ethylacetate (90 %/ 10% v/v) up to hexanes/ethylacetate (70 % / 30% v/v) to afford the product as a brownish oil (1.13 g, 54 %). ^{1}H-NMR (acetone-d^6): δ = 9.46 (s, 1H), 7.56 (d, 1H, J = 4.4 Hz), 6.07 (d, 1H, J = 4.4 Hz), 3.49 (q, 4H, J = 7.1 Hz), 1.23 (t, 6H, J = 7.1 Hz). ^{13}C-NMR (acetone-d^6): δ = 179.2, 166.0, 140.8, 125.9, 102.8, 47.6, 11.8. HRMS(+) calculated for $[C_9H_{13}NOS+H]^+$: 184.07906, found: 184.07913.

2-Amino-thiophene-3-carbonitrile (I-3). To a solution of 1,4-dihydroxy-dithiol (12.12 g, 78 mmol) and malenonitrile (10.52 g, 156 mmol) in DMF (55 mL) at 0°C was slowly added 1,8-diazabicyclo[5.4.0]undec-7-ene (DBU) (12 mL, 94 mmol). The solution was stirred for 8 hours at 60 °C. The reaction mixture was then hydrolysed with 0.4 M acetic acid (120 mL), extracted with ether, and dried over $MgSO_4$. The solvent was removed and the crude product was purified by recrystallization in ethylacetate /

dichloromethane (70 % / 30 % v/v) to give a light yellow solid (11.2 g, 57 %). M.p.: 97-99 °C. ^{1}H-NMR ($CDCl_3$): δ = 6.73 (d, 1H, *J* = 5.8 Hz), 6.35 (d, 1H, *J* = 5.8 Hz). ^{13}C-NMR ($CDCl_3$): δ = 163.3, 125.6, 115.3, 110.3, 88.4. HRMS(+) calculated for $[C_5H_5N_2S+H]^+$: 125.01679, found: 125.0172.

5-Methyl-thiophene-2-carbaldehyde (I-4). Phosphorous chloride (2 mL, 20 mmol) was added in anhydrous DMF (10 mL) at 0°C. After 20 minutes, 2-methyl-thiophene (0.5 mL, 5 mmol) was slowly added to the solution. The flask was carefully heated at 50 °C for 3 hours and the mixture was poured with stirring into a beaker containing crushed-ice (10 g). The aqueous layer was extracted with ethylacetate (7 times), while the organic layers were combined, then dried over anhydrous magnesium sulphate, and finally concentrated. The crude mixture was purified by chromatography (SiO_2) eluted with hexanes/ethylacetate (50 % / 50 % v/v). The product was isolated as a yellow oil (160 mg, 25 %). ^{1}H-NMR ($CDCl_3$): δ = 9.85 (s, 1H), 7.78 (d, 1H, *J* = 3.7 Hz), 7.03 (d, 1H, *J* = 3.7 Hz), 2.58 (s, 3H). ^{13}C-NMR ($CDCl_3$): δ = 184.0, 152.4, 143.8, 139.2, 128.9, 16.6. HRMS(+) calculated for $[C_6H_6S+H]^+$: 127.02121, found: 127.02137.

2-Amino-5-[(thiophen-2-ylmethylene)-amino]-thiophene-3,4-dicarboxylic acid diethyl ester (I-5). In a 50 mL round bottom flask was added **I-1** (50 mg, 0.19 mmol) in absolute ethanol (20 mL) to which was added 2-thiophene carboxaldehyde (24 mg, 0.21 mmol) and a catalytic amount of trifluoroacetic acid (TFA). The mixture was refluxed for 20 hours under normal atmosphere. Complete removal of the solvent led to an orange solid which was purified by flash chromatography (SiO_2) and eluted with

hexanes/ethylacetate (80 % / 20 %). The product was isolated as an orange solid (81 %). M.p.: 114-116 °C. ^{1}H-NMR (acetone-d^6): δ = 8.24 (s, 1H), 7.63 (d, 1H, *J* = 5.0Hz), 7.52 (dd, 1H, *J* = 3.7 Hz and *J* = 0.7 Hz), 7.48 (s, 2H), 7.14 (dd, 1H, *J* = 5.0 Hz and 3.7 Hz), 4.32 (q, 2H, *J* = 7.2 Hz), 4.19 (q, 2H, *J* = 7.1 Hz), 1.37 (t, 3H, *J* = 7.1 Hz), 1.26 (t, 3H, *J* = 7.1 Hz). ^{13}C-NMR (acetone-d^6): δ = 165.0, 164.3, 161.1, 161.0, 146.1, 143.2, 132.8, 132.1, 130.5, 128.4, 101.8, 61.0, 60.0, 14.3, 14.1. HRMS(+) calculated for $[C_{15}H_{16}O_4N_2S_2+H]^+$: 353.06242, found: 353.06251.

2-Amino-5-[(5-nitro-thiophen-2-ylmethylene)-amino]-thiophene-3,4-dicarboxylic acid diethyl ester (I-6). In a 50 mL round bottom flask, **I-1** (30 mg, 0.12 mmol) was dissolved in isopropanol (20 mL). To this, was added with vigorous stirring, 5-nitro-2-thiophene carboxaldehyde (91 mg, 0.58 mmol) and catalytic TFA followed by refluxing for 30 minutes. The title compound was isolated as a dark black-purple powder (87 %) by flash chromatography (SiO_2) eluted with hexanes/ethylacetate (90 % / 10 % v/v) up to hexanes/ethylacetate (50% / 50 % v/v). M.p.: 194-196 °C. ^{1}H-NMR (acetone-d^6): δ = 8.21 (s, 1H), 8.00 (d, 1H, *J* = 4.4 Hz), 7.74 (s, 2H), 7.50 (d, 1H, *J* = 4.4 Hz), 4.37 (q, 2H, *J* = 7.1 Hz), 4.22 (q, 2H, *J* = 7.1 Hz), 1.40 (t, 3H, *J* = 7.1 Hz), 1.27 (t, 3H, *J*= 7.1 Hz). ^{13}C-NMR (acetone-d^6): δ = 164.6, 164.1, 162.8, 162.7, 152.7, 149.7, 143.7, 134.3, 131.4, 130.1, 129.7, 61.4, 60.3, 14.3, 14.0. HRMS(+) calculated for $[C_{15}H_{16}O_6N_3S_2+H]^+$: 398.04750, found: 398.04794.

2-Amino-5-[(5-diethylamino-thiophen-2-ylmethylene)-amino]-thiophene-3,4-dicarboxylic acid diethyl ester (I-7). In a 50 mL round bottom flask was added **I-1**

(67 mg, 0.26 mmol) dissolved in 20 mL of anhydrous toluene to which was subsequently added 1,4-diazabicyclo[2.2.2]octane (DABCO) (32 mg, 0.29 mmol), $TiCl_4$ 1.0 M solution in toluene (286 μL, 0.29 mmol) at 0 ^oC and then **2** (52 mg, 0.29 mmol) was added. The mixture was then refluxed for two hours after which the solvent was removed. Purification by flash chromatography (SiO_2) with hexanes/ethylacetate (90 % / 10 % v/v) and increased up to hexanes/ethylacetate (50 % / 50 % v/v) yielded the title product as a yellow-orange solid (67 %). M. decomp.: 95 °C. ^{1}H-NMR (acetone-d^6): δ = 7.96 (s, 1H), 7.23 (s, 2H), 7.21 (d, 1H, *J* = 4.4 Hz), 5.93 (d, 1H, *J* = 4.2 Hz), 4.27 (q, 2H, *J* = 7.2 Hz), 4.17 (q, 2H, *J* = 7.1 Hz), 3.43 (q, 4H, *J* = 7.1 Hz), 1.35 (t, 3H, *J* = 7.1 Hz), 1.24 (t, 3H, *J* = 7.1 Hz), 1.21 (t, 6H, *J* = 7.1 Hz). ^{13}C-NMR (acetone-d^6): δ = 164.5, 162.3, 159.3, 159.3, 146.9, 135.7, 135.5, 125.5, 124.5, 102.2, 101.7, 60.7, 59.7, 47.3, 14.2, 14.1, 12.0. HRMS(+) calculated for $[C_{19}H_{25}O_4N_3S_2+H]^+$: 424.13592, found: 424.13520.

Diethyl-2-((5-methylthiophen-2-yl)methyleneamino)-5-aminothiophene-3,4-dicarboxylate (I-8). **I-1** (30 mg, 0.12 mmol) and **I-4** (16 mg, 0.13 mmol) were mixed in anhydrous isopropanol with a catalytic amount of TFA and refluxed for 20 hours. The reaction was then purified by flash chromatography eluted with hexanes/ethylacetate (90 % / 10 % v/v) up to hexanes/ethylacetate (60 % / 40 % v/v) to afford the product as an orange viscous oil (30 mg, 70 %). ^{1}H-NMR (acetone-d^6): δ = 8.15 (s, 1H), 7.45 (s, 2H), 7.33 (d, 1H, ^3J = 3.6 Hz), 6.84 (dd, 1H, *J* = 3.7 Hz and 1.0 Hz), 4.33 (q, 2H, *J* = 7.2 Hz), 4.21 (q, 2H, *J* = 7.2 Hz), 2.51 (s, 3H), 1.39 (t, 3H, *J* = 7.2 Hz), 1.28 (t, 3H, *J* = 7.1 Hz). ^{13}C-NMR (acetone-d^6): δ = 165.0, 164.4, 160.8, 146.3, 145.7, 141.1, 139.7, 136.7, 132.6,

129.8, 127.0, 60.9, 59.9, 15.3, 14.3, 14.1. HRMS(+) calculated for $[C_{16}H_{18}N_2O_4S_2+H]^+$: 367.07807, found: 367.07862.

2-[(Thiophen-2-ylmethylene)-amino]-thiophene-3-carbonitrile (I-9). **I-3** (50 mg, 0.40 mmol) and thiophene-2-carboxaldehyde (54 mg, 0.48 mmol) were mixed in anhydrous isopropanol with a catalytic amount of TFA and then refluxed for 20 hours. The reaction was then purified by flash chromatography eluted with hexanes/ethylacetate (90 % / 10 % v/v) up to hexanes/ethylacetate (60 % / 40 % v/v) to afford the product as an orange solid (61 mg, 70 %). M.p.: 58-60 °C. ^{1}H-NMR (acetone-d^6): δ = 8.49 (s, 1H), 7.90 (d, 1H, J = 5.0 Hz), 7.82 (dd, 1H, ^3J = 3.7 Hz and 1.0 Hz), 7.42 (d, 1H, J = 5.7 Hz), 7.26 (d, 1H, J = 5.6 Hz), 7.26 (dd, 1H, J = 4.8 Hz and J = 3.5 Hz). ^{13}C-NMR (acetone-d^6): δ = 163.4, 155.4, 141.8, 136.2, 133.9, 129.0, 128.1, 122.5, 114.6, 105.8. HRMS(+) calculated for $[C_{10}H_6N_2S_2+H]^+$: 219.00452, found: 219.00514.

2-[(5-Nitro-thiophen-2-ylmethylene)-amino]-thiophene-3-carbonitrile (I-10). **I-3** (30 mg, 0.24 mmol) and 5-nitro-thiophene-2-carboxaldehyde (41 mg, 0.26 mmol) were mixed in anhydrous isopropanol with catalytic TFA and refluxed for 28 hours. The reaction was then purified by flash chromatography eluted with hexanes/ethylacetate (90 % / 10 %) up to hexanes/ethylacetate (70 % / 30 %) to afford the compound as an orange powder (45 mg, 71 %). M.p.: 192°-194°C. ^{1}H-NMR (acetone-d^6): δ = 8.98 (s, 1H), 8.12 (d, 1H, J = 4.3 Hz), 7.85 (d, 1H, J = 4.3 Hz), 7.61 (d, 1H, J = 5.7 Hz), 7.38 (d, 1H, J = 5.7 Hz). ^{13}C-NMR (acetone-d^6): δ = 161.2, 154.3, 147.3, 133.7, 130.0, 128.6,

125.9, 125.1, 109.5, 108.5. HRMS(+) calculated for $[C_{10}H_5O_2N_3S_2+H]^+$: 263.98959, found: 263.99006.

2-[(5-Diethylamino-thiophen-2-ylmethylene)-amino]-thiophene-3-carbonitrile (I-11). In a 50 mL round bottom flask was added **I-3** (30 mg, 0.24 mmol) in 20 mL anhydrous isopropanol to which was added **I-2** (48 mg, 0.26 mmol) and a catalytic amount of TFA. The mixture was refluxed for 3 hours. Complete removal of the solvent afforded an orange oil which was purified by flash chromatography (SiO_2) eluted with hexanes/ethylacetate (90 % / 10 % v/v) up to hexanes/ethylacetate (65 % / 35 % v/v). The product was isolated as an orange viscous oil (44 mg, 63 %). ^{1}H-NMR (acetone-d^6): δ = 8.44 (s, 1H), 7.54 (d, 1H, J = 4.5 Hz), 7.09 (s, 2H), 6.13 (d, 1H, J = 4.5 Hz), 3.54 (q, 4H, J = 7.1 Hz), 1.27 (t, 6H, J = 7.1 Hz). ^{13}C-NMR (acetone-d^6): δ = 166.1, 153.2, 141.2, 131.9, 127.9, 123.3, 118.8, 116.0, 104.5, 101.5, 48.2, 12.4. HRMS(+) calculated for $[C_{14}H_{15}N_3S_2+H]^+$: 290.07802, found: 290.07887.

2-((5-Methylthiophen-2-yl)methyleneamino)thiophene-3-carbonitrile (I-12). In anhydrous isopropanol was added **I-3** (30 mg, 0.24 mmol) and **I-4** (30 mg, 0.24 mmol) with a catalytic amount of TFA and then refluxed for 20 hours. The reaction was purified by flash chromatography eluted with hexanes/ethylacetate (90 % / 10 % v/v) up to hexanes/ethylacetate (60 % / 40 % v/v) to afford an orange oil (47 mg, 85%). ^{1}H-NMR (acetone-d^6): δ = 8.79 (s, 1H), 7.65 (d, 1H, J = 3.7 Hz), 7.39 (d, 1H, ^3J = 5.7 Hz), 7.27 (d, 1H, J = 5.7 Hz), 6.99 (dd, 1H, J = 3.7 Hz), 2.60 (s, 3H). ^{13}C-NMR (acetone-d^6): δ =163.7,

155.1, 149.7, 139.8, 136.9, 128.0, 127.8, 122.0, 114.6, 105.3, 15.5. HRMS(+) calculated for $[C_{11}H_8N_2S_2+H]^+$: 233.02017, found: 233.02054.

2-((5-formylthiophen-2-yl)methyleneamino)thiophene-3-carbonitrile (I-13). 2,5-thiophene dicarboxaldehyde (60 mg, 0.42 mmol) and **I-3** (26 mg, 0.21 mmol) were dissolved in anhydrous isopropanol with a catalytic amount of TFA and then refluxed for 15 hours. The reaction was precipitated twice from ethylacetate/hexanes to give a light orange solid (20 mg, 39 %). M.p.: 214-217 °C. ^{1}H-NMR (acetone-d^6): δ = 10.07 (s, 1H), 9.00 (s, 1H), 8.07 (d, 1H, *J* = 3.9 Hz), 7.95 (d, 1H, *J* = 3.9 Hz), 7.56 (d, 1H, *J* = 5.7 Hz), 7.35 (d, 1H, *J* = 5.6 Hz). ^{13}C-NMR (acetone-d^6): δ = 184.4, 161.9, 154.8, 148.6, 147.8, 137.3, 135.5, 128.5, 124.3, 114.2, 107.7. HRMS(+) calculated for $[C_{11}H_6N_2OS_2+H]^+$: 246.99943, found: 246.99979.

2,5-Bis-[(thiophen-2-ylmethylene)-amino]-thiophene-3,4-dicarboxylic acid diethyl ester (I-14). I-1 (100 mg, 0.4 mmol) and 2-thiophene carboxaldehyde (198.8 mg, 1.6 mmol) were refluxed in anhydrous isopropanol (10 ml), which turned from orange then red in color within 125 hours under nitrogen. The solution was then concentrated under vacuum to near dryness. The crude product was loaded onto a silica column and eluted with hexanes/ethylacetate (85 % / 15 % v/v) up to hexanes/ethylacetate (75 % / 25 %) to give a red solid (65 mg, 36 %). M.p.: 125-126 °C. ^{1}H-NMR (acetone-d^6): δ = 8.75 (s, 2H), 7.85 (d, 2H, *J* = 5.0 Hz), 7.76 (d, 2H, *J* = 3.7 Hz), 7.26 (dd, 2H, *J* = 5.2 and 3.7 Hz), 4.32 (q, 4H, *J* = 7.2 Hz), 1.37 (t, 6H, *J* = 7.2 Hz). ^{13}C-NMR (acetone-d^6): δ = 163.0,

153.6, 149.2, 142.4, 135.1, 133.2, 128.9, 127.5, 61.2, 14.2. HRMS(+) calculated for $[C_{20}H_{18}O_4N_2S_3+H]^+$: 447.05015, found: 447.04921.

Diethyl-2,5-bis((5-nitrothiophen-2-yl)methyleneamino)thiophene-3,4-dicarboxylate (I-15). 5-Nitrothiophene-2-carbaldehyde (40 mg, 0.25 mmol) was dissolved in anhydrous toluene at 0 °C with DABCO (29 mg, 0.25 mmol) and the slow addition of $TiCl_4$ 1.0 M solution in toluene (255 μL, 0.25 mmol). **I-1** (33 mg, 0.13 mmol) was added and the mixture was then refluxed for 4 hours. The title compound was isolated as a purple-grey solid after flash chromatography with hexanes/ethylacetate (90 % / 10 % v/v) up to hexanes/ethylacetate (60 % / 40 % v/v) (26 mg, 38 %). M.p.: 255-257 °C. ^{1}H-NMR (acetone-d^6): δ = 8.84 (s, 2H), 8.10 (d, 2H, *J* = 4.5 Hz), 7.80 (d, 2H, *J* = 4.4 Hz), 4.37 (q, 4H, *J* = 7.1 Hz), 1.39 (t, 6H, *J* = 7.1 Hz). ^{13}C-NMR (acetone-d^6): δ = 164.8, 163.3, 156.2, 147.0, 137.5, 131.3, 130.0, 127.8, 60.6, 14.4. HRMS(+) calculated for $[C_{20}H_{16}O_8N_4S_3+H]^+$: 563.10872, found: 537.01931.

Diethyl-2,5-bis((5-(diethylamino)thiophen-2-yl)methyleneamino) thiophene-3,4-dicarboxylate (I-16). I-2 (50 mg, 0.27 mmol) was dissolved with DABCO (31 mg, 0.27 mmol) in anhydrous toluene (25 mL) at 0 °C and the slow addition of $TiCl_4$ 1.0 M solution in toluene (273 μL, 0.27 mmol). **I-1** (32 mg, 0.12 mmol) was added and then refluxed for 3 hours. The solvent was removed and the product isolated as a purple-grey solid after purification by flash chromatography with hexanes/ethylacetate (90 % / 10 % v/v) up to hexanes/ethylacetate (50 % / 50 % v/v) (64 mg, 88 %). M. decomp.: 86 °C. ^{1}H-NMR (acetone-d^6): δ = 8.26 (s, 2H), 7.39 (d, 2H, *J* = 4.4 Hz), 6.05 (d, 2H, *J* = 4.4 Hz),

4.24 (q, 4H, *J* =7.1 Hz), 3.49 (q, 8H, *J* =7.1 Hz), 1.34 (t, 6H, *J* = 7.1Hz), 1.25 (t, 12H, *J* = 7.1Hz). ^{13}C-NMR (acetone-d^6): δ = 164.2, 163.8, 150.6, 149.1, 138.4, 124.3, 124.2, 103.3, 60.5, 47.6, 14.2, 12.0. HRMS(+) calculated for $[C_{28}H_{36}O_4N_4S_3+H]^+$: 589.19714, found: 589.19778.

2-[(5-Nitro-thiophen-2-ylmethylene)-amino]-5-[(thiophen-2-ylmethylene)-amino]-thiophene-3,4-dicarboxylic acid diethyl ester (I-17). 5-Nitrothiophene-2-carbaldehyde (9 mg, 0.06 mmol) was dissolved in anhydrous toluene under nitrogen at 0 ^{o}C with DABCO (7 mg, 0.06 mmol), $TiCl_4$ 1.0 M solution in toluene (59 μL, 0.06 mmol) was slowly added follow by **I-14** (12 mg, 0.03 mmol). The mixture was refluxed for 6 hours, after which the solution was evaporated and the product was isolated as a red powder (7 mg, 48 %) after purification by flash chromatography eluted with hexanes/ethylacetate (90 % / 10 % v/v) up to hexanes/ethylacetate (60 % / 40 % v/v). M.p.: 220-222 °C. ^{1}H-NMR (acetone-d^6): δ = 8.81 (s, 1H), 8.79 (s, 1H), 8.10 (d, 1H, *J* = 3.2 Hz), 7.91 (d, 1H, *J* = 4.1 Hz), 7.81 (d, 1H, *J* = 2.9 Hz), 7.78 (d, 1H, *J* = 4.6 Hz), 7.29 (dd, 1H, *J* = 2.7 Hz and 3.8 Hz), 4.38 (q, 2H, *J* = 5.3 Hz), 4.32 (q, 2H, *J* = 5.3 Hz), 1.41 (t, 3H, *J* = 5.3 Hz), 1.36 (t, 3H, *J* = 5.3 Hz). ^{13}C-NMR (acetone-d^6): δ = 176.9, 174.2, 169.1, 166.5, 155.1, 151.7, 146.6, 142.2, 140.9, 136.1, 135.9, 134.0, 132.7, 130.0, 129.0, 127.5, 61.5, 61.3, 14.2, 14.0. HRMS(+) calculated for $[C_{20}H_{17}O_6N_3S_3+H]^+$: 492.03522, found: 492.03561.

2-[(5-Diethylamino-thiophen-2-ylmethylene)-amino]-5-[(5-nitro-thiophen-2-ylmethylene)-amino]-thiophene-3,4-dicarboxylic acid diethyl ester (I-18).

5-Nitrothiophene-2-carbaldehyde (23 mg, 0.15 mmol) was dissolved in anhydrous toluene under nitrogen at 0 °C with DABCO (16 mg, 0.15 mmol), $TiCl_4$ 1.0 M solution in toluene (146 µL, 0.15 mmol) followed by **I-7** (56 mg, 0.13 mmol). The solution was then refluxed for 7 hours. The product was obtained as a purple-grey powder (53 mg, 72%) after purification by flash chromatography eluted with hexanes/ethylacetate (90 % / 10 % v/v) up to hexanes/ethylacetate (50 % / 50 % v/v). M. decomp.: 170 °C. ^{1}H-NMR (acetone-d^6): δ = 8.55 (s, 1H), 8.36 (s, 1H), 8.06 (d, 1H, *J* = 4.3 Hz), 7.66 (d, 1H, *J* = 4.4 Hz), 7.55 (d, 1H, *J* = 4.6 Hz), 6.19 (d, 1H, *J* = 4.6 Hz), 4.36 (q, 2H, *J* = 7.3 Hz), 4.25 (q, 2H, *J* = 7.1 Hz), 3.55 (q, 4H, *J* = 7.5 Hz), 1.39 (t, 3H, *J* = 7.1 Hz), 1.34 (t, 3H, *J* = 7.2 Hz), 1.28 (t, 6H, *J* = 7.1 Hz). ^{13}C-NMR (acetone-d^6): δ = 173.0, 167.5, 164.1, 162.9, 149.7, 143.7, 132.9, 131.6, 131.3, 130.2, 130.1, 129.7, 129.1, 127.6, 114.0, 104.9, 61.4, 60.2, 39.2, 14.2, 13.8, 10.8. HRMS(+) calculated for $[C_{24}H_{26}O_6N_4S_3+H]^+$: 563.10872, found: 563.10838.

Diethyl-2,5-bis((5-methylthiophen-2-yl)methyleneamino)thiophene-3,4-dicarboxylate (I-19). **I-4** (52 mg, 0.41 mmol) was dissolved in anhydrous toluene under nitrogen at 0 °C with DABCO (260 mg, 2.32 mmol), $TiCl_4$ 1.0 M solution in toluene (580 µL, 0.58 mmol) and **I-1** (30 mg, 0.12 mmol). The solution was then refluxed for 2 hours. The product was obtained as a red viscous oil (15 mg, 26%) after filtration and washing with acetone and then with hexanes. ^{1}H-NMR (acetone-d^6): δ = 8.60 (s, 2H), 7.55 (d, 2H, *J* = 3.5 Hz), 6.95 (d, 2H, *J* = 3.6 Hz), 4.30 (q, 4H, *J* = 7.2 Hz), 2.56 (s, 6H), 1.36 (t, 6H, *J* = 7.2 Hz). ^{13}C-NMR (acetone-d^6): δ = 163.1, 153.2, 149.2, 148.8, 140.4, 135.7, 127.6, 127.1, 61.1, 15.5, 14.1. HRMS(+) calculated for $[C_{22}H_{22}N_2O_4S_3+H]^+$: 475.08145, found: 475.08065.

(13E)-N-((5-((E)-(3-Cyanothiophen-2-ylimino)methyl)thiophen-2-yl)methylene)-3-cyanothiophen-2-amine (I-20). 2,5-Thiophene dicarboxaldehyde (30 mg, 0.21 mmol) was dissolved along with **I-3** (134 mg, 1.07 mmol) in *n*-butanol in a 50 mL round bottom flask. The resulting solution was refluxed for 48 hours after which the product precipitated from solution. It was then filtered and washed with cold absolute ethanol to yield the title compound as a dark brown powder (58 mg, 77 %). M.p.: 244°-246°C. ^{1}H-NMR (acetone-d^6): δ = 8.96 (s, 2H), 7.91 (s, 2H), 7.53 (d, 2H, ^{3}J = 5.7Hz), 7.34 (d, 2H, ^{3}J = 5.6Hz). ^{13}C-NMR (acetone-d^6): δ = 154.7, 147.0, 140.8, 136.1, 128.4, 123.9, 117.3, 107.3. HRMS(+) calculated for $[C_{16}H_9N_4S_3+H]^+$: 352.9984, found: 352.9994.

N-((Thiophen-2-yl)methylene)butan-1-amine (I-21). In a 50 mL round bottom flask was added 2-thiophene carboxaldehyde (100 mg, 0.89 mmol) diluted in *n*-butylamine (72 mg, 0.98 mmol). The reaction was mixed at room temperature for 4 hours after which the excess *n*-butylamine was removed under vacuum to give the pure product as a clear liquid (144 mg, 93 %). ^{1}H-NMR (acetone-d^6): δ = 8.42 (s, 1H), 7.51 (d, 1H, J = 5.0 Hz), 7.38 (d, 1H, J = 3.1 Hz), 7.11 (dd, 1H, J = 4.9 Hz and 3.2 Hz), 3.55 (t, 2H, J = 6.8 Hz), 1.64 (m(5), 2H, J = 7.0 Hz), 1.39 (m(6), 2H, J = 7.5 Hz), 0.95 (t, 3H, J = 7.4 Hz). ^{13}C-NMR (acetone-d^6): δ = 154.1, 143.7, 130.6, 129.0, 127.7, 61.0, 33.5, 20.8, 14.0. HRMS(+) calculated for $[C_9H_{13}NS+H]^+$: 168.08415, found: 168.08410.

N-((5-((Butylimino)methyl)thiophen-2-yl)methylene)butan-1-amine (I-22). In a 50 mL round bottom flask was added 2,5-thiophene dicarboxaldehyde (100 mg, 0.71 mmol) dissolved in *n*-butylamine (1 mL, 10.1 mmol). The reaction was stirred at room temperature for 20 hours. The excess *n*-butylamine was removed under vacuum to give the pure product as a light yellow solid (160 mg, 90%). M.p.: 34-35 °C. ^{1}H-NMR (acetone-d^6): δ = 8.41 (s, 2H), 7.36 (s, 2H), 3.56 (t, 4H, J = 6.7 Hz), 1.62 (m(5), 4H, J = 7.7 Hz), 1.39 (m(6), 4H, J = 7.6 Hz), 0.93 (t, 6H, J = 7.4 Hz). ^{13}C-NMR (acetone-d^6): δ = 154.4, 145.5, 130.6, 60.8, 33.3, 20.6, 13.6. HRMS(+) calculated for $[C_{14}H_{22}N_2S+H]^+$: 251.15765, found: 251.15882.

Absorption and Emission spectra

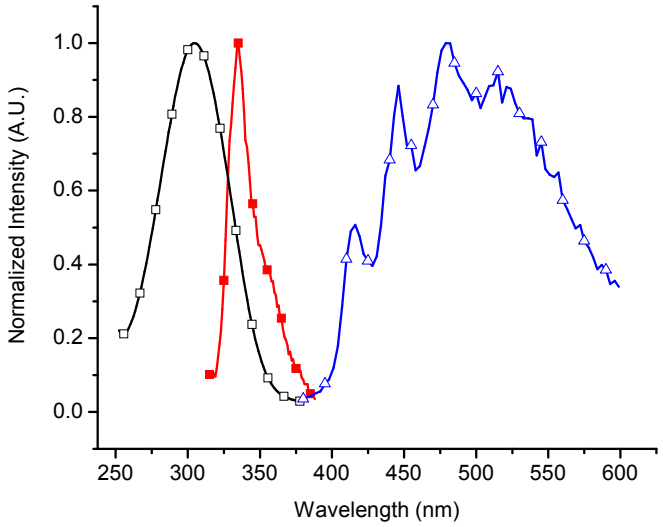

Figure AI-1. Normalized absorption (open squares), fluorescence (closed squares), and phosphorescence (open triangles) spectra of **I-1** in acetonitrile.

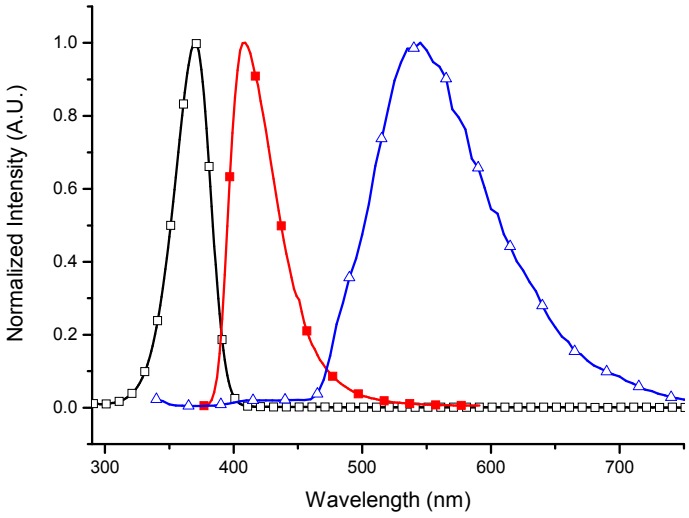

Figure AI-2. Normalized absorption (open squares), fluorescence (closed squares), and phosphorescence (open triangles) spectra of **I-2** in acetonitrile.

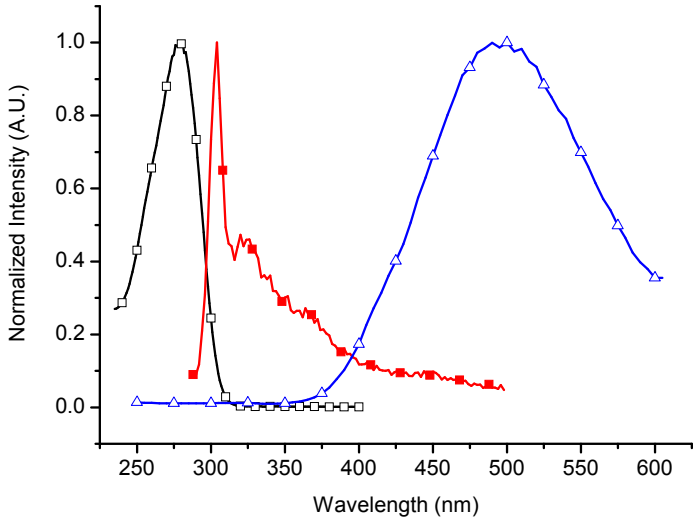

Figure AI-3. Normalized absorption (open squares), fluorescence (closed squares), and phosphorescence (open triangles) spectra of **I-3** in acetonitrile.

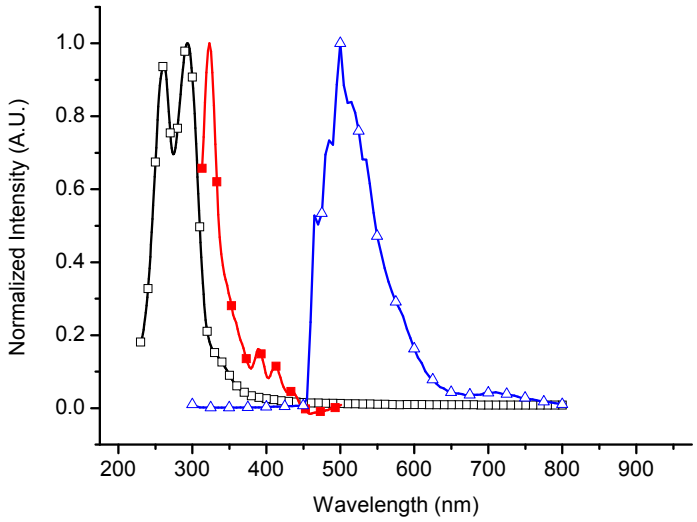

Figure AI-4. Normalized absorption (open squares), fluorescence (closed squares), and phosphorescence (open triangles) spectra of **I-4** in acetonitrile.

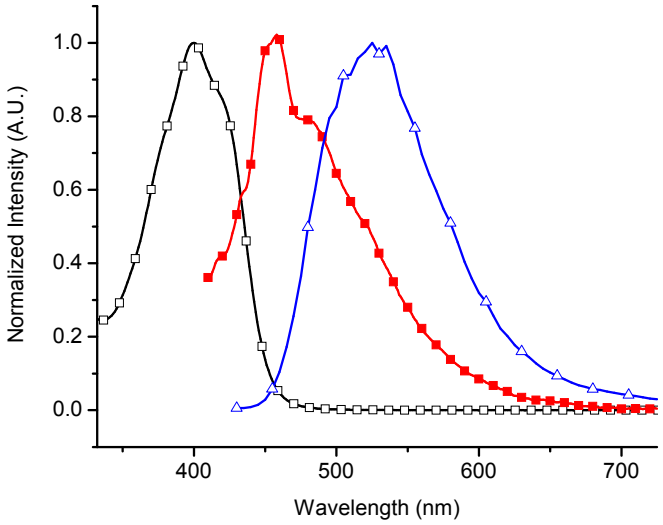

Figure AI-5. Normalized absorption (open squares), fluorescence (closed squares), and phosphorescence (open triangles) spectra of **I-5** in acetonitrile.

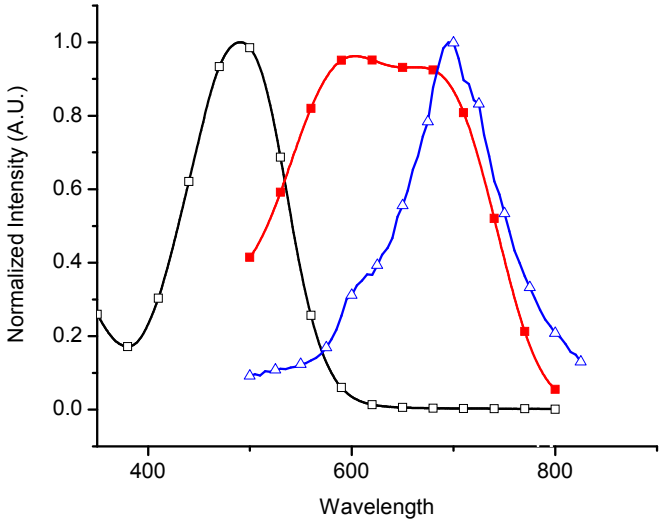

Figure AI-6. Normalized absorption (open squares), fluorescence (closed squares), and phosphorescence (open triangles) spectra of **I-6** in acetonitrile.

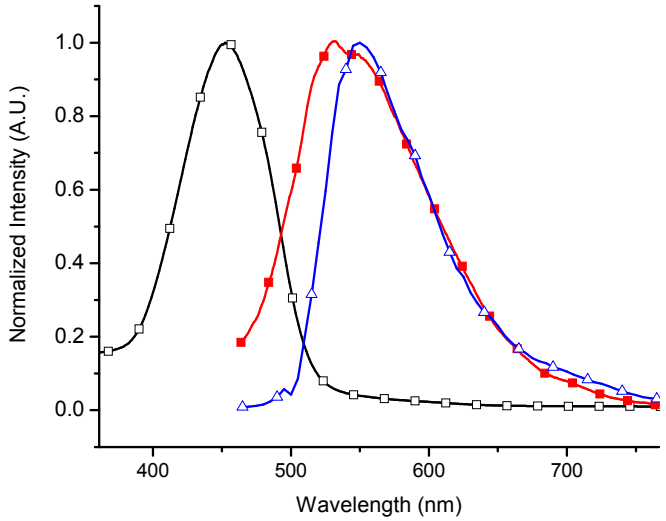

Figure AI-7. Normalized absorption (open squares), fluorescence (closed squares), and phosphorescence (open triangles) spectra of **I-7** in acetonitrile.

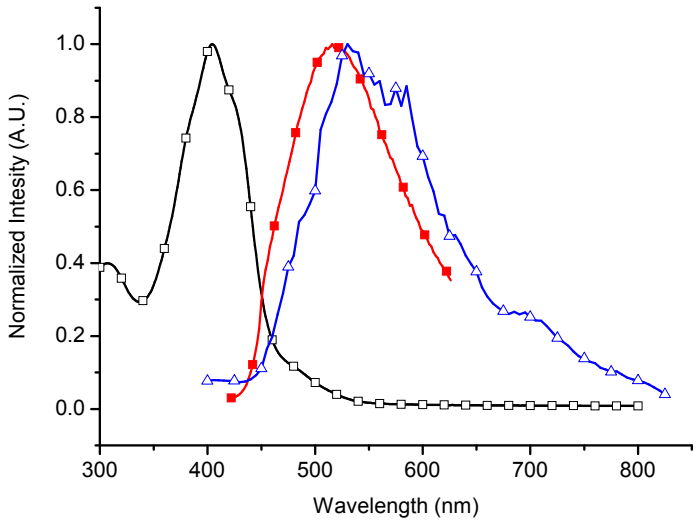

Figure AI-8. Normalized absorption (open squares), fluorescence (closed squares), and phosphorescence (open triangles) spectra of **I-8** in acetonitrile.

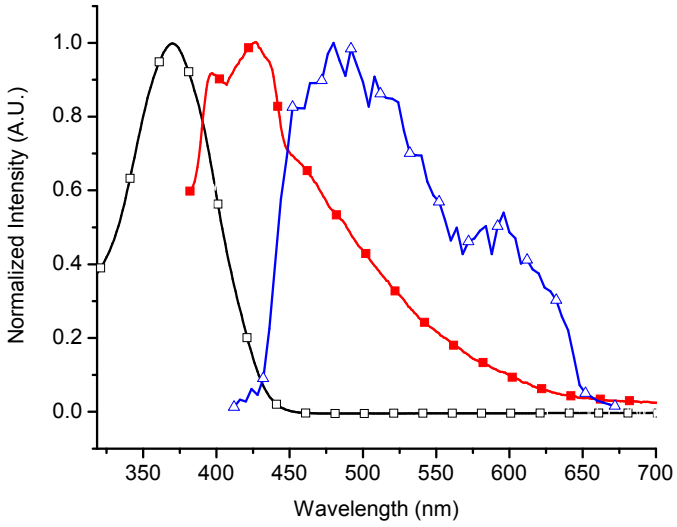

Figure AI-9. Normalized absorption (open squares), fluorescence (closed squares), and phosphorescence (open triangles) spectra of **I-9** in acetonitrile.

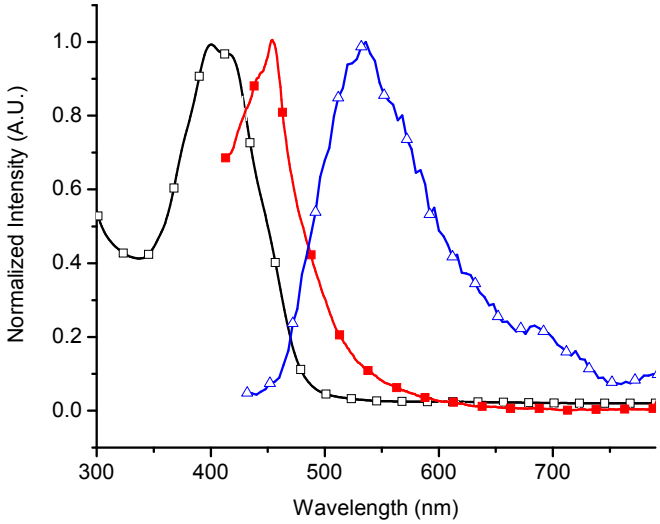

Figure AI-10. Normalized absorption (open squares), fluorescence (closed squares), and phosphorescence (open triangles) spectra of **I-10** in acetonitrile.

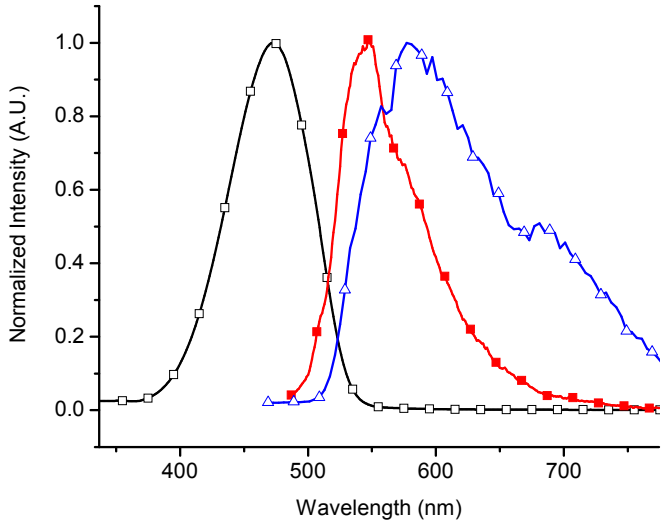

Figure AI-11. Normalized absorption (open squares), fluorescence (closed squares), and phosphorescence (open triangles) spectra of **I-11** in acetonitrile.

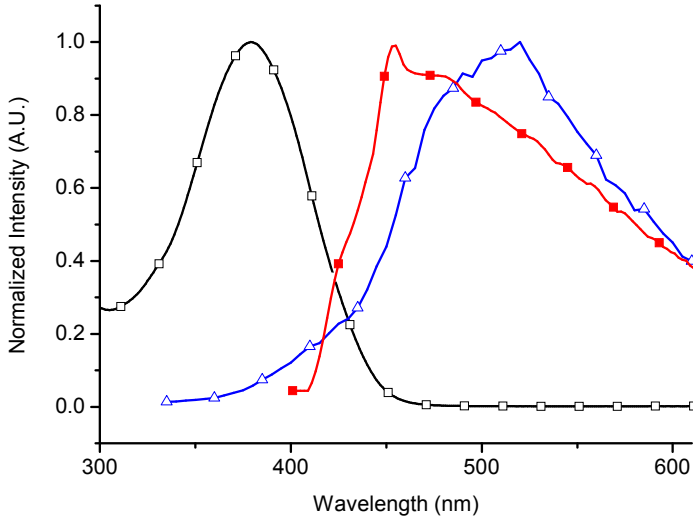

Figure AI-12. Normalized absorption (open squares), fluorescence (closed squares), and phosphorescence (open triangles) spectra of **I-12** in acetonitrile.

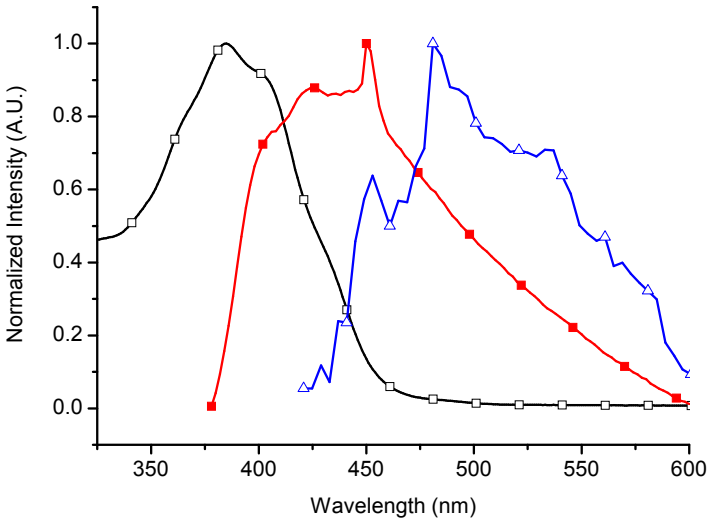

Figure AI-13. Normalized absorption (open squares), fluorescence (closed squares), and phosphorescence (open triangles) spectra of **I-13** in acetonitrile.

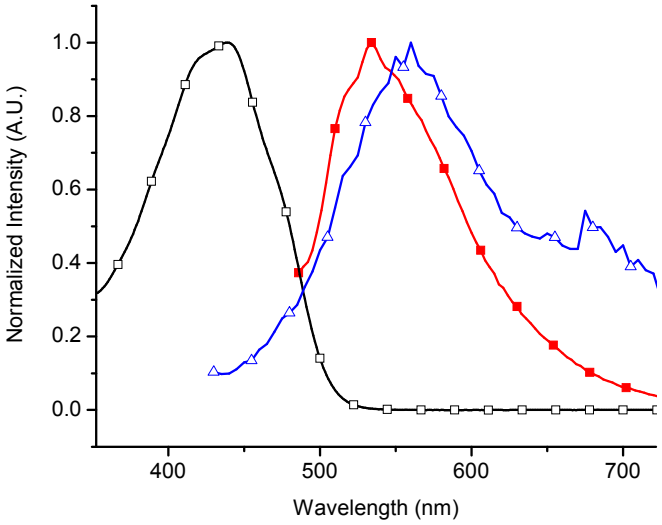

Figure AI-14. Normalized absorption (open squares), fluorescence (closed squares), and phosphorescence (open triangles) spectra of **I-14** in acetonitrile.

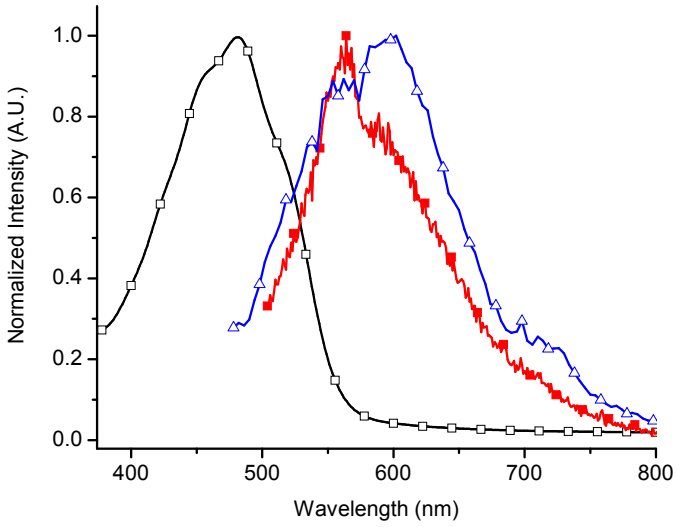

Figure AI-15. Normalized absorption (open squares), fluorescence (closed squares), and phosphorescence (open triangles) spectra of **I-15** in acetonitrile.

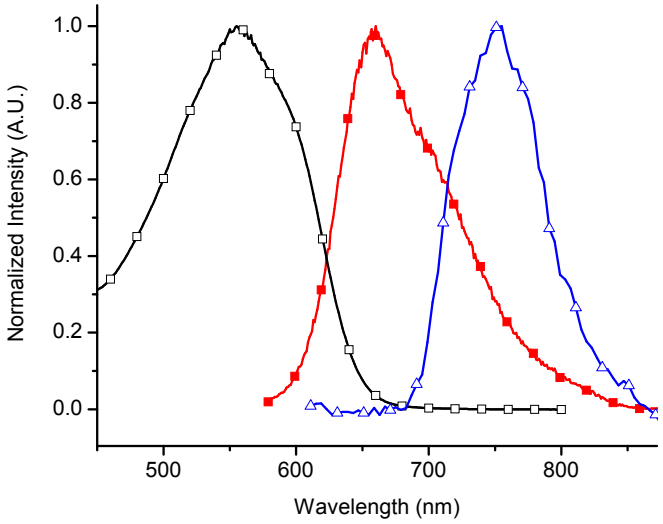

Figure AI-16. Normalized absorption (open squares), fluorescence (closed squares), and phosphorescence (open triangles) spectra of **I-16** in acetonitrile.

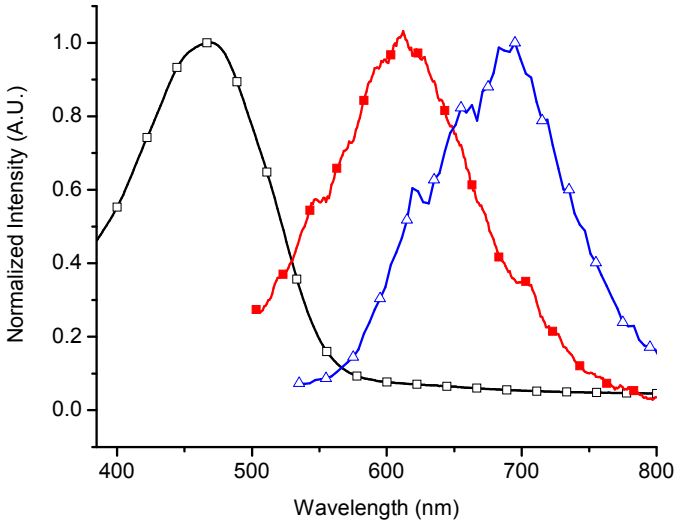

Figure AI-17. Normalized absorption (open squares), fluorescence (closed squares), and phosphorescence (open triangles) spectra of **I-17** in acetonitrile.

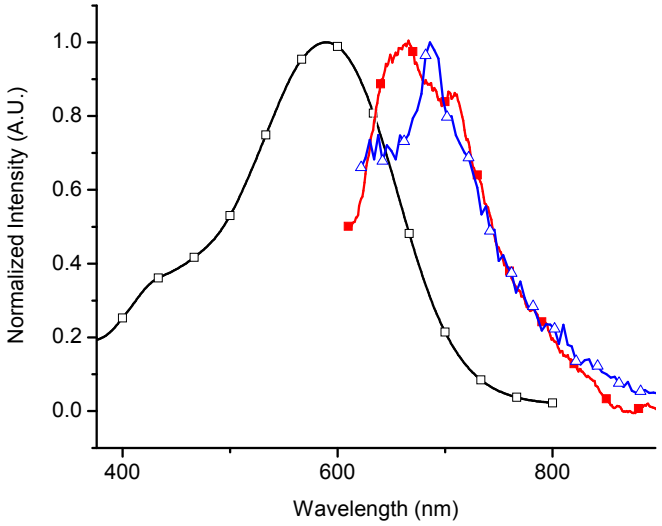

Figure AI-18. Normalized absorption (open squares), fluorescence (closed squares), and phosphorescence (open triangles) spectra of **I-18** in acetonitrile.

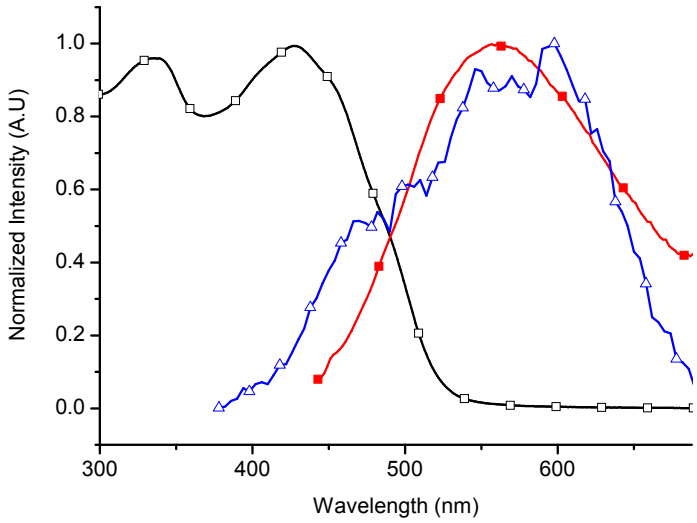

Figure AI-19. Normalized absorption (open squares), fluorescence (closed squares), and phosphorescence (open triangles) spectra of **I-19** in acetonitrile.

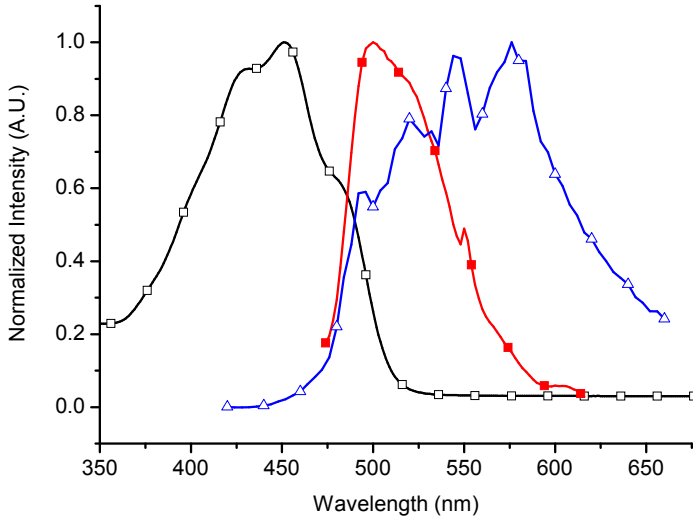

Figure AI-20. Normalized absorption (open squares), fluorescence (closed squares), and phosphorescence (open triangles) spectra of **I-20** in acetonitrile.

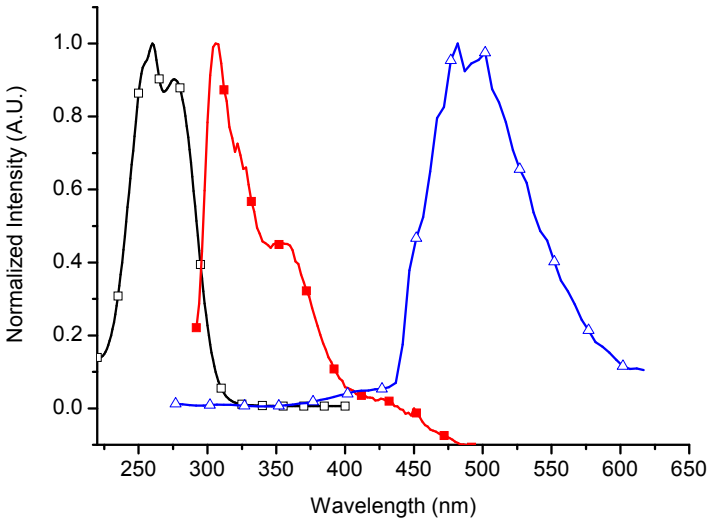

Figure AI-21. Normalized absorption (open squares), fluorescence (closed squares), and phosphorescence (open triangles) spectra of **I-21** in acetonitrile.

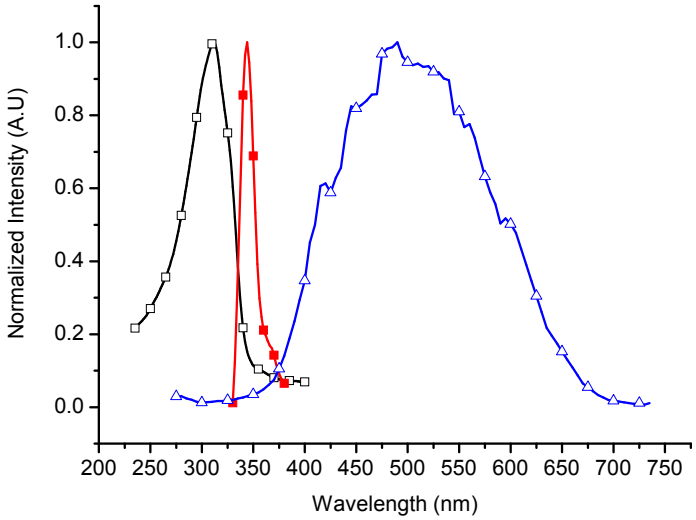

Figure AI-22. Normalized absorption (open squares), fluorescence (closed squares), and phosphorescence (open triangles) spectra of **I-22** in acetonitrile.

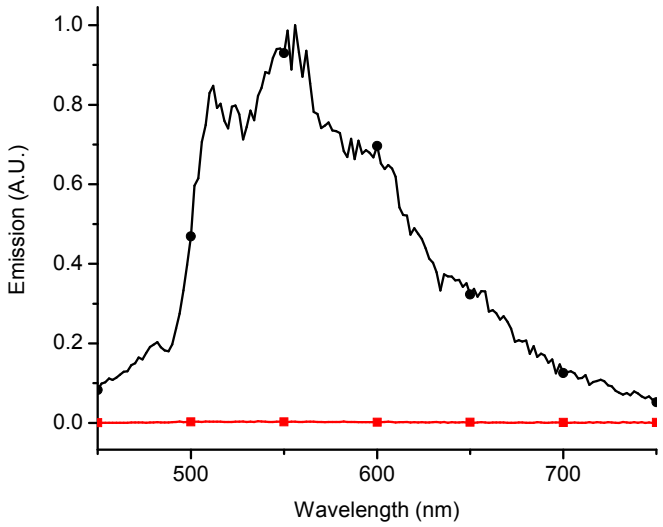

Figure AI-23. Emission specta of **I-14** at 77 K (closed circles) relative to room temperature (closed squares).

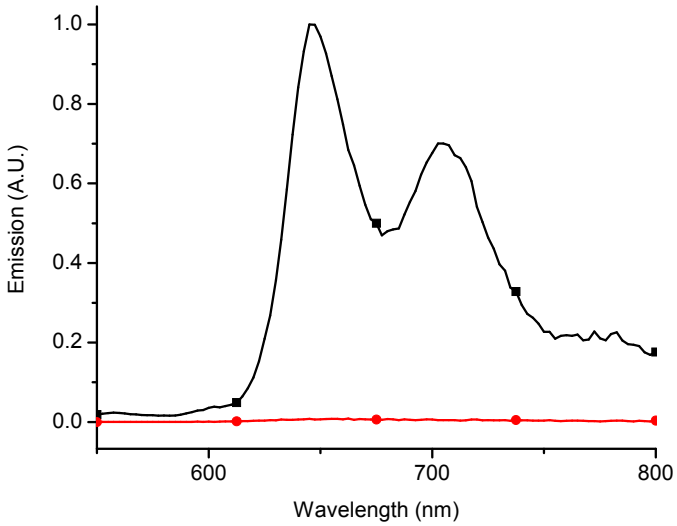

Figure AI-24. Emission specta of **I-15** at 77 K (closed circles) relative to room temperature (closed squares).

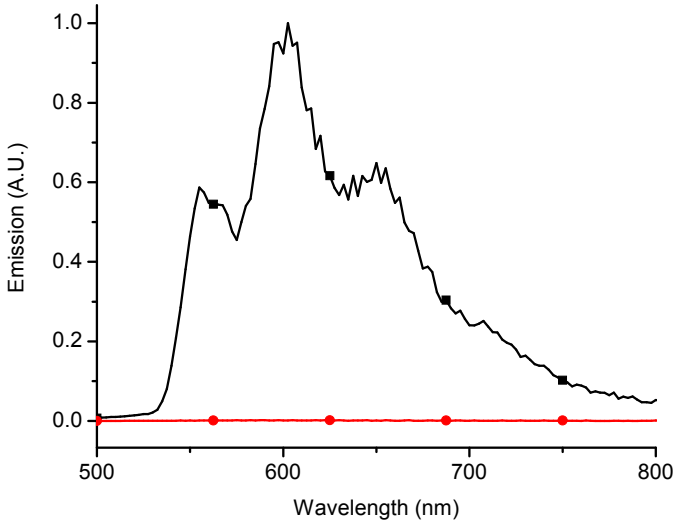

Figure AI-25. Emission specta of **I-16** at 77 K (closed circles) relative to room temperature (closed squares).

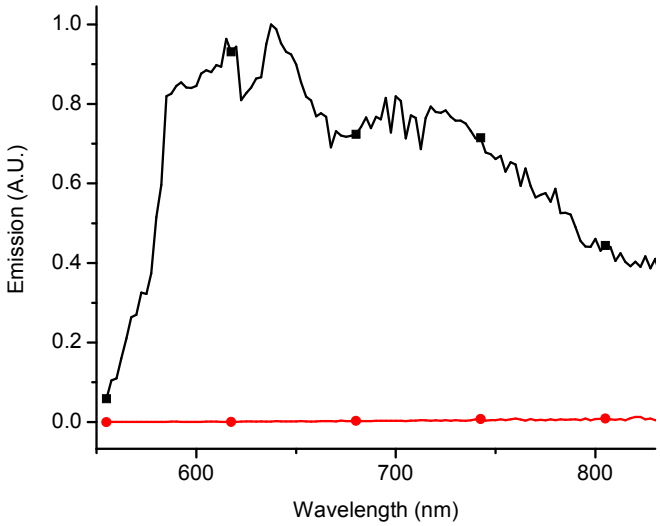

Figure AI-26. Emission specta of **I-18** at 77 K (closed circles) relative to room temperature (closed squares).

Cyclic voltammetry

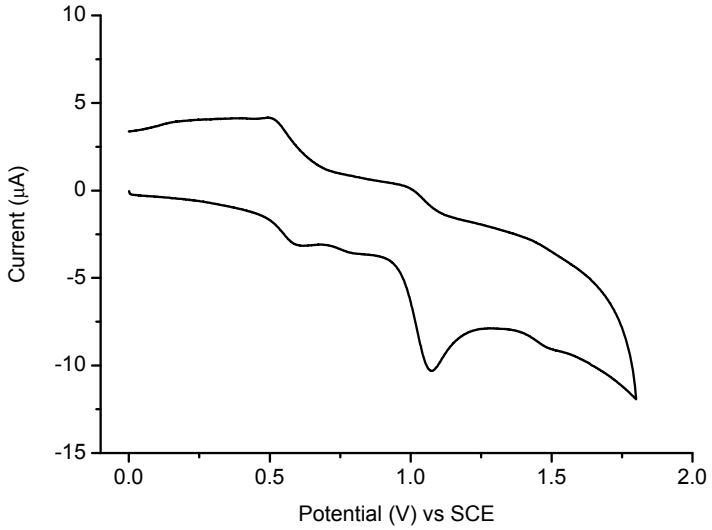

Figure AI-27. Cyclic voltammogram of **I-1** in anhydrous and deaerated dichloromethane.

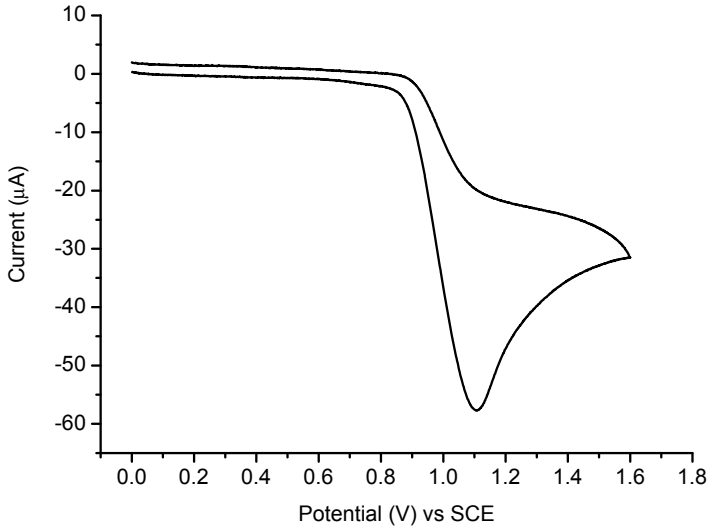

Figure AI-28. Cyclic voltammogram of **I-2** in anhydrous and deaerated dichloromethane.

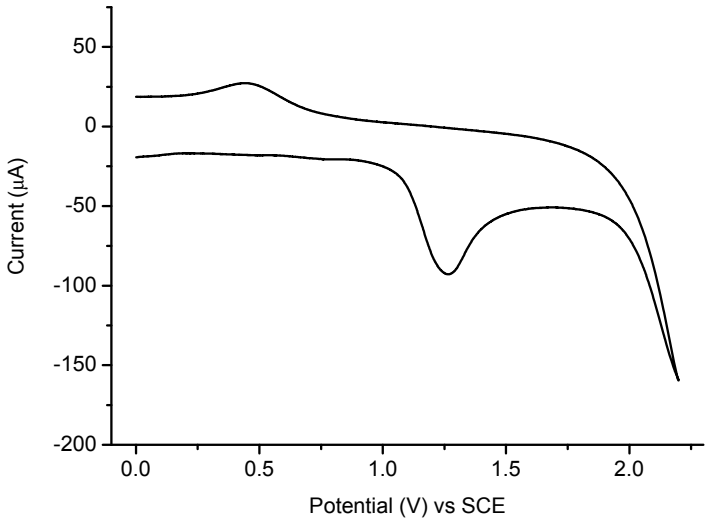

Figure AI-29. Cyclic voltammogram of **I-3** in anhydrous and deaerated dichloromethane.

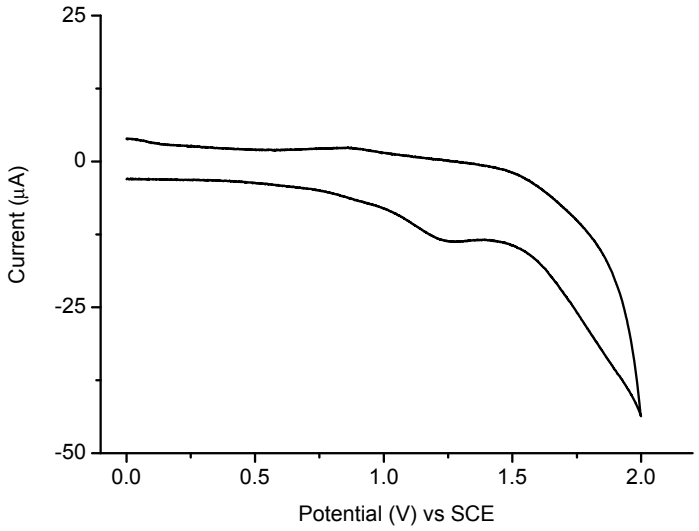

Figure AI-30. Cyclic voltammogram of **I-4** in anhydrous and deaerated dichloromethane.

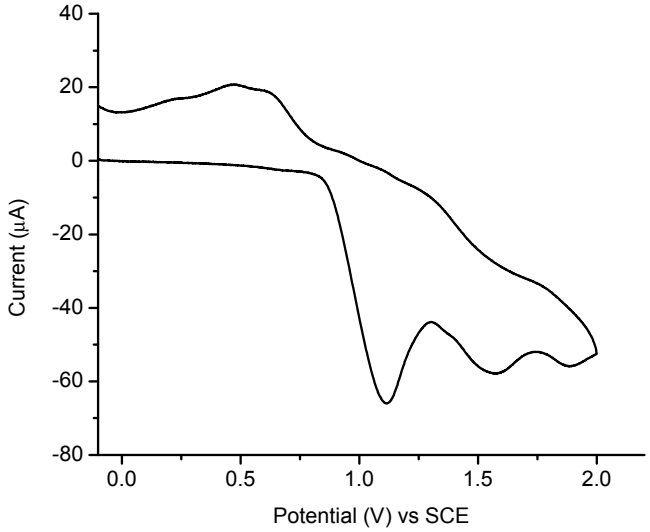

Figure AI-31. Cyclic voltammogram of **I-5** in anhydrous and deaerated dichloromethane.

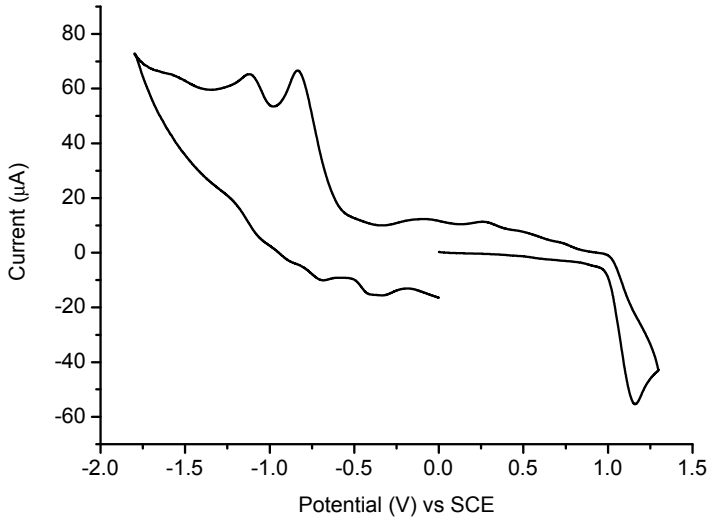

Figure AI-32. Cyclic voltammogram of **I-6** in anhydrous and deaerated dichloromethane.

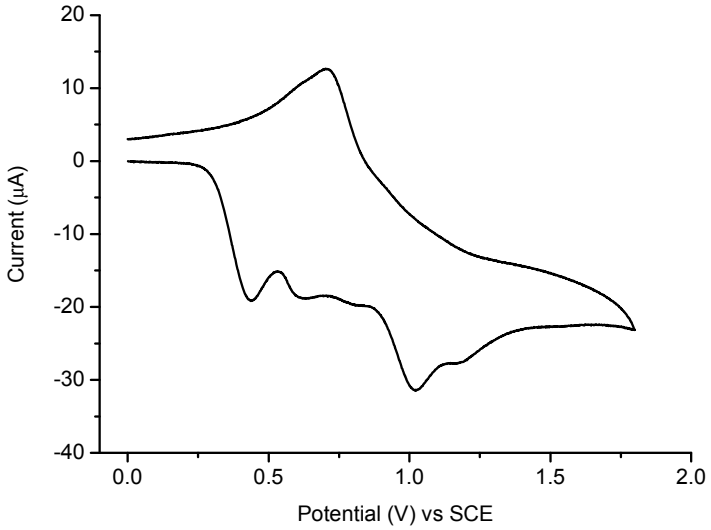

Figure AI-33. Cyclic voltammogram of **I-7** in anhydrous and deaerated dichloromethane.

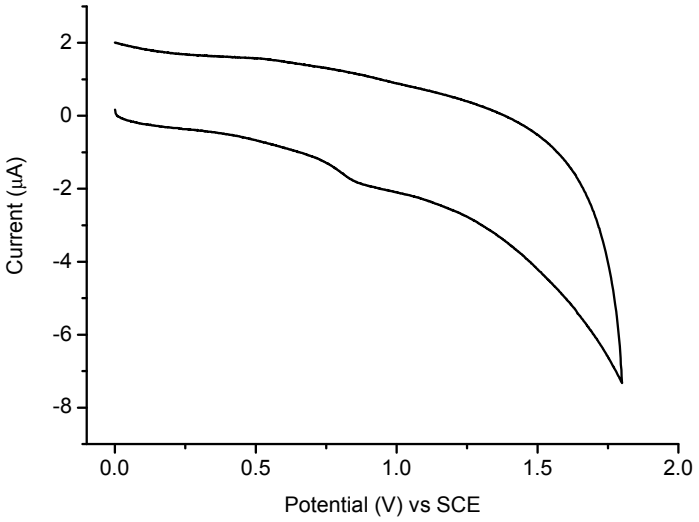

Figure AI-34. Cyclic voltammogram of **I-8** in anhydrous and deaerated dichloromethane.

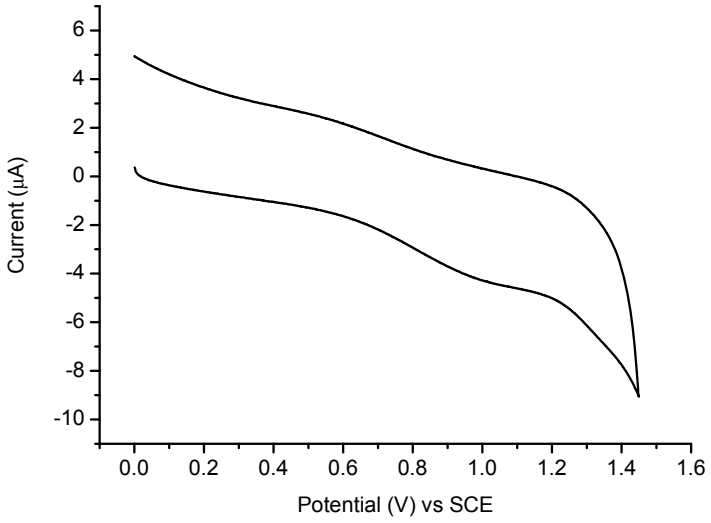

Figure AI-35. Cyclic voltammogram of **I-9** in anhydrous and deaerated dichloromethane.

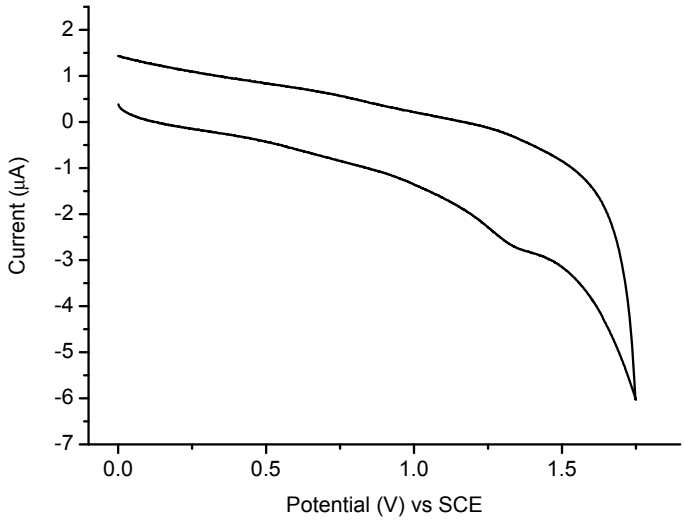

Figure AI-36. Cyclic voltammogram of **I-10** in anhydrous and deaerated dichloromethane.

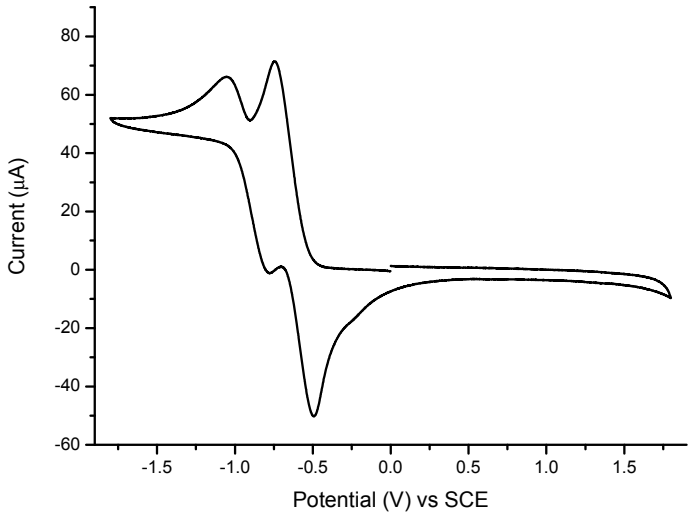

Figure AI-37. Cyclic voltammogram of **I-10** in anhydrous and deaerated dichloromethane.

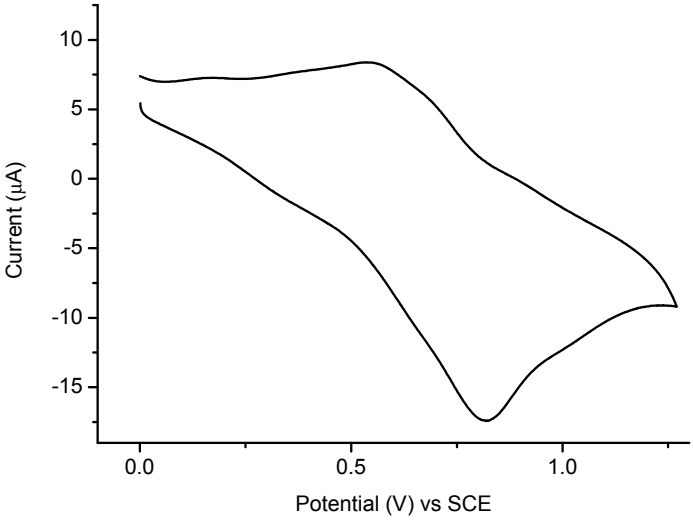

Figure AI-38. Cyclic voltammogram of **I-11** in anhydrous and deaerated dichloromethane.

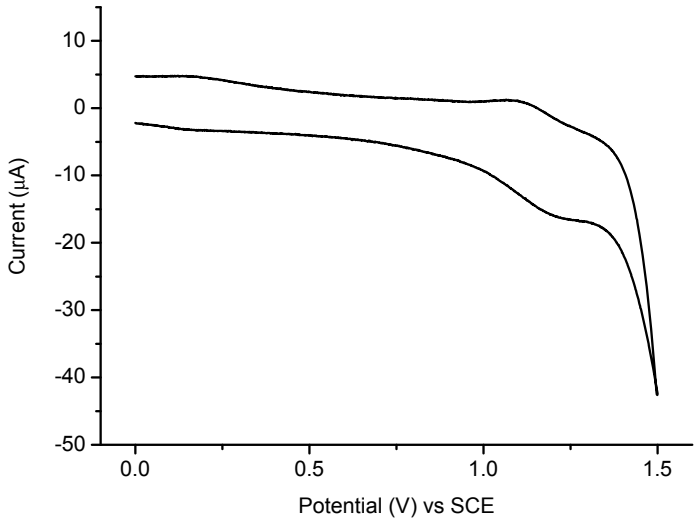

Figure AI-39. Cyclic voltammogram of **I-12** in anhydrous and deaerated dichloromethane.

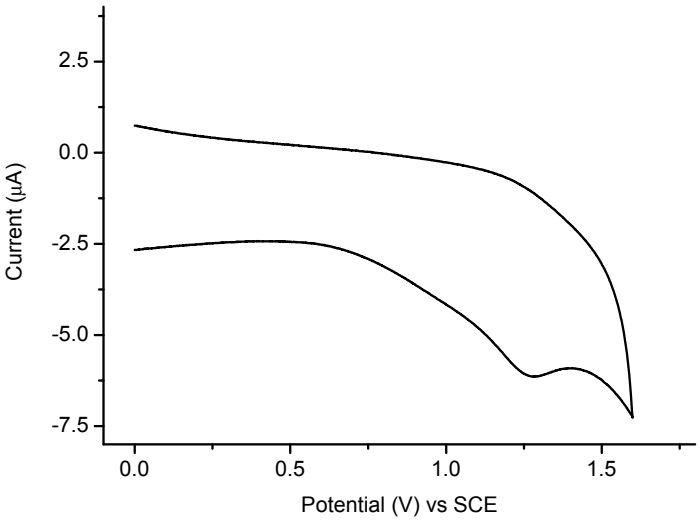

Figure AI-40. Cyclic voltammogram of **I-13** in anhydrous and deaerated dichloromethane.

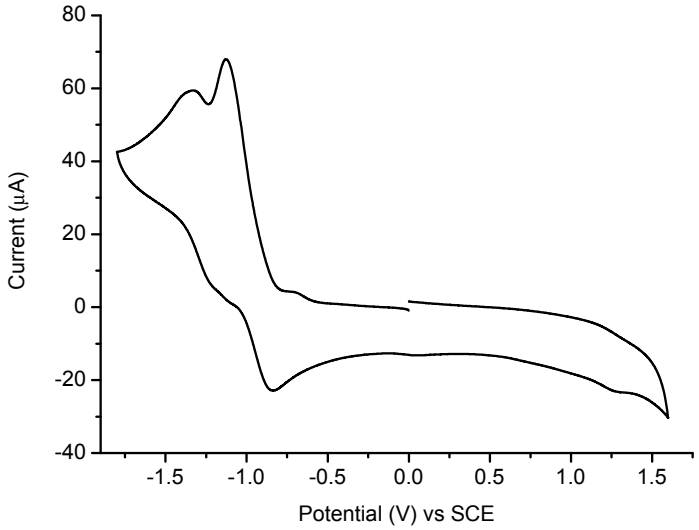

Figure AI-41. Cyclic voltammogram of **I-13** in anhydrous and deaerated dichloromethane.

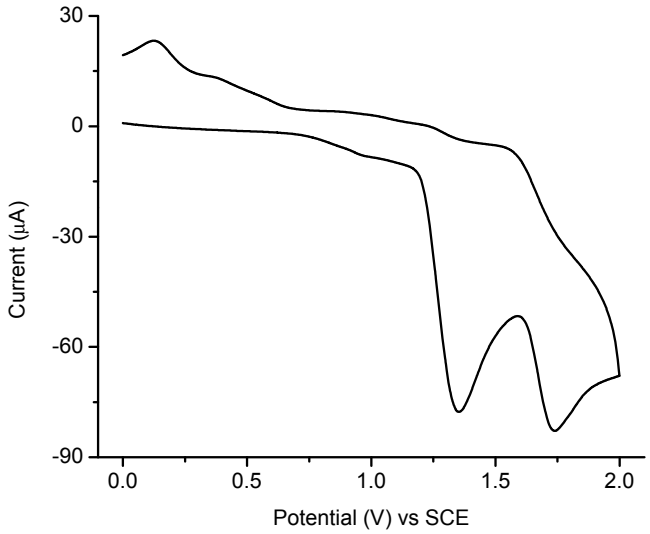

Figure AI-42. Cyclic voltammogram of **I-14** in anhydrous and deaerated dichloromethane.

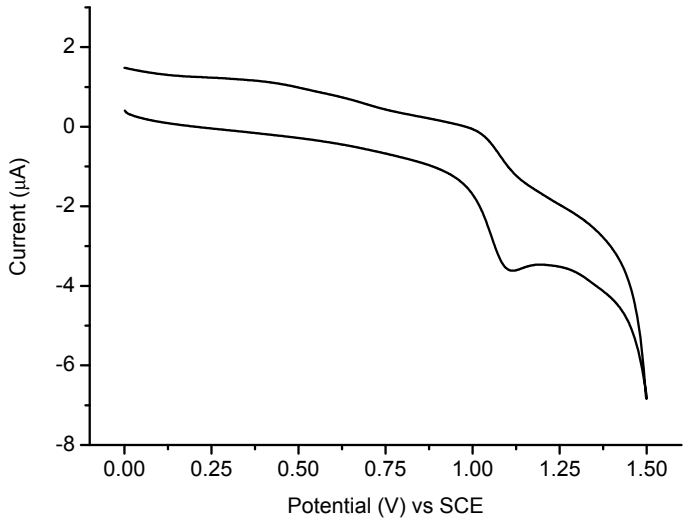

Figure AI-43. Cyclic voltammogram of **I-15** in anhydrous and deaerated dichloromethane.

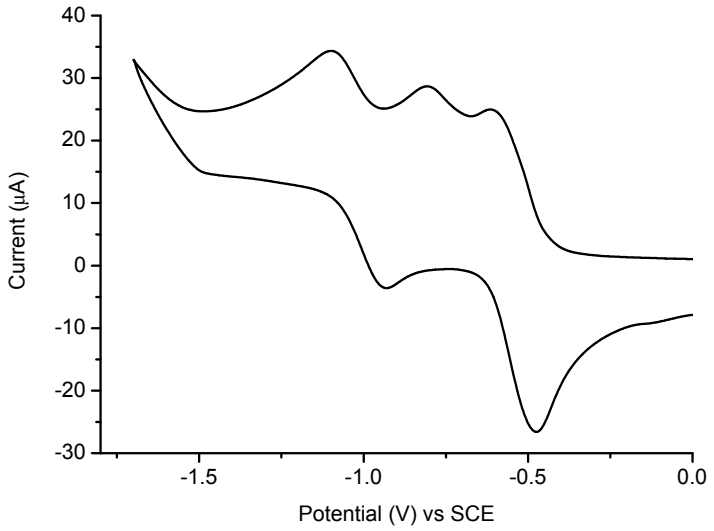

Figure AI-44. Cyclic voltammogram of **I-15** in anhydrous and deaerated dichloromethane.

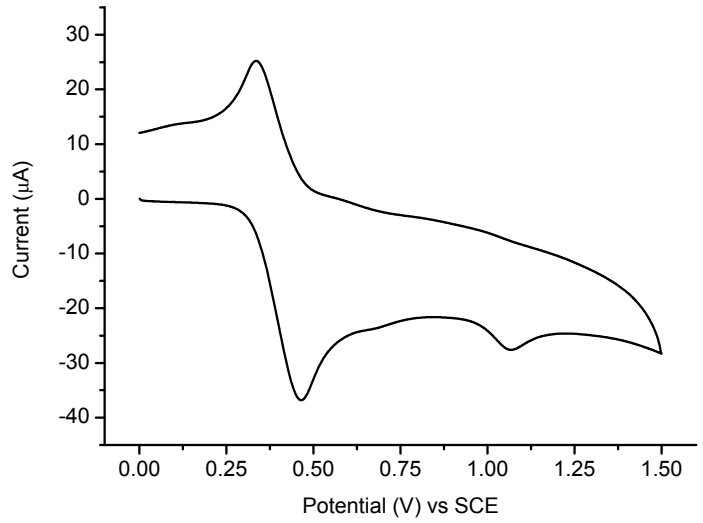

Figure AI-45. Cyclic voltammogram of **I-16** in anhydrous and deaerated dichloromethane.

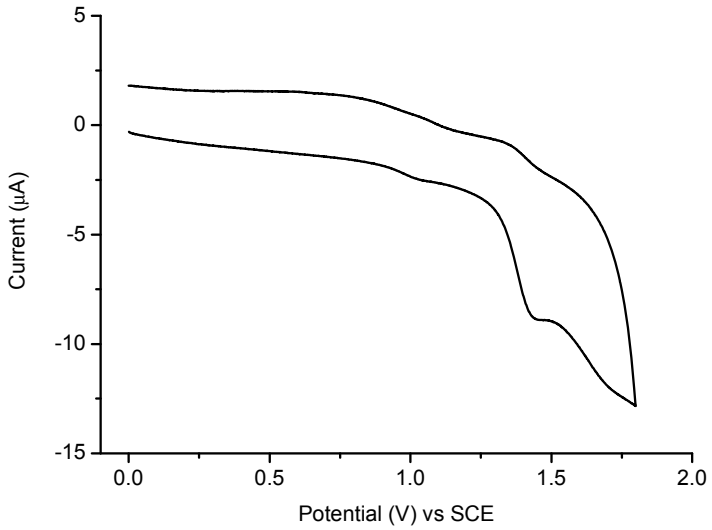

Figure AI-46. Cyclic voltammogram of **I-17** in anhydrous and deaerated dichloromethane.

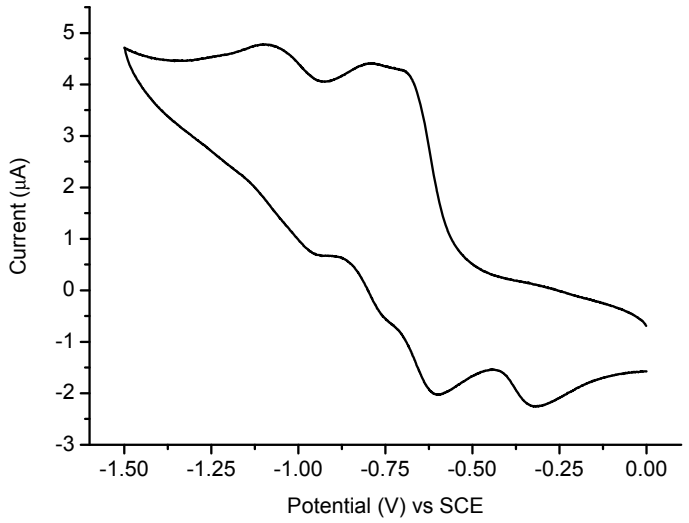

Figure AI-47. Cyclic voltammogram of **I-17** in anhydrous and deaerated dichloromethane.

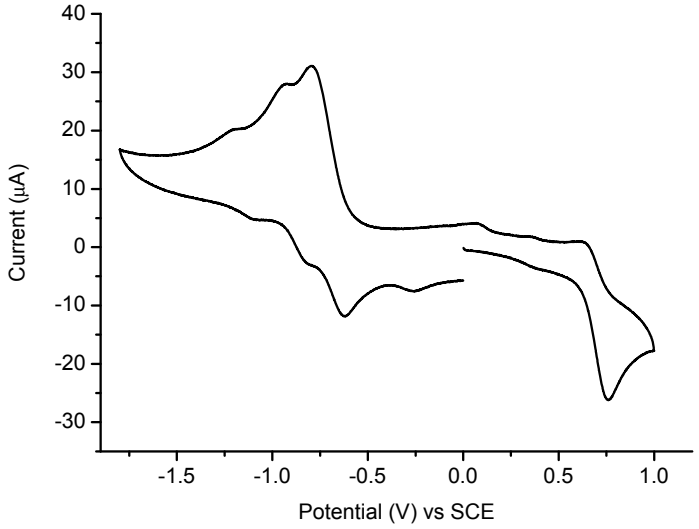

Figure AI-48. Cyclic voltammogram of **I-18** in anhydrous and deaerated dichloromethane.

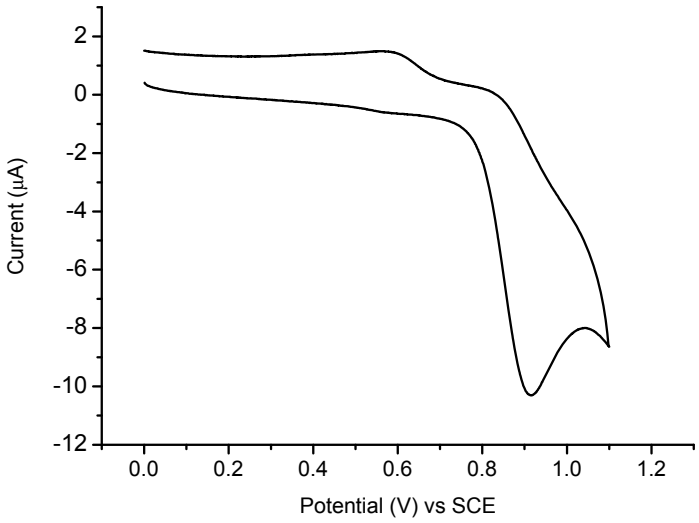

Figure AI-49. Cyclic voltammogram of **I-19** in anhydrous and deaerated dichloromethane.

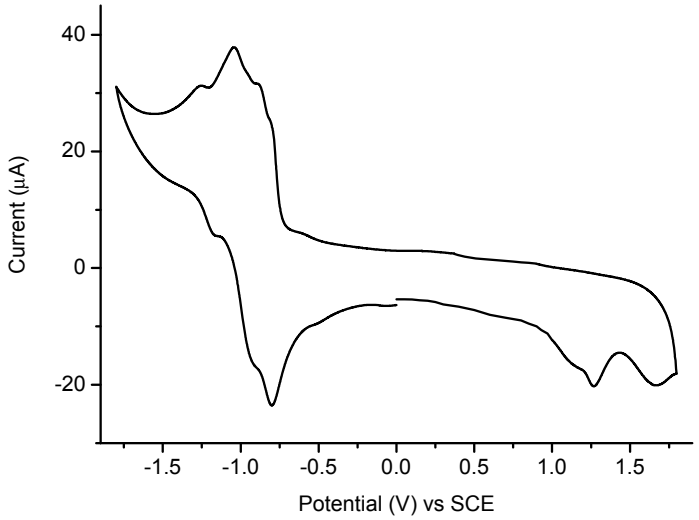

Figure AI-50. Cyclic voltammogram of **I-20** in anhydrous and deaerated dichloromethane.

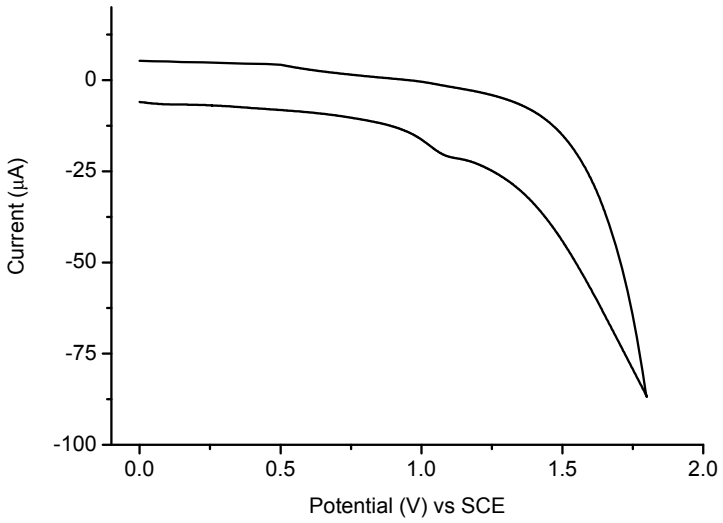

Figure AI-51. Cyclic voltammogram of **I-21** in anhydrous and deaerated dichloromethane.

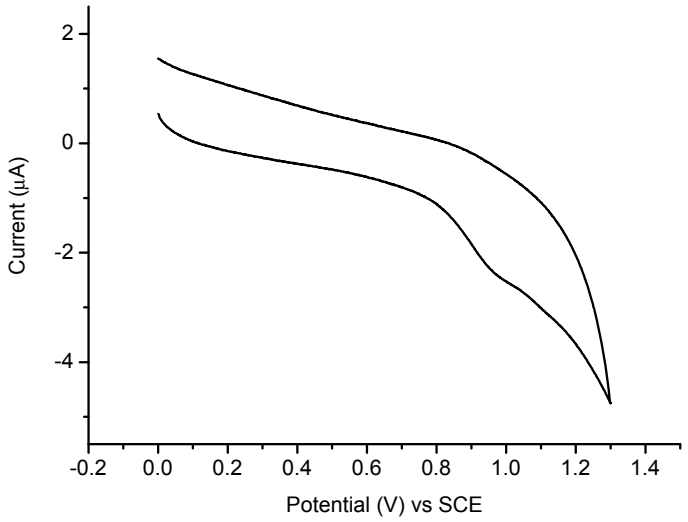

Figure AI-52. Cyclic voltammogram of **I-22** in anhydrous and deaerated dichloromethane.

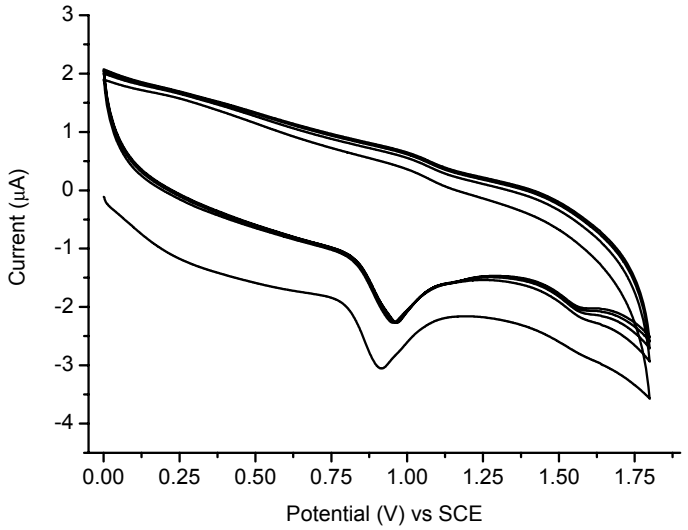

Figure AI-53. Repeated cyclic voltammogram of **I-2** leading to oxidative coupling.

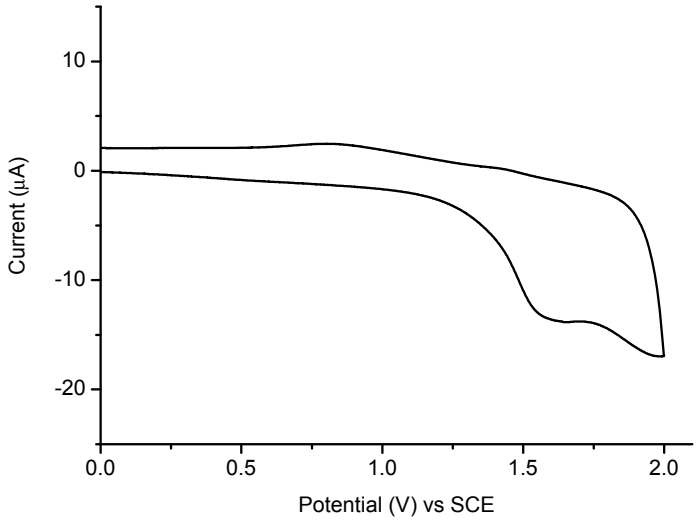

Figure AI-54. Cyclic voltammogram of the dimer obtained by oxidative coupling from **I-5**.

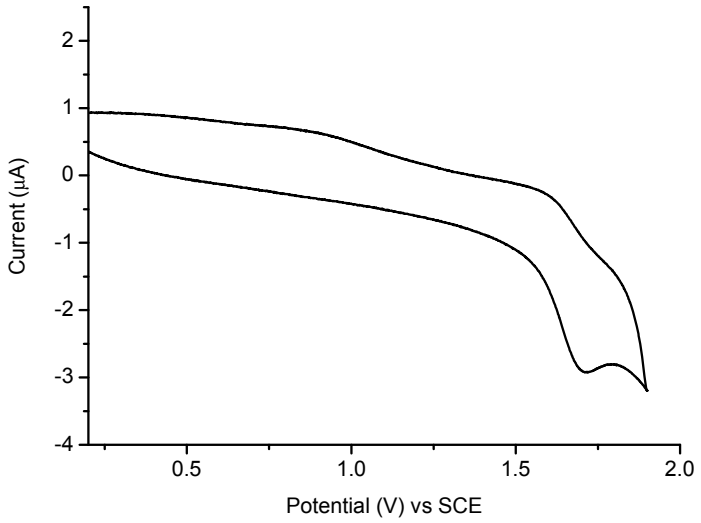

Figure AI-55. Cyclic voltammogram of the dimer obtained by oxidative coupling from **I-9**.

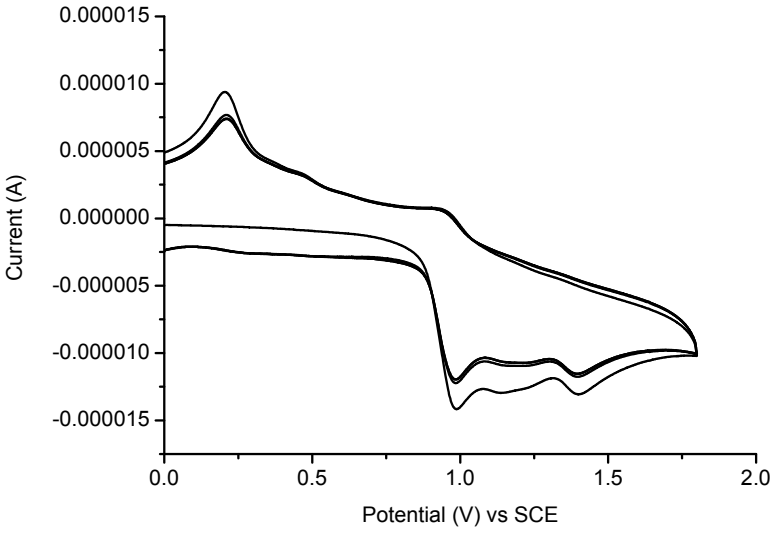

Figure AI-56. Repeated cyclic voltammogram of **I-14** leading to oxidative coupling.

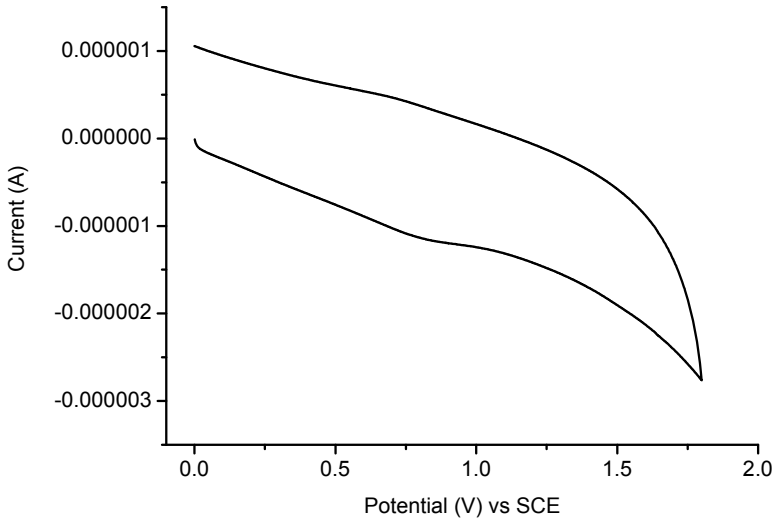

Figure AI-57. Cyclic voltammogram of the polymer obtained by oxidative coupling from **I-14**.

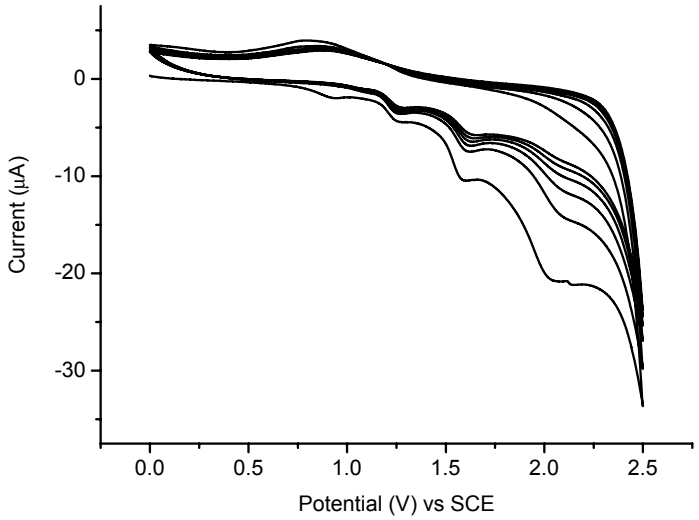

Figure AI-58. Repeated cyclic voltammogram of **I-17** leading to oxidative coupling.

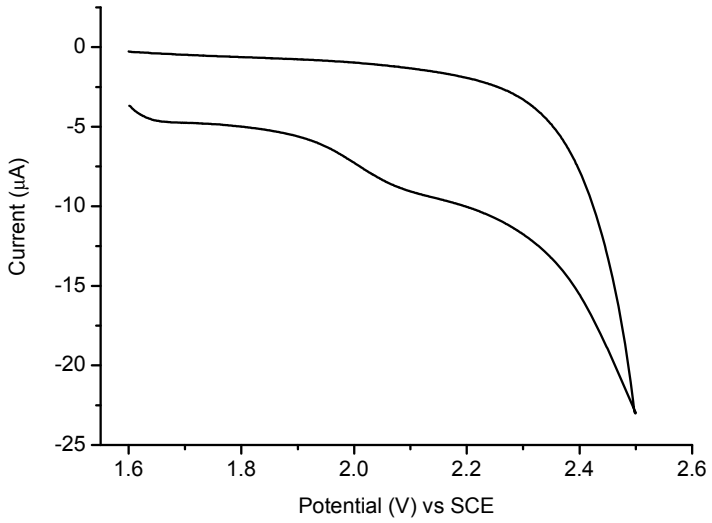

Figure AI-59. Cyclic voltammogram of the dimer made by oxidative coupling from **I-17**.

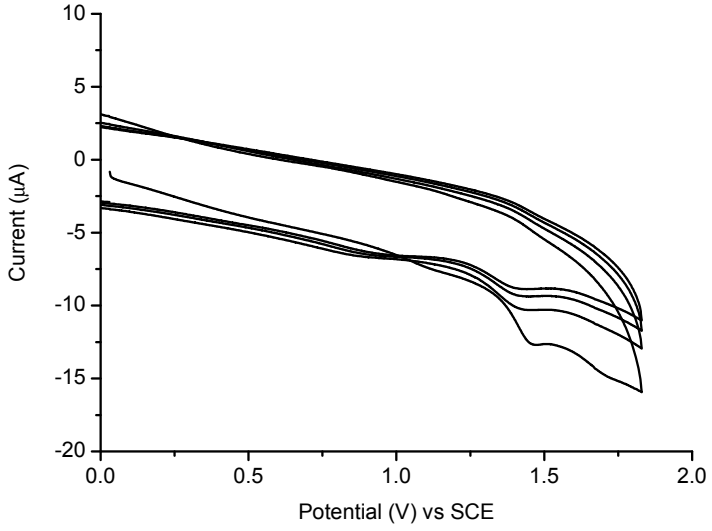

Figure AI-60. Repeated cyclic voltammogram of **I-21** leading to oxidative coupling.

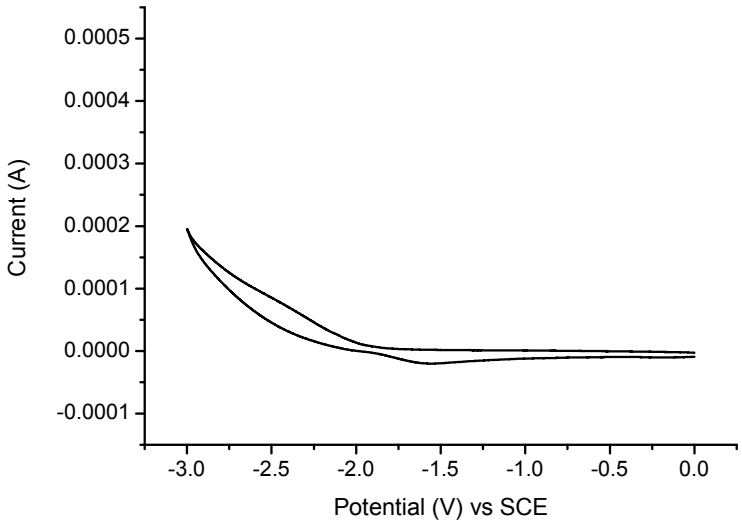

Figure AI-61. Reduction analysis of **I-14** in deaerated and anhydrous DMF.

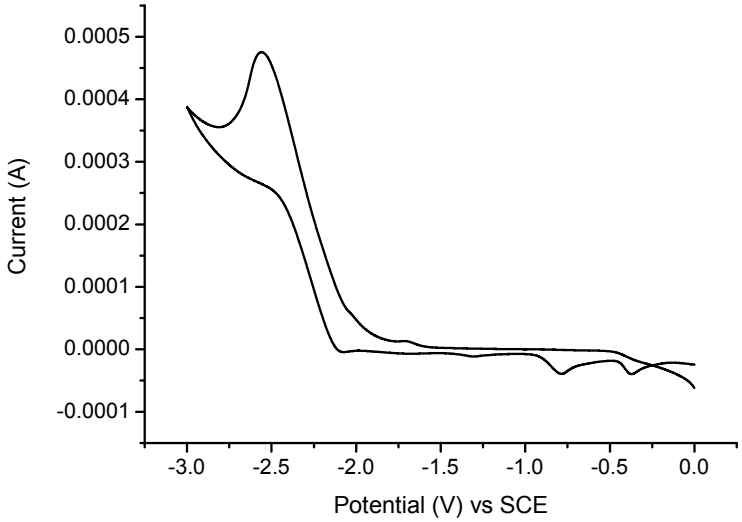

Figure AI-62. Reduction analysis of **I-21** in deaerated and anhydrous DMF.

References

1. (a) Becker, R. S.; Seixas de Melo, J.; Maçanita, A. L.; Elisei F. J. Phys. Chem. **1996**, 100, 18683-18695. (b) Seixas de Melo, J.; Elisei F.; Becker R. S. J. Chem. Phys. **2002**, 117, 4428-4435. (c) Seixas de Melo, J.; Burrows, H. D.; Svensson, M.; Andersson, M. R.; Monkman, A. P. J. Chem. Phys. **2003**, 118, 1550-1556. (d) Seixas de Melo, J.; Silva, L. M.; Arnaut, L. G.; Becker, R. S. J. Chem. Phys. **1999**, 111, 5427-5433. (e) Seixas de Melo, J.; Elisei, F.; Gartner, C.; Aloisi, G. G.; Becker, R.S. J. Phys. Chem. A **2000**, 104, 6907-6911.

2. (a) Scaiano, J. C. CRC Handbook of Organic Photochemistry, CRC Press, Boca Raton, 1989. (b) Carmichael, I.; Hug, G. L. J. Phys. Chem. Ref. Data **1986**, 15, 1-250.

3. (a) Andrews, L. J.; Deroulede, A.; Linschltz, H. J. Phys. Chem. **1978**, 82, 2304-2309. (b) Murphy, R. S.; Moorlag, C. P.; Green, W. H.; Bohne, C. J. Photochem. Photobiol. A **1997**, 110, 123-129.

4. Gewald, V. K.; Kleinert, M.; Thiele, B.; Hentschel, M. J. Prak. Chem. **1972**, 314, 303-314.

AII. ANNEXE II - CHAPITRE II

Table of Contents

NMR Spectra

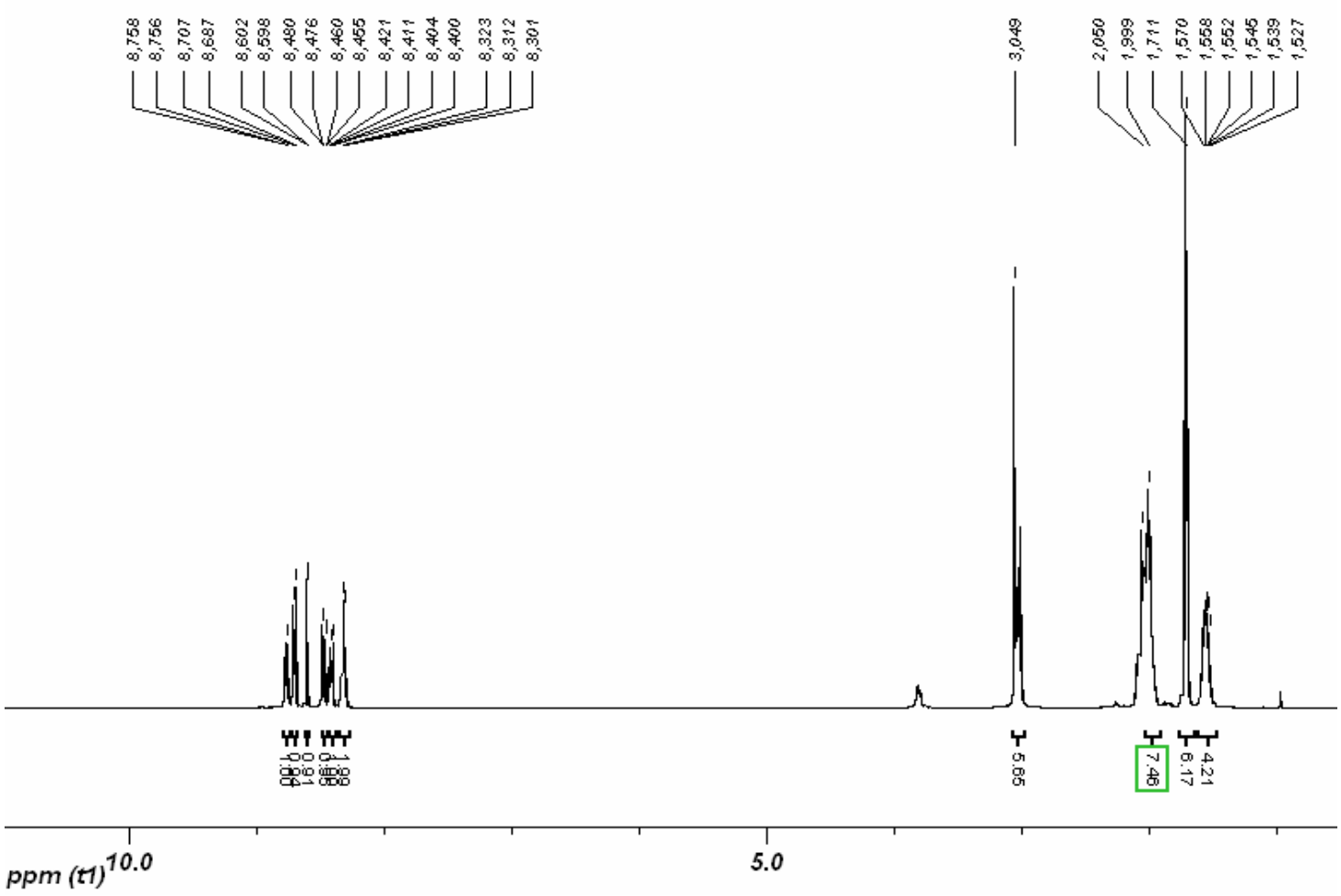

Figure AII-1. ^{1}H- NMR of **II-3.**

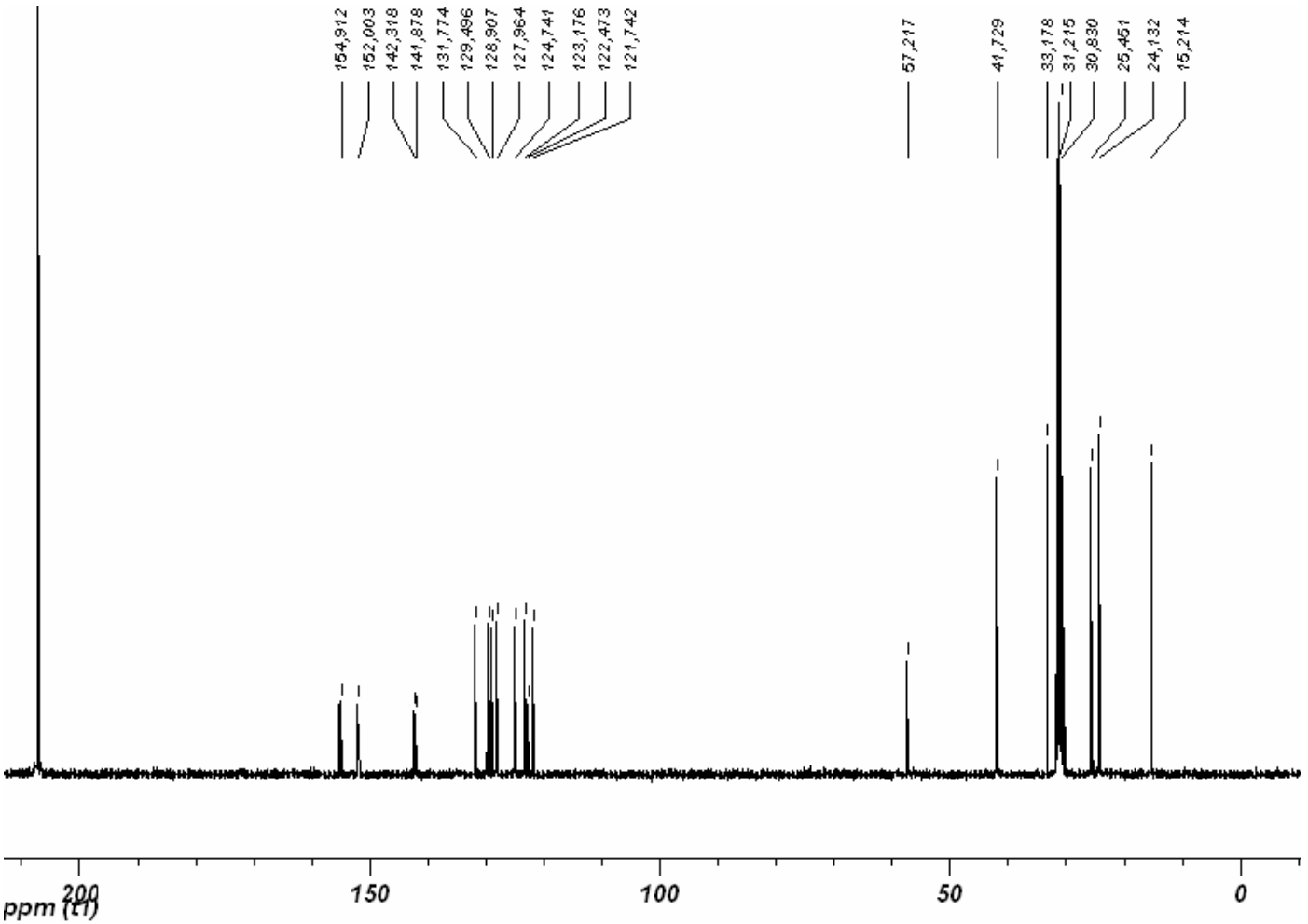

Figure AII-2. ^{13}C- NMR of **II-3.**

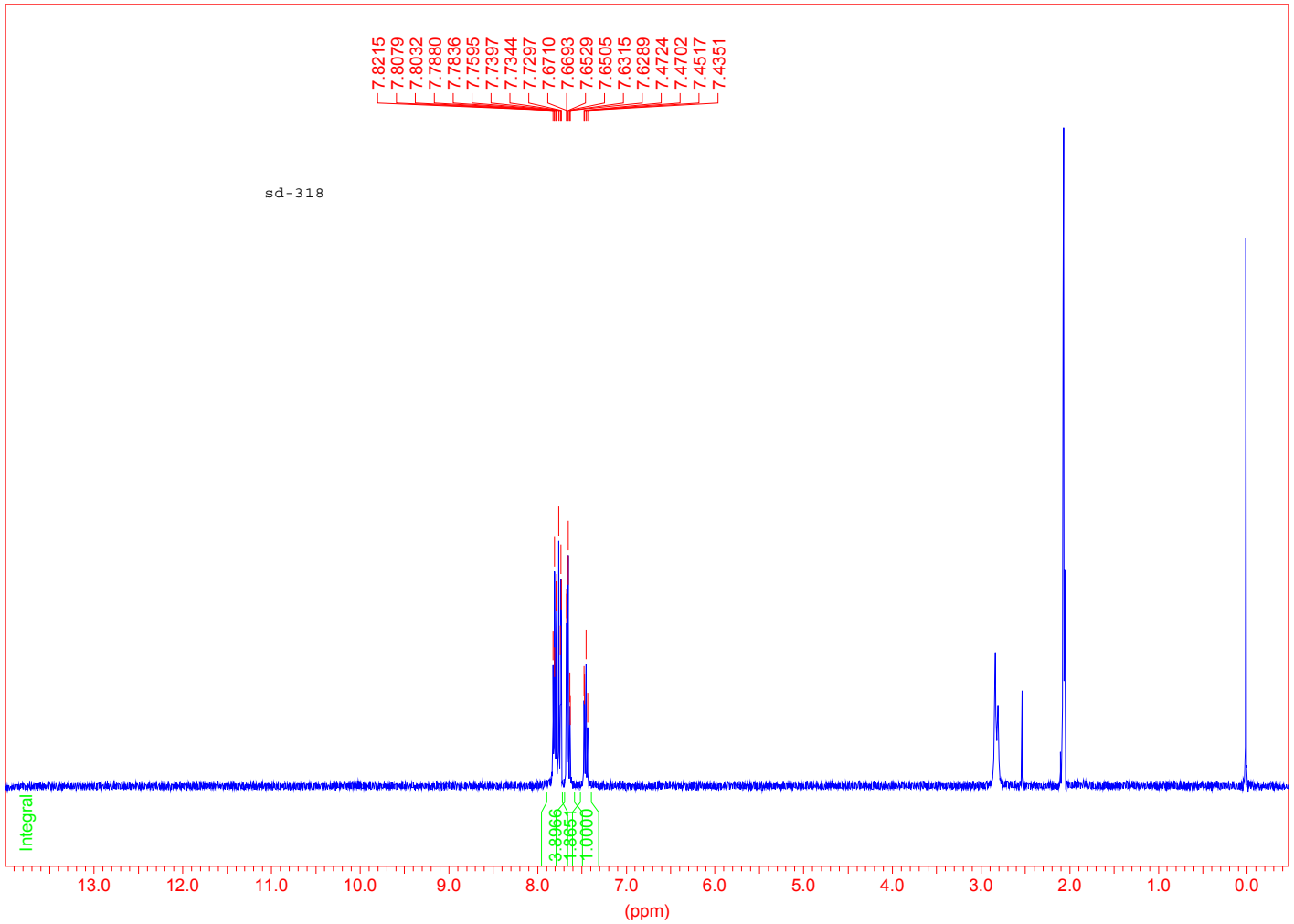

Figure AII-3. ^{1}H- NMR of **II-6.**

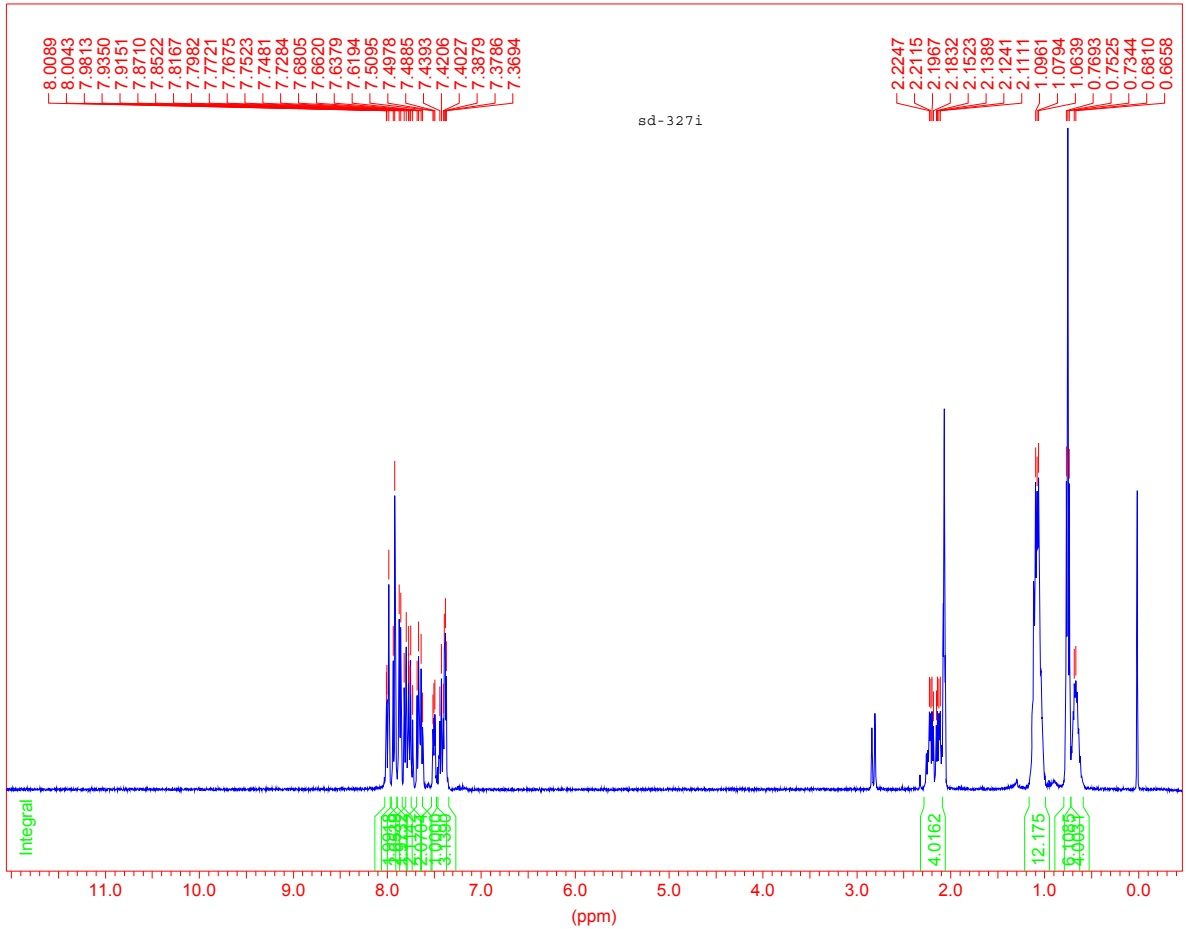

Figure AII-4. ^{1}H- NMR of **II-10.**

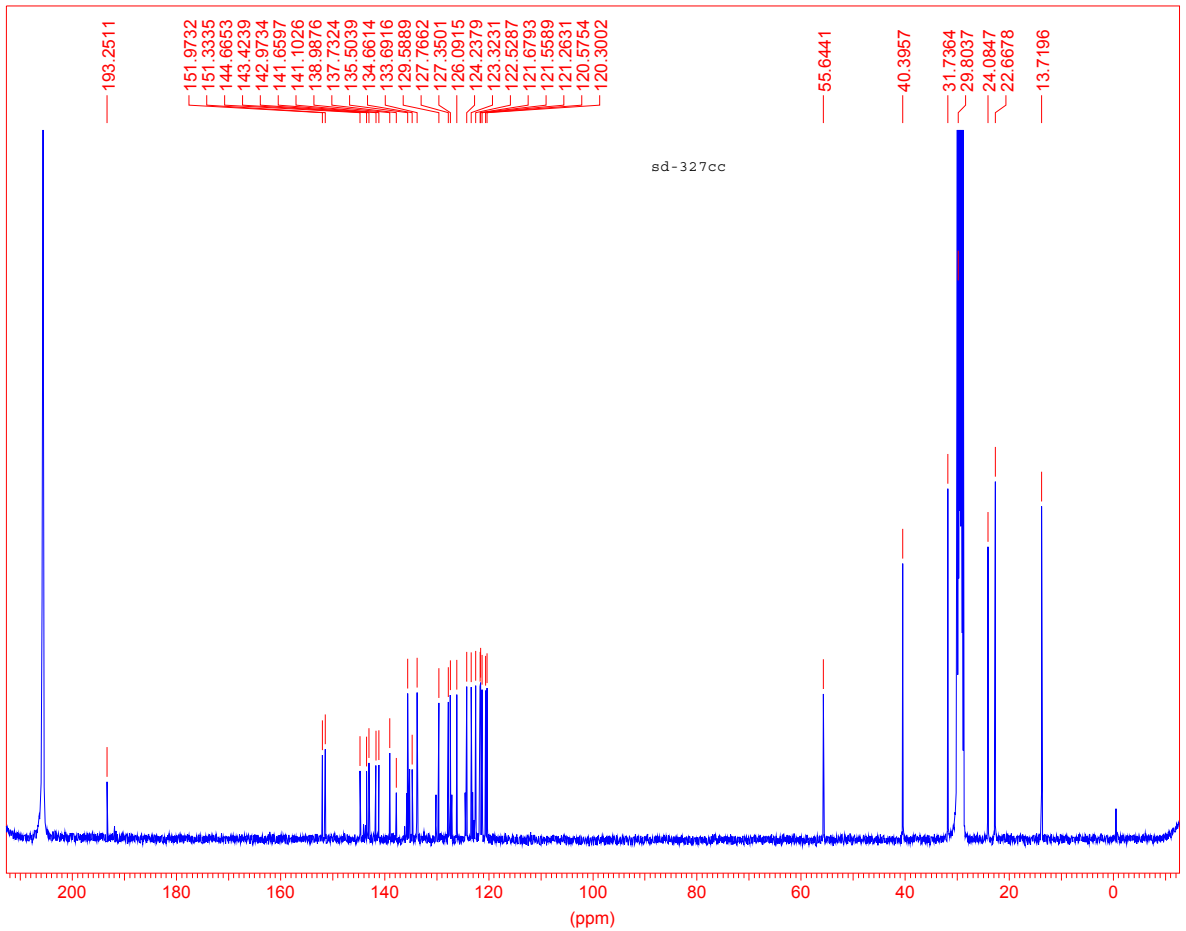

Figure AII-5. ^{13}C- NMR of **II-10.**

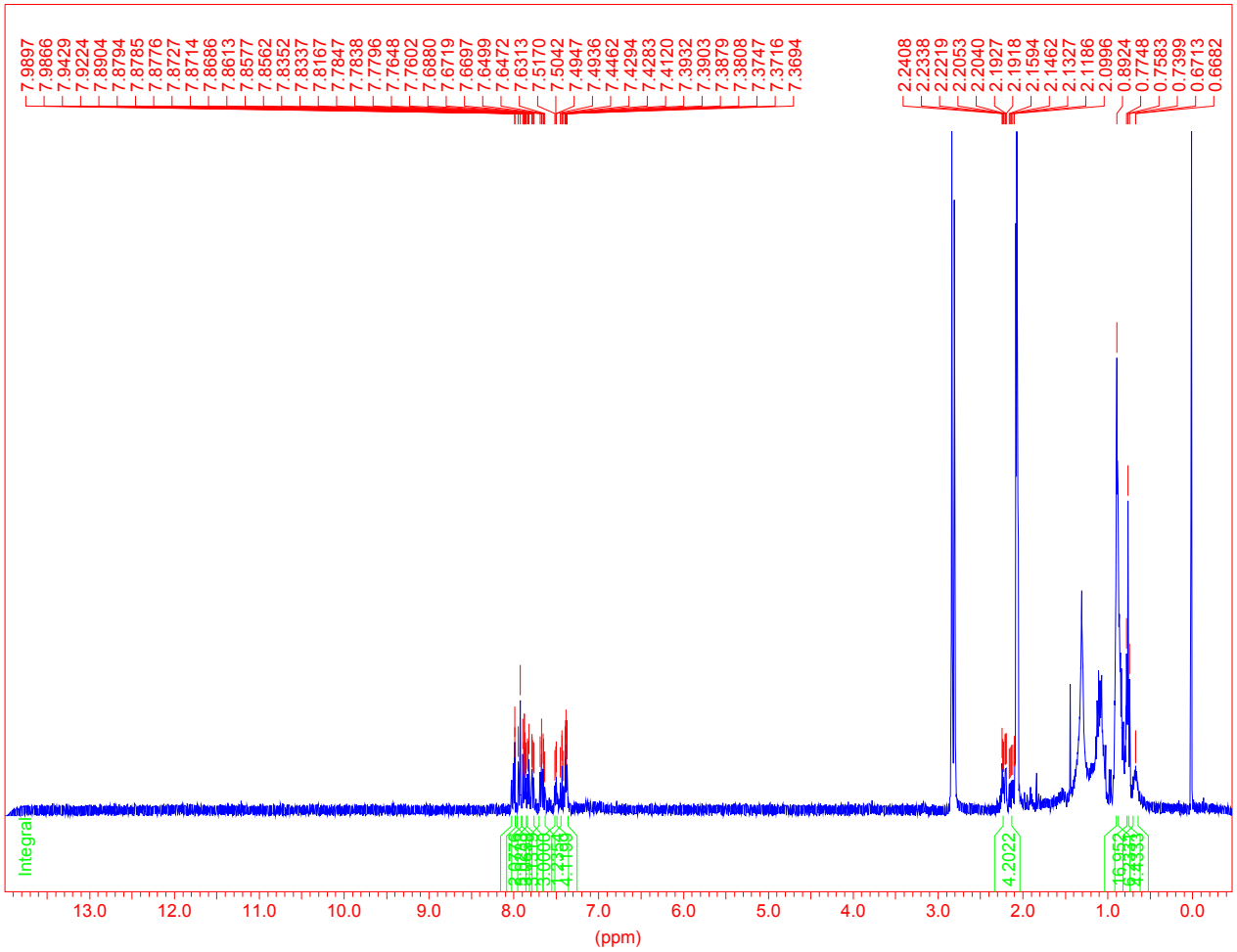

Figure AII-6. ^{1}H- NMR of **II-11.**

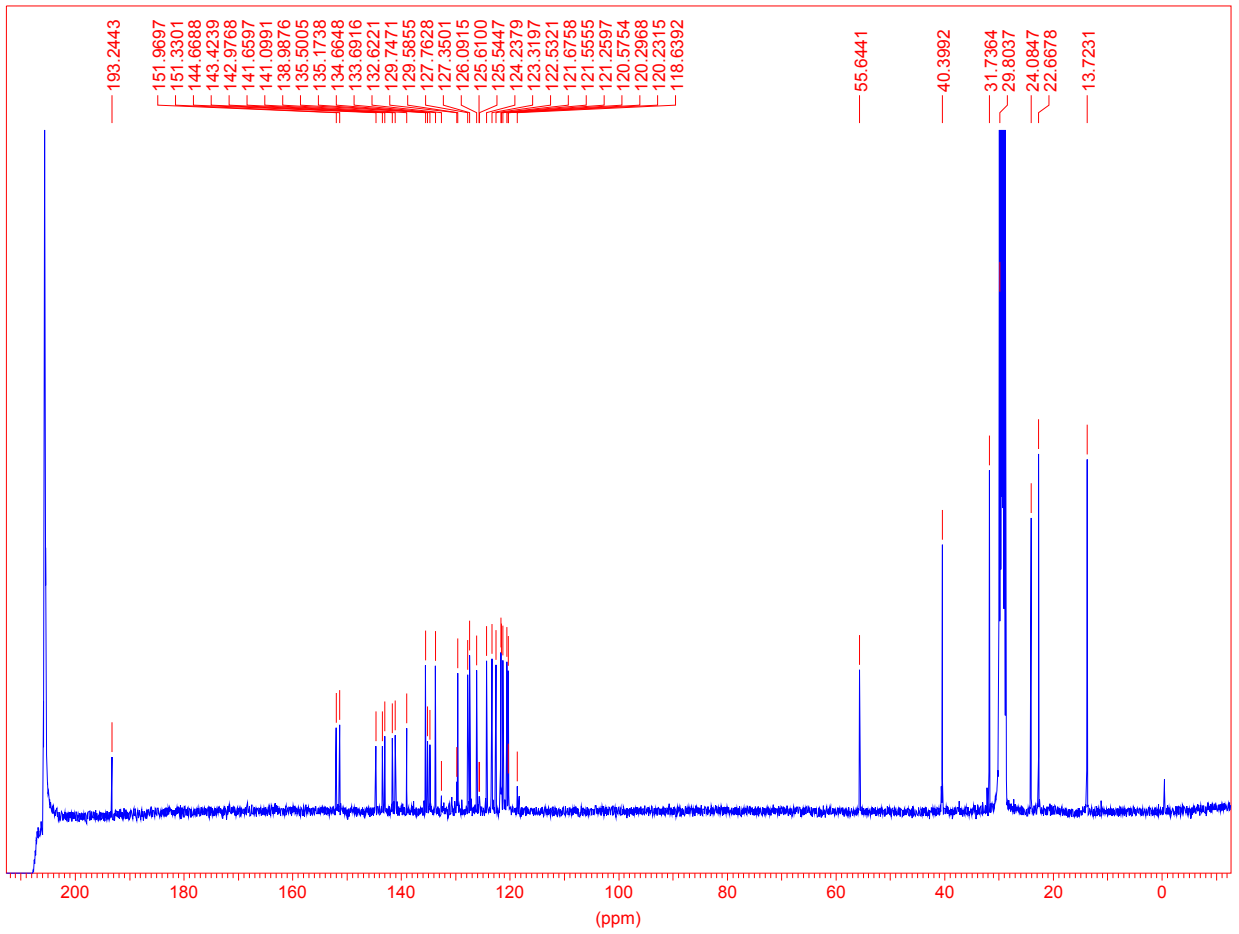

Figure AII-7. ^{13}C- NMR of **II-11.**

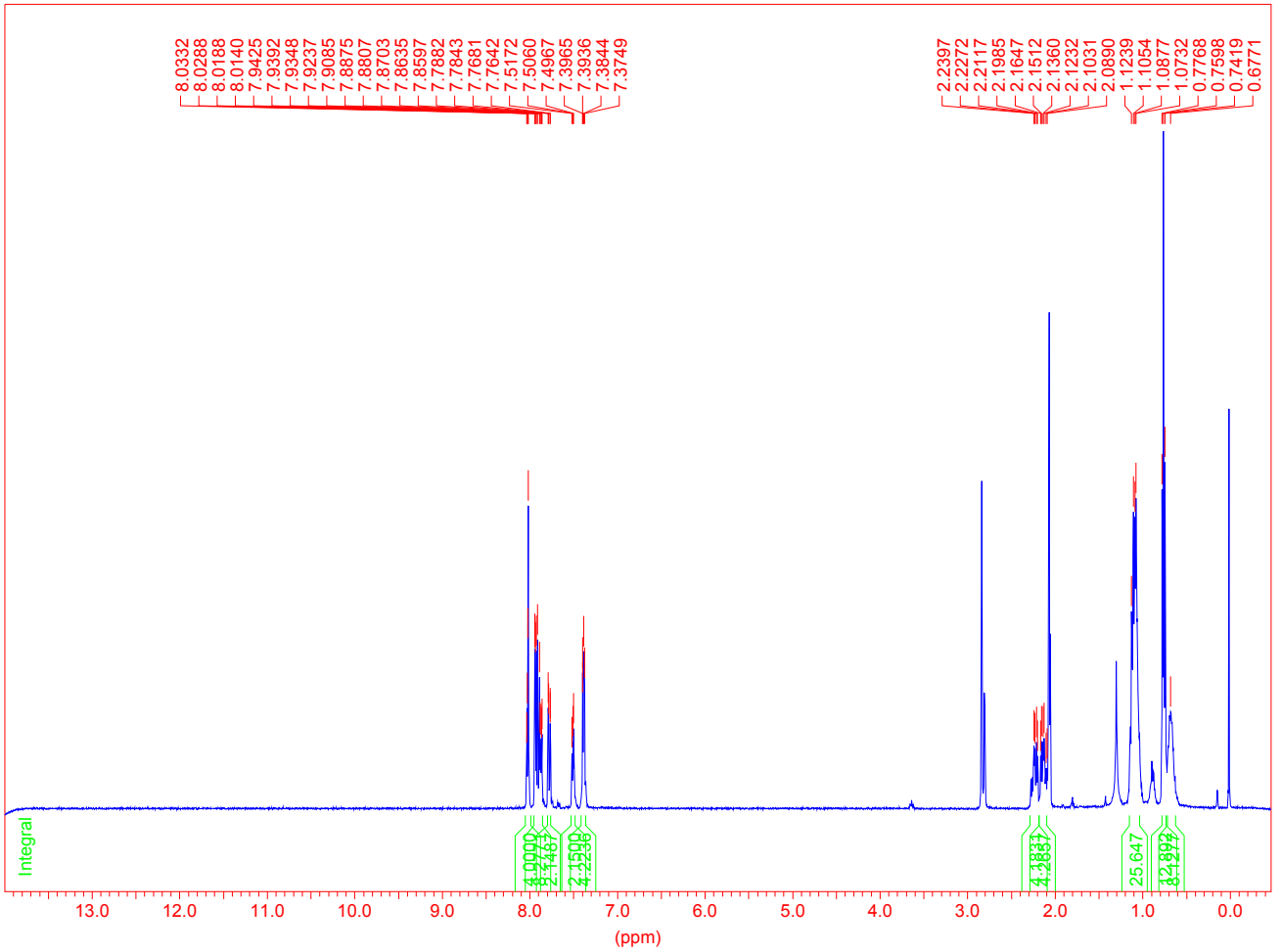

Figure AII-8. ^{1}H- NMR of **II-12**.

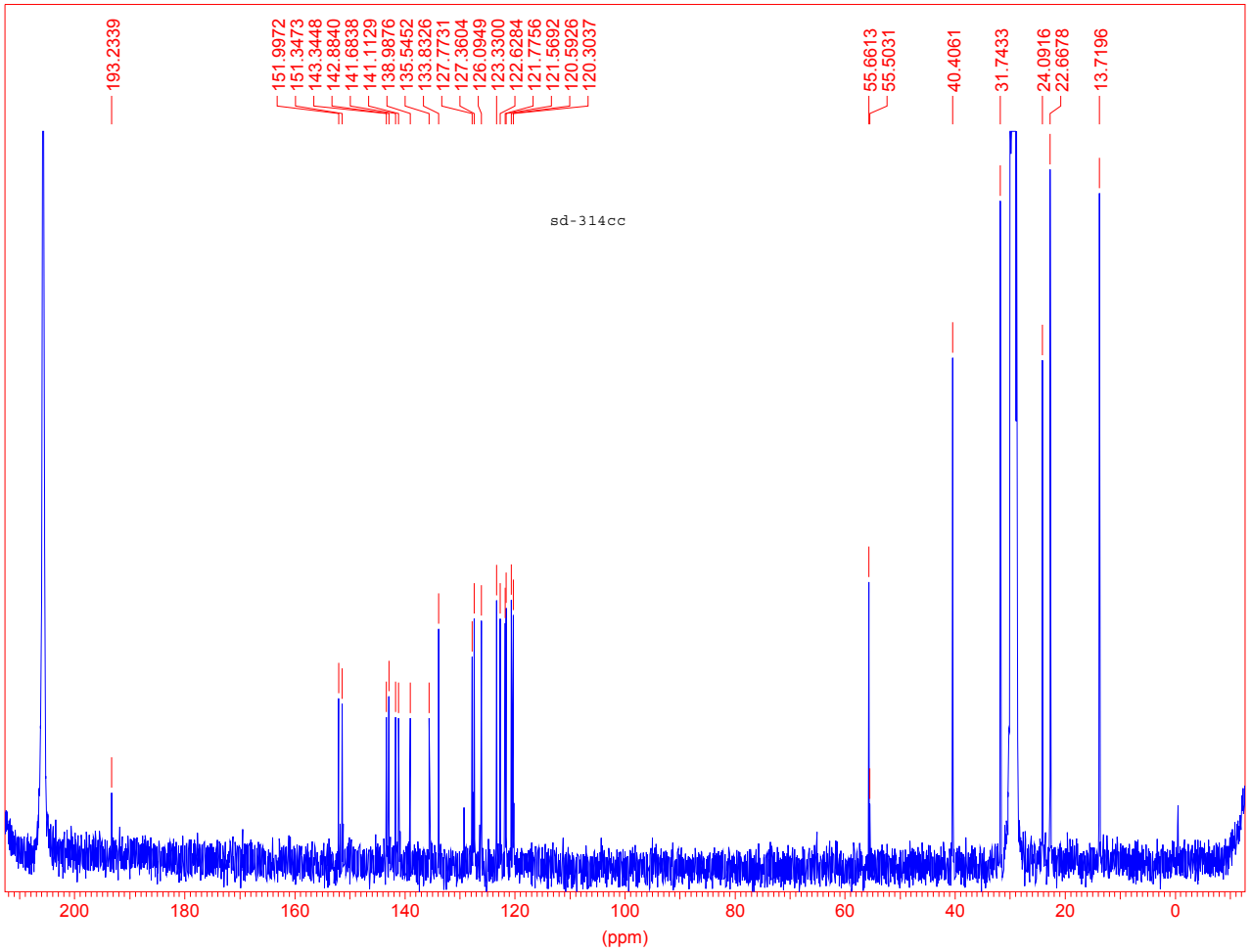

Figure AII-9. ^{13}C- NMR of **II-12**.

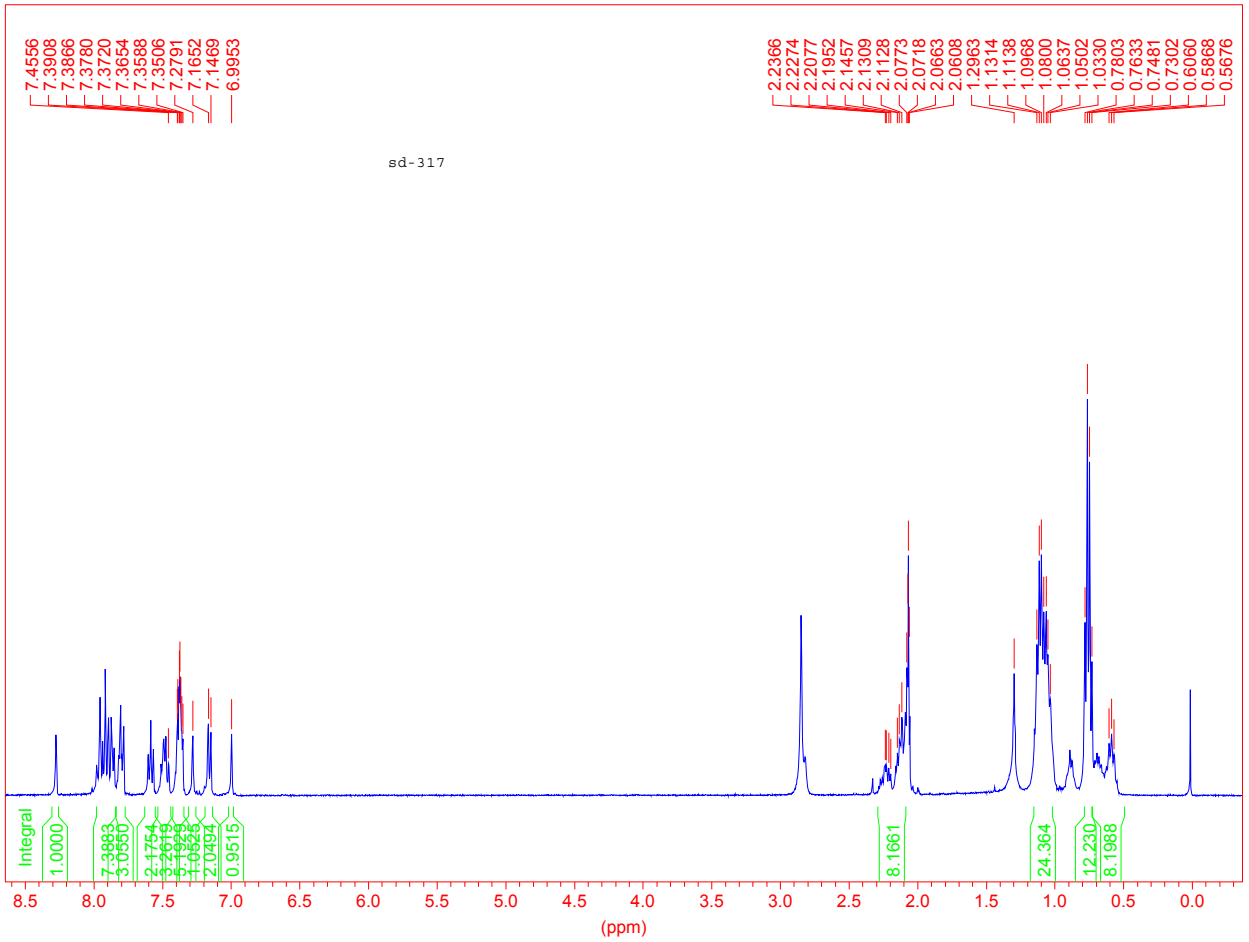

Figure AII-10. ^{1}H- NMR of **II-13**.

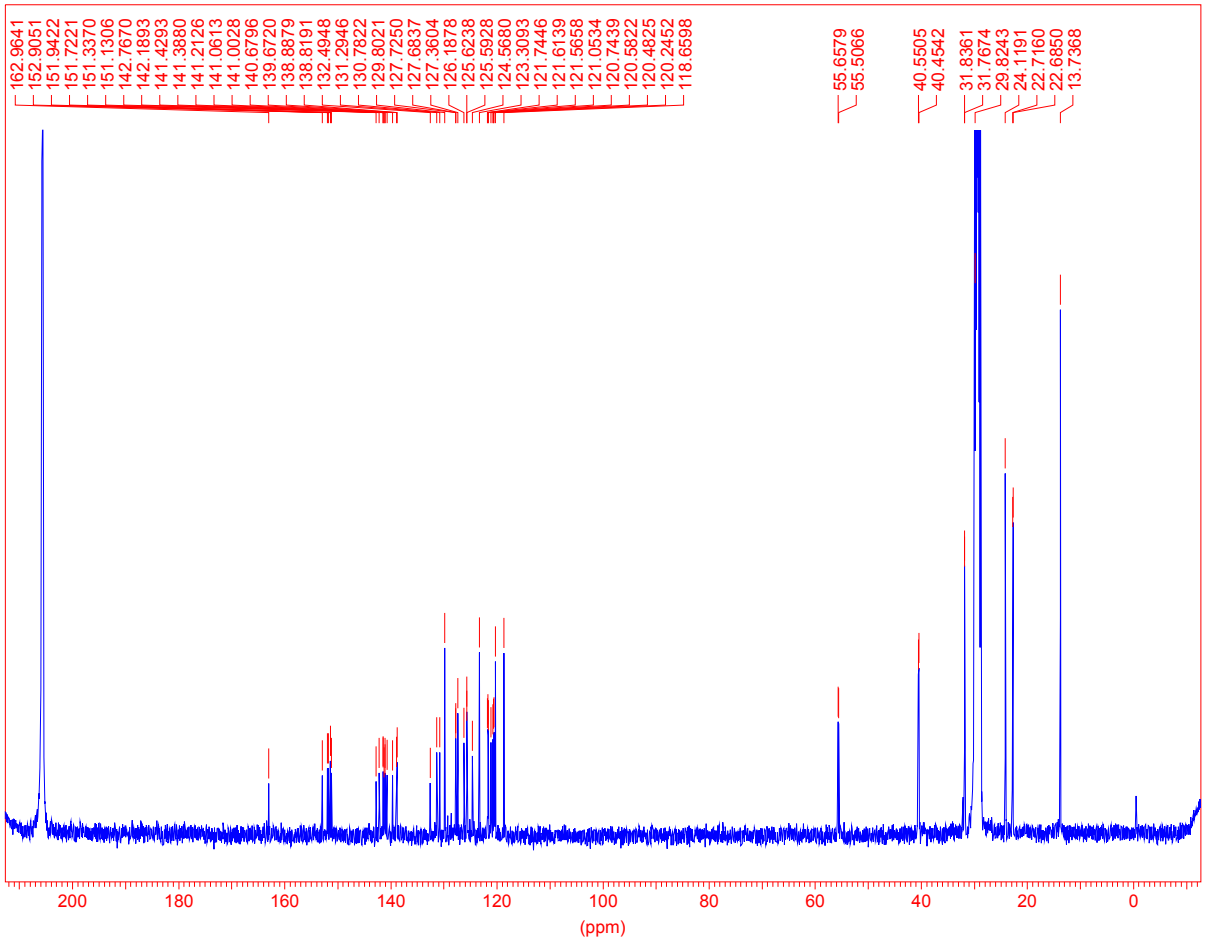

Figure AII-11. ^{13}C- NMR of **II-13**.

Absorption and Emission spectra

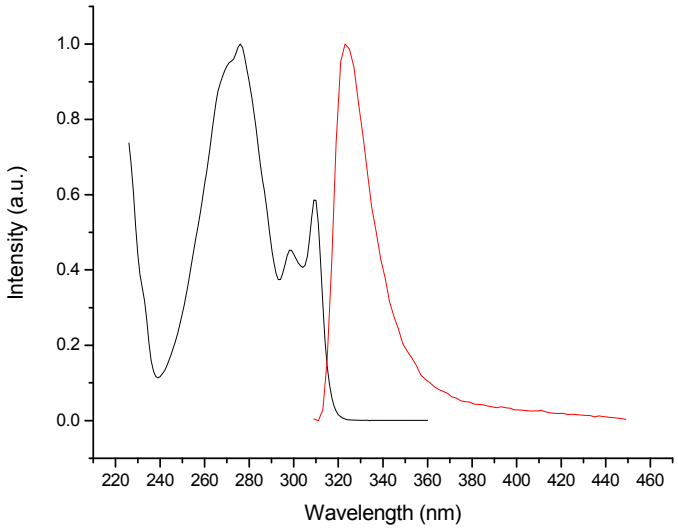

Figure AII-12. Absorbance and fluorescence spectra of **II-3**.

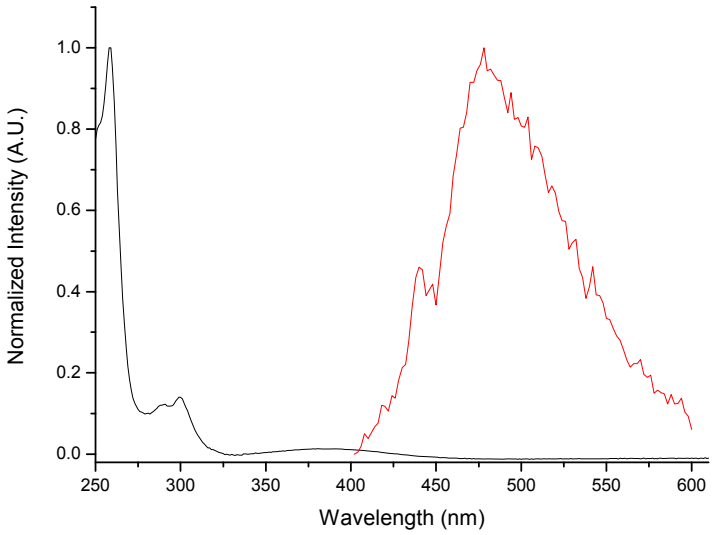

Figure AII-13. Absorbance and fluorescence spectra of **II-4**.

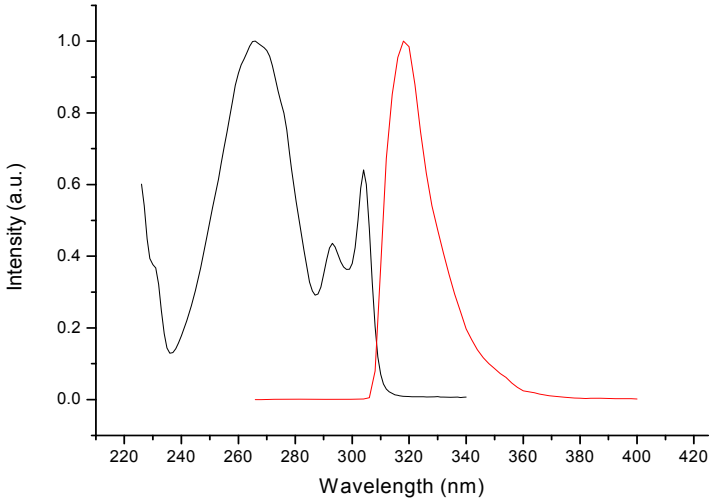

Figure AII-14. Absorbance and fluorescence spectra of **II-5**.

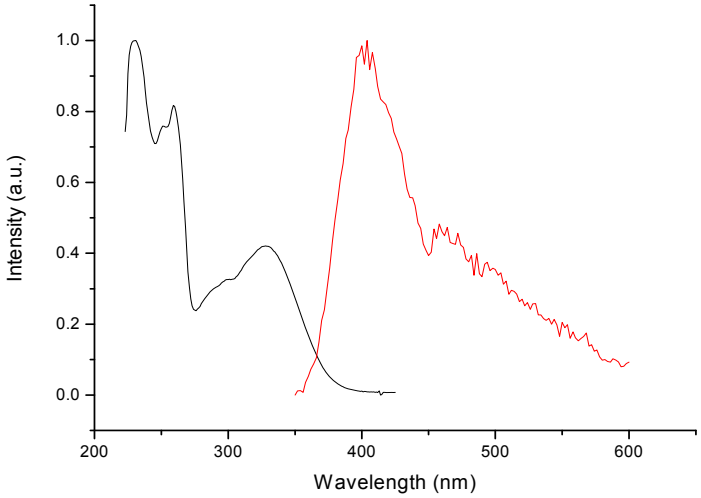

Figure AII-15. Absorbance and fluorescence spectra of **II-7.**

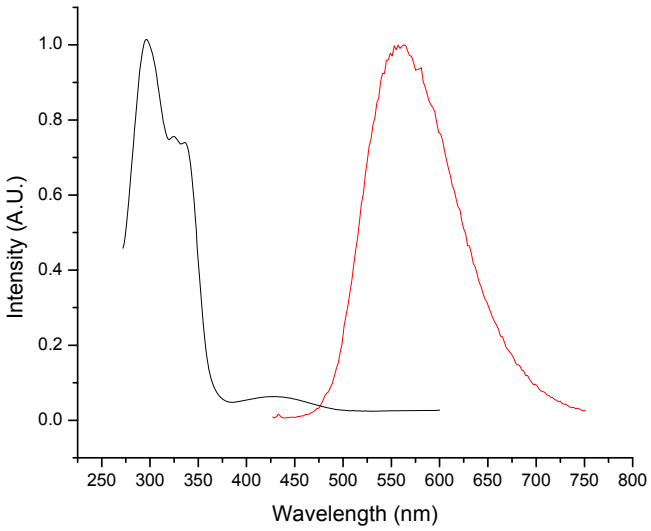

Figure AII-16. Absorbance and fluorescence spectra of **II-10**.

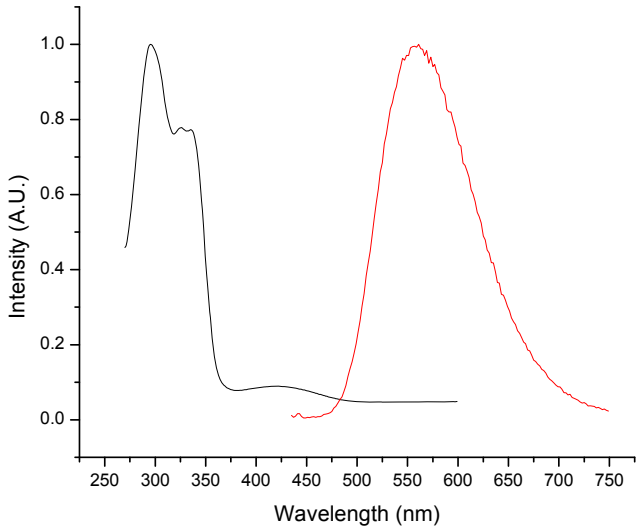

Figure AII-17. Absorbance and fluorescence spectra of **II-11**.

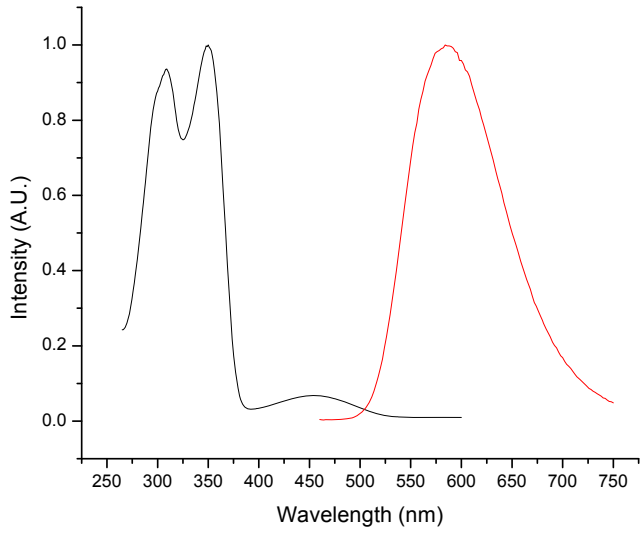

Figure AII-18. Absorbance and fluorescence spectra of **II-12**.

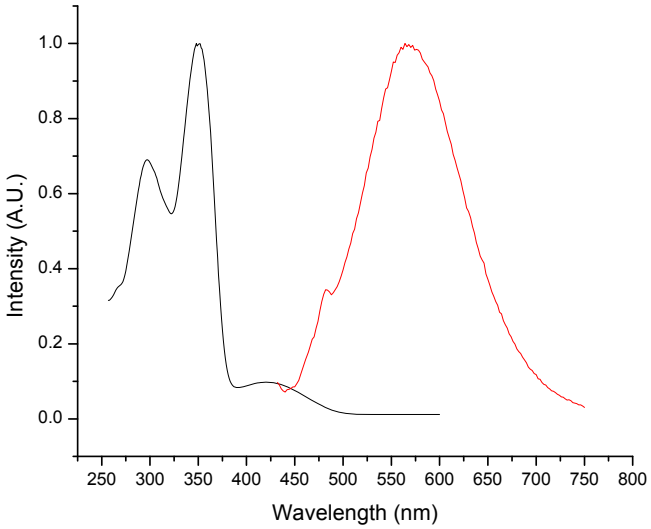

Figure AII-19. Absorbance and fluorescence spectra of **II-13**.

Cyclic voltammetry

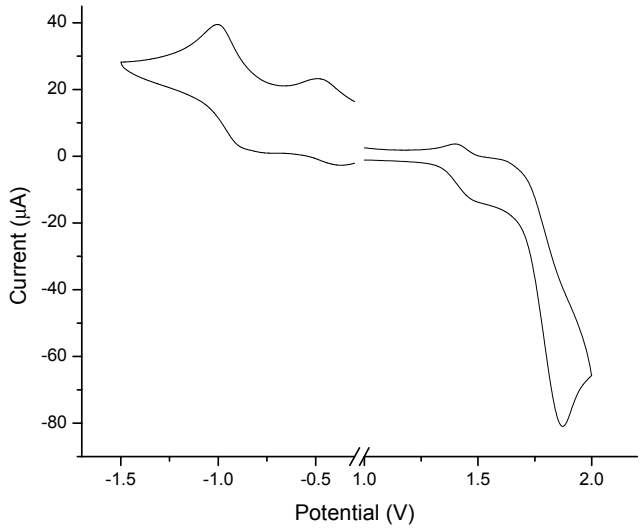

Figure AII-20. Cyclic voltammetry of **II-1** in dichloromethane with 0.1 M $TBAPF_6$.

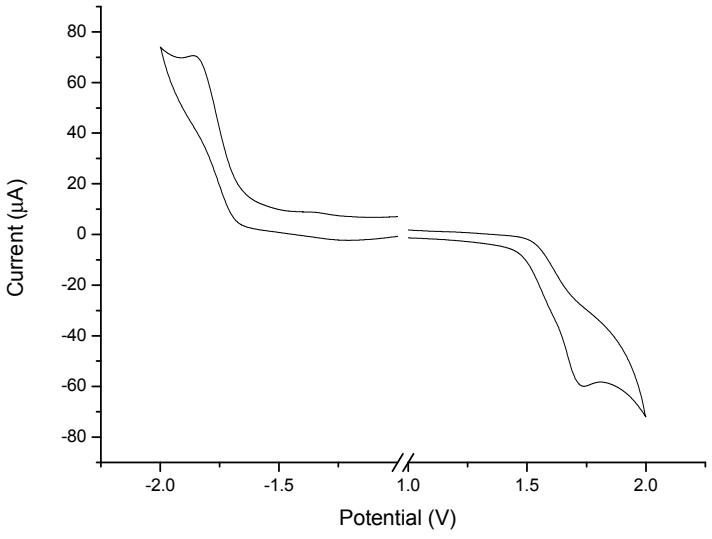

Figure AII-21. Cyclic voltammetry of **II-7** in dichloromethane with 0.1 M $TBAPF_6$.

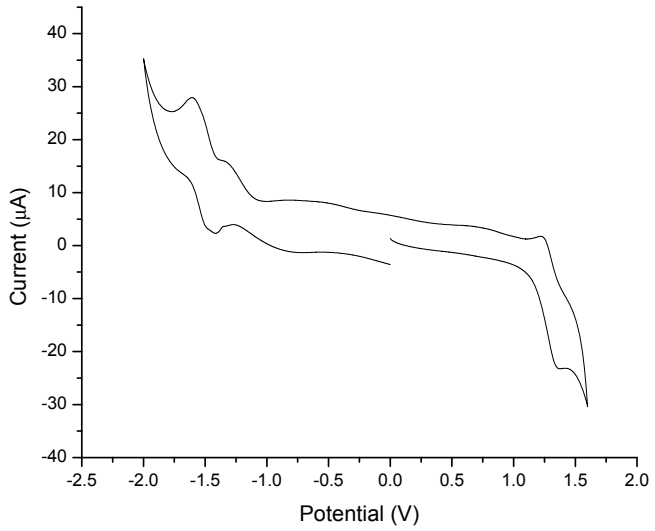

Figure AII-22. Cyclic voltammetry of **II-10** in dichloromethane with 0.1 M $TBAPF_6$.

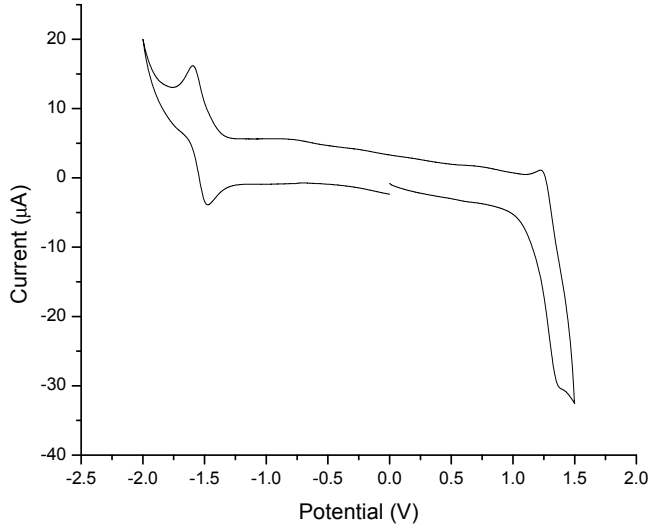

Figure AII-23. Cyclic voltammetry of **II-11** in dichloromethane with 0.1 M $TBAPF_6$.

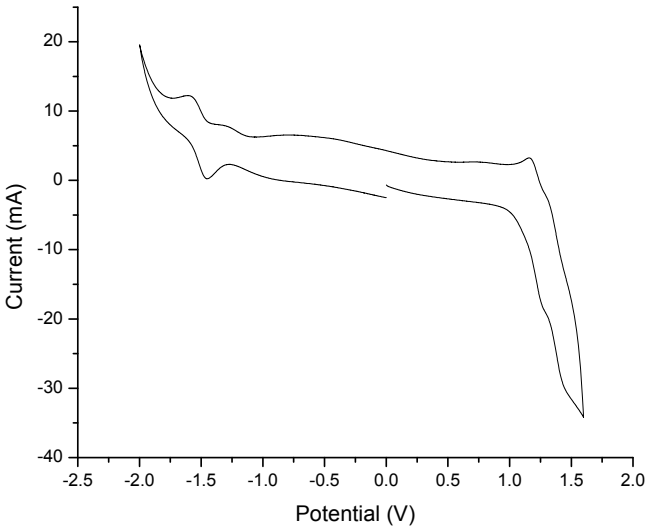

Figure AII-24. Cyclic voltammetry of **II-12** in dichloromethane with 0.1 M $TBAPF_6$.

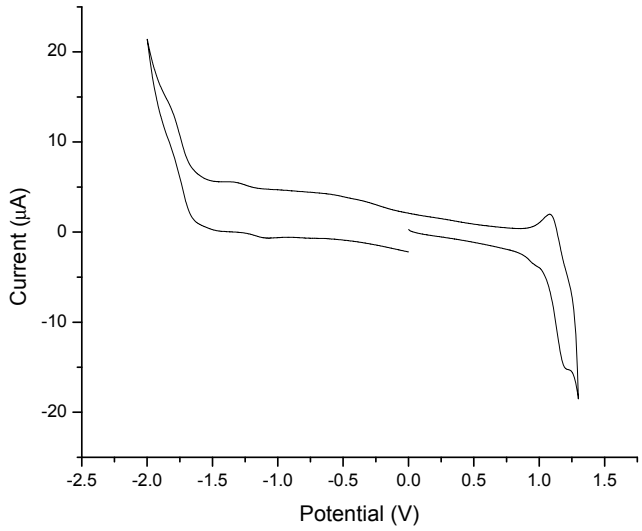

Figure AII-25. Cyclic voltammetry of **II-13** in dichloromethane with 0.1 M $TBAPF_6$.

Quenching studies

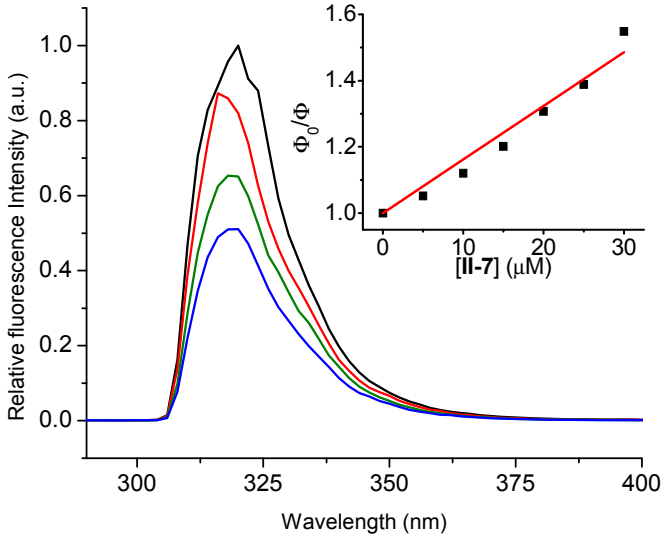

Figure AII-26. Quenching of **II-1** with **II-7** in DCM.

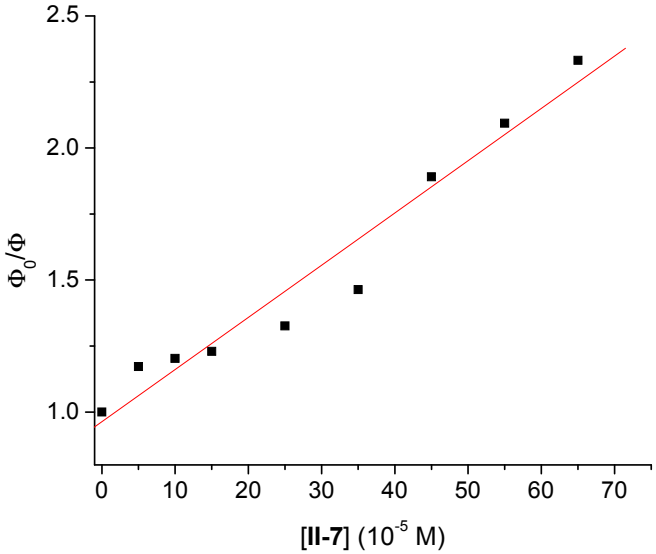

Figure AII-27. Quenching of **II-5** with **II-7** in DCM.

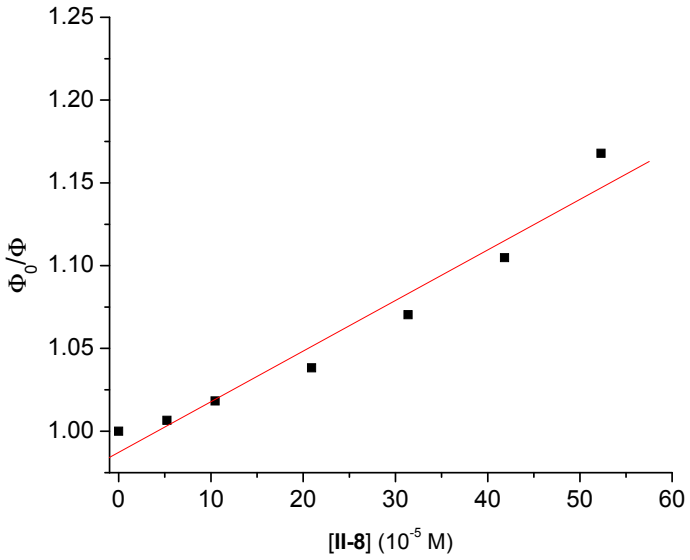

Figure AII-28. Quenching of **II-1** with **II-8** in DCM.

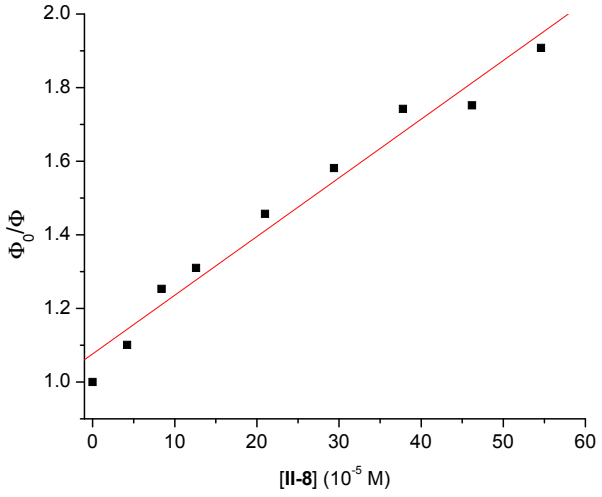

Figure AII-29. Quenching of **II-5** with **II-8** in DCM.

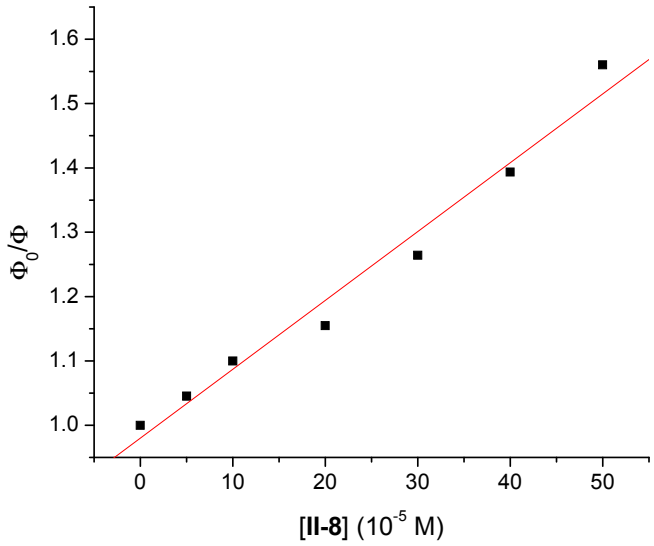

Figure AII-30. Quenching of **II-9** with **II-8** in DCM.

AIII. ANNEXE III - CHAPITRE III

Table of contents

Absorption and Emission spectra

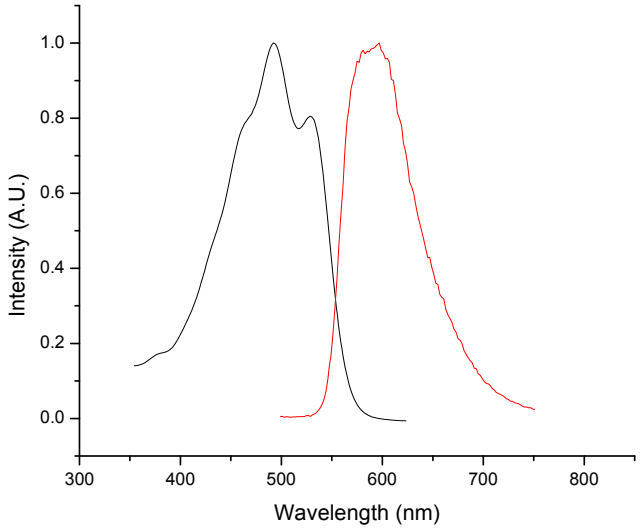

Figure AIII-1. Absorbance (black) and fluorescence (red) of **III-2** in dichloromethane.

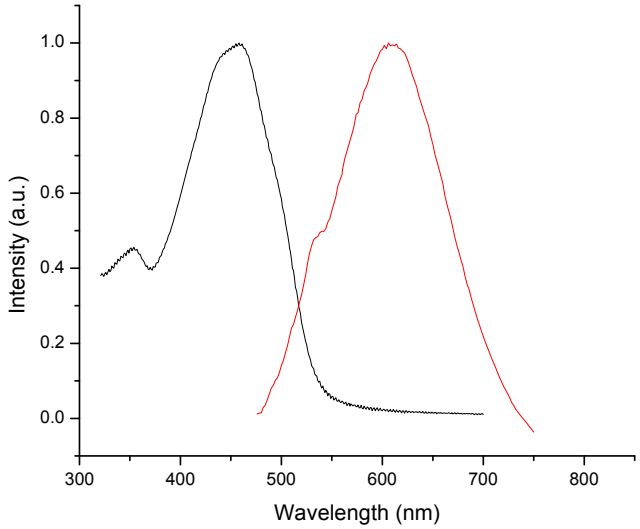

Figure AIII-2. Absorbance (black) and fluorescence (red) of **III-4** in dichloromethane.

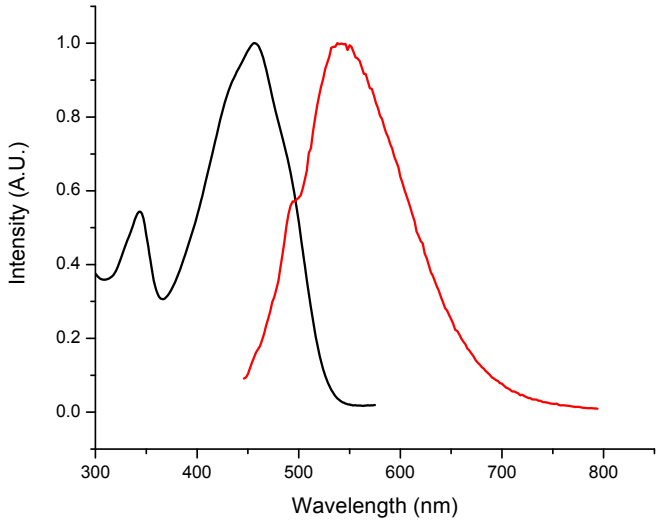

Figure AIII-3. Absorbance (black) and fluorescence (red) of **III-5** in dichloromethane.

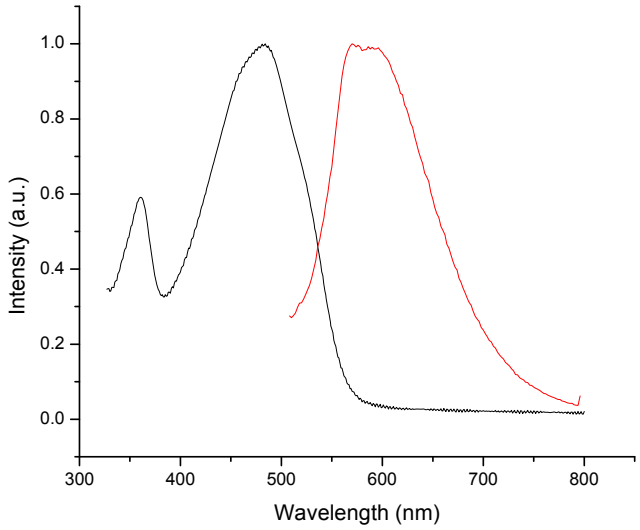

Figure AIII-4. Absorbance (black) and fluorescence (red) of **III-6** in dichloromethane.

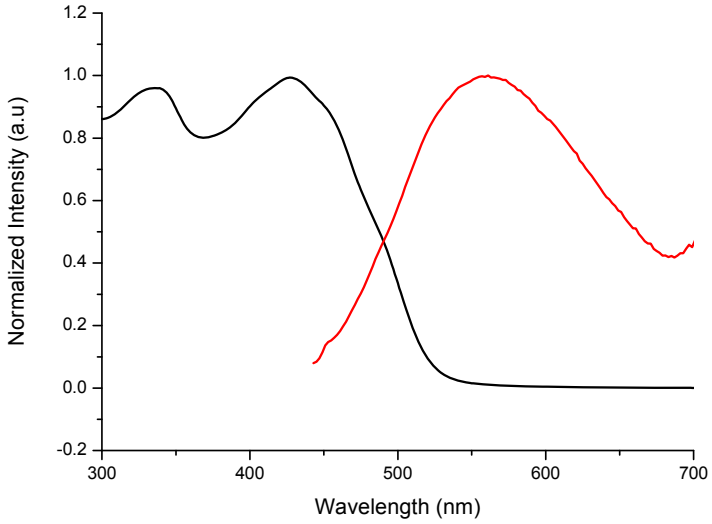

Figure AIII-5. Absorbance (black) and fluorescence (red) of **III-7** in dichloromethane.

Cyclic voltammetry

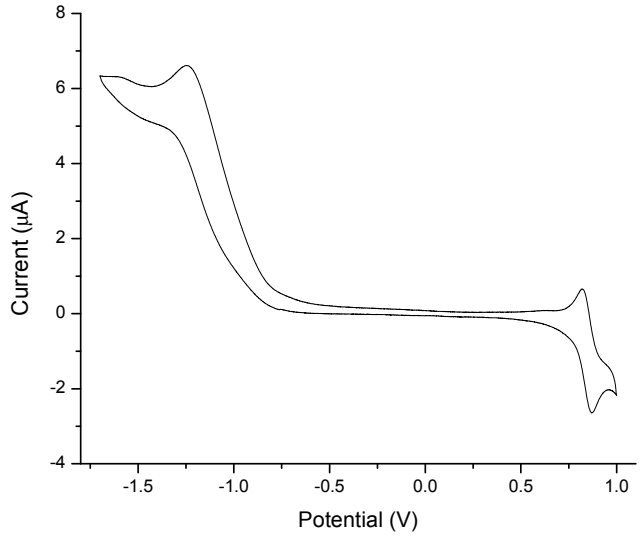

Figure AIII-6. Cyclic voltammogram of **III-2** with 0.1M $TBAPF_6$ in dichloromethane.

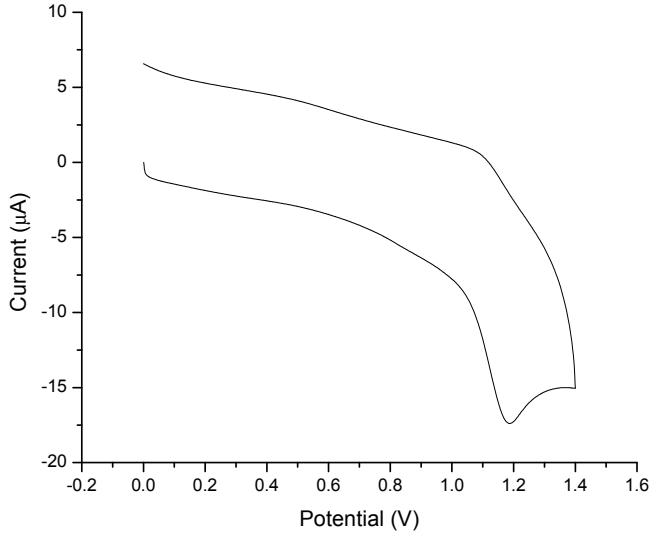

Figure AIII-7. Cyclic voltammogram of **III-4** with 0.1M $TBAPF_6$ in dichloromethane.

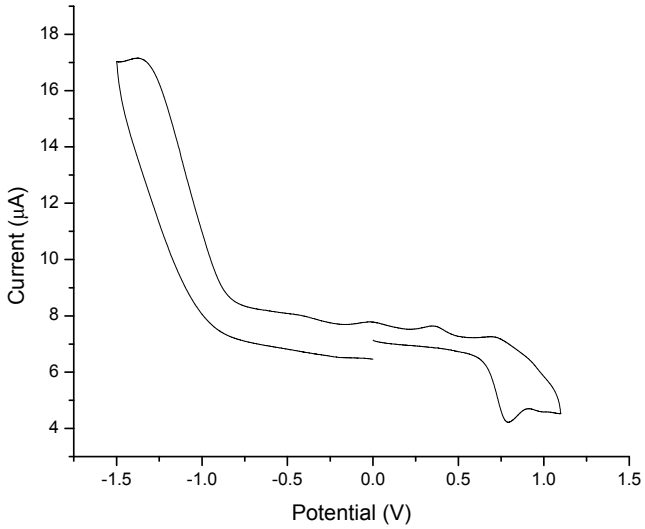

Figure AIII-8. Cyclic voltammogram of **III-5** with 0.1M $TBAPF_6$ in dichloromethane.

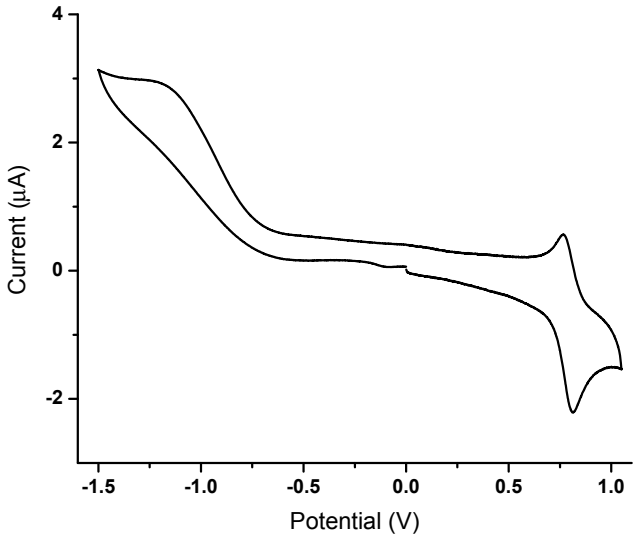

Figure AIII-9. Cyclic voltammogram of **III-6** with 0.1M $TBAPF_6$ in dichloromethane.

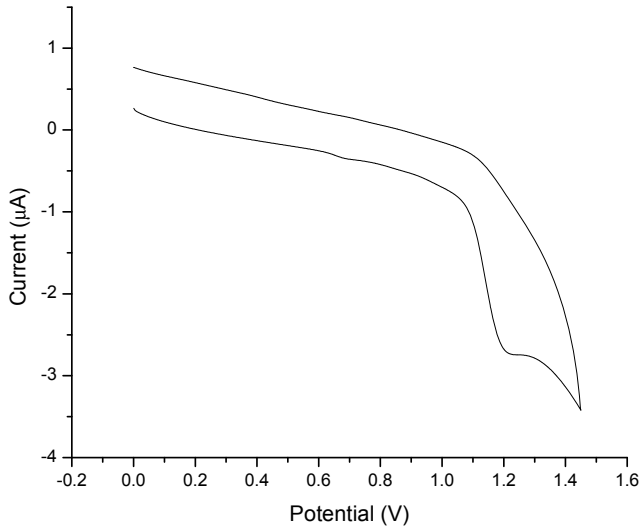

Figure AIII-10. Cyclic voltammogram of **III-7** with 0.1M $TBAPF_6$ in dichloromethane.

NMR spectra

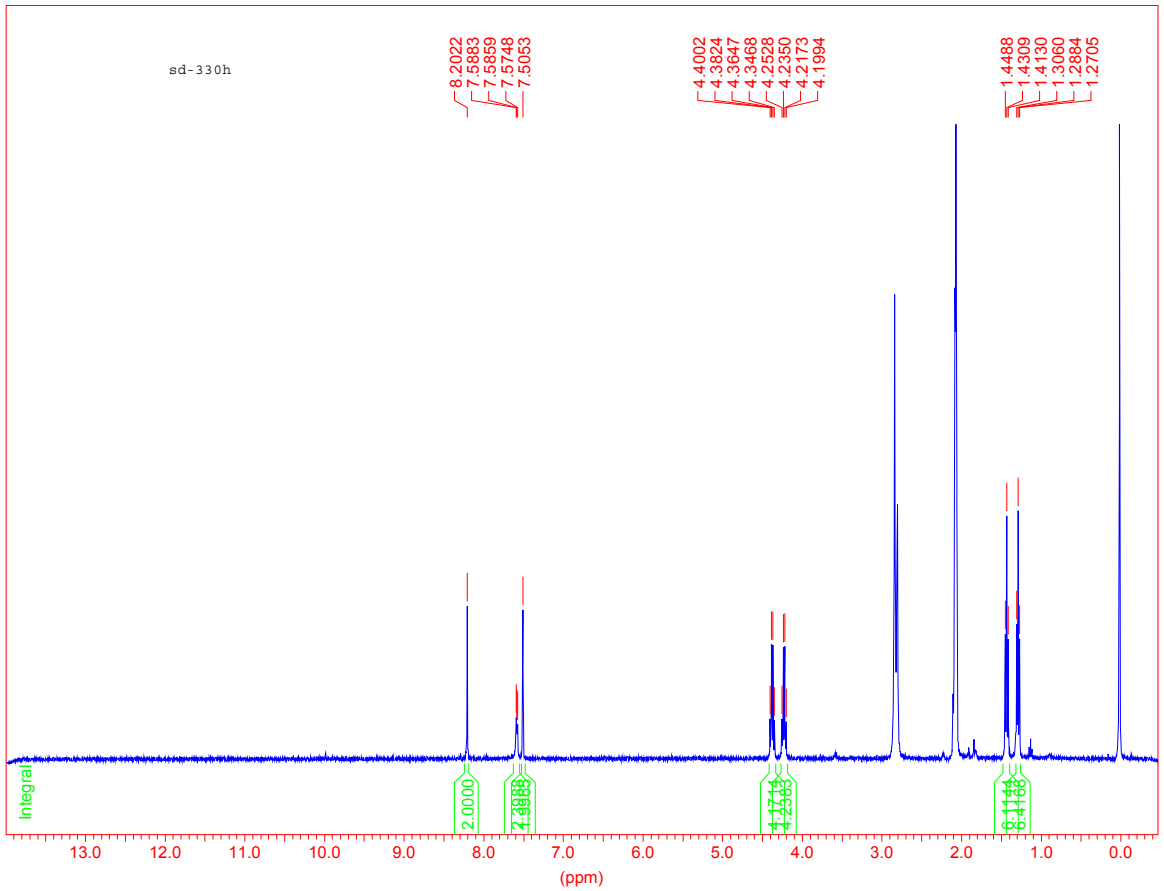

Figure AIII-11. ^{1}H NMR spectrum of **III-2** in deuterated acetone.

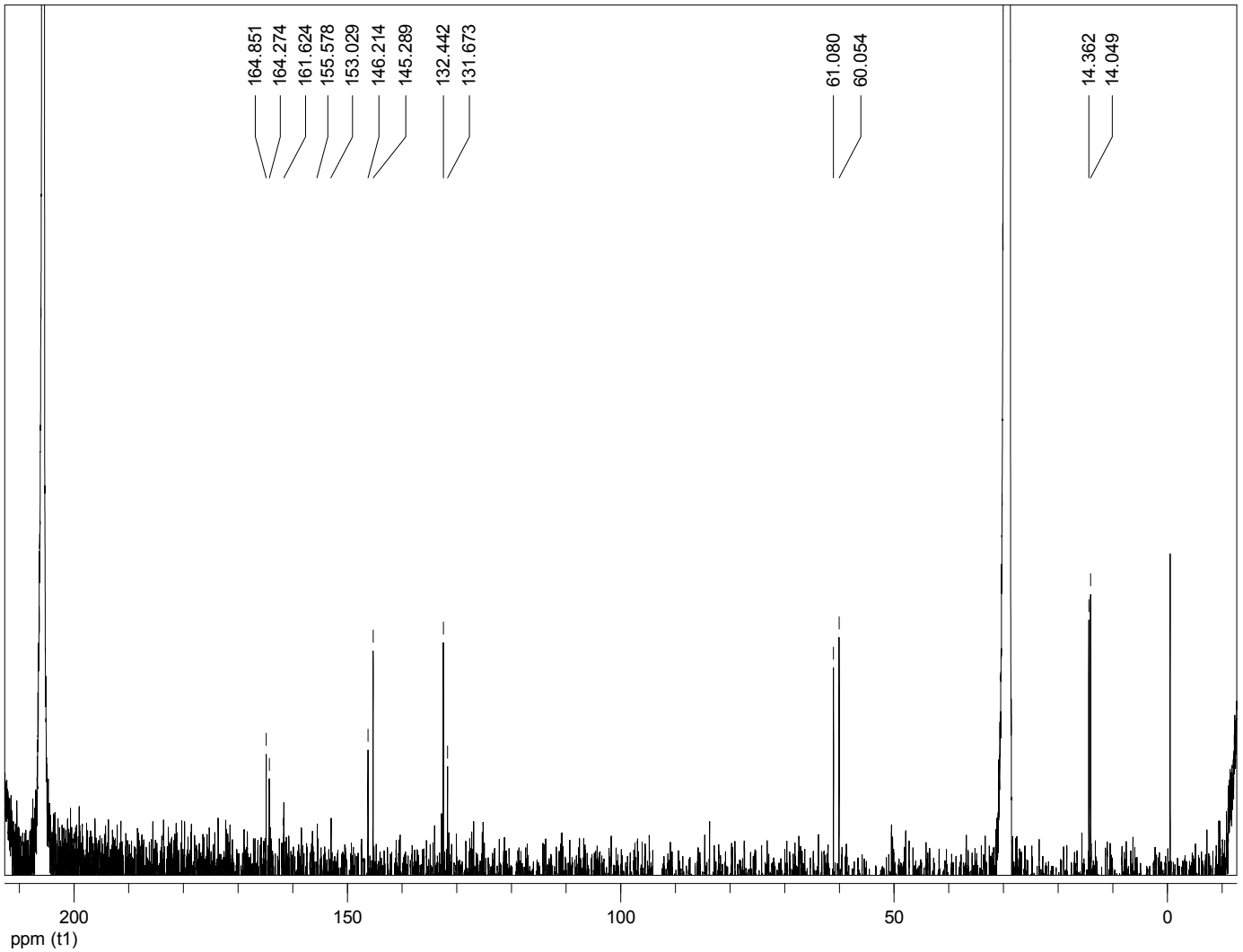

Figure AIII-12. ^{13}C NMR spectrum of **III-2** in deuterated acetone.

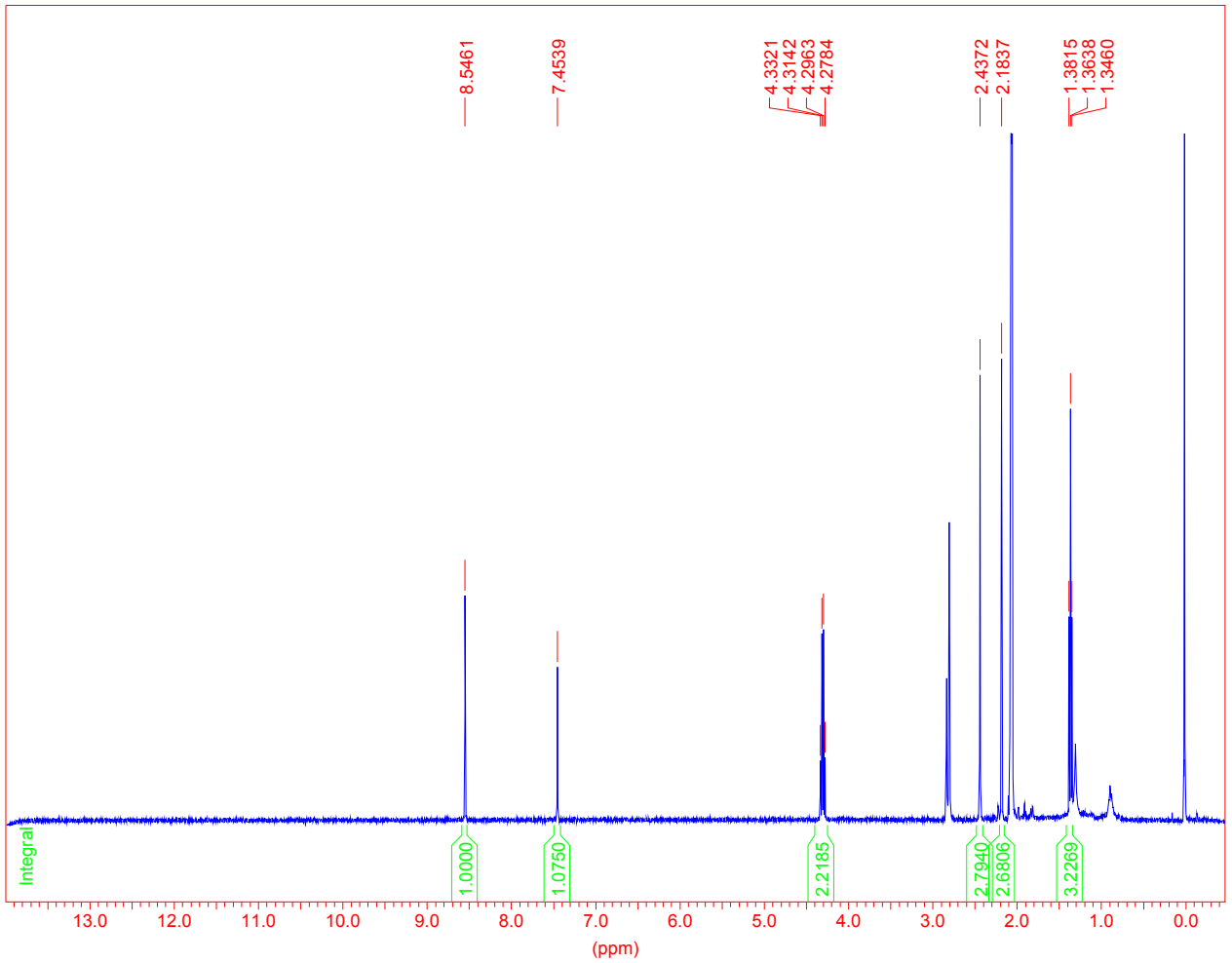

Figure AIII-13. ^{1}H NMR spectrum of **III-4** in deuterated acetone.

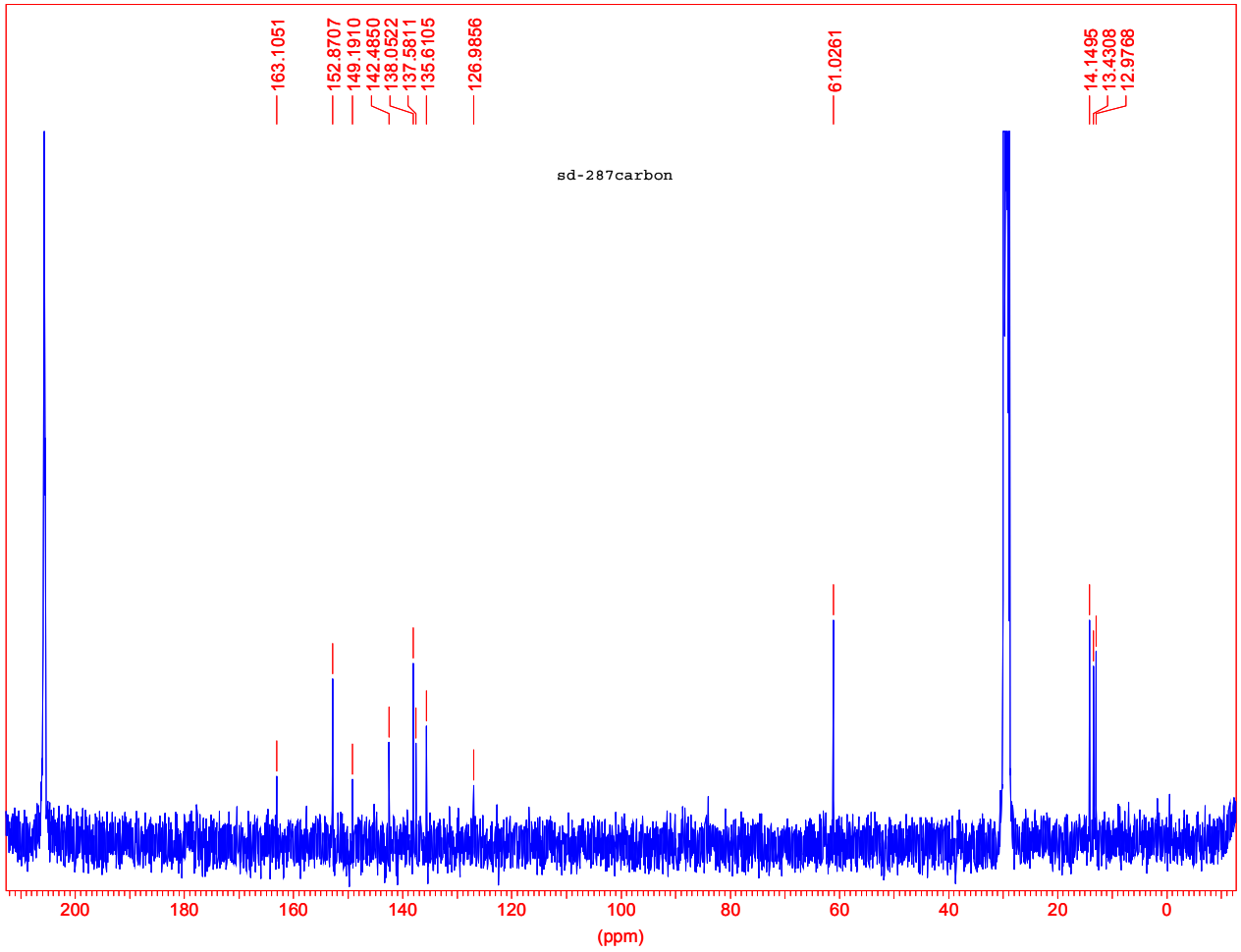

Figure AIII-14. ^{13}C NMR spectrum of **III-4** in deuterated acetone.

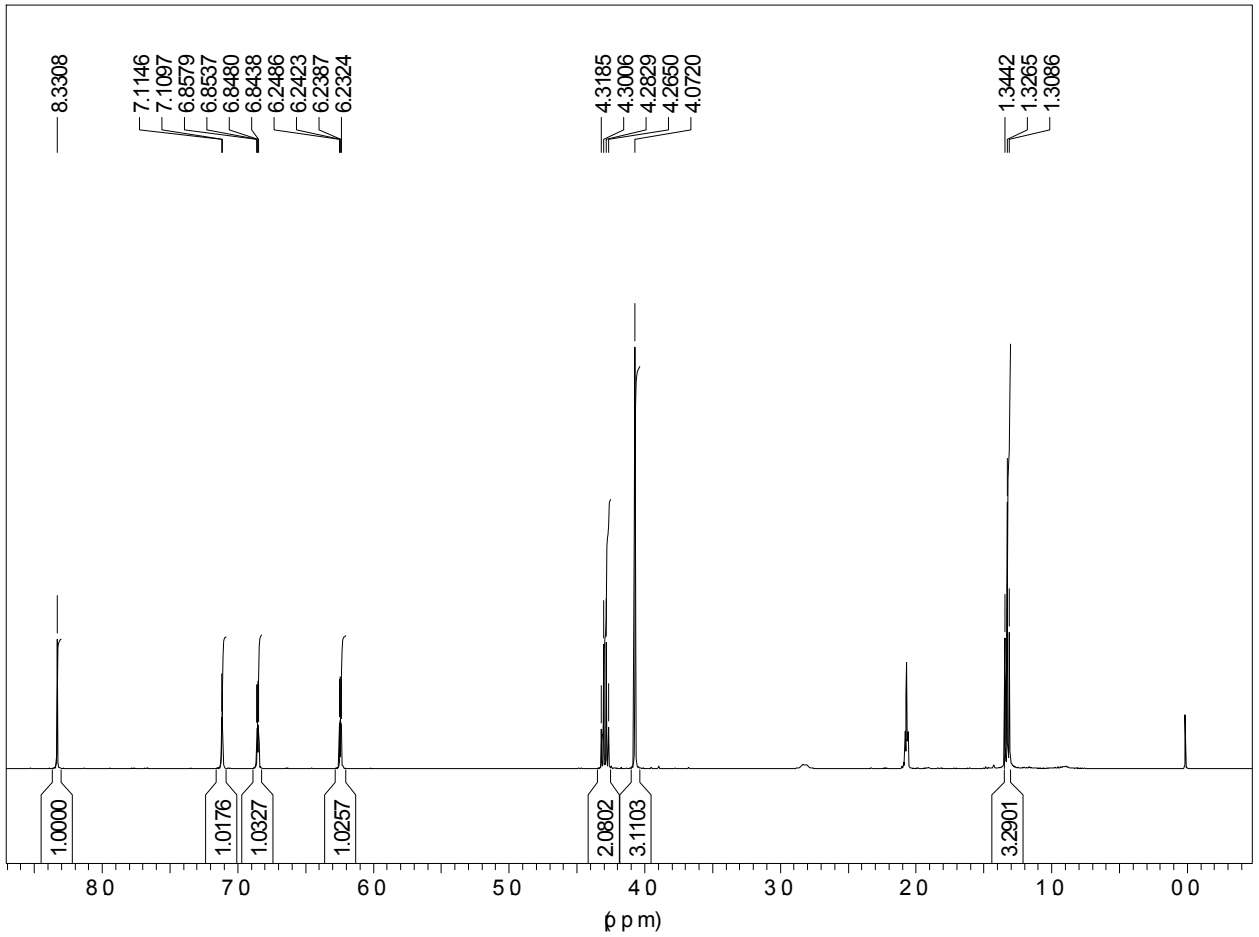

Figure AIII-15. ^{1}H NMR spectrum of **III-5** in deuterated acetone.

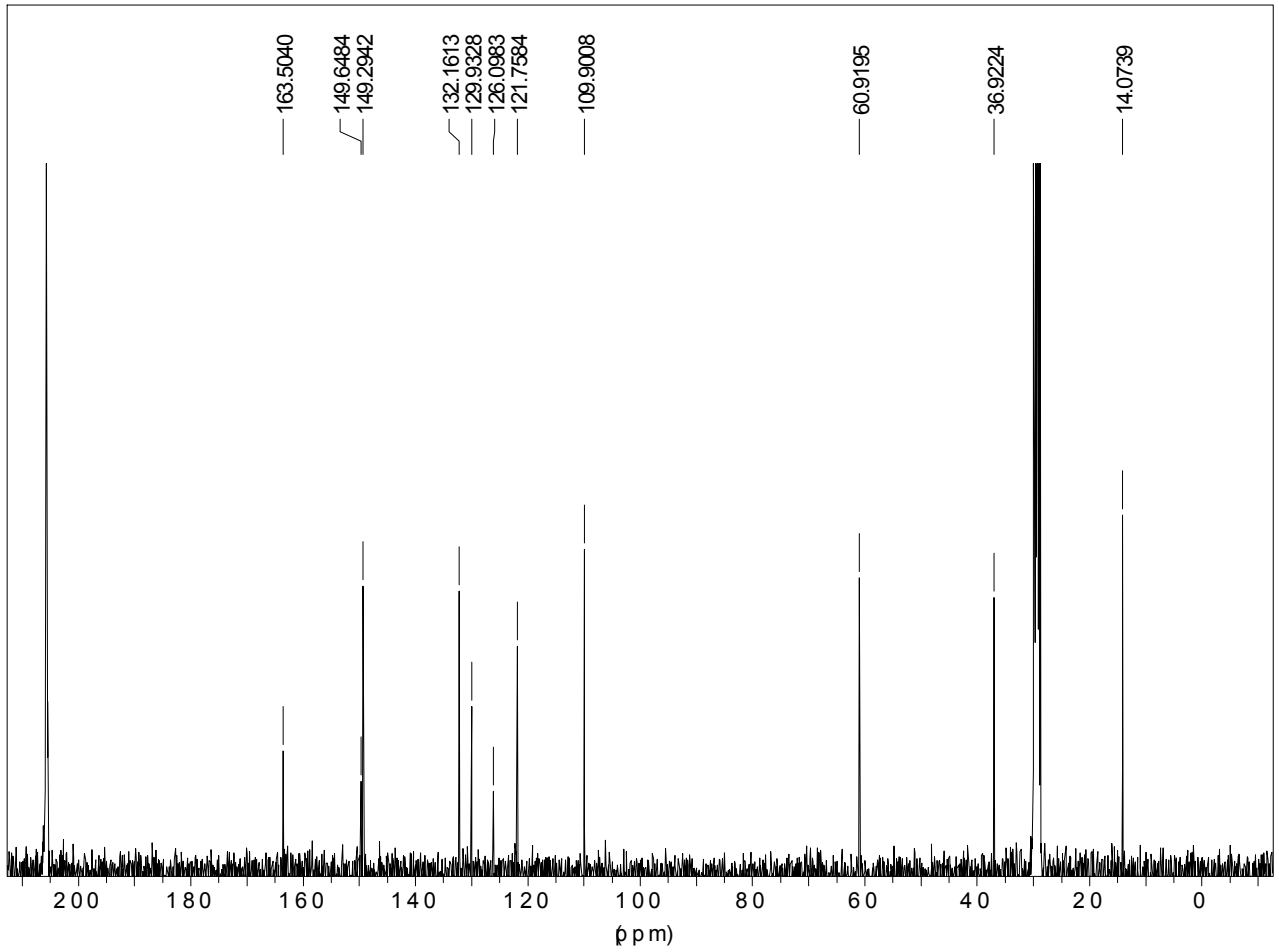

Figure AIII-16. ^{13}C NMR spectrum of **III-5** in deuterated acetone.

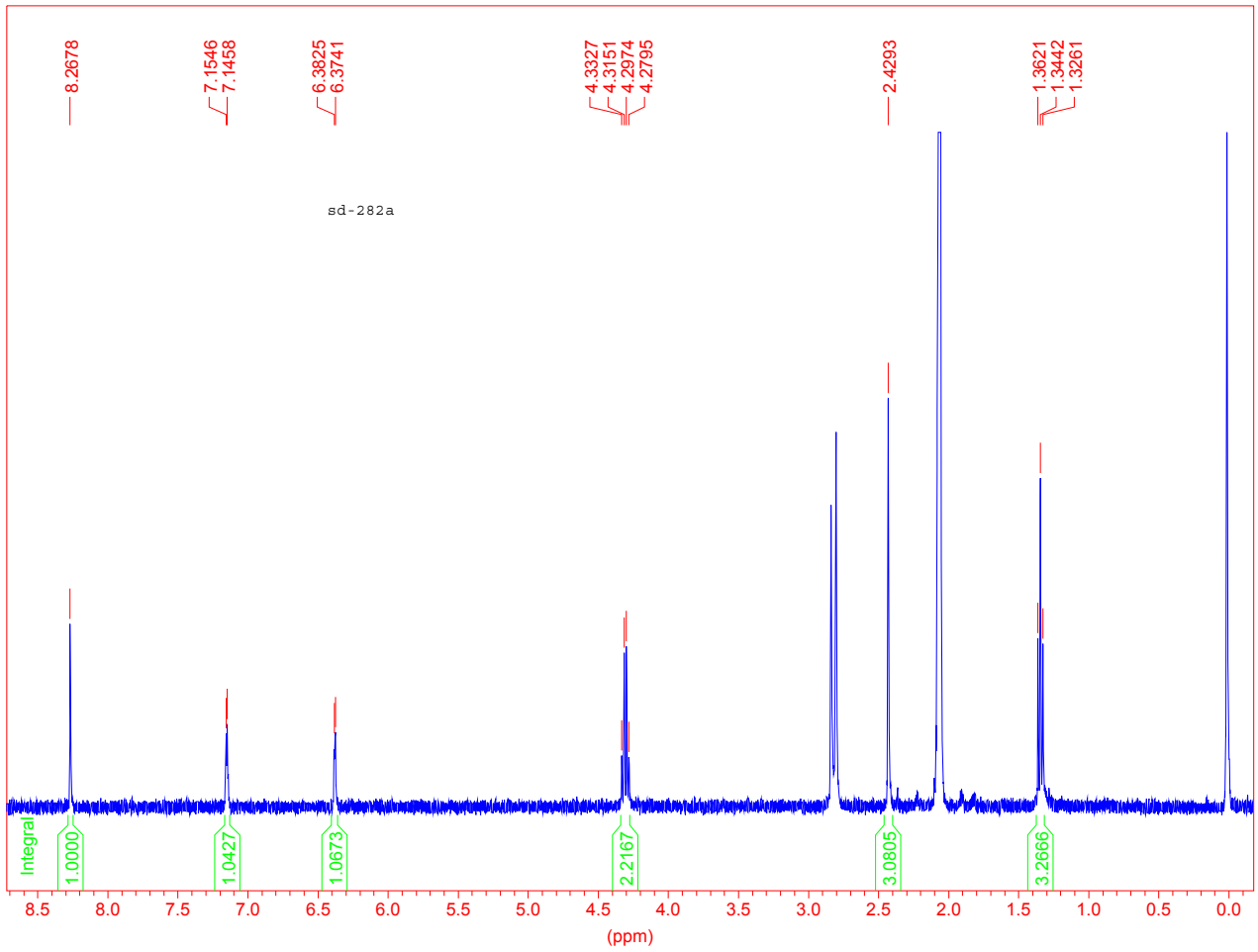

Figure AIII-17. ^{1}H NMR spectrum of **III-6** in deuterated acetone.

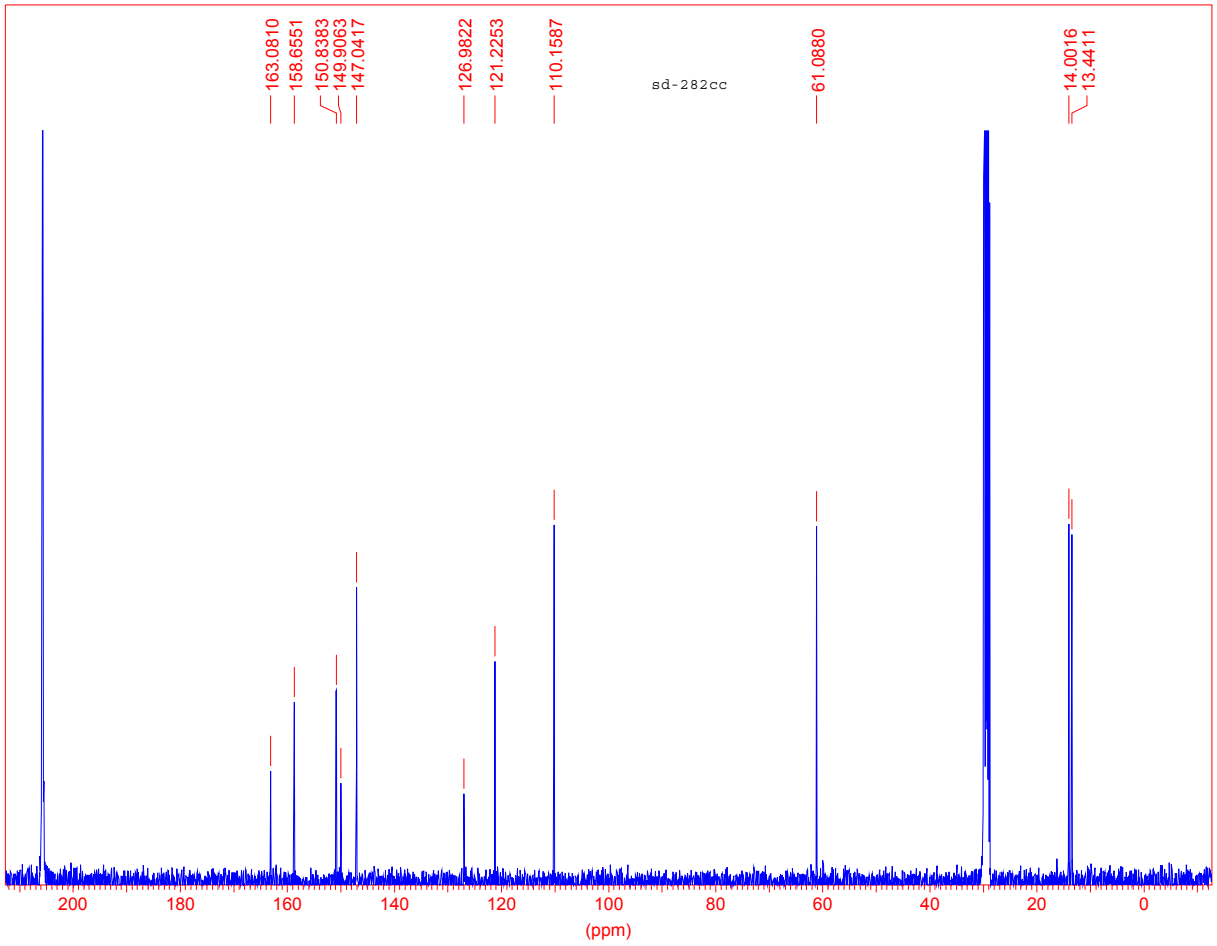

Figure AIII-18. ^{13}C NMR spectrum of **III-6** in deuterated acetone.

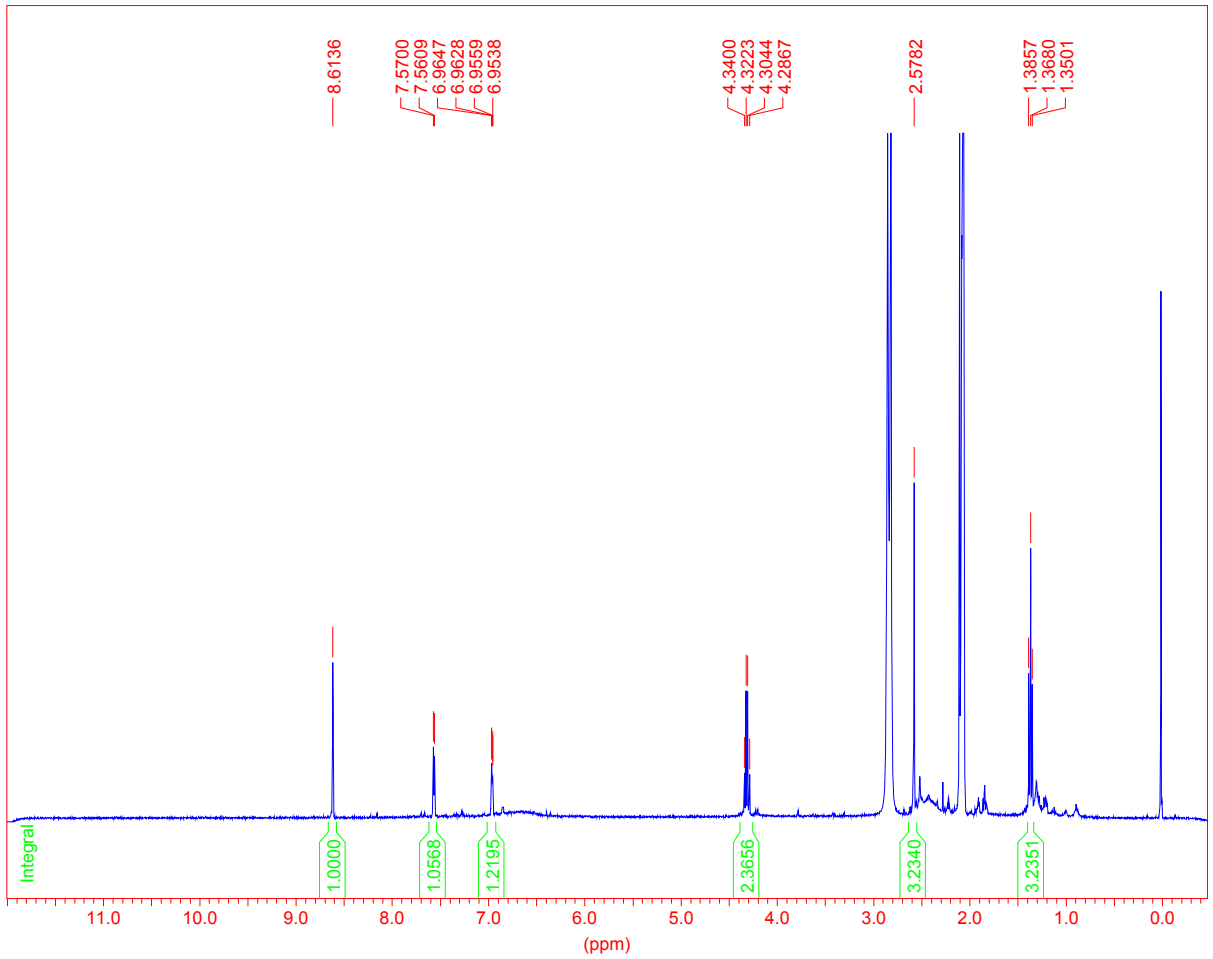

Figure AIII-19. ^{1}H NMR spectrum of **III-7** in deuterated acetone.

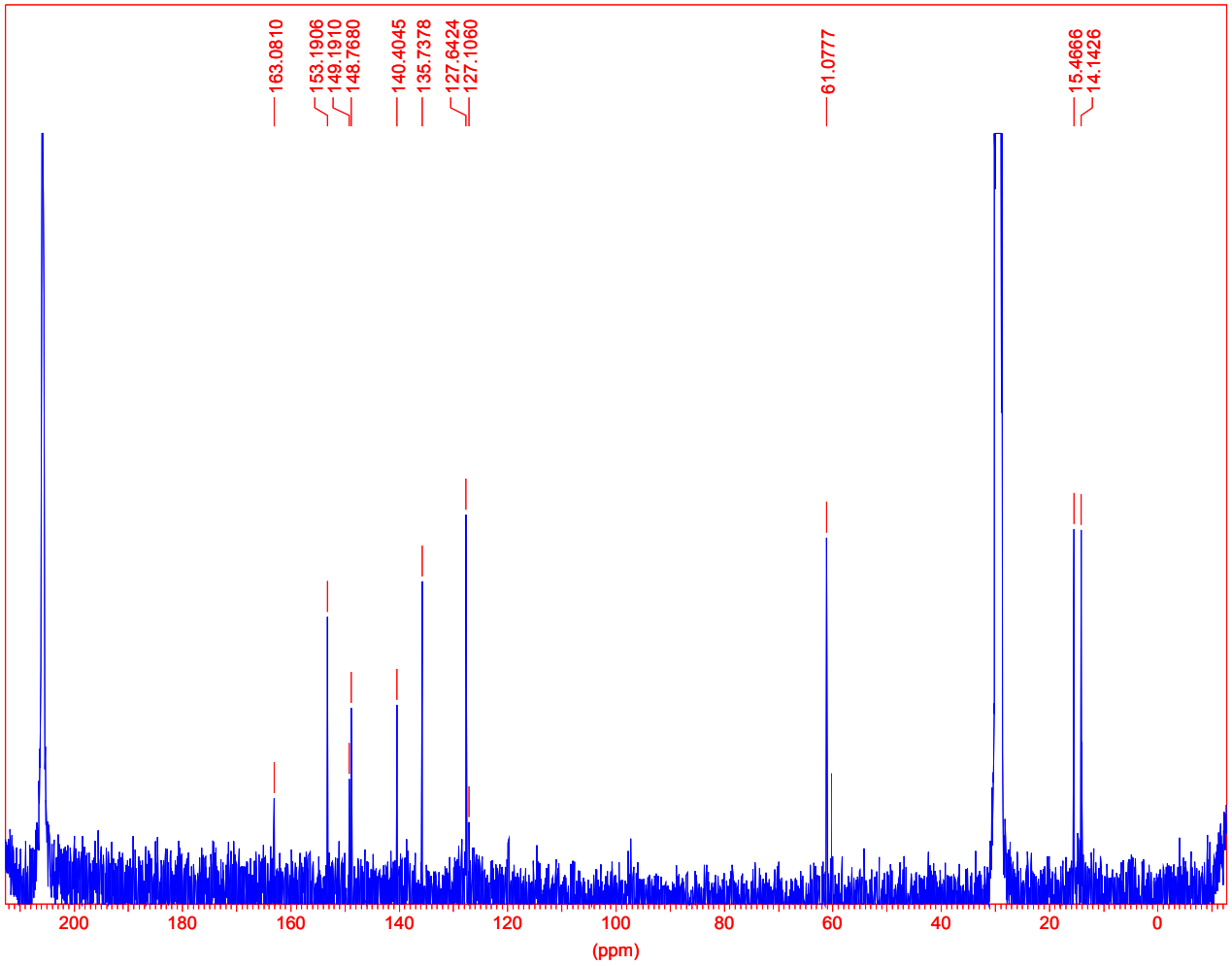

Figure AIII-20. ^{13}C NMR spectrum of **III-7** in deuterated acetone.

AV. ANNEXE IV - CHAPITRE IV

Table of Contents

Absorption and Emission spectra

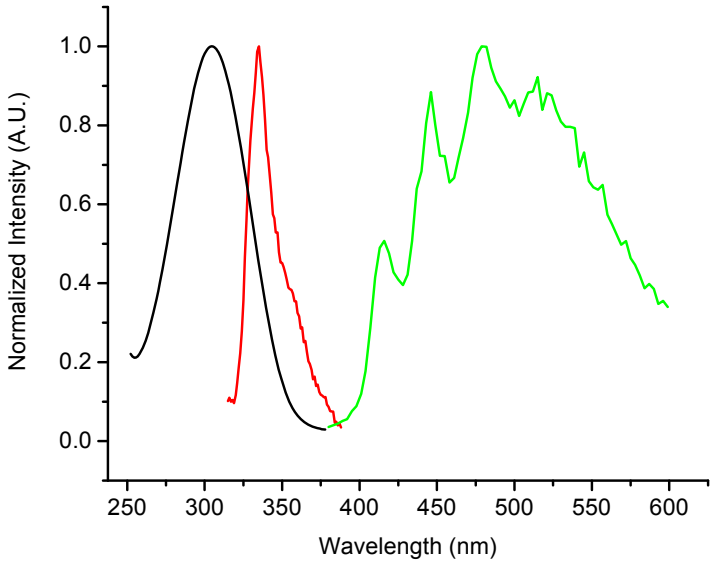

Figure AIV-1. Absorption, fluorescence and phosphorescence spectra of **IV-1.**

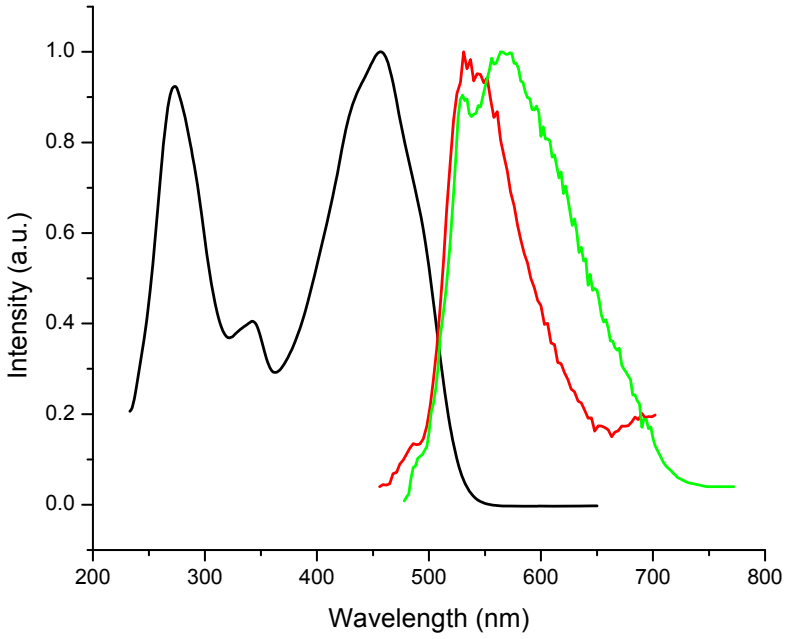

Figure AIV-2. Absorption, fluorescence and phosphorescence spectra of **IV-6.**

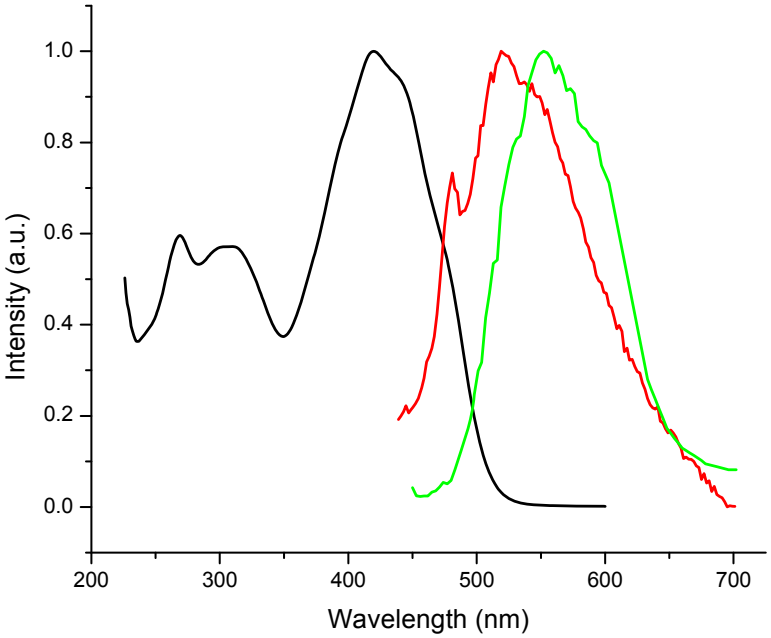

Figure AIV-3. Absorption, fluorescence and phosphorescence spectra of **IV-7.**

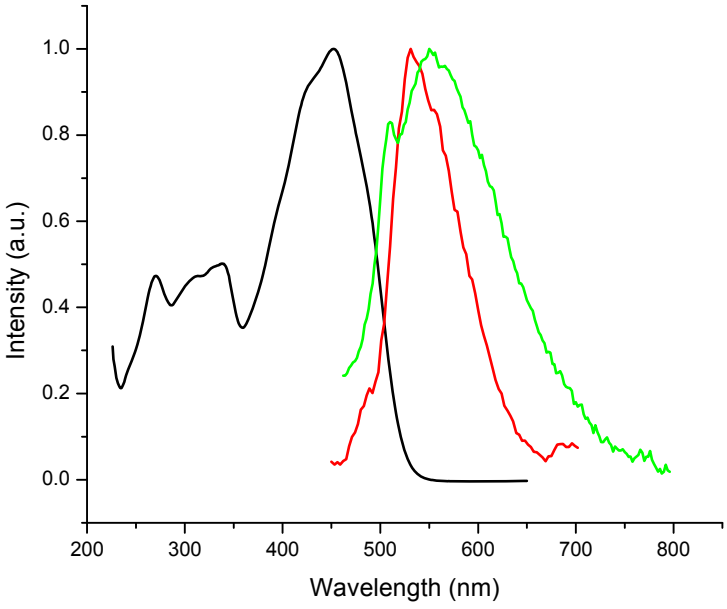

Figure AIV-4. Absorption, fluorescence and phosphorescence spectra of **IV-8.**

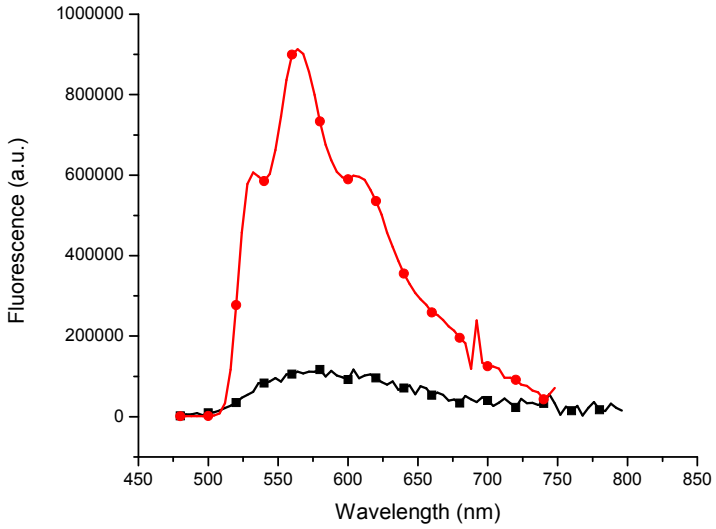

Figure AIV-5. Fluorescence of **IV-6** measured at RT (■) and magnified 100 times relative to the fluorescence at 77 K measured in a 4:1 ethanol/methanol glass matrix (●).

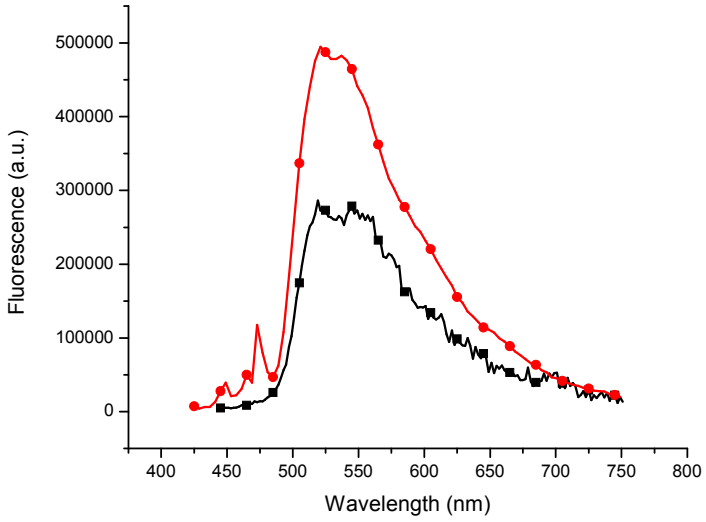

Figure AIV-6. Fluorescence of **IV-7** measured at RT (■) and magnified 50 times relative to the fluorescence at 77 K measured in a 4:1 ethanol/methanol glass matrix (●).

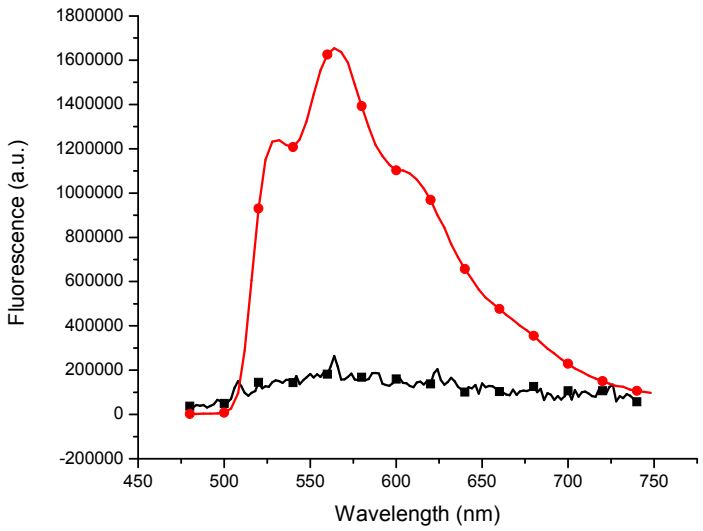

Figure AIV-7. Fluorescence of **IV-8** measured at RT (■) and magnified 100 times relative to the fluorescence at 77 K measured in a 4:1 ethanol/methanol glass matrix (●).

Cyclic voltammetry

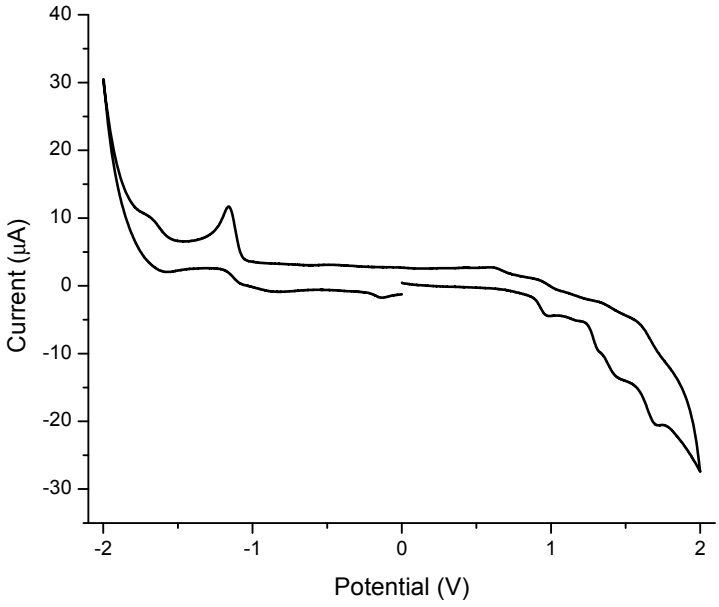

Figure AIV-8. Cyclic voltammetry of **IV-6.**

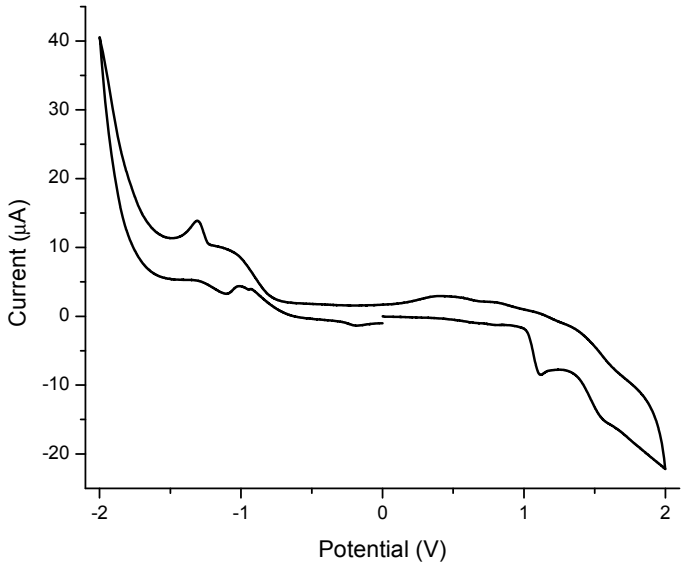

Figure AIV-9. Cyclic voltammetry of **IV-7.**

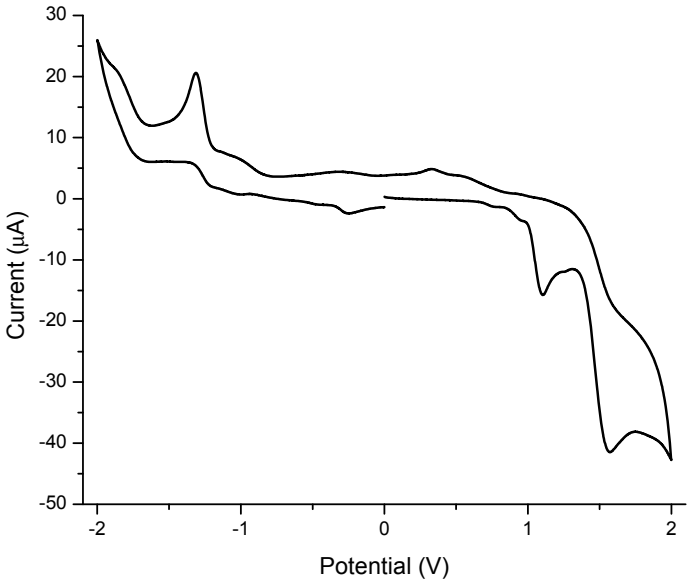

Figure AIV-10. Cyclic voltammetry of **IV-8.**

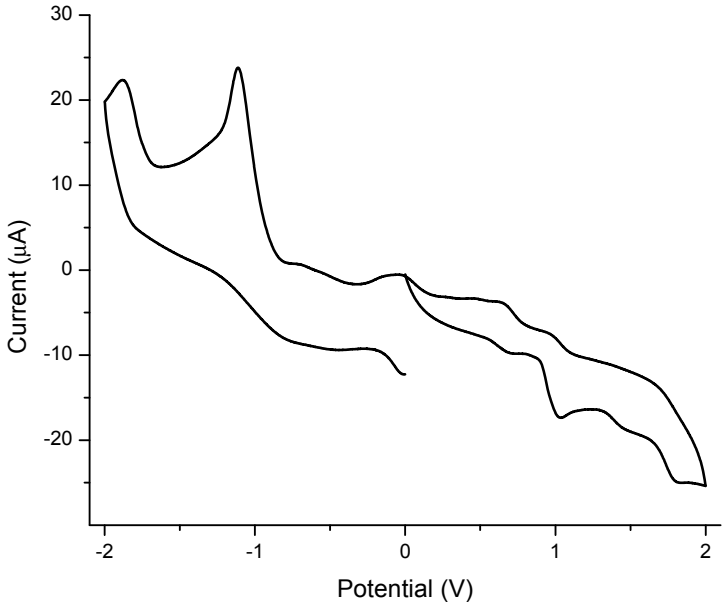

Figure AIV-11. Cyclic voltammetry of **IV-11** in DCM made by oxydative coupling of **IV-6**.

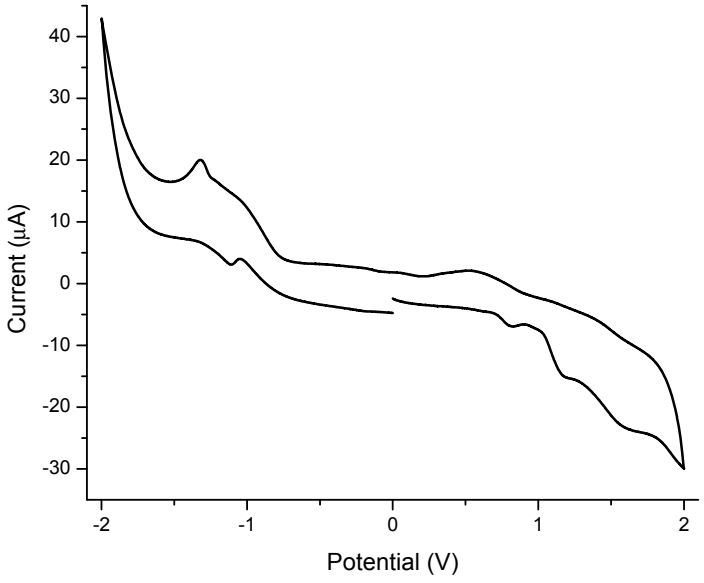

Figure AIV-12. Cyclic voltammetry of **IV-12** in DCM made by oxydative coupling of **IV-7.**

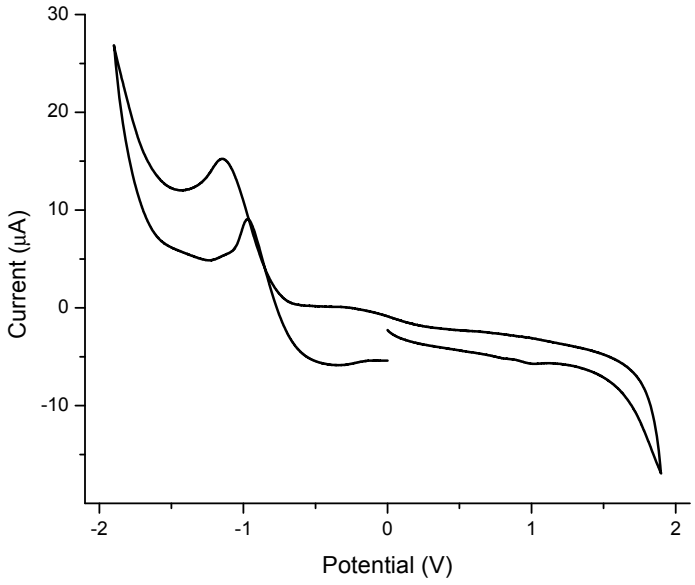

Figure AIV-13. Cyclic voltammetry of **IV-13** in DCM made by oxydative coupling of **IV-8.**

NMR spectra

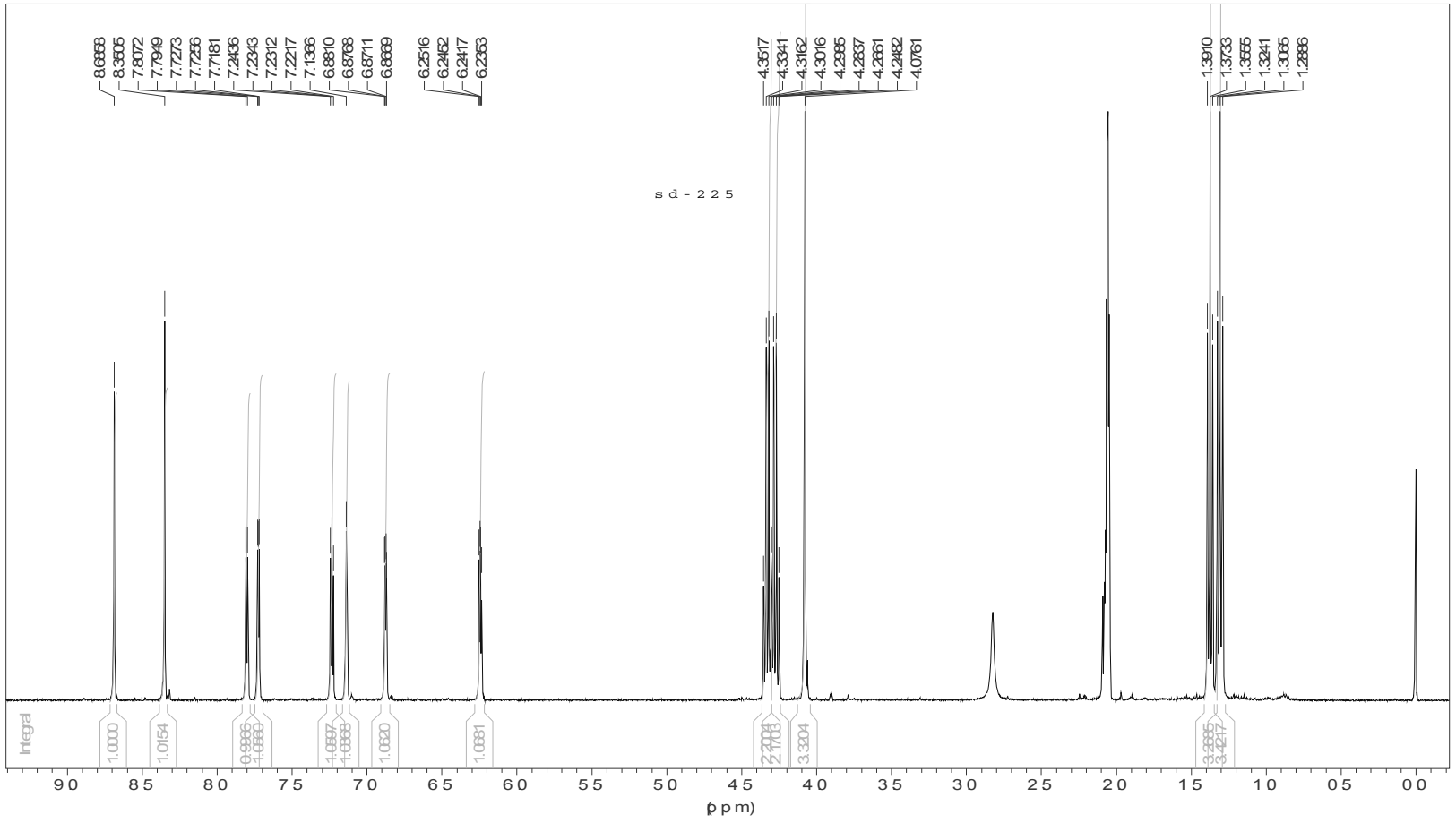

Figure AIV-14. ^{1}H NMR spectra of **IV-6** in deuterated acetone.

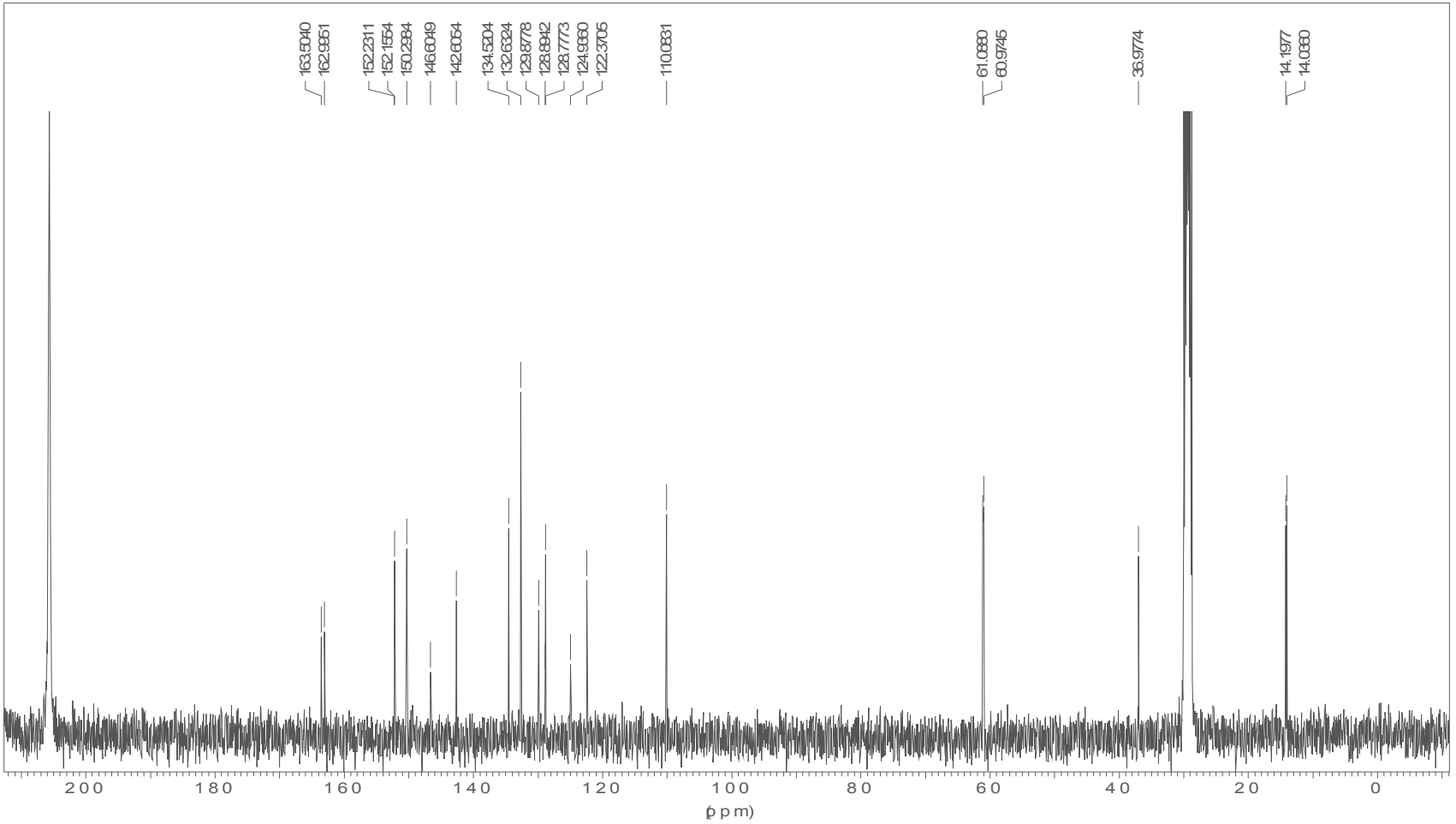

Figure AIV-15. ^{13}C NMR spectra of **IV-6** in deuterated acetone.

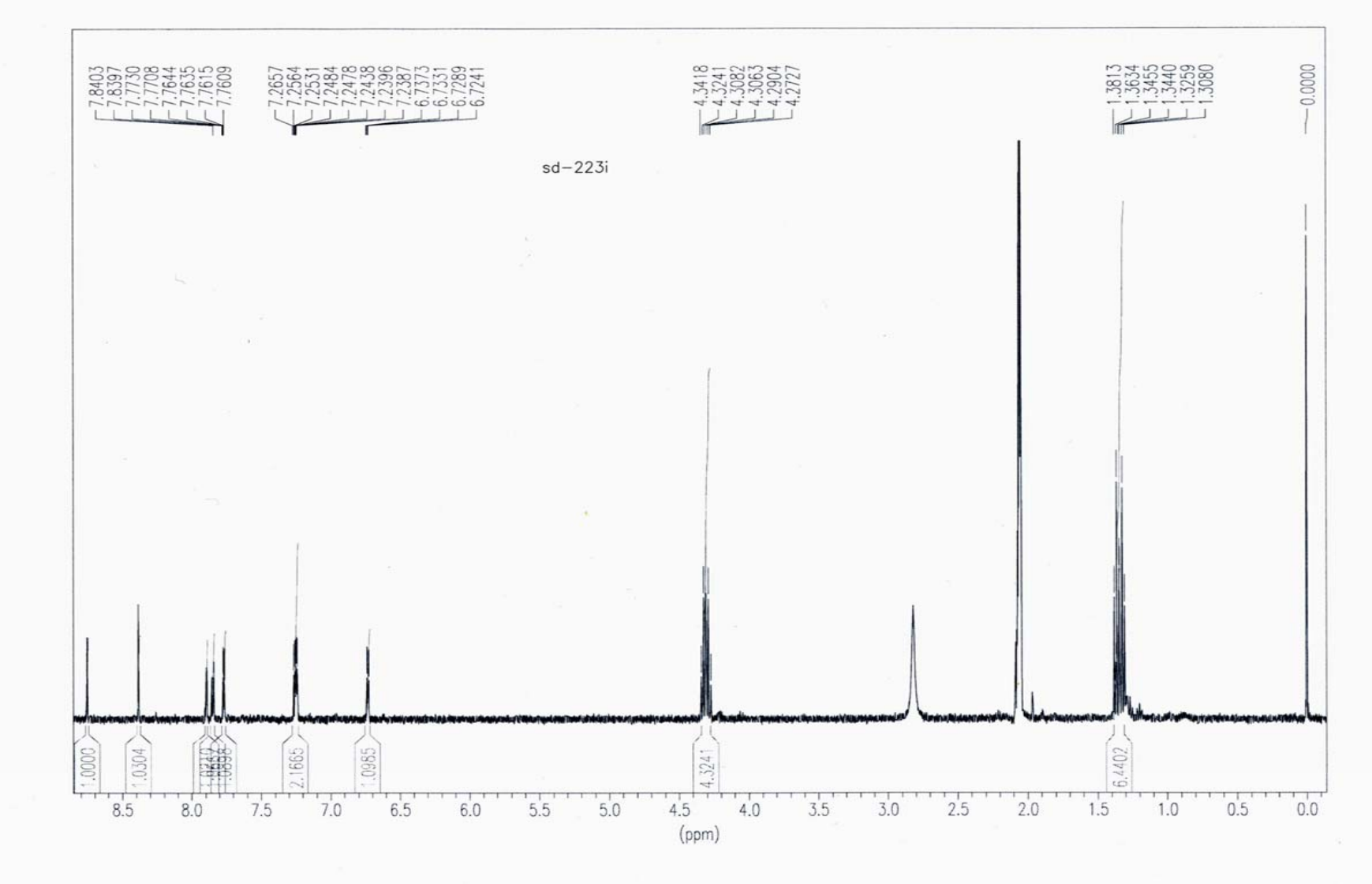

Figure AIV-16. ^{1}H NMR spectra of **IV-7** in deuterated acetone.

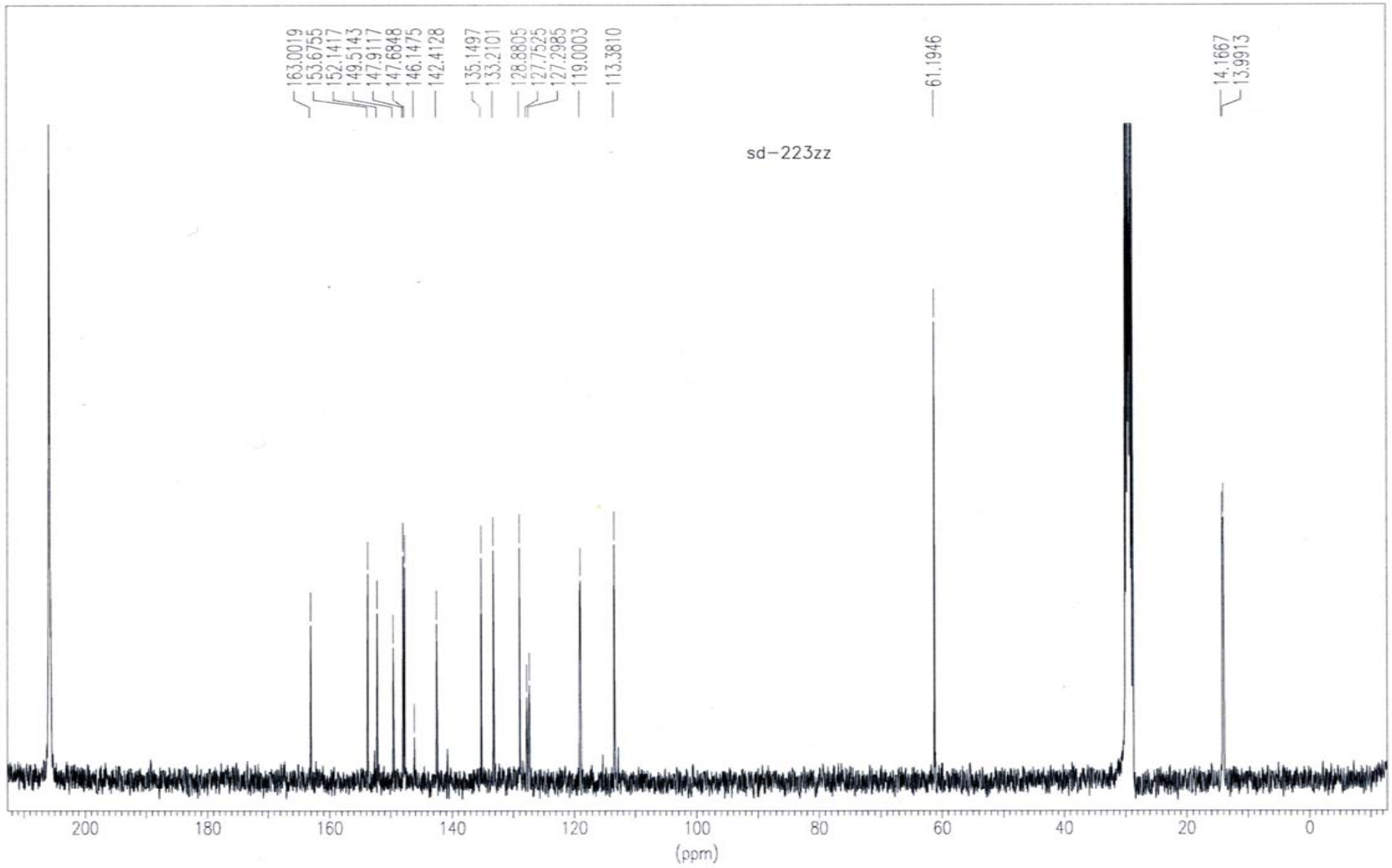

Figure AIV-17. ^{13}C NMR spectra of **IV-7** in deuterated acetone.

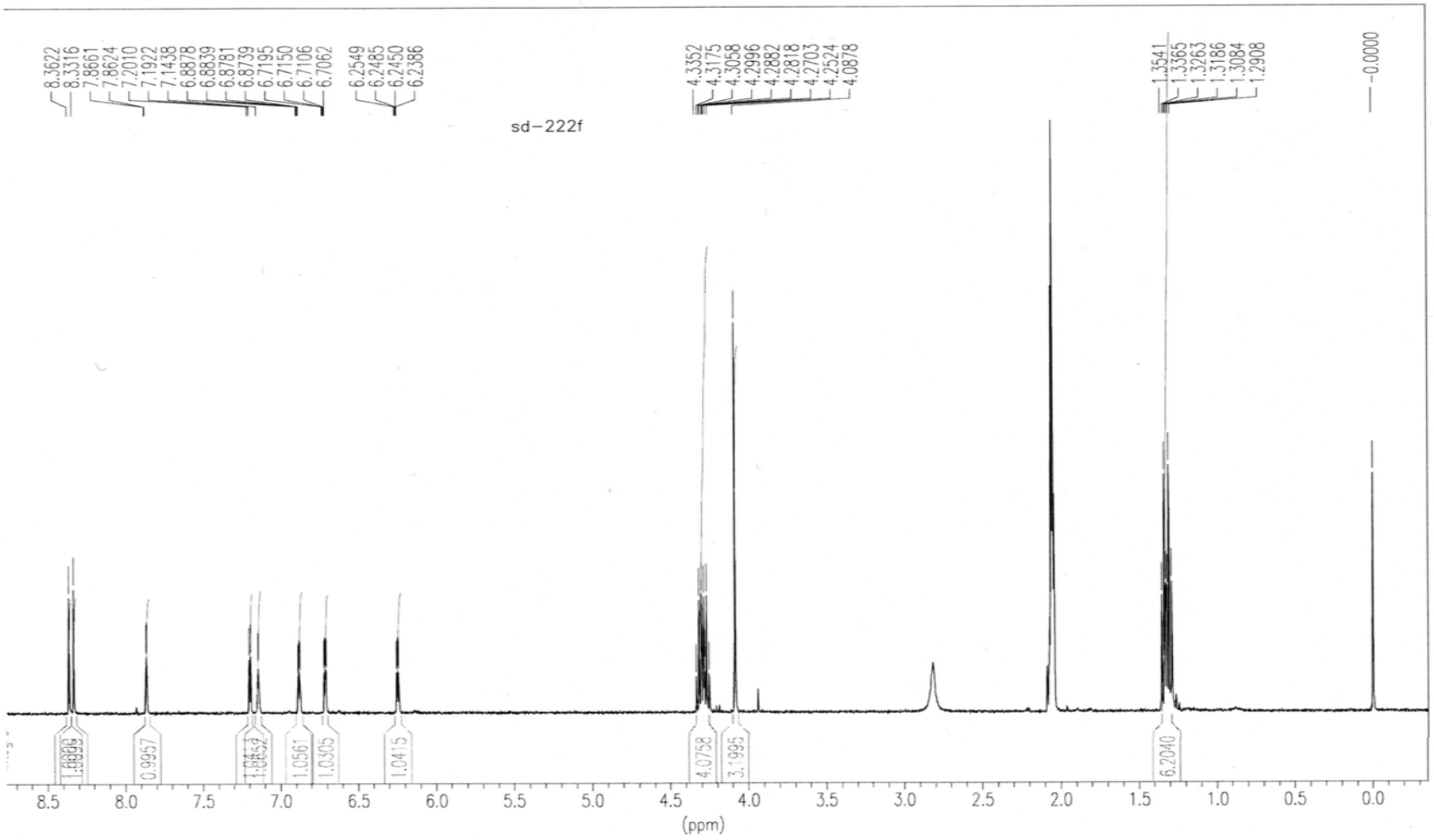

Figure AIV-18. ^{1}H NMR spectra of **IV-8** in deuterated acetone.

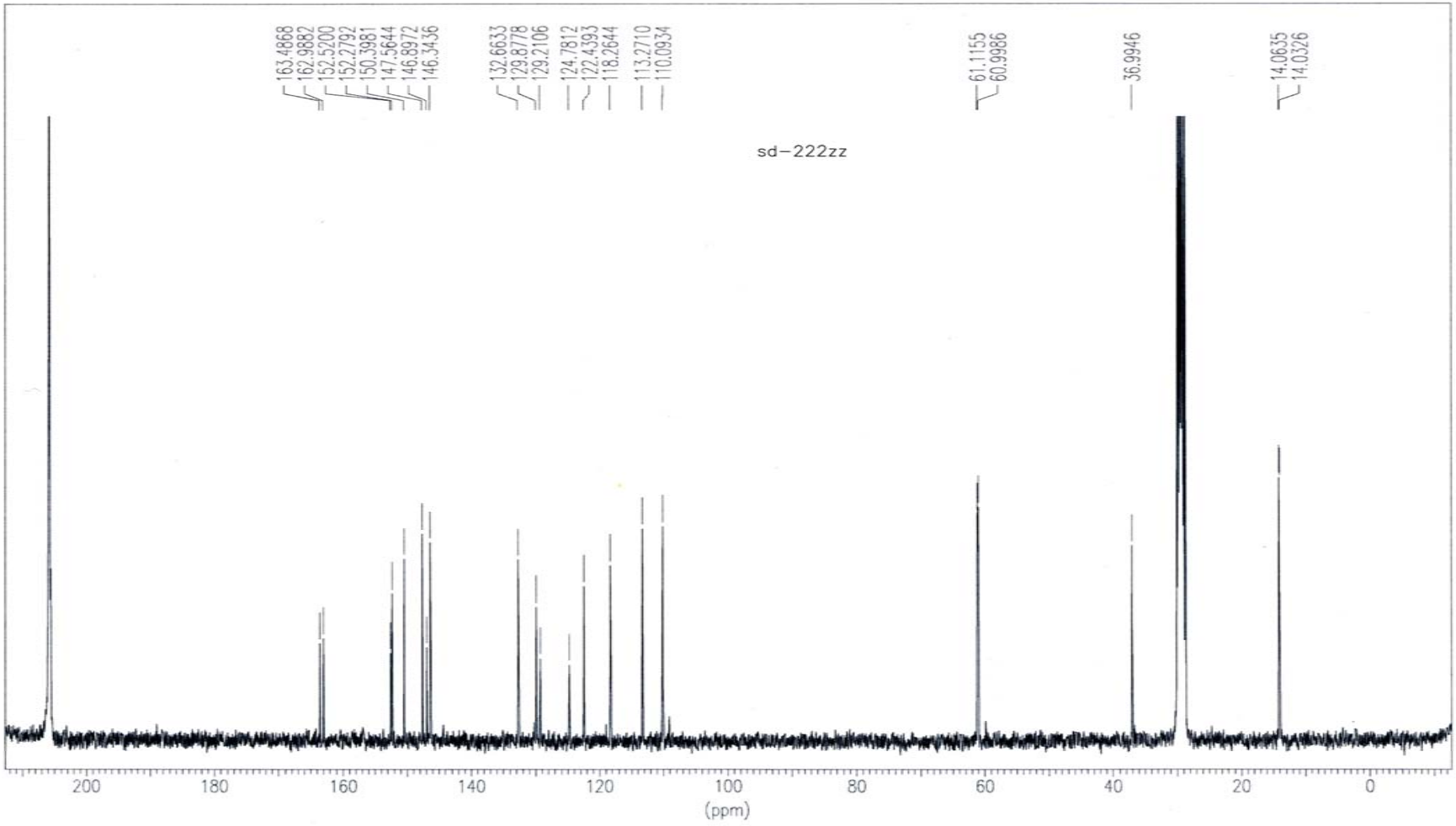

Figure AIV-19. ^{13}C NMR spectra of **IV-8** in deuterated acetone.

AV. ANNEXE V - CHAPITRE V

Table of content

Absorption and Emission spectra

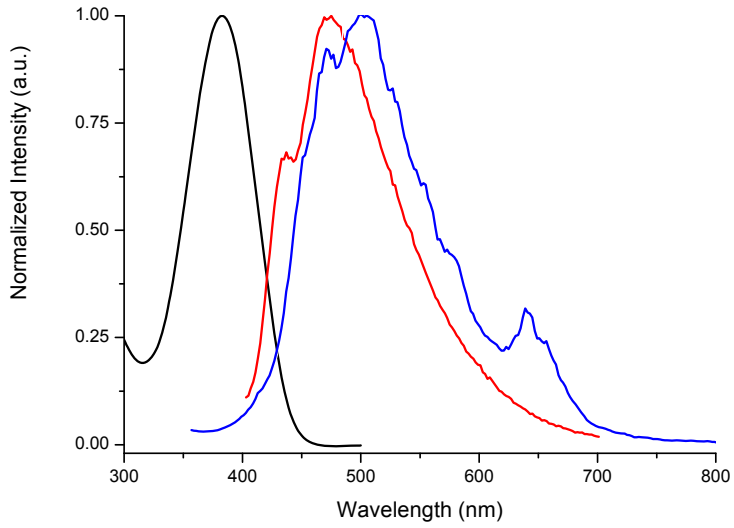

Figure AV-1. Absorption (black, left), fluorescence (red, middle) and phosphorescence spectra (blue, right) of **V-7**.

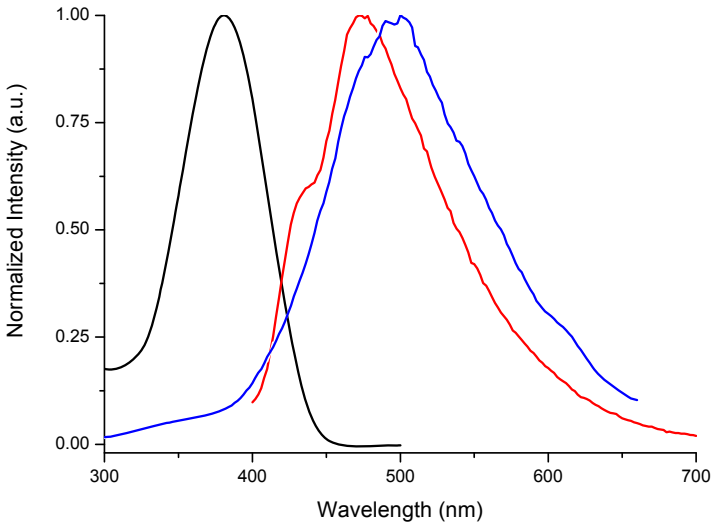

Figure AV-20. Absorption (black, left), fluorescence (red, middle) and phosphorescence spectra (blue, right) of **V-8**.

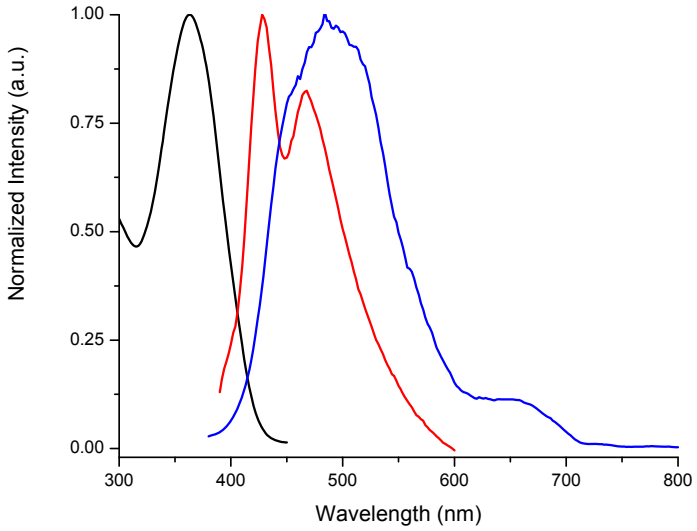

Figure AV-3. Absorption (black, left), fluorescence (red, middle) and phosphorescence spectra (blue, right) of **V-10**.

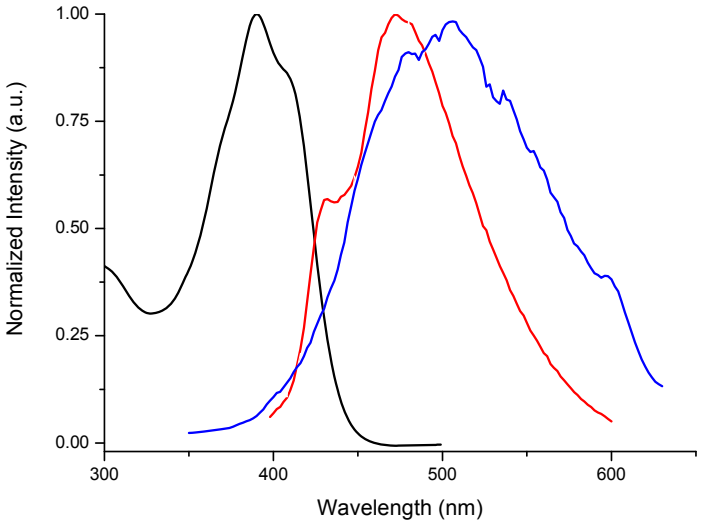

Figure AV-4. Absorption (black, left), fluorescence (red, middle) and phosphorescence spectra (blue, right) of **V-11.**

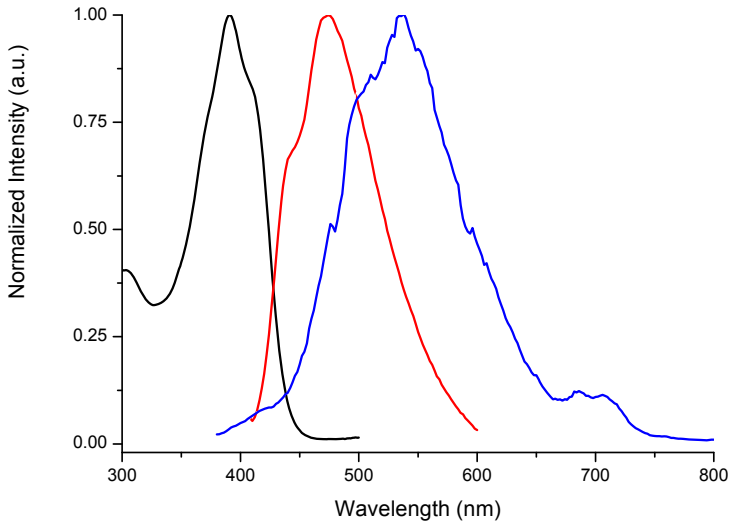

Figure AV-5. Absorption (black, left), fluorescence (red, middle) and phosphorescence spectra (blue, right) of **V-12**.

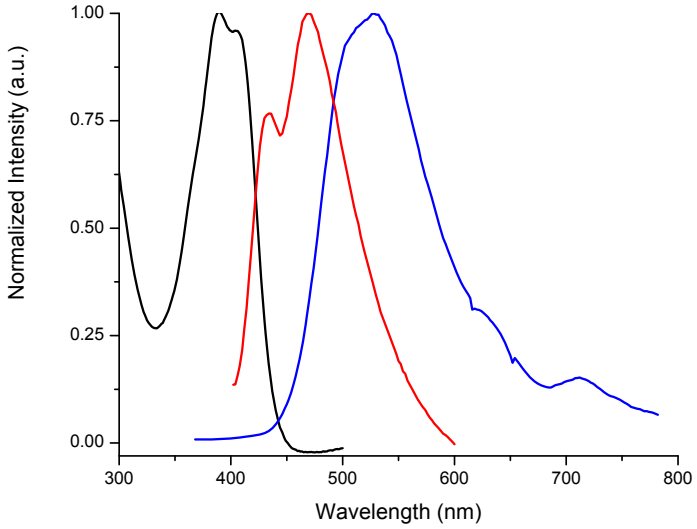

Figure AV-6. Absorption (black, left), fluorescence (red, middle) and phosphorescence spectra (blue, right) of **V-14**.

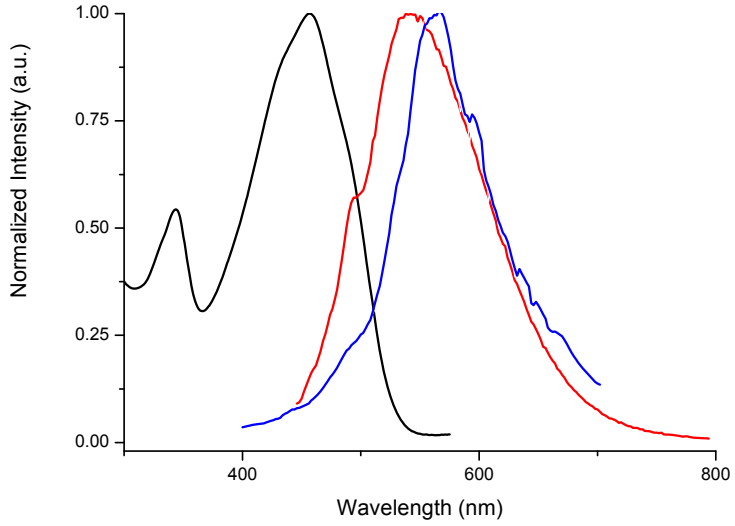

Figure AV-7. Absorption (black, left), fluorescence (red, middle) and phosphorescence spectra (blue, right) of **V-15**.

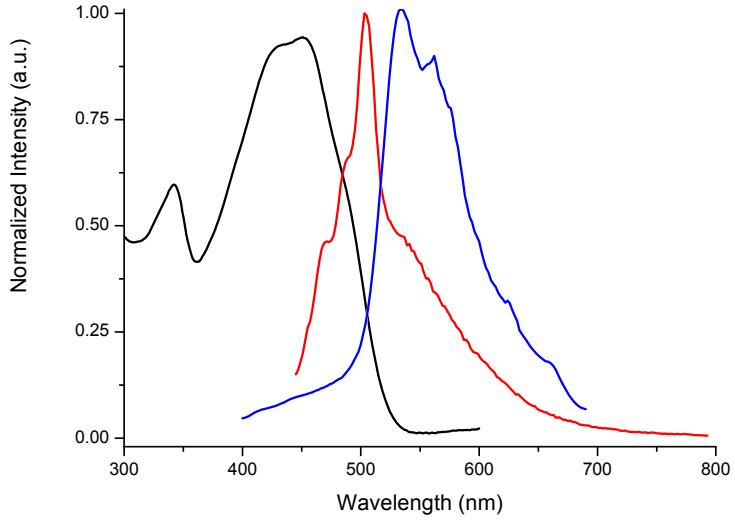

Figure AV-8. Absorption (black, left), fluorescence (red, middle) and phosphorescence spectra (blue, right) of **V-16**.

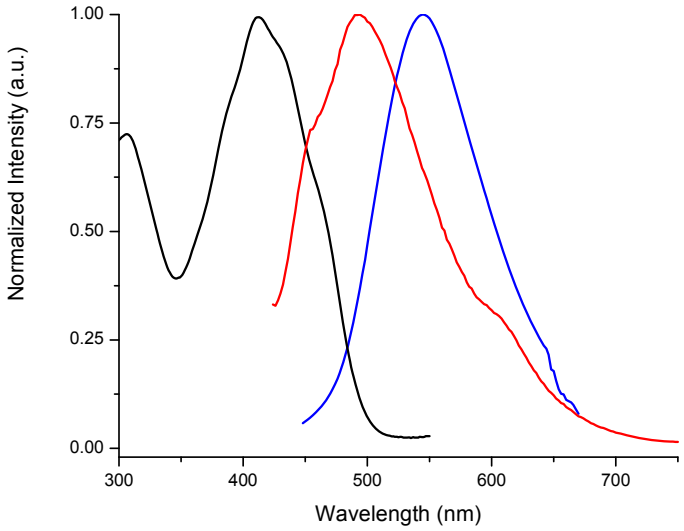

Figure AV-9. Absorption (black, left), fluorescence (red, middle) and phosphorescence spectra (blue, right) of **V-18.**

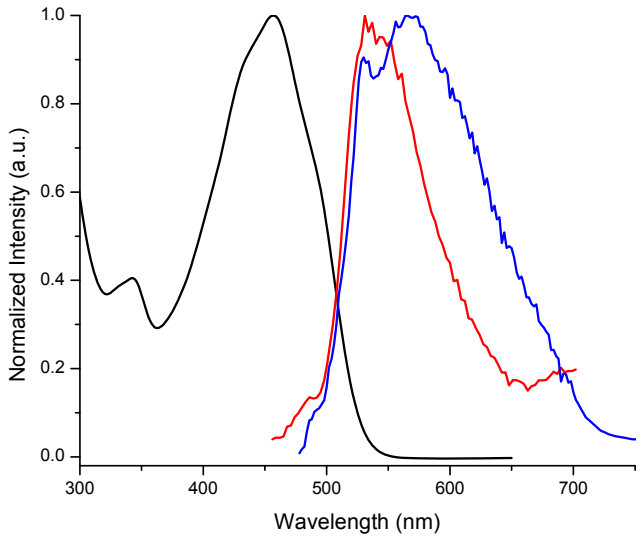

Figure AV-10. Absorption (black, left), fluorescence (red, middle) and phosphorescence spectra (blue, right) of **V-19.**

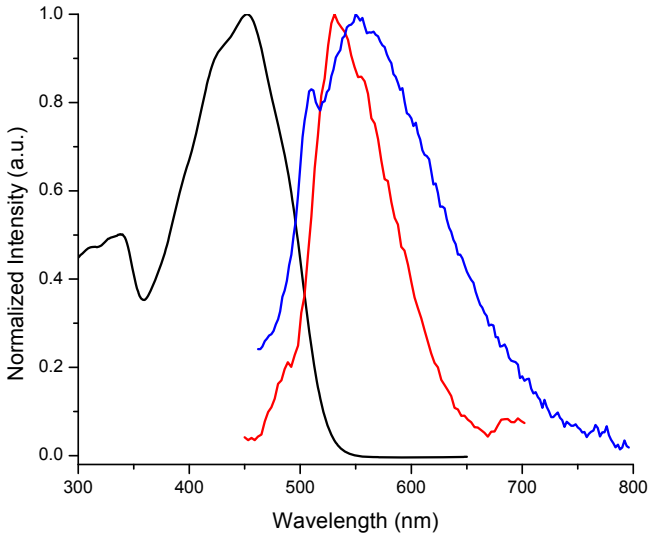

Figure AV-11. Absorption (black, left), fluorescence (red, middle) and phosphorescence spectra (blue, right) of **V-20.**

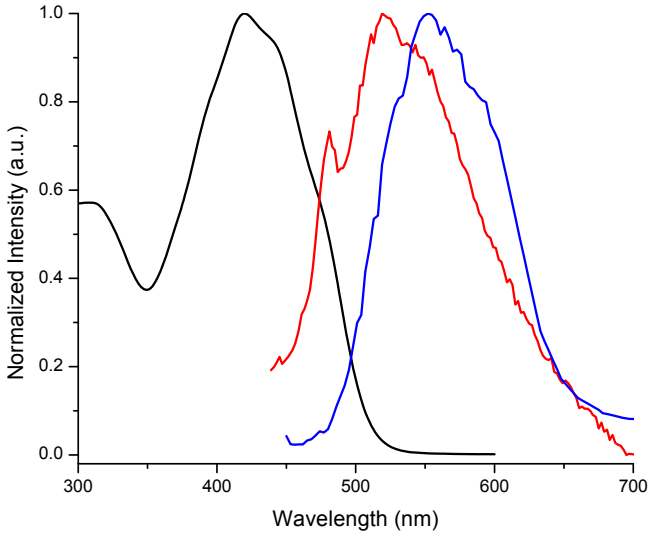

Figure AV-12. Absorption (black, left), fluorescence (red, middle) and phosphorescence spectra (blue, right) of **V-21**.

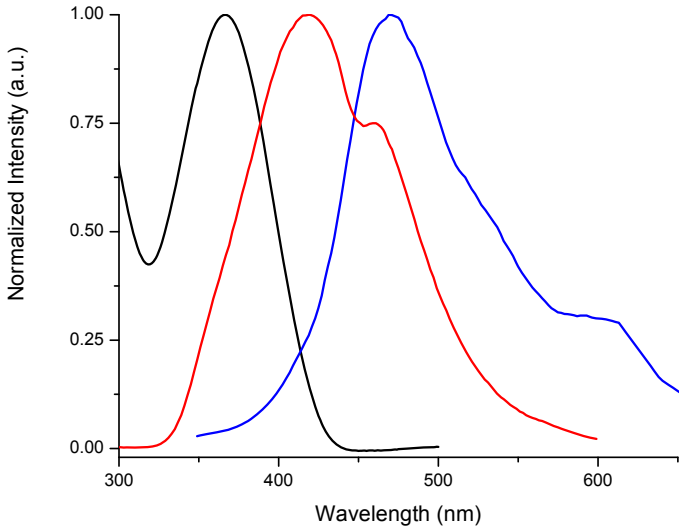

Figure AV-13. Absorption (black, left), fluorescence (red, middle) and phosphorescence spectra (blue, right) of **V-22**.

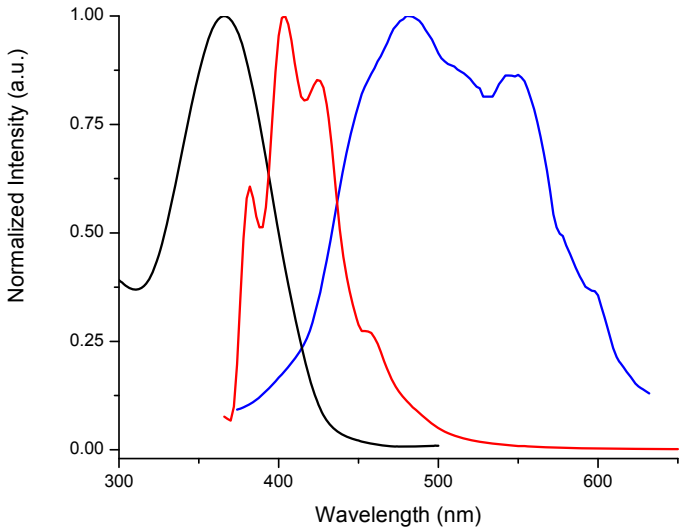

Figure AV-14. Absorption (black, left), fluorescence (red, middle) and phosphorescence spectra (blue, right) of **V-23**.

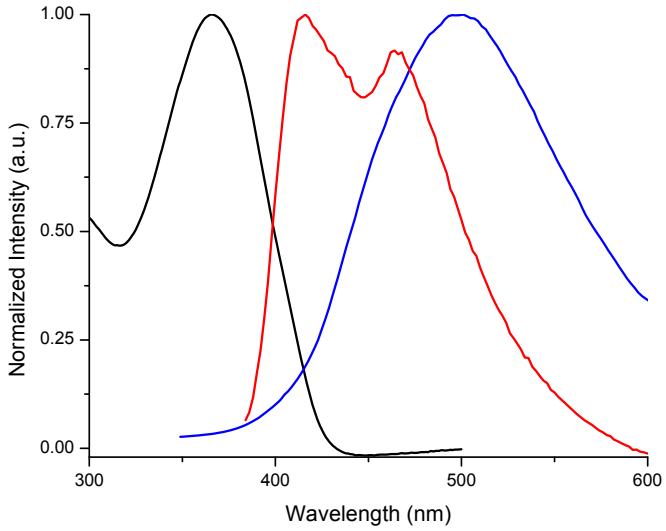

Figure AV-15. Absorption (black, left), fluorescence (red, middle) and phosphorescence spectra (blue, right) of **V-24**.

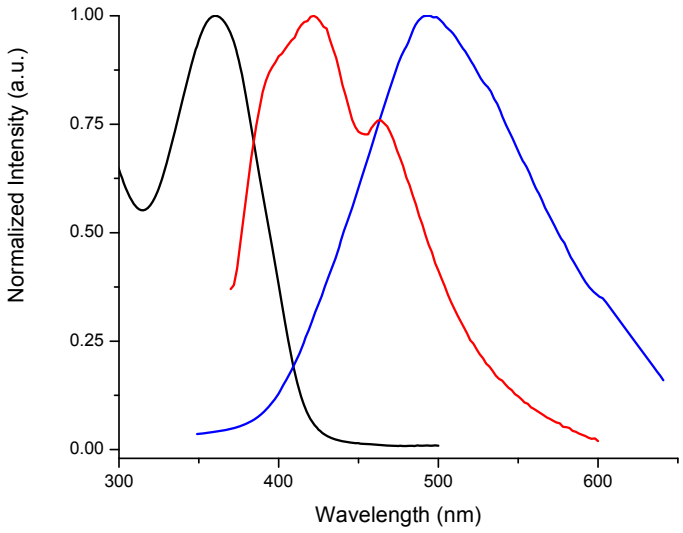

Figure AV-16. Absorption (black, left), fluorescence (red, middle) and phosphorescence spectra (blue, right) of **V-25.**

Cyclic voltammetry

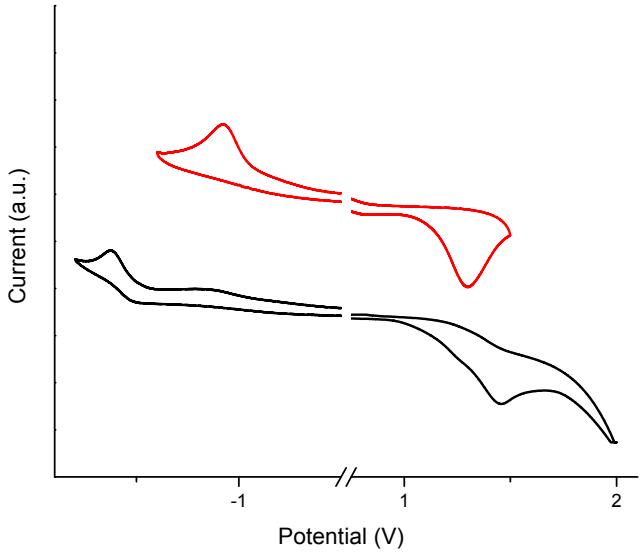

Figure AV-17. Cyclic voltammetry of mol **V-7** (bottom) and its anodically coupled product **V-P7** (top) on a platinum button electrode.

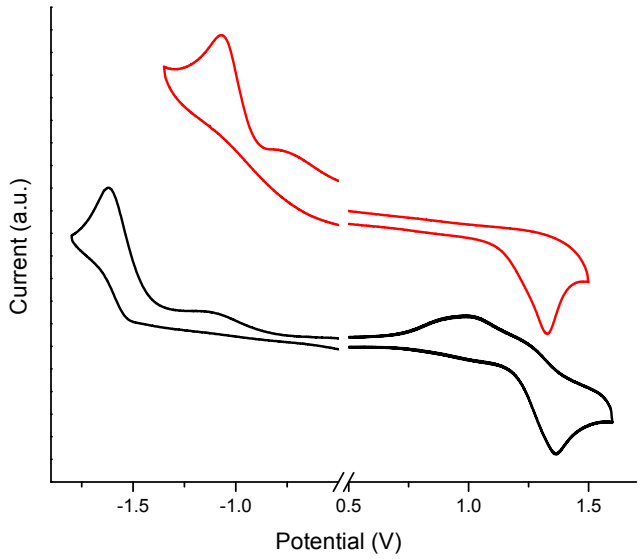

Figure AV-18. Cyclic voltammetry of mol **V-8** (bottom) and its anodically coupled product **V-P8** (top) on a platinum button electrode.

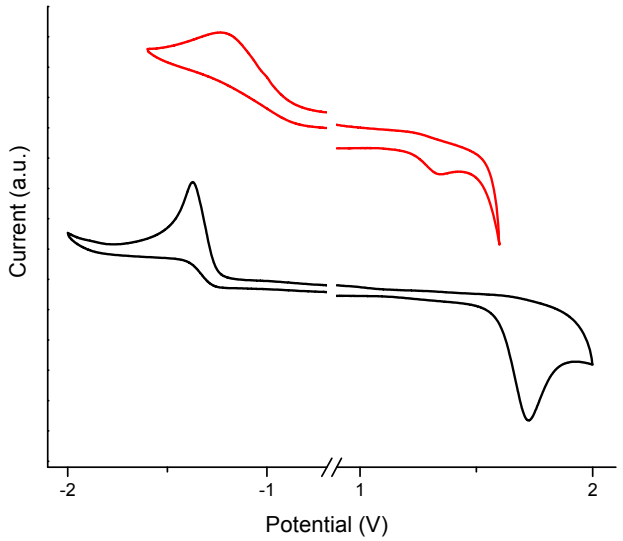

Figure AV-19. Cyclic voltammetry of mol **V-9** (bottom) and its anodically coupled product **V-P9** (top) on a platinum button electrode.

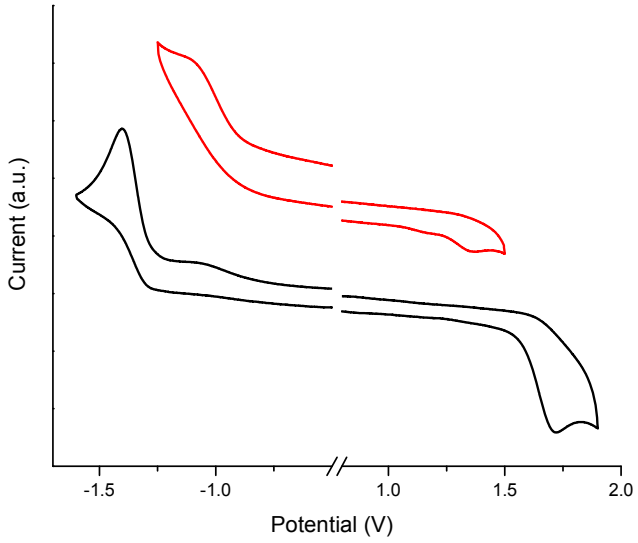

Figure AV-20. Cyclic voltammetry of mol **V-10** (bottom) and its anodically coupled product **V-P10** (top) on a platinum button electrode.

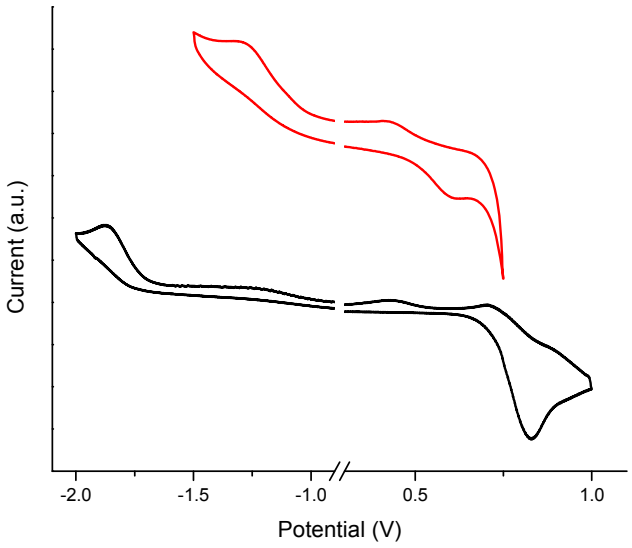

Figure AV-21. Cyclic voltammetry of mol **V-11** (bottom) and its anodically coupled product **V-P11** (top) on a platinum button electrode.

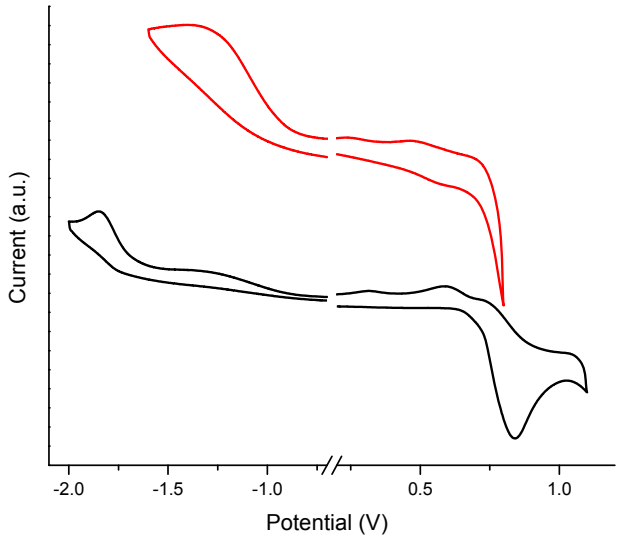

Figure AV-22. Cyclic voltammetry of mol **V-12** (bottom) and its anodically coupled product **V-P12** (top) on a platinum button electrode.

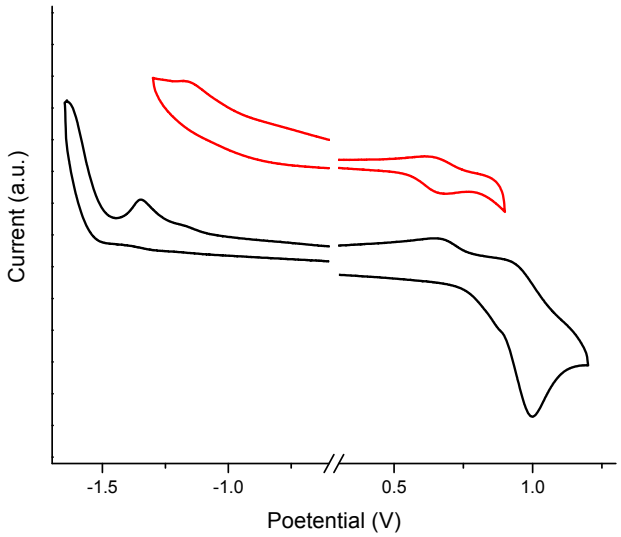

Figure AV-23. Cyclic voltammetry of mol **V-13** (bottom) and its anodically coupled product **V-P13** (top) on a platinum button electrode.

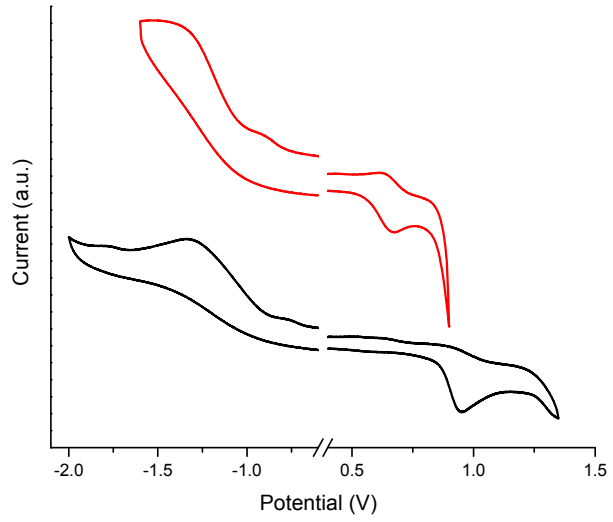

Figure AV-24. Cyclic voltammetry of mol **V-14** (bottom) and its anodically coupled product **V-P14** (top) on a platinum button electrode.

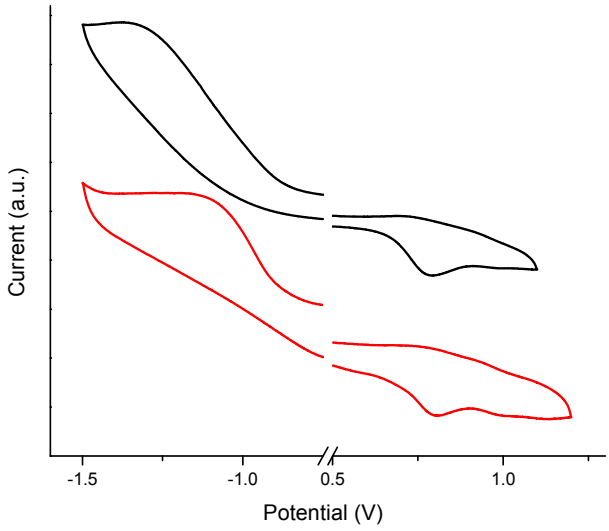

Figure AV-25. Cyclic voltammetry of mol **V-15** (bottom) and its anodically coupled product **V-P15** (top) on a platinum button electrode.

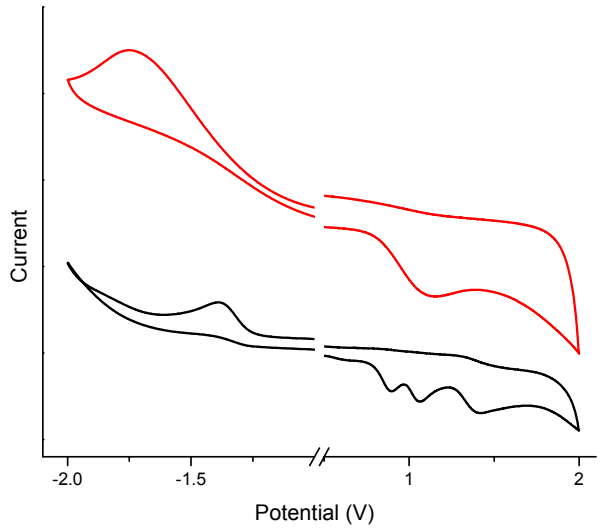

Figure AV-26. Cyclic voltammetry of mol **V-16** (bottom) and its anodically coupled product **V-P16** (top) on a platinum button electrode.

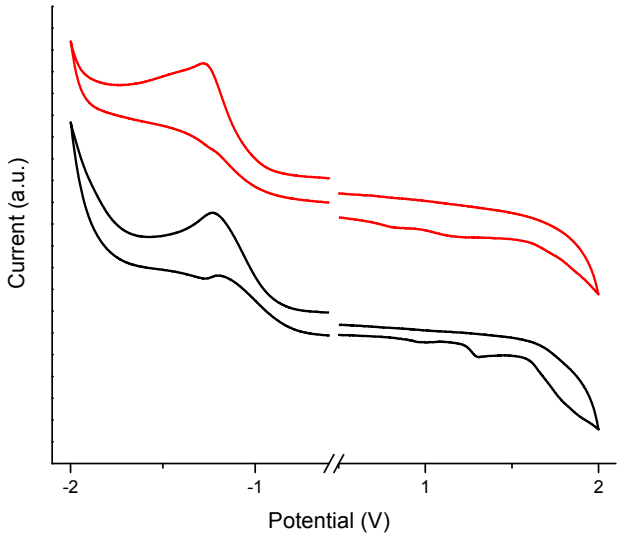

Figure AV-27. Cyclic voltammetry of mol **V-18 (**bottom) and its anodically coupled product **V-P18** (top) on a platinum button electrode.

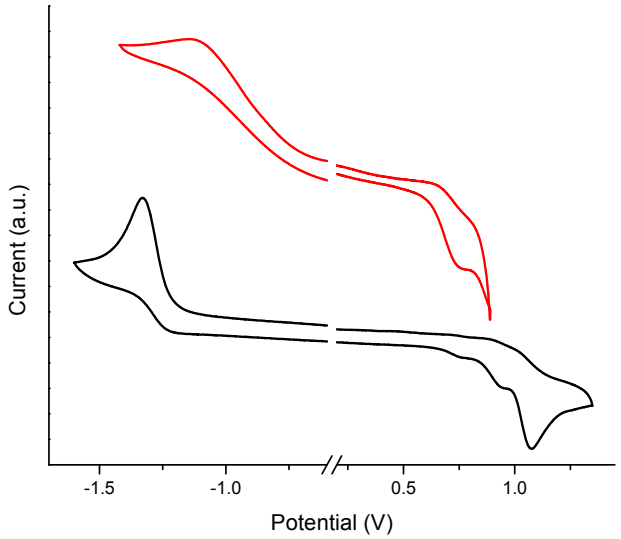

Figure AV-28. Cyclic voltammetry of mol **V-19** (bottom) and its anodically coupled product **V-P19** (top) on a platinum button electrode.

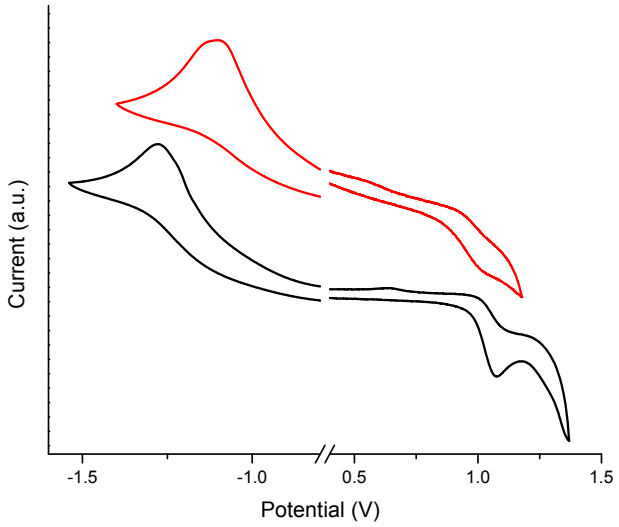

Figure AV-29. Cyclic voltammetry of mol **V-20** (bottom) and its anodically coupled product **V-P20** (top) on a platinum button electrode.

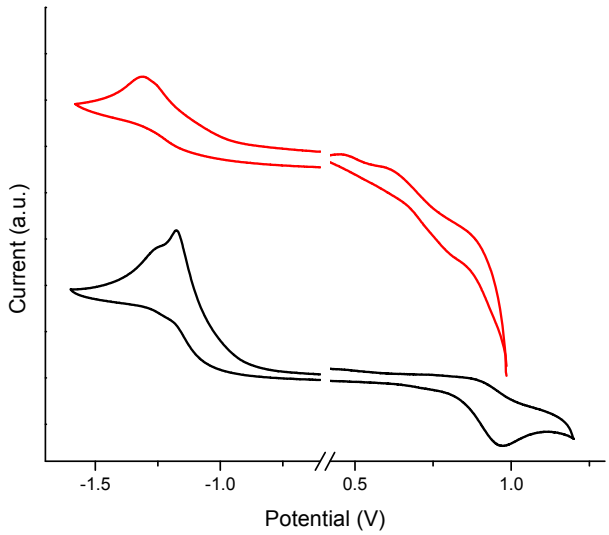

Figure AV-30. Cyclic voltammetry of mol **V-21** (bottom) and its anodically coupled product **V-P21** (top) on a platinum button electrode.

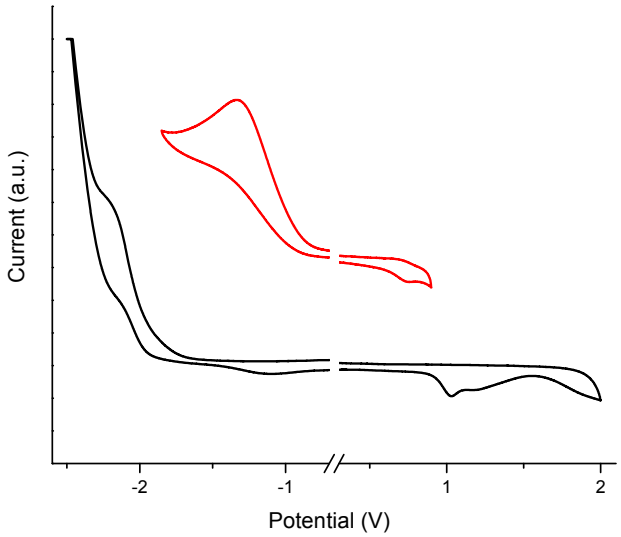

Figure AV-31. Cyclic voltammetry of mol **AV-22** (bottom) and its anodically coupled product **AV-P22** (top) on a platinum button electrode.

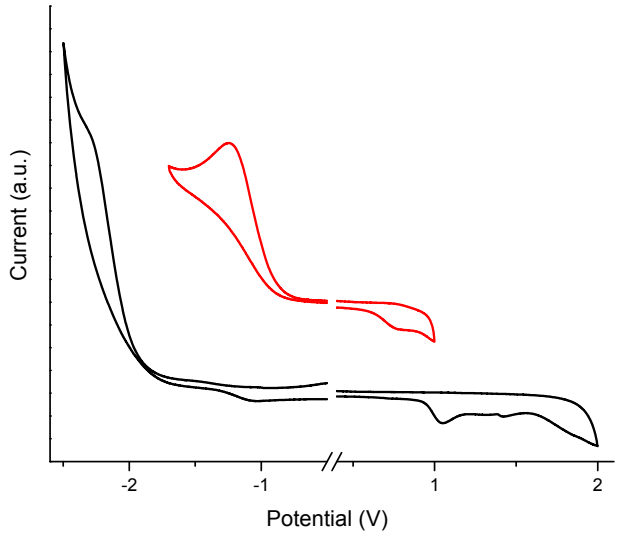

Figure AV-32. Cyclic voltammetry of mol **V-23** (bottom) and its anodically coupled product **V-P23** (top) on a platinum button electrode.

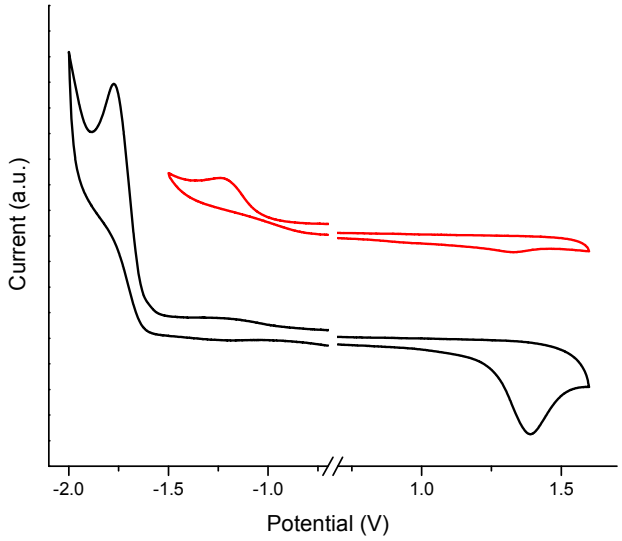

Figure AV-33. Cyclic voltammetry of mol **V-24** (bottom) and its anodically coupled product **V-P24** (top) on a platinum button electrode.

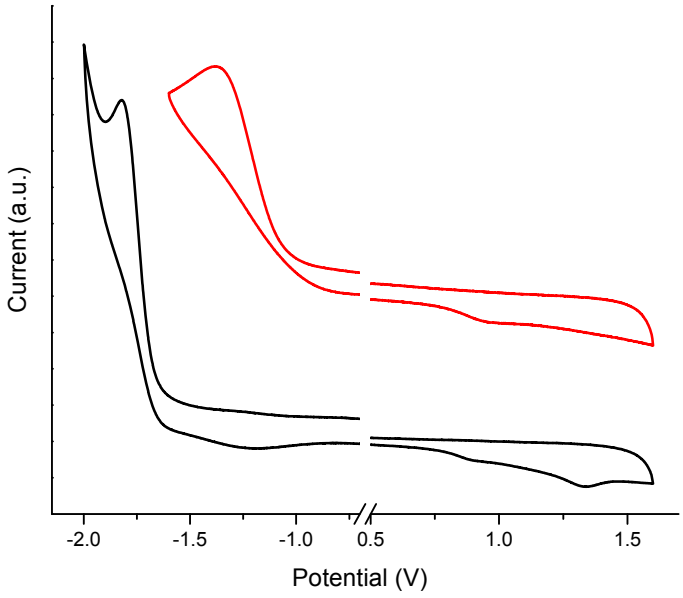

Figure AV-34. Cyclic voltammetry of mol **V-25** (bottom) and its anodically coupled product **V-P25** (top) on a platinum button electrode**.**

NMR spectra

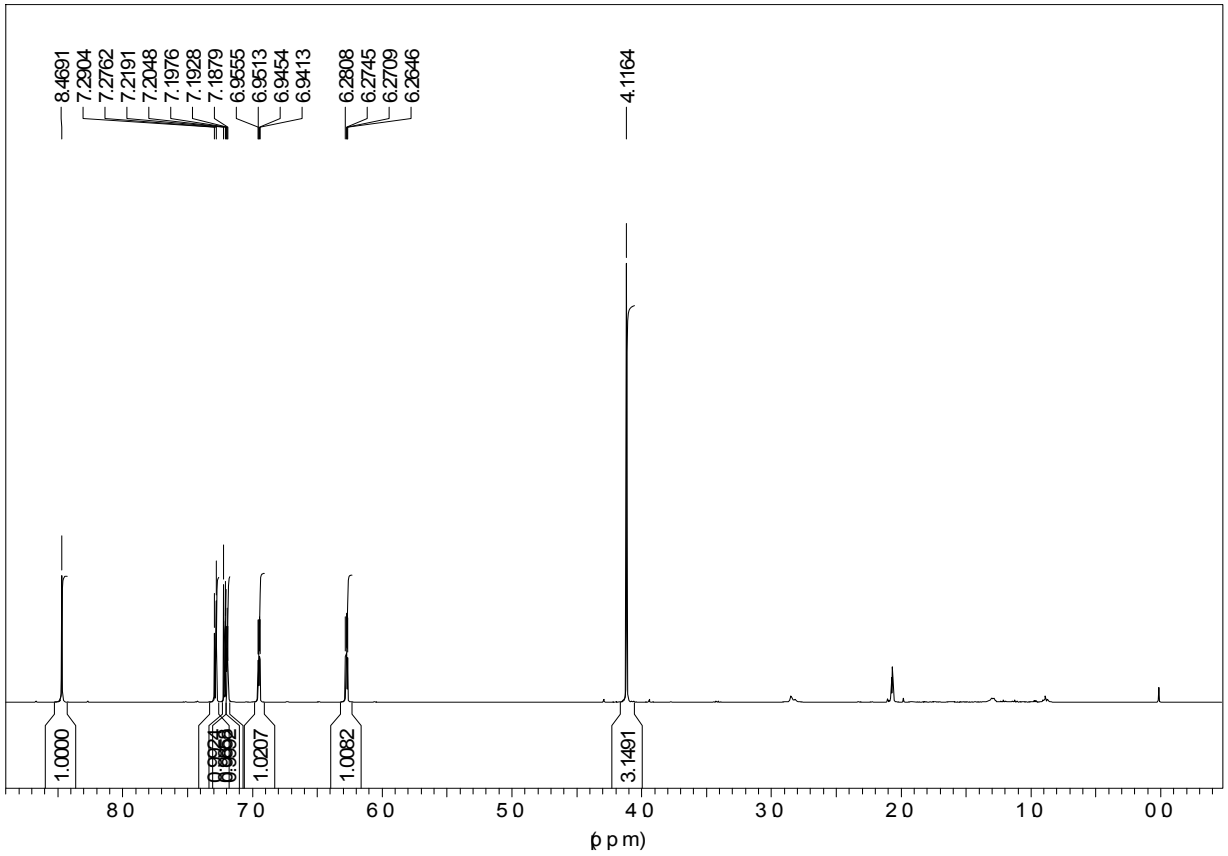

Figure AV-35. ^{1}H NMR spectrum of **V-7** in deuterated acetone.

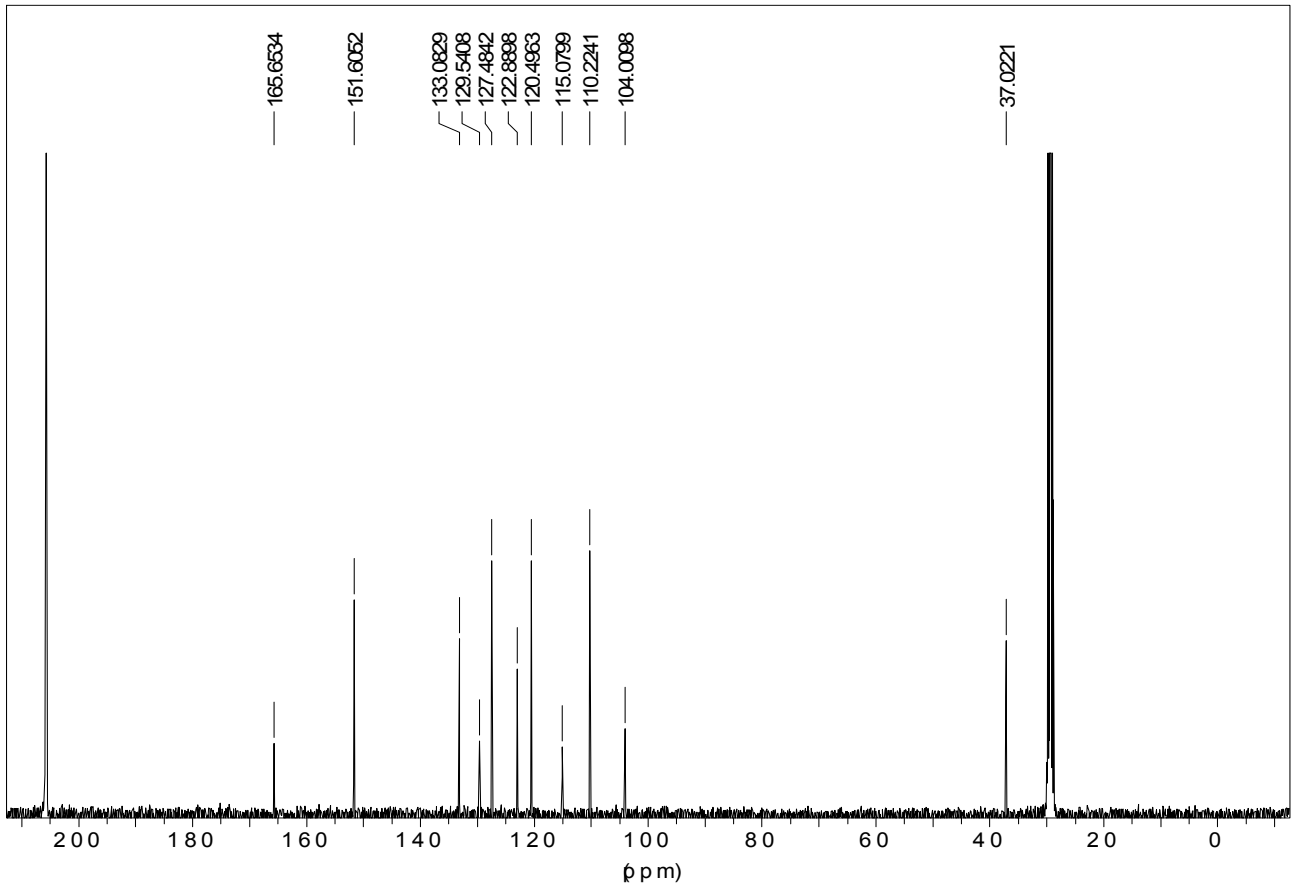

Figure AV-36. ^{13}C NMR spectrum of **V-7** in deuterated acetone.

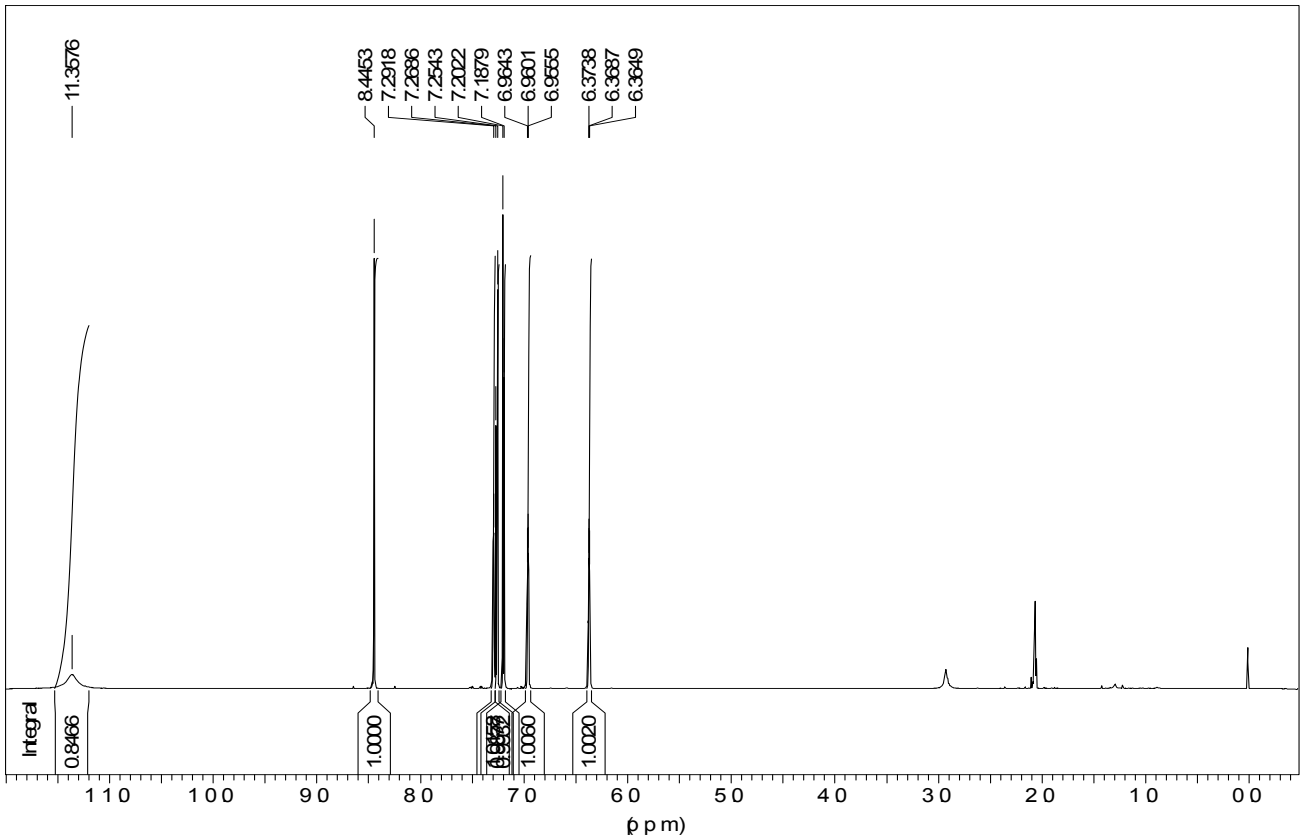

Figure AV-37. ^{1}H NMR spectrum of **V-8** in deuterated acetone.

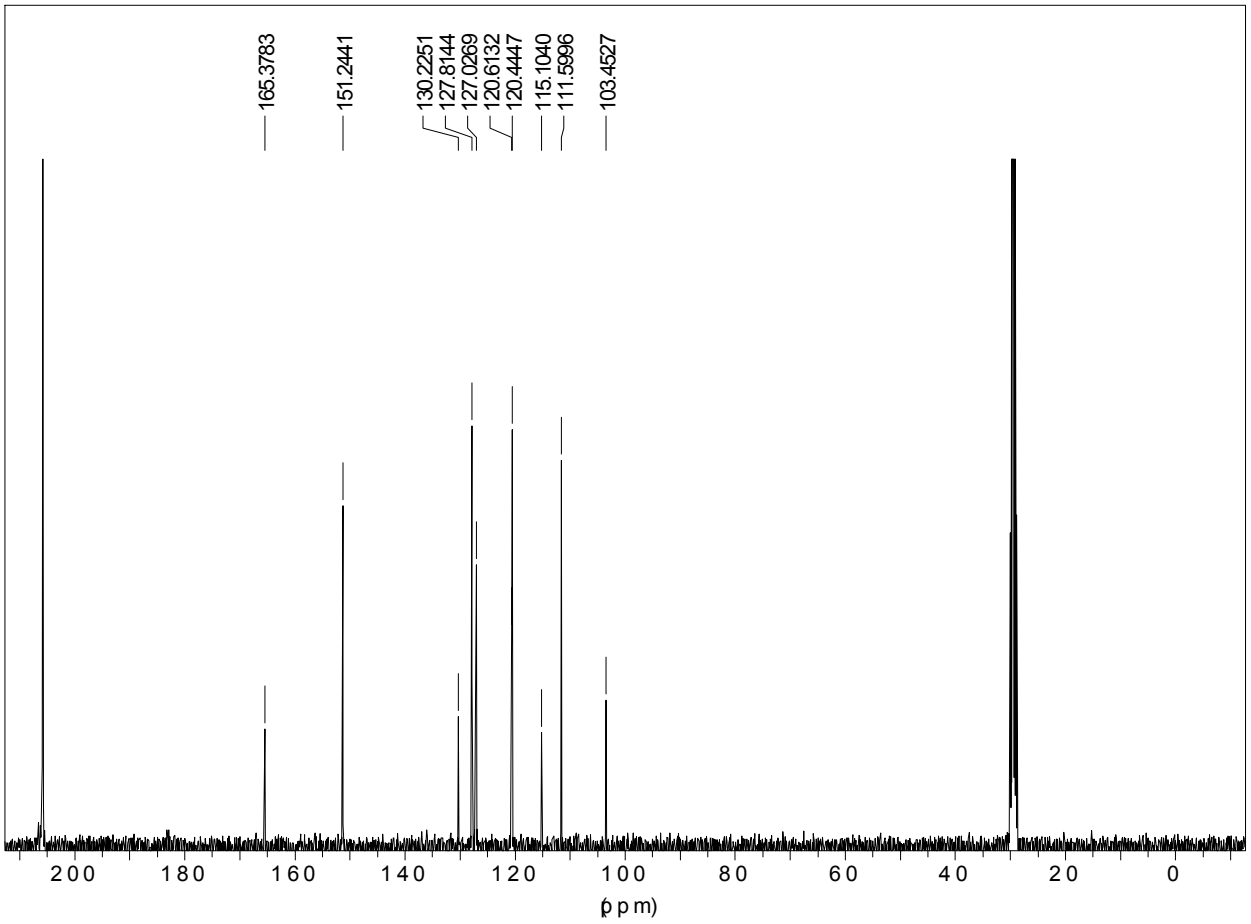

Figure AV-38. ^{13}C NMR spectrum of **V-8** in deuterated acetone.

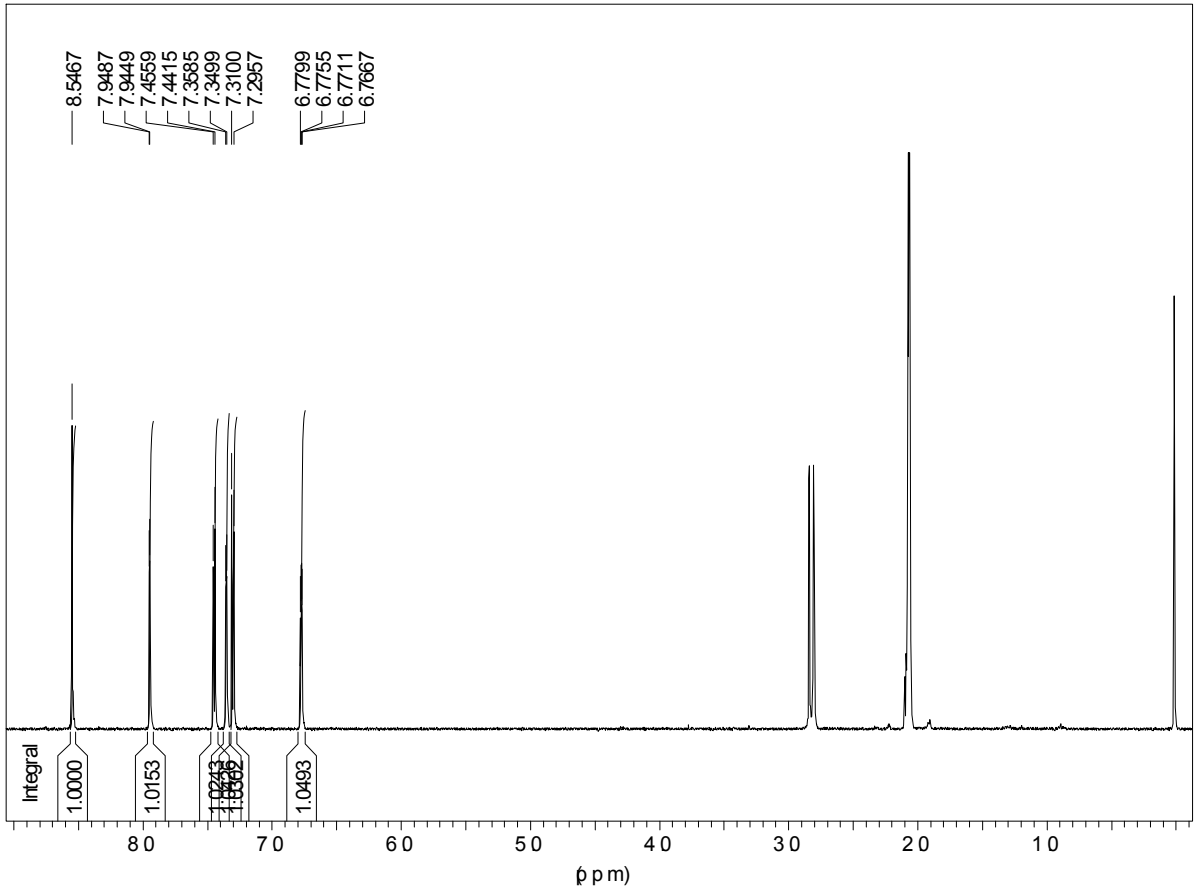

Figure AV-39. ^{1}H NMR spectrum of **V-10** in deuterated acetone.

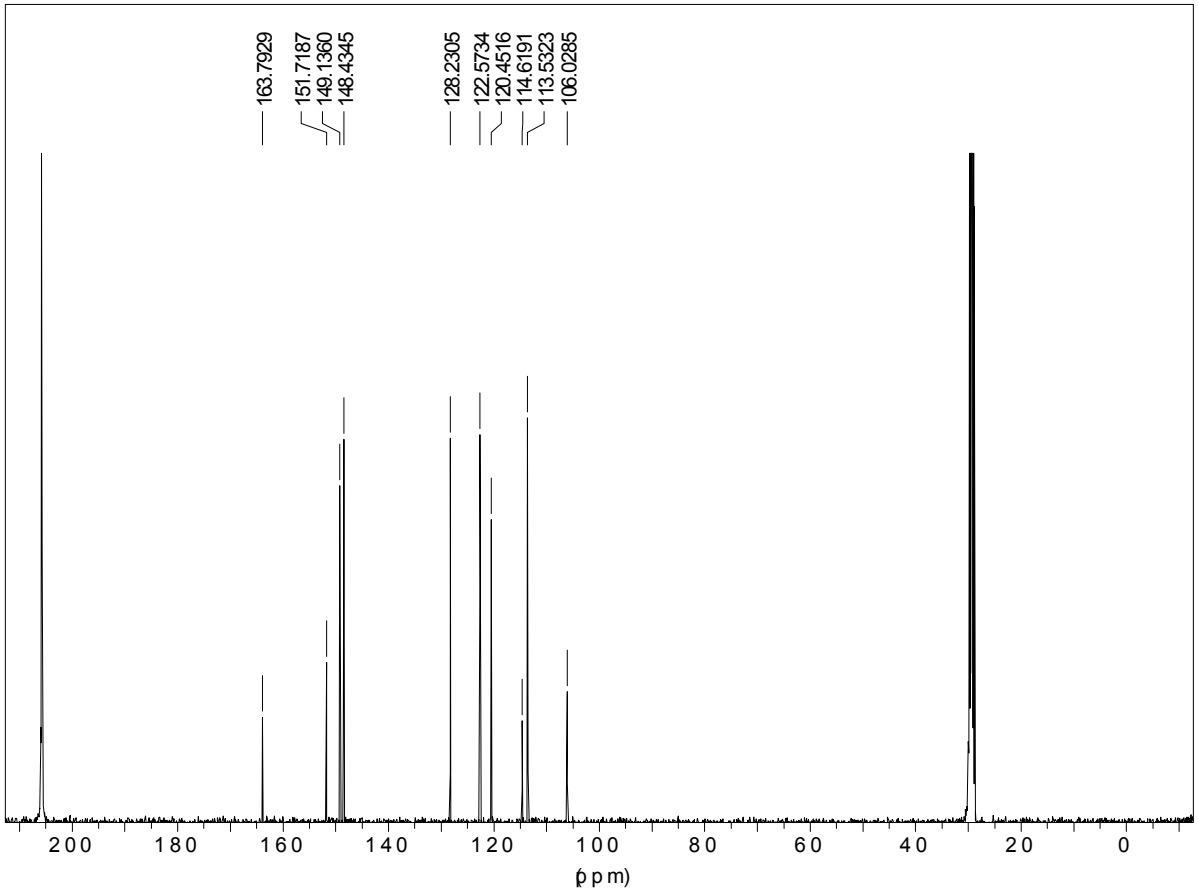

Figure AV-40. ^{13}C NMR spectrum of **V-10** in deuterated acetone.

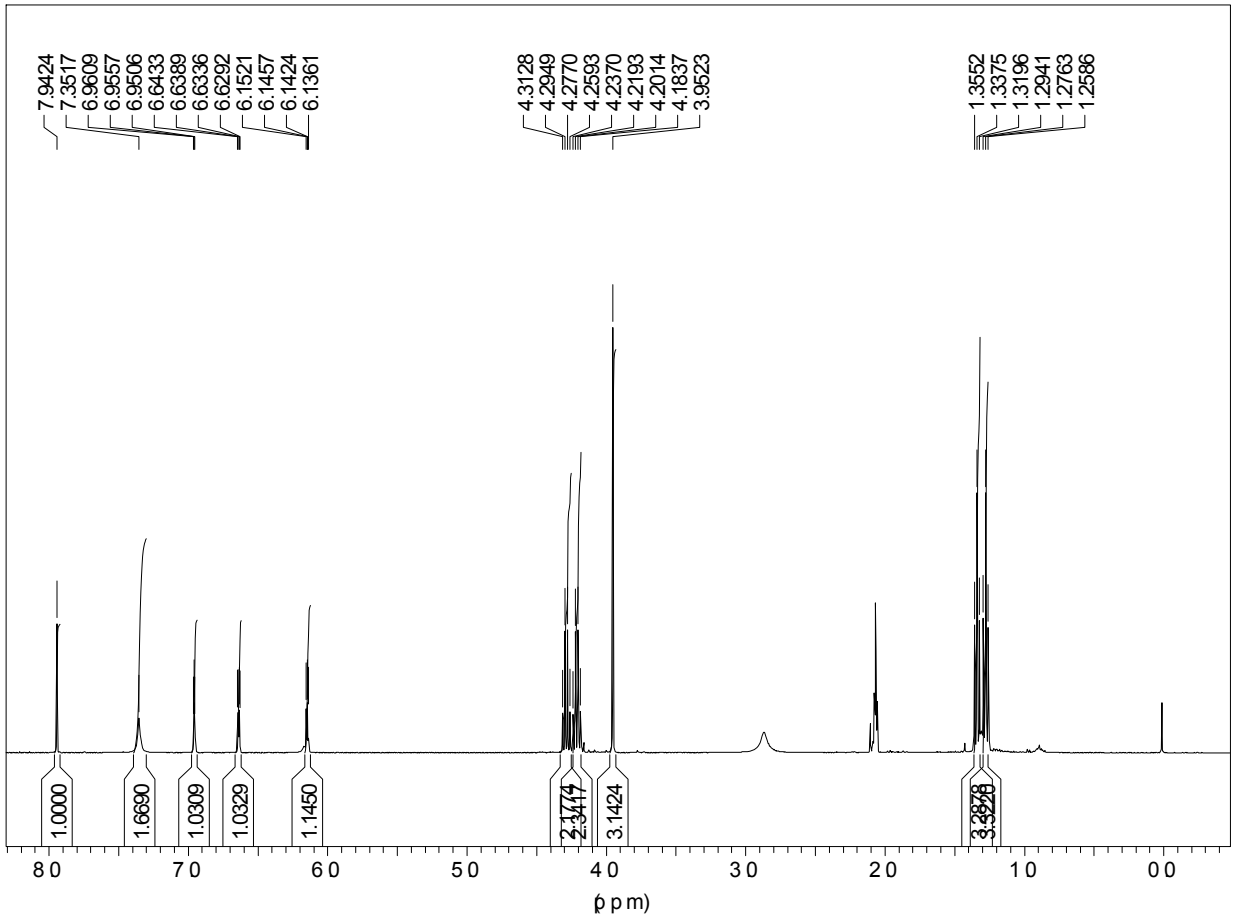

Figure AV-41. ^{1}H NMR spectrum of **V-11** in deuterated acetone.

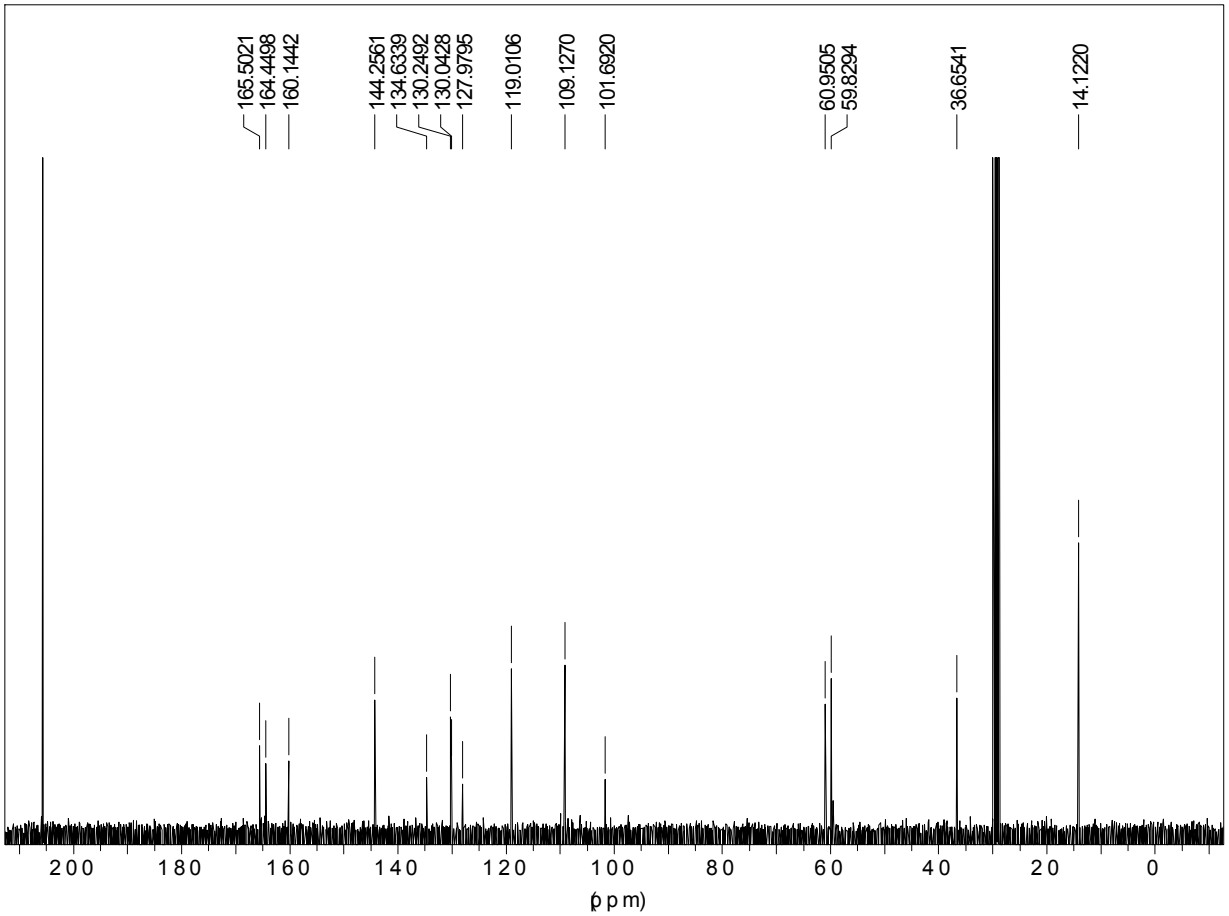

Figure AV-42. ^{13}C NMR spectrum of **V-11** in deuterated acetone.

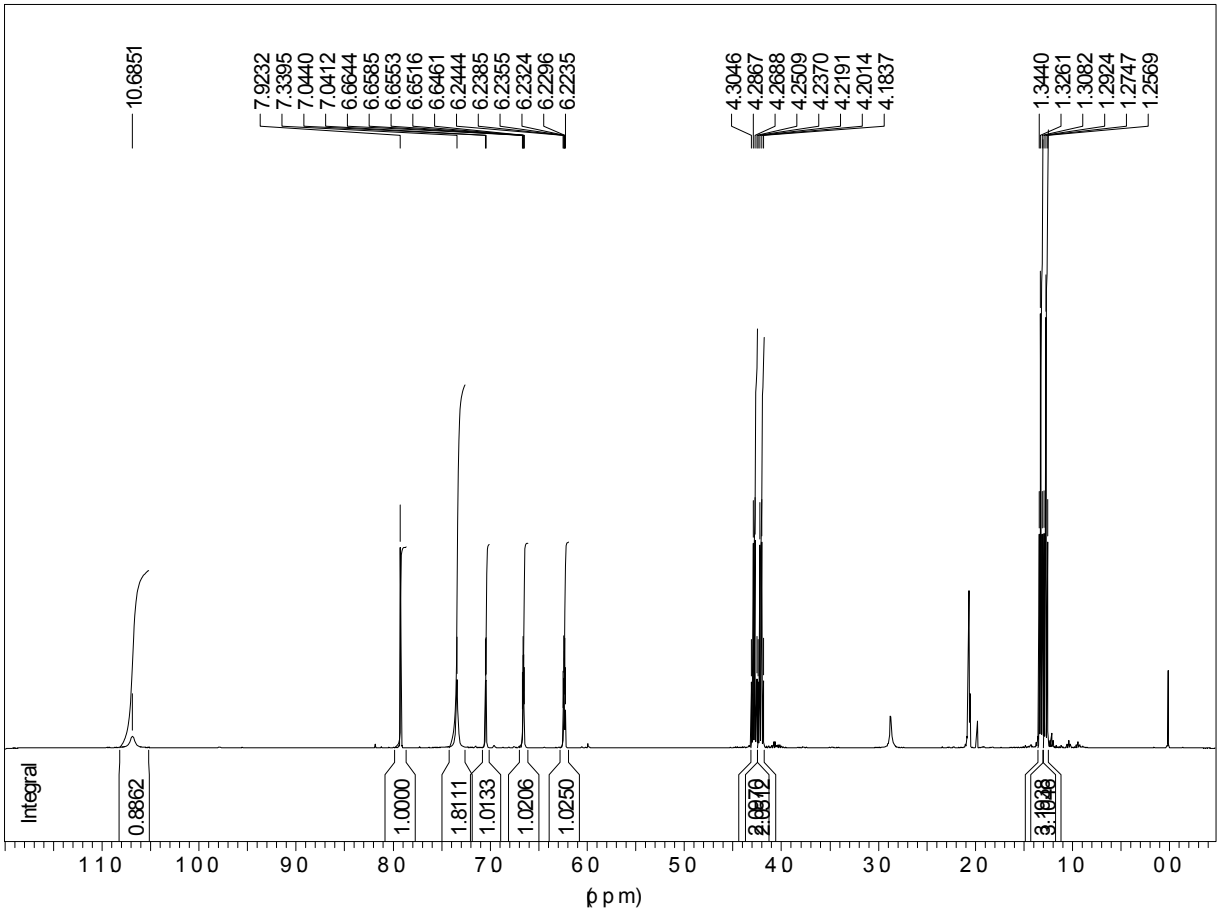

Figure AV-43. ^{1}H NMR spectrum of **V-12** in deuterated acetone.

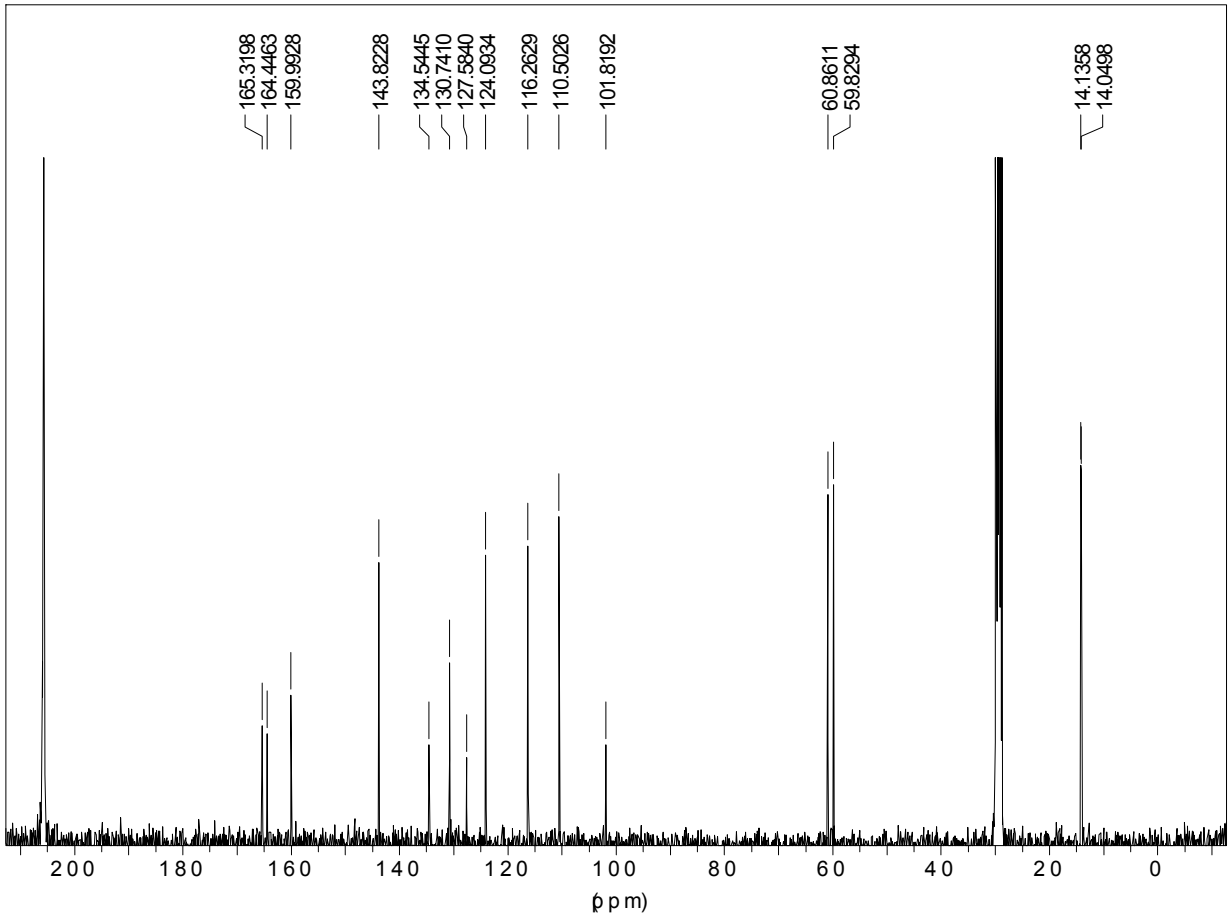

Figure AV-44. ^{13}C NMR spectrum of **V-12** in deuterated acetone.

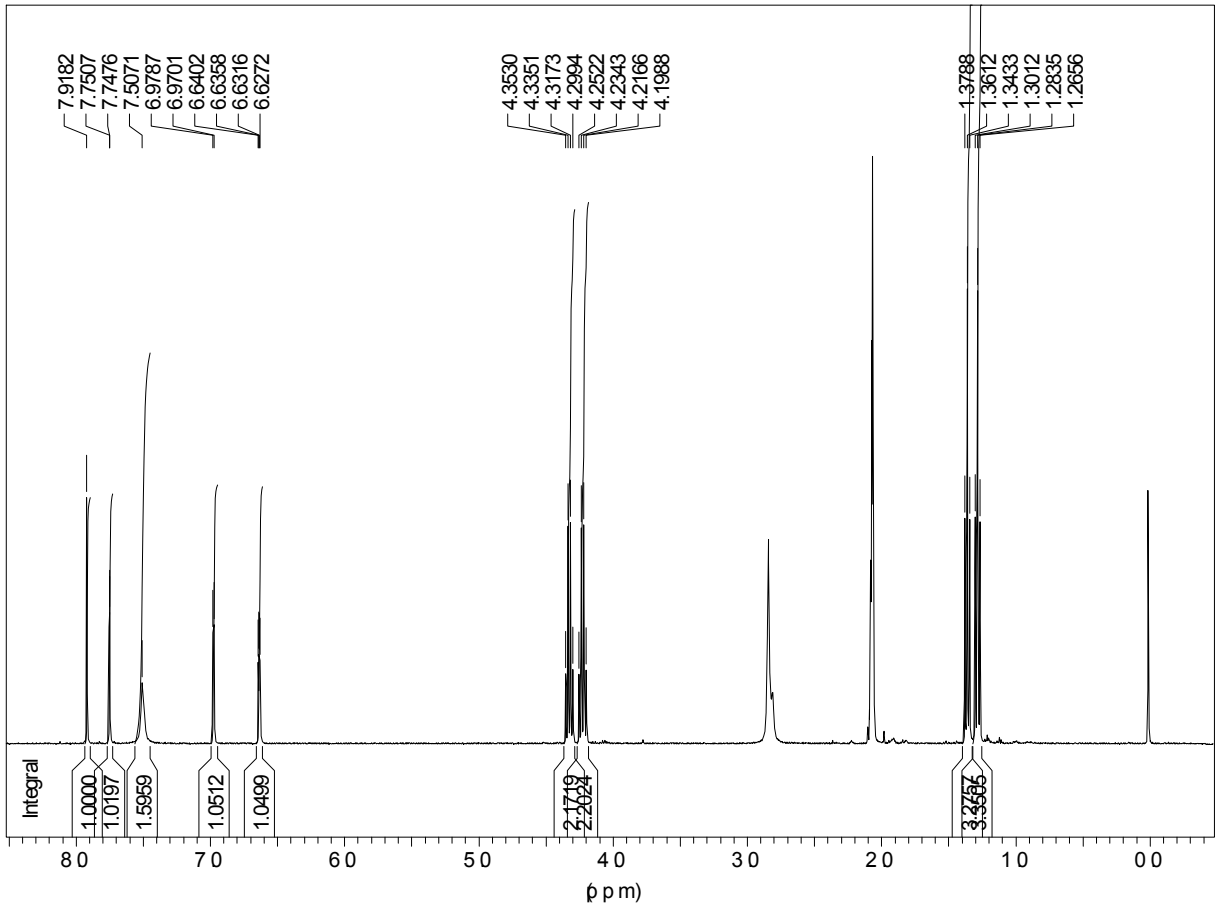

Figure AV-45. ^{1}H NMR spectrum of **V-14** in deuterated acetone.

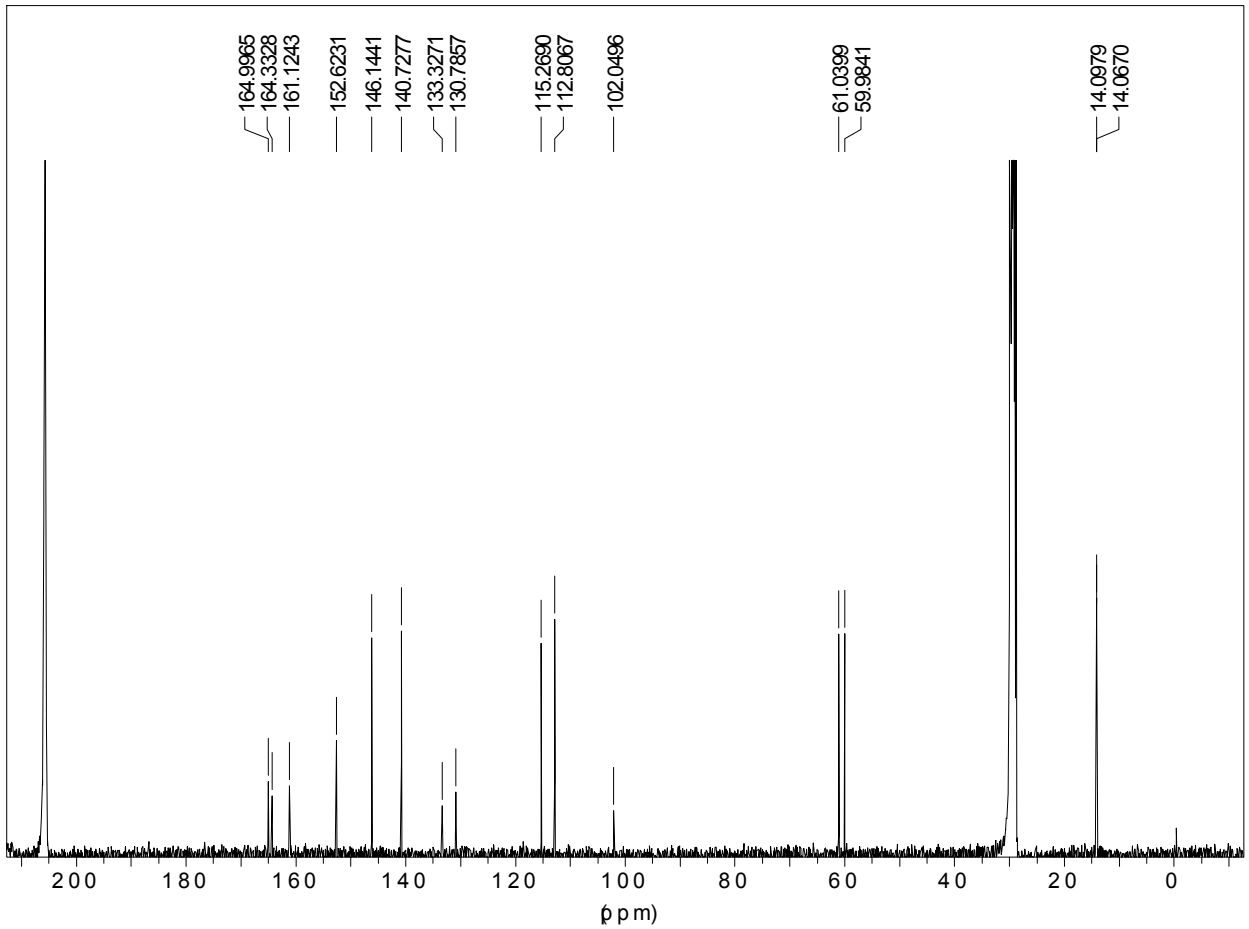

Figure AV-46. ^{13}C NMR spectrum of **V-14** in deuterated acetone.

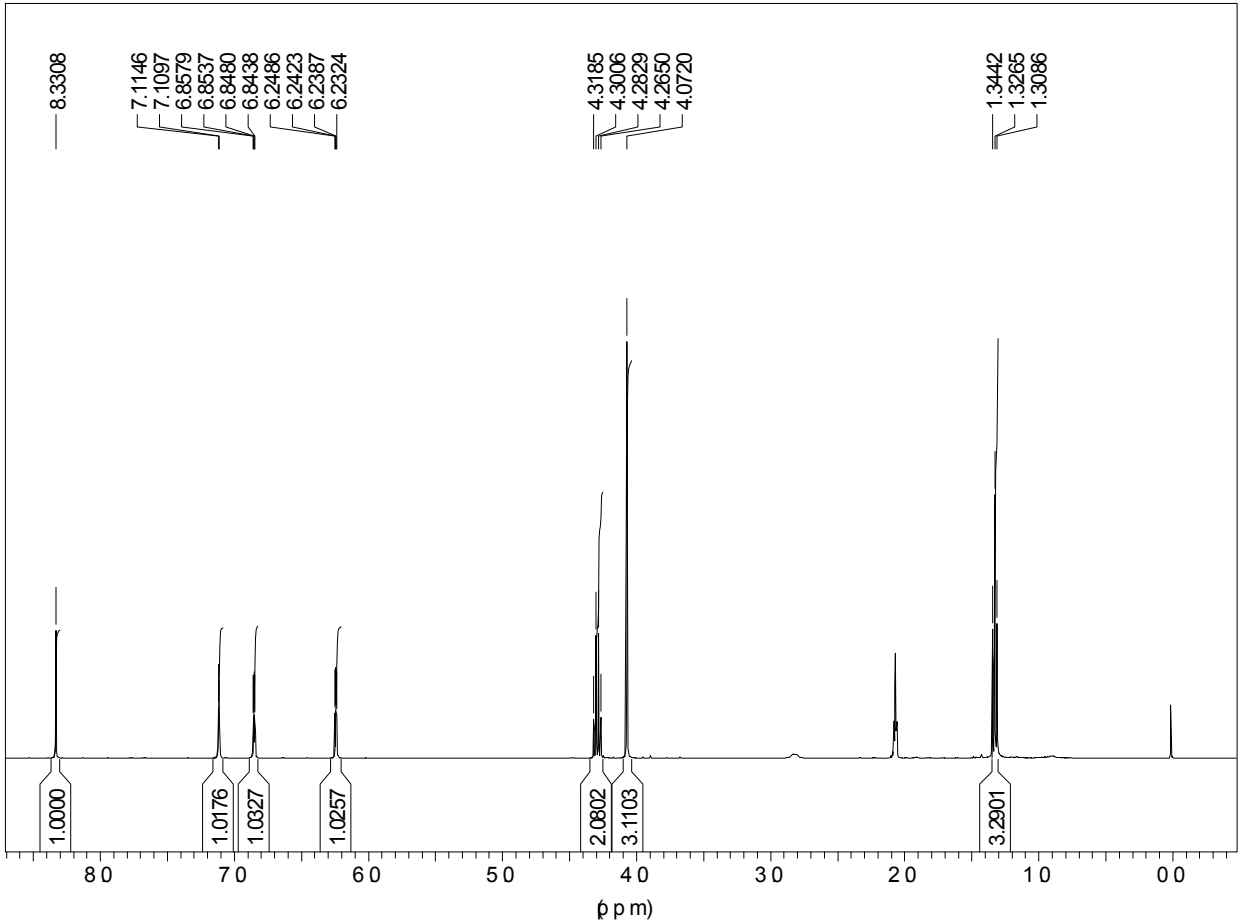

Figure AV-47. ^{1}H NMR spectrum of **V-15** in deuterated acetone.

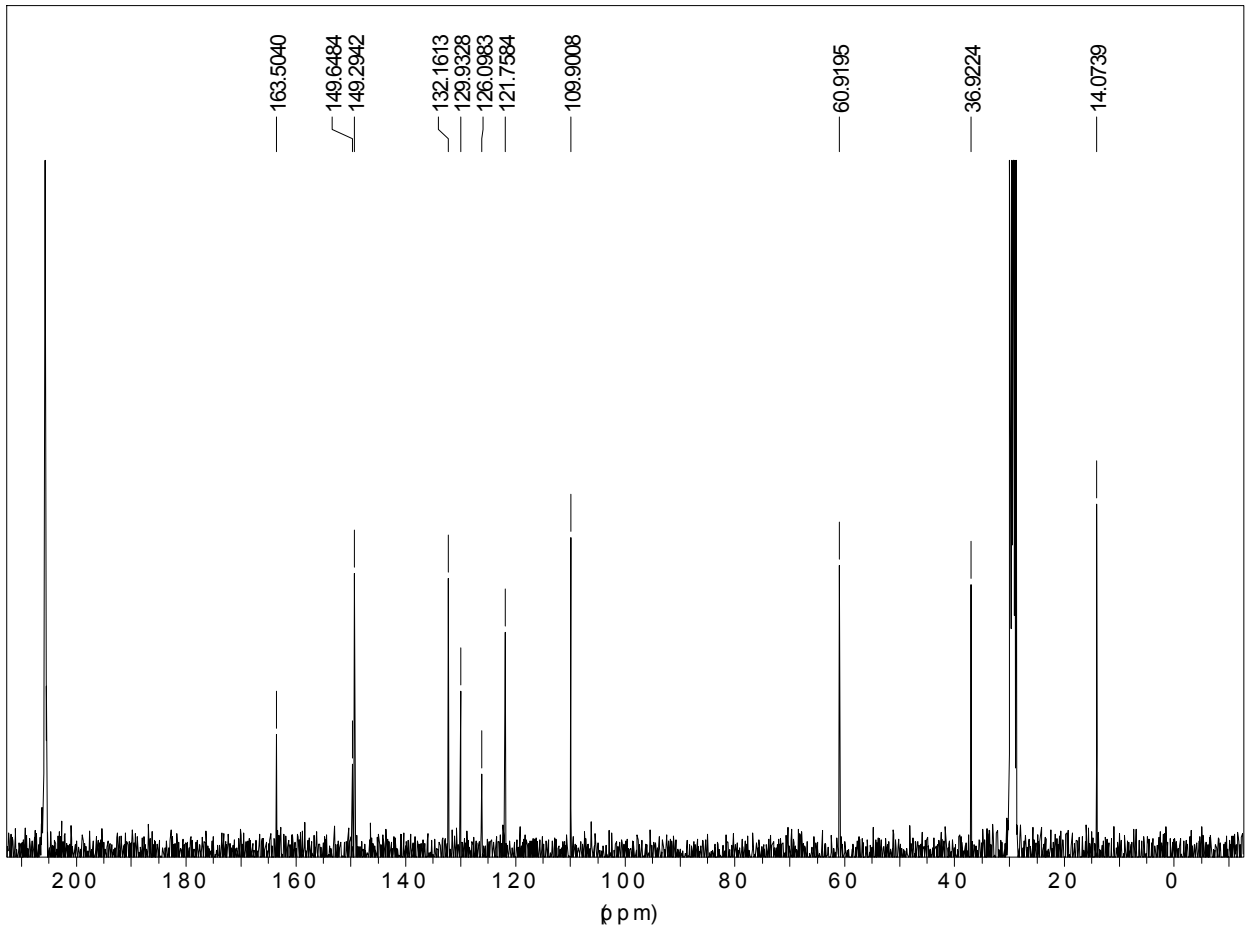

Figure AV-48. ^{13}C NMR spectrum of **V-15** in deuterated acetone.

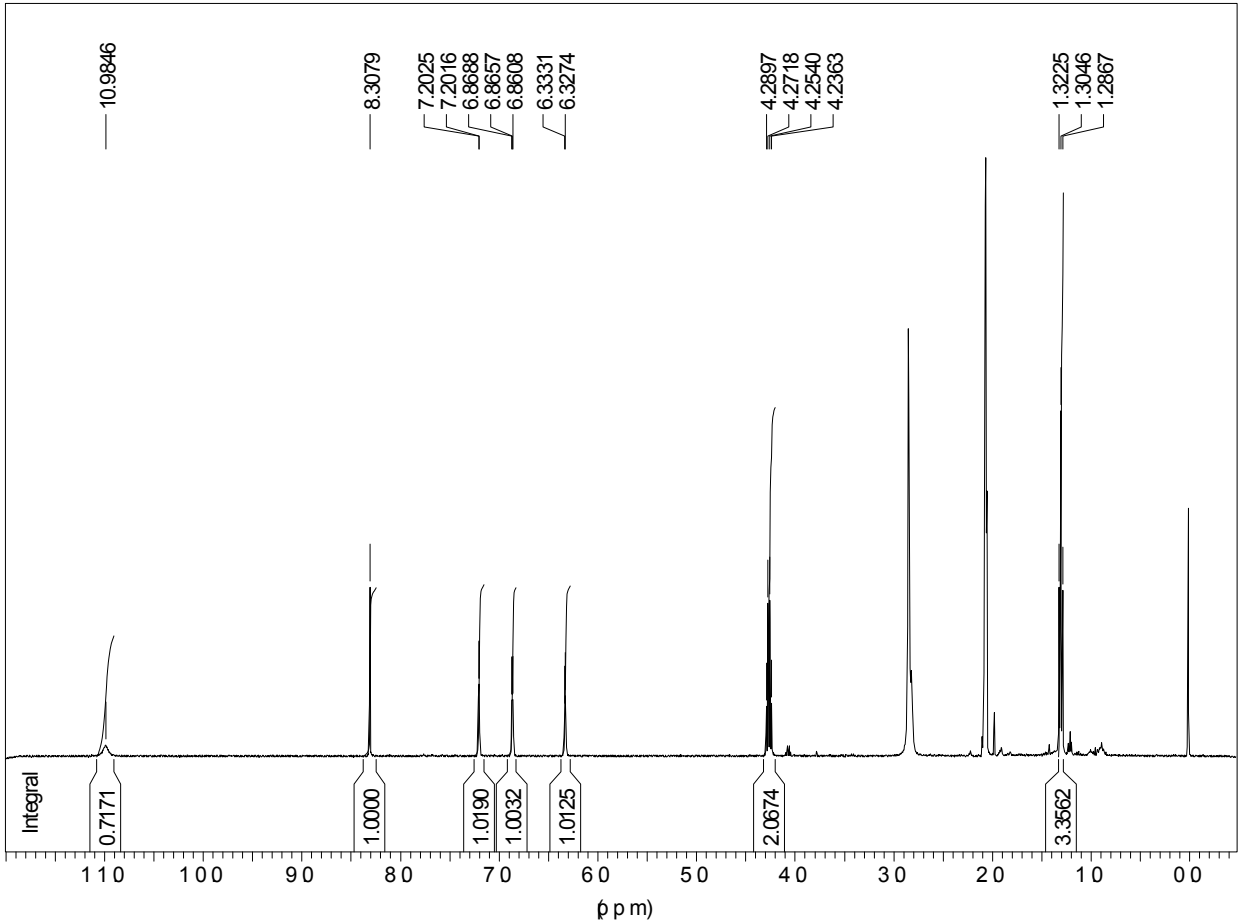

Figure AV-49. ^{1}H NMR spectrum of **V-16** in deuterated acetone.

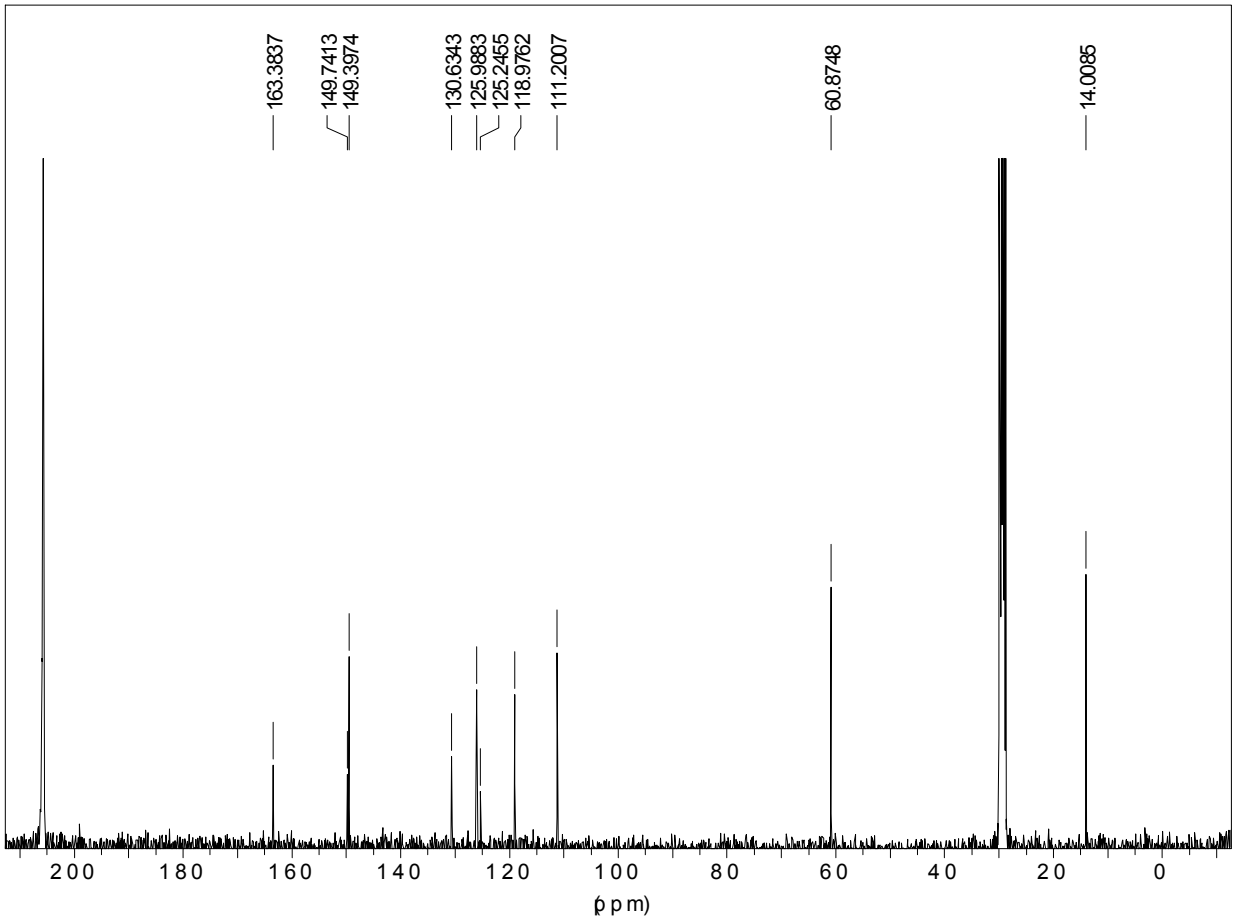

Figure AV-50. ^{13}C NMR spectrum of **V-16** in deuterated acetone.

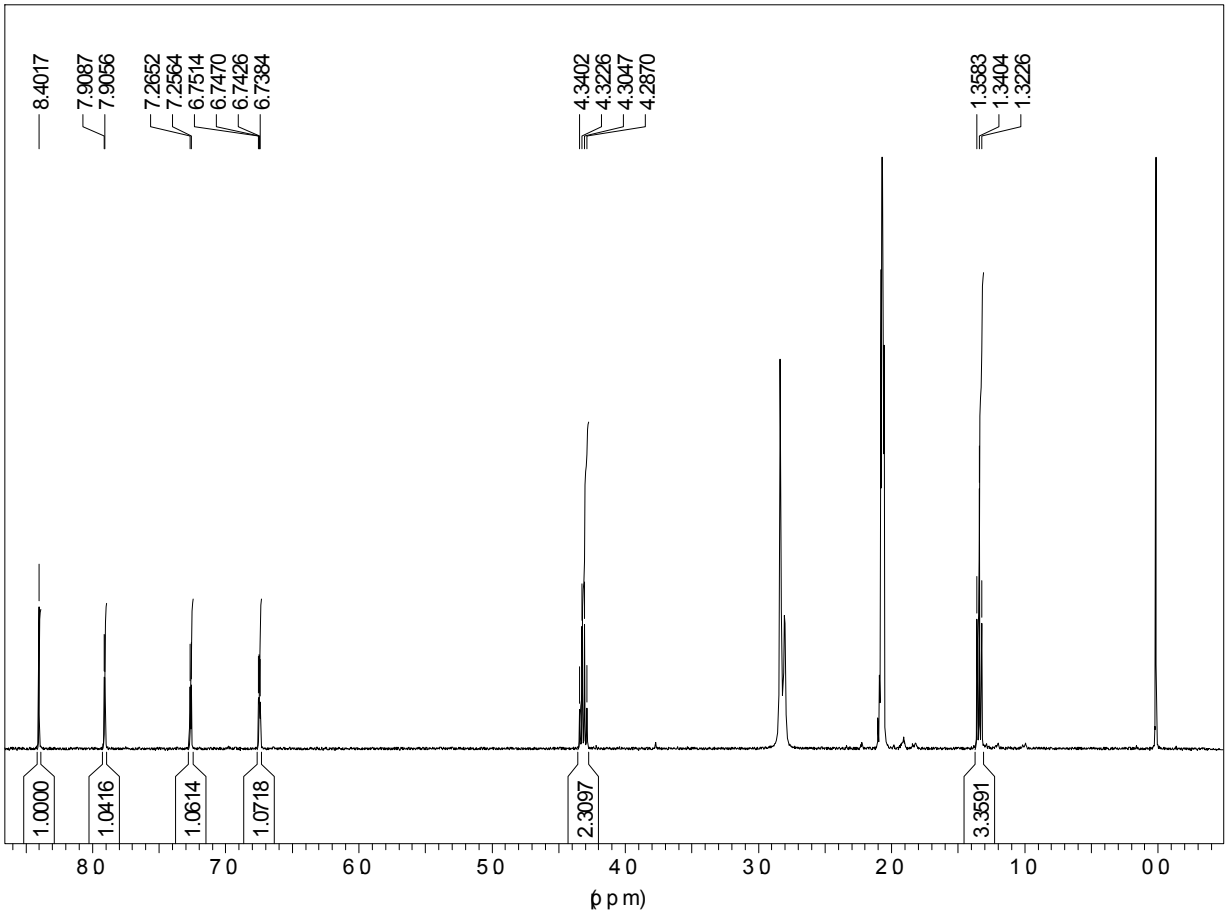

Figure AV-51. ^{1}H NMR spectrum of **V-18** in deuterated acetone.

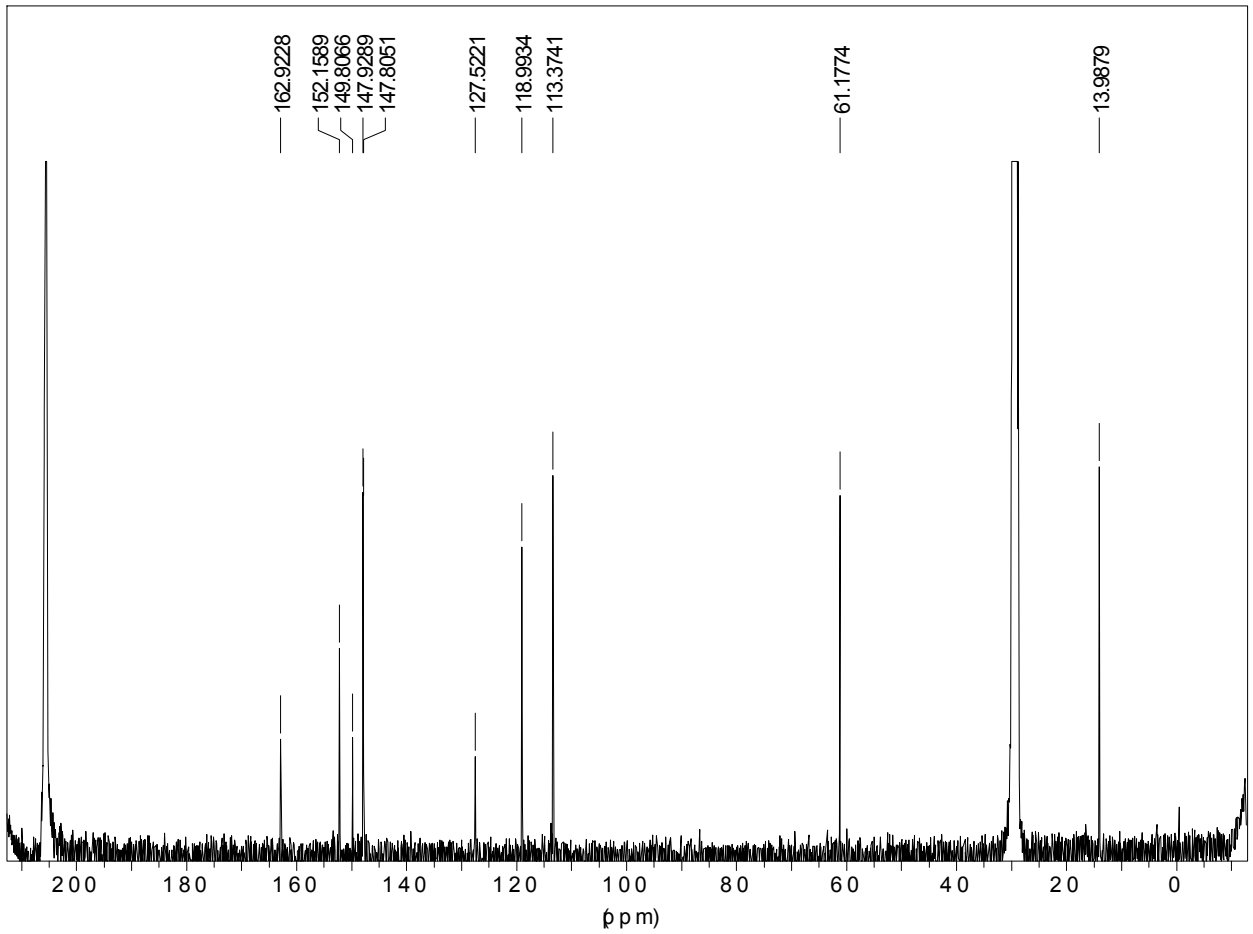

Figure AV-52. ^{13}C NMR spectrum of **V-18** in deuterated acetone.

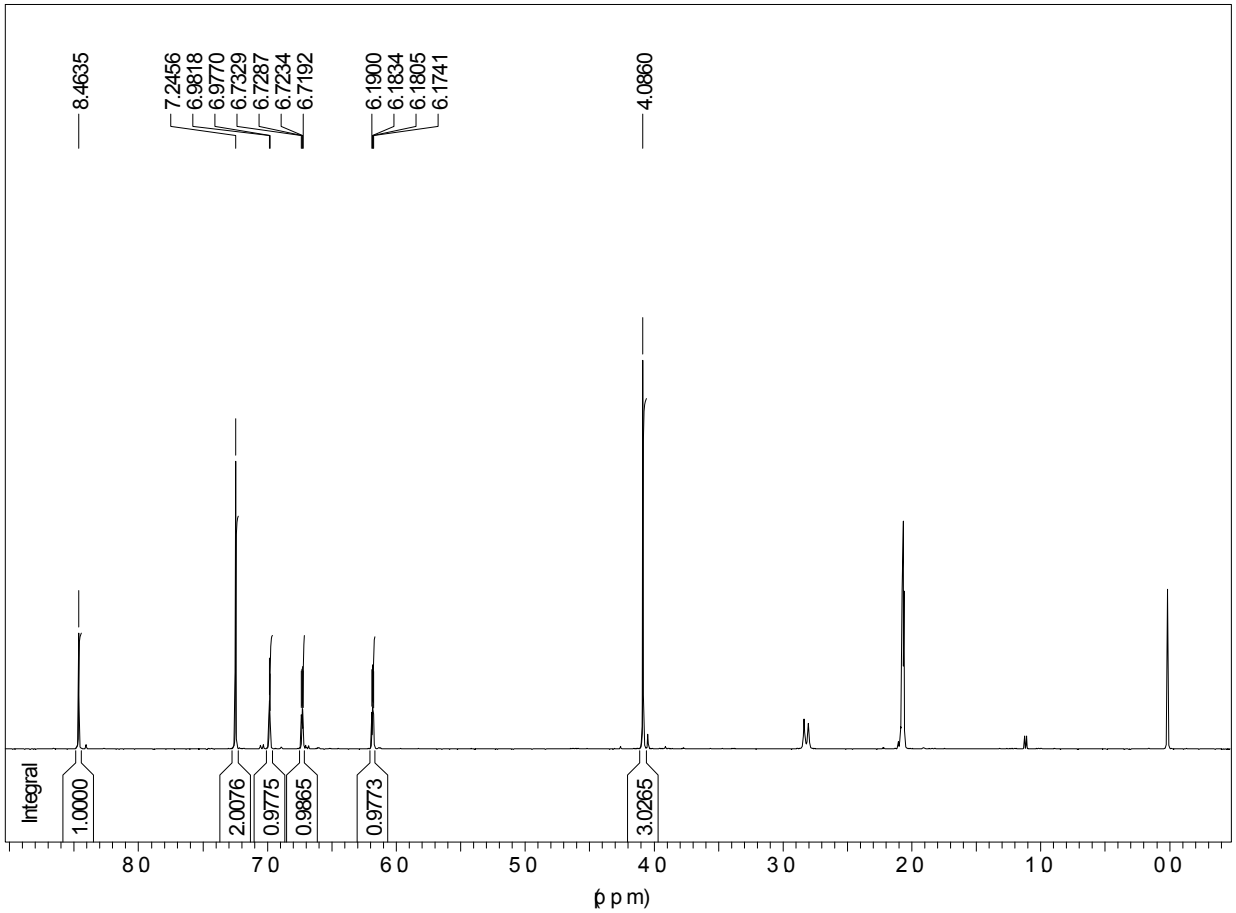

Figure AV-53. ^{1}H NMR spectrum of **V-22** in deuterated acetone.

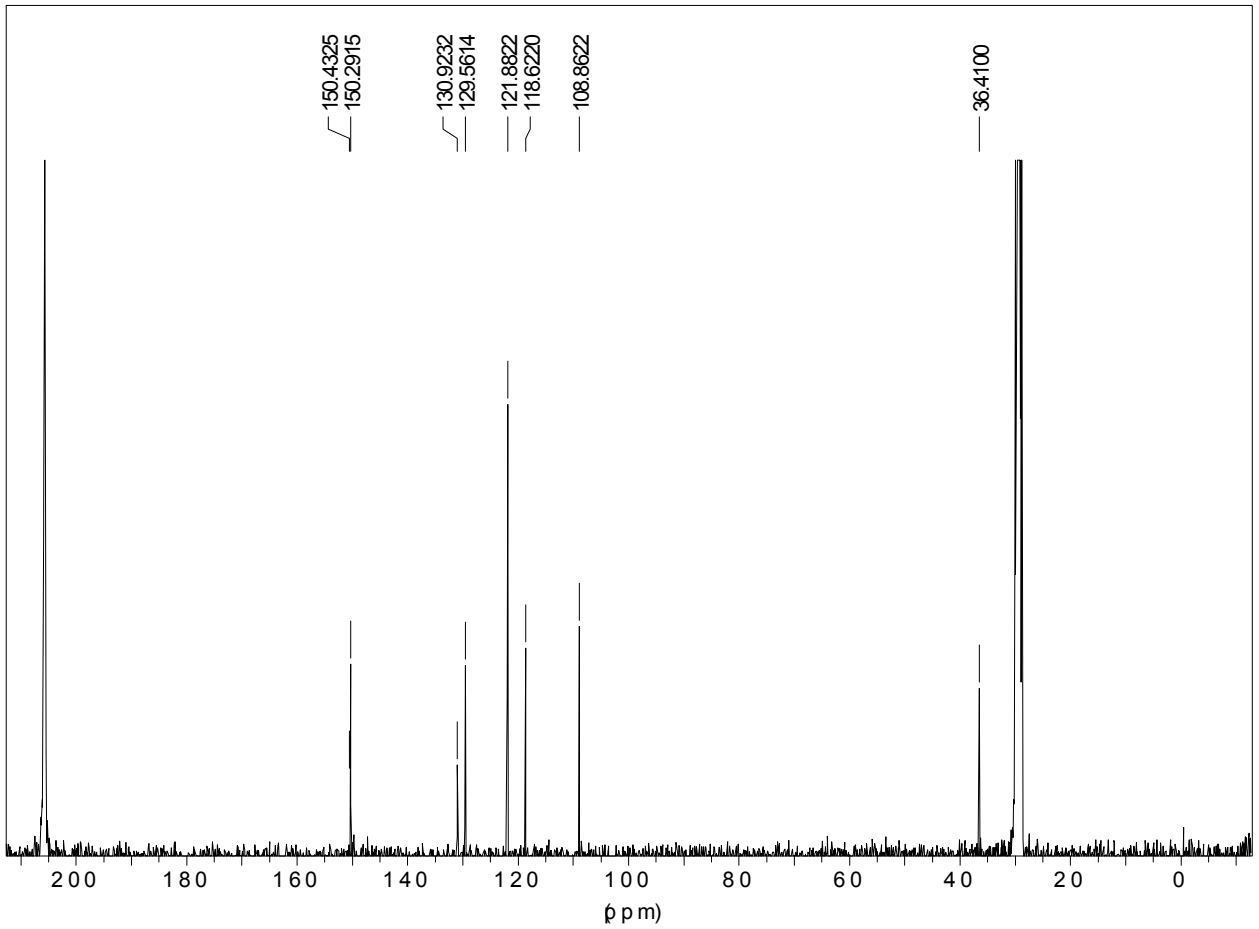

Figure AV-54. ^{13}C NMR spectrum of **V-22** in deuterated acetone.

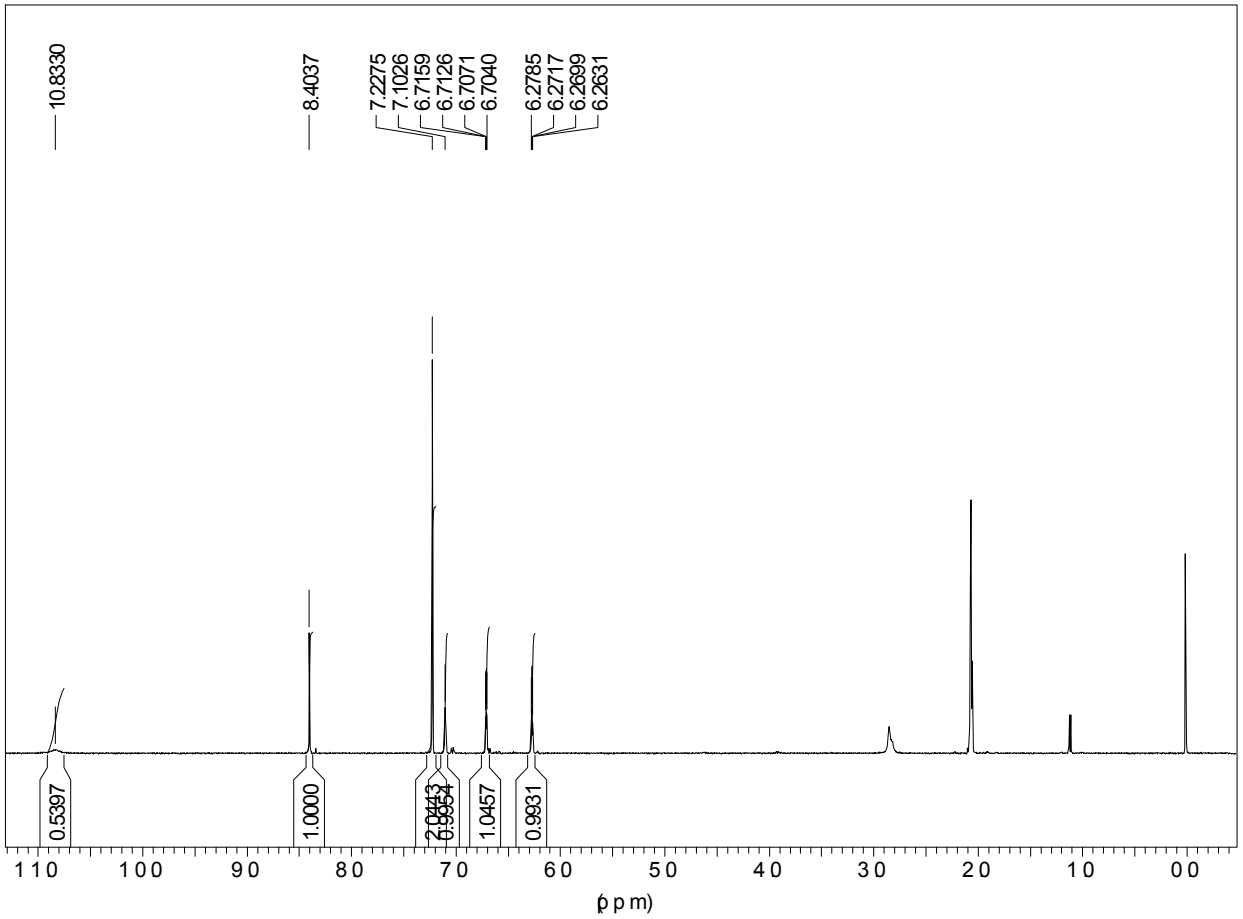

Figure AV-55. ^{1}H NMR spectrum of **V-23** in deuterated acetone.

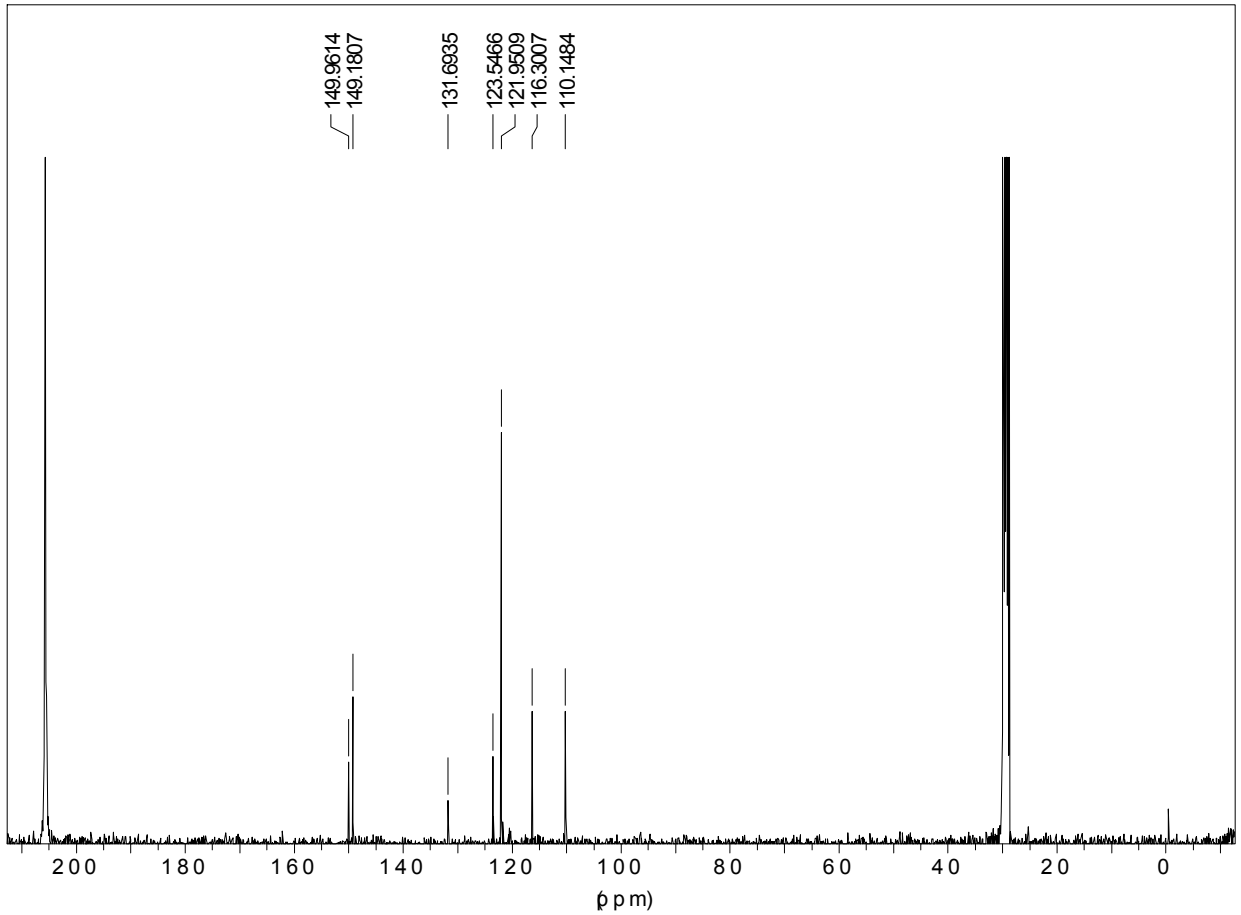

Figure AV-56. ^{13}C NMR spectrum of **V-23** in deuterated acetone.

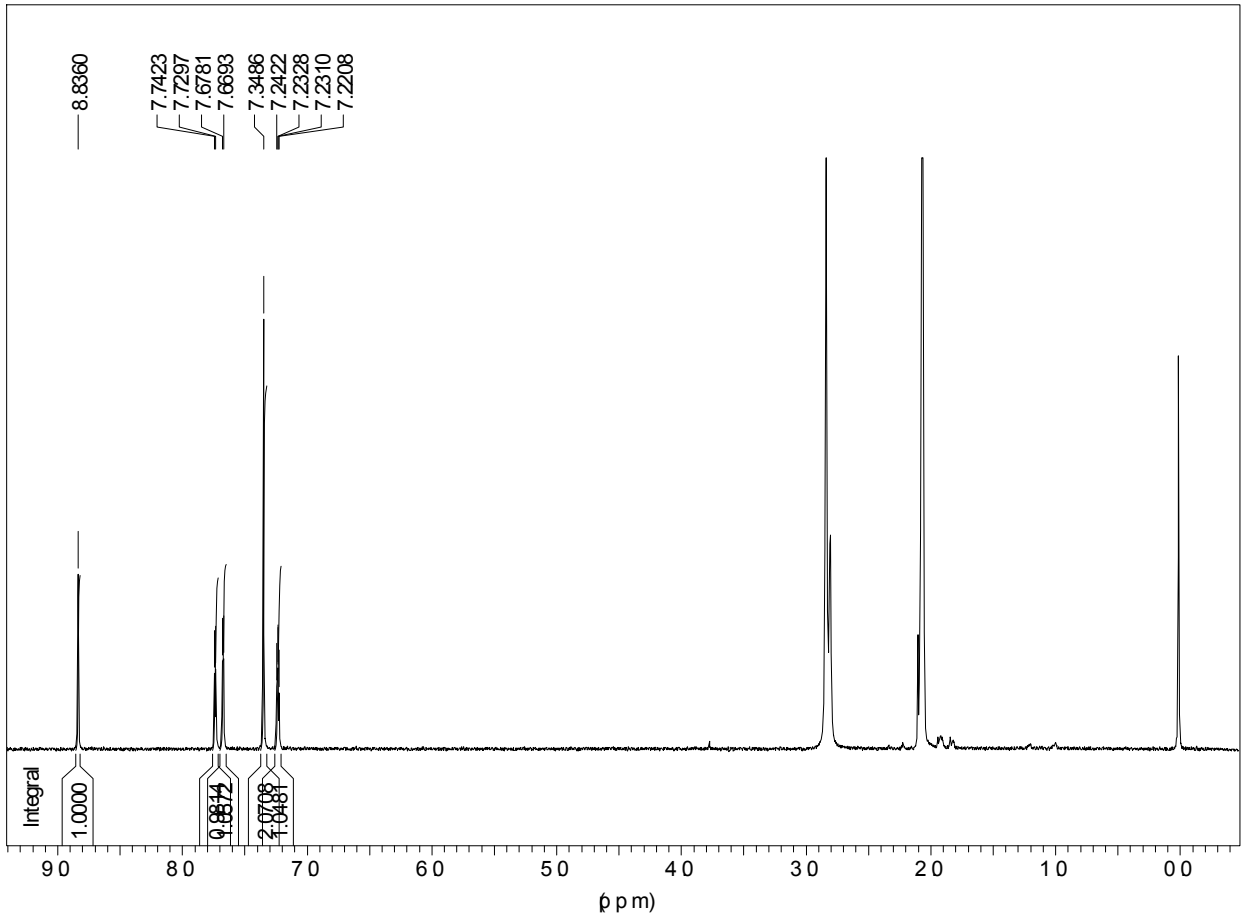

Figure AV-57. ^{1}H NMR spectrum of **V-24** in deuterated acetone.

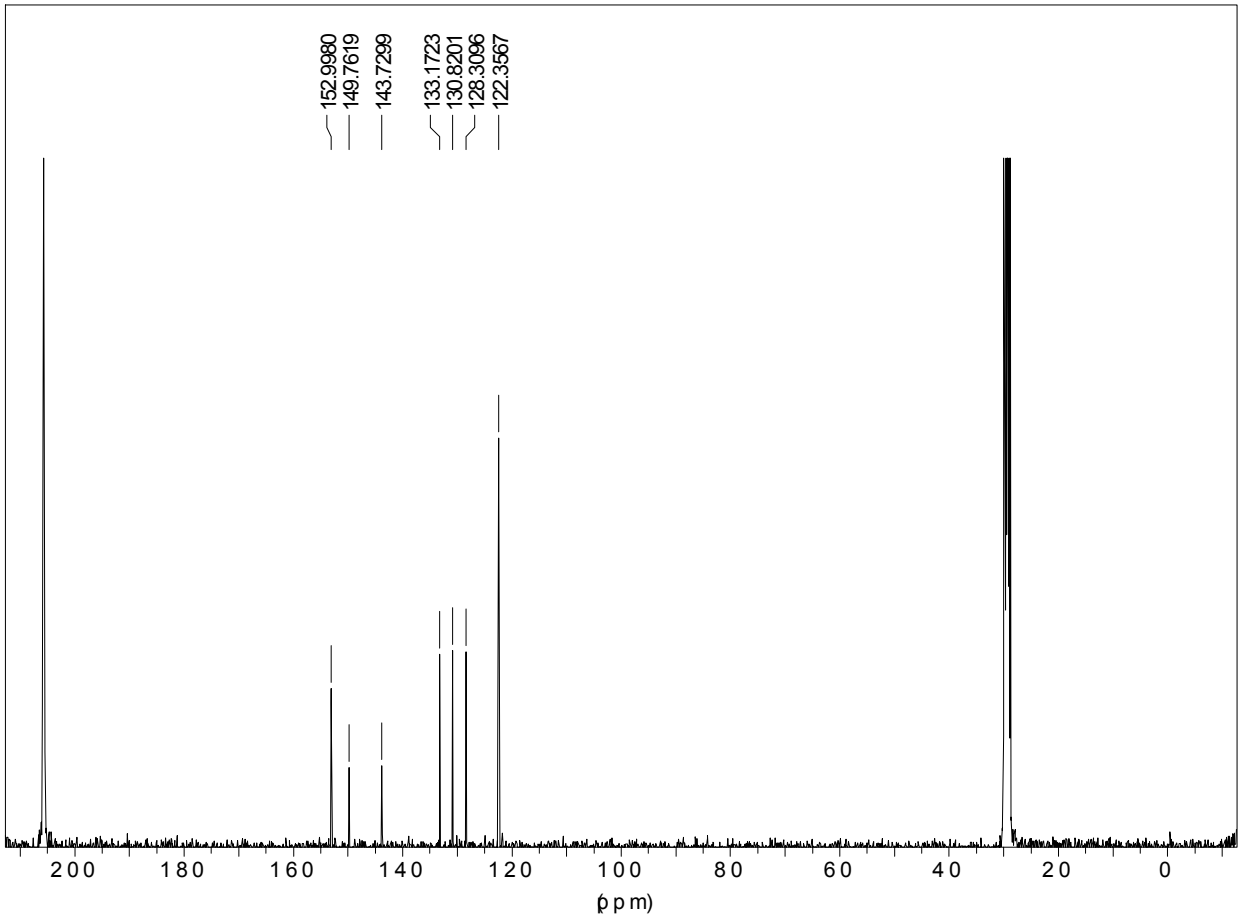

Figure AV-58. ^{13}C NMR spectrum of **V-24** in deuterated acetone.

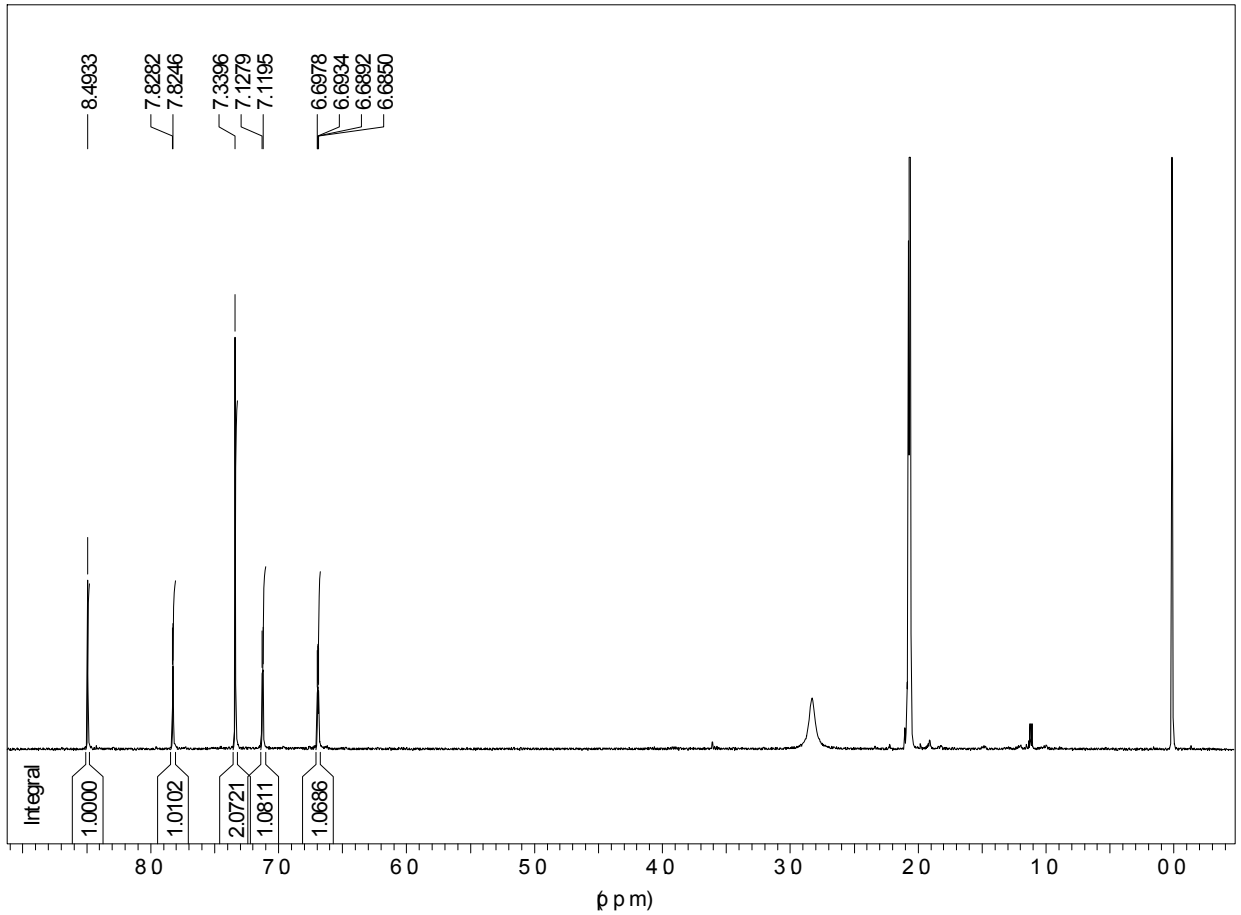

Figure AV-59. ^{1}H NMR spectrum of **V-25** in deuterated acetone.

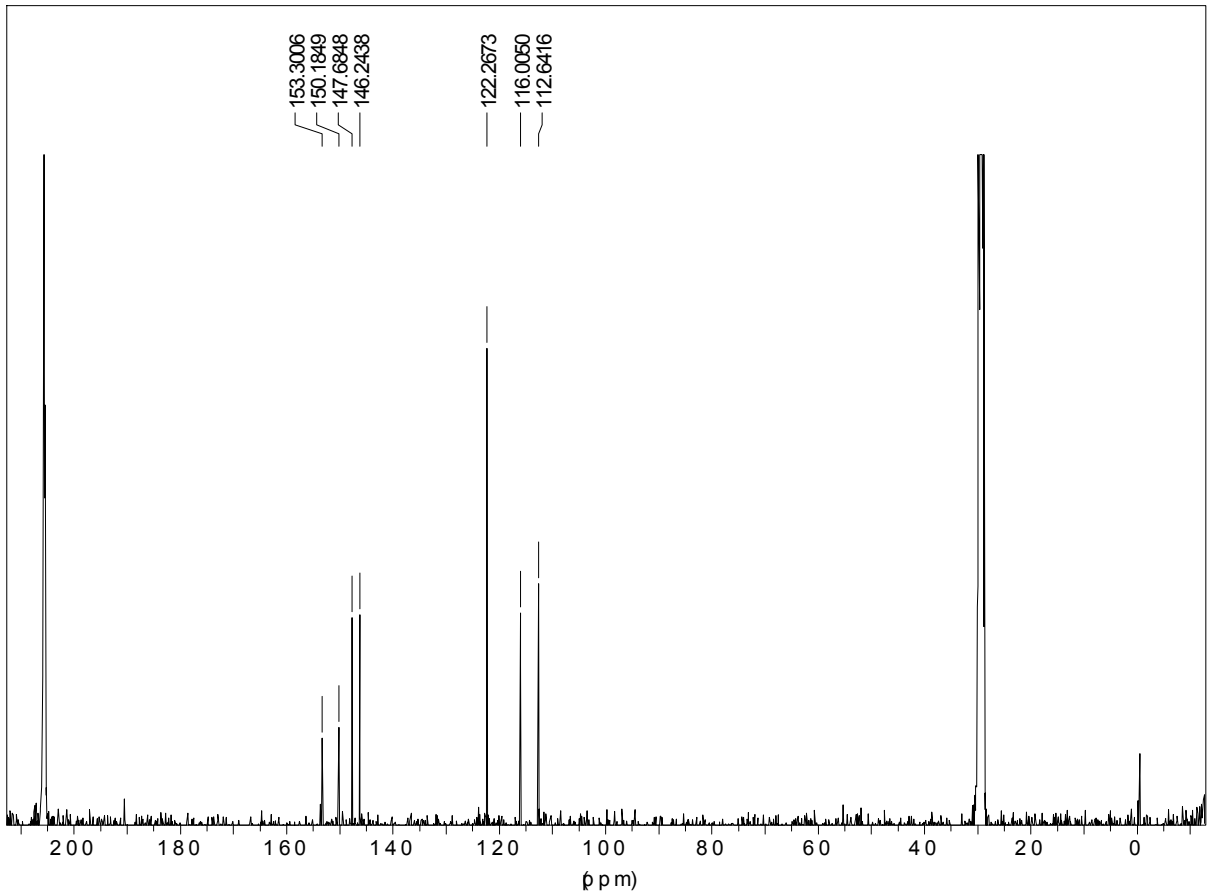

Figure AV-60. ^{13}C NMR spectrum of **V-25** in deuterated acetone.

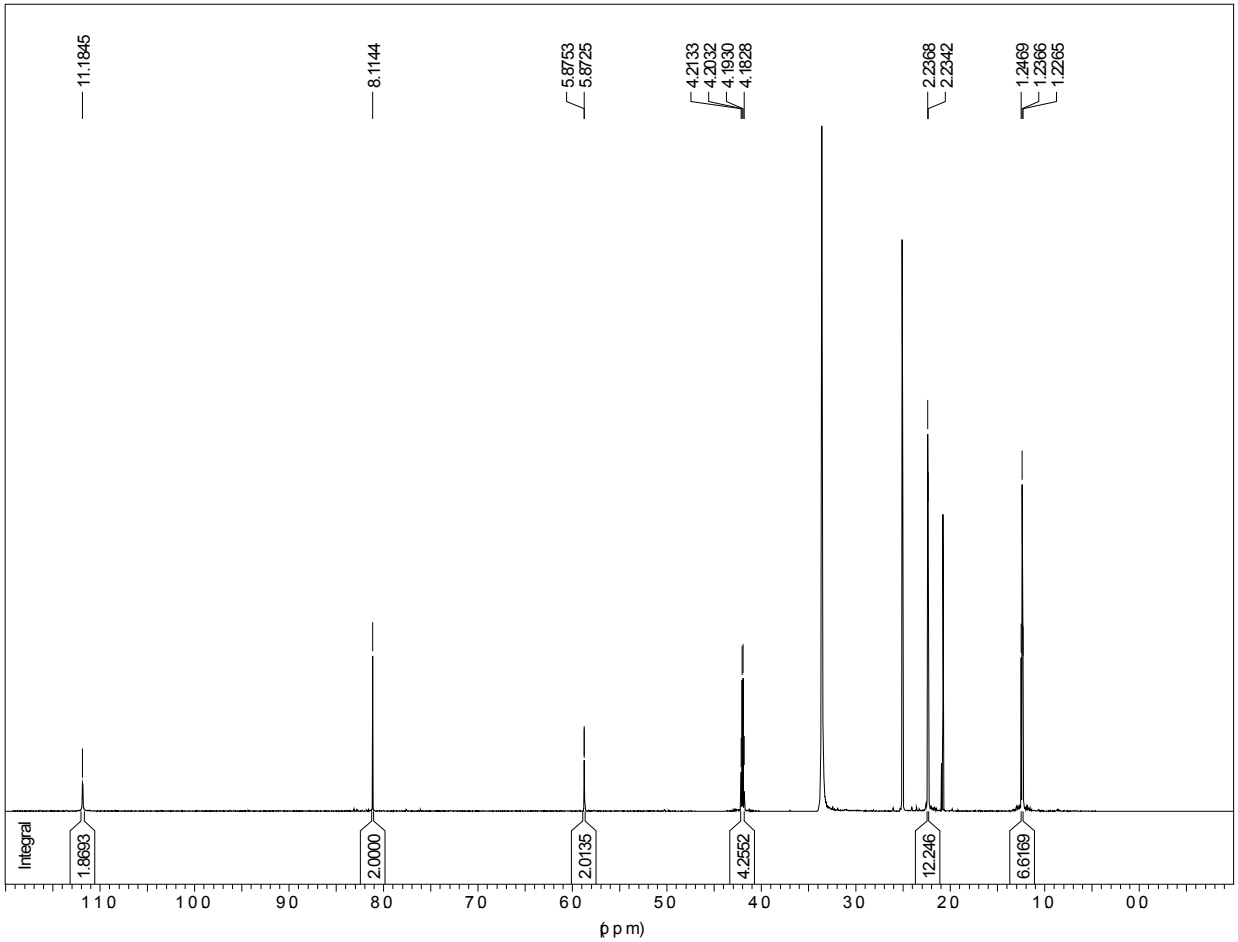

Figure AV-61. ^{1}H NMR spectrum of **V-26** in deuterated DMSO.

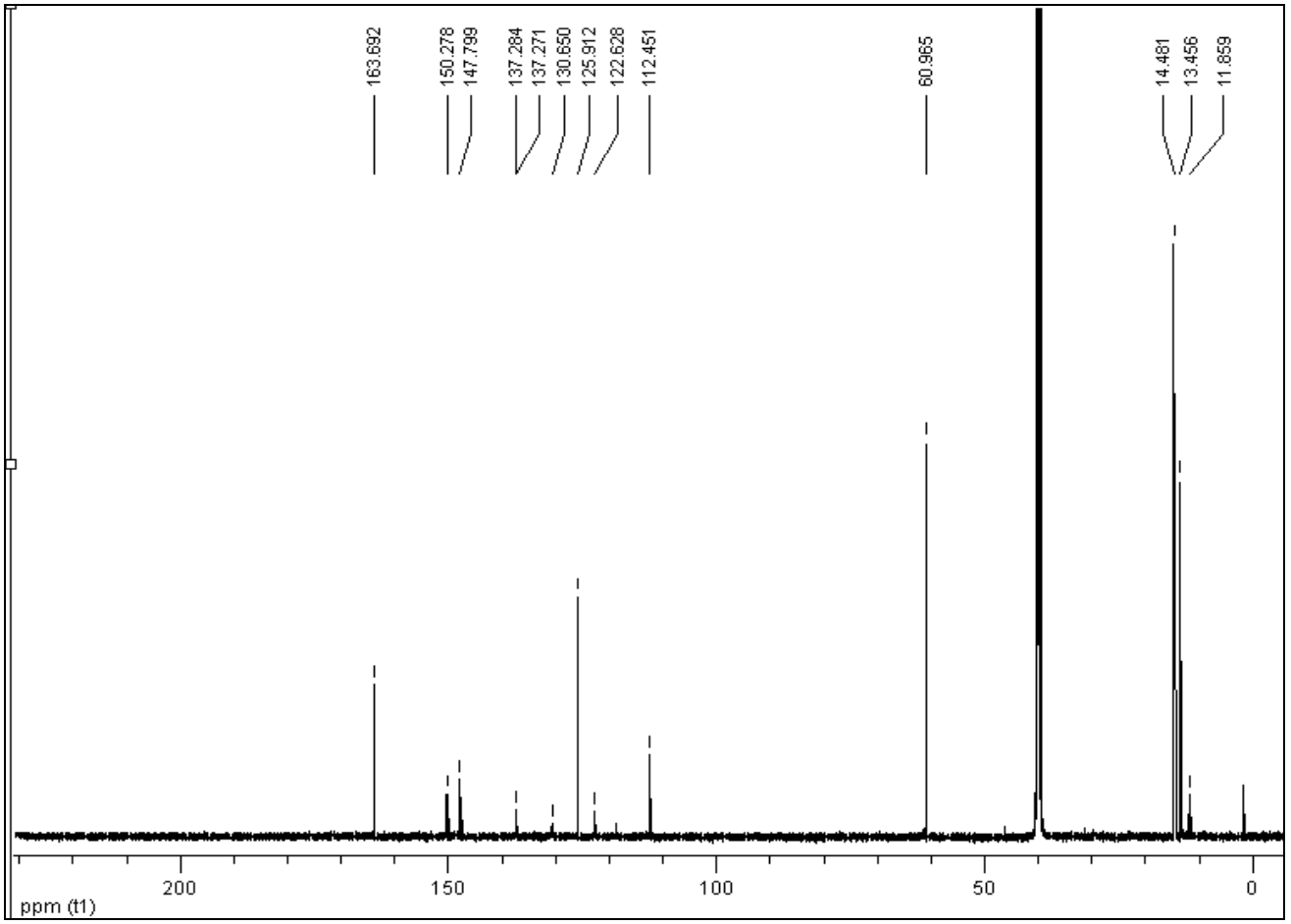

Figure AV-62. ^{13}C NMR spectrum of **V-26** in deuterated DMSO.

Table AV-1. Additional spectroscopic and electrochemical results for each comonomer.

	Compound	ε (L/mol*cm)	τ^a(ns)	Phospho	E_T (kcal/mol)	$k_r{}^b$ ($10^3 s^{-1}$)	$k_{nr}{}^c$ ($10^6 s^{-1}$)	E_{pa2} (V)	$E_{pa(ITO)}$ (V)
	V-1	37000	13.5	479	60	185	74	1.1	-
	V-2	15000	3.9	493	58	0.77	257	-	-
Dyads	V-7	23000	1.8	500	57	52	553	1.6	1.5
	V-8	27000	3.7	500	57	30	273	1.9	1.2
	V-9	17000	5.4	480	60	722	184	-	1.3
	V-10	21000	2.3	484	59	100	435	-	1.4
	V-11	29500	10.2	506	57	42	98	1.2	1.2
	V-12	30000	2.6	538	53	100	385	1.3	1.2
	V-13	19000	14.0	525	54	207	71	1.4	1.2
	V-14	24500	2.0	528	54	385	500	1.4	1.1
Triads	V-15	31500	7.3	566	51	699	136	1.3	1.1
	V-16	22500	4.4	534	54	568	227	1.3	1.0
	V-17	27000	13.2	560	51	212	76	1.3	0.9
	V-18	24500	8.0	544	53	120	125	1.3	1.0
	V-19	29000	3.1	566	51	123	324	1.4	0.9
	V-20	29000	1.3	550	52	923	768	1.6	1.0
	V-21	32500	2.1	552	52	310	477	1.5	0.8
Analogue	V-22	40000	1.9	469	61	632	526	1.2	1.3
	V-23	39000	0.9	480	60	3667	1108	1.3	1.1
	V-24	33000	6.4	493	58	58	157	-	1.2
	V-25	25000	2.0	501	57	230	500	1.4	1.0

[a]Monoexponential fluorescence lifetime measured at λ_{em} max. [b]$k_R = \Phi_{fl}/\tau_{fl}$. [c]$k_{NR} = k_R(1-\Phi_{fl})/\Phi_{fl}$.

Table AV-2. Details of crystal structure determination of **V-20**.

Formula	$C_{21}H_{21}N_3O_5S$
CCSD no.	see remark 1
Mw (g/mol); F(000)	427.47 g/mol ; 896
Crystal color and form	Red plate
Crystal size (mm)	0.15 x 0.09 x 0.05
T (K); $d_{calcd.}$ (g/cm^3)	150 (2) ; 1.407
Crystal System	Monoclinic
Space Group	$P2_1/c$
Unit Cell: a (Å)	15.041 (3)
b (Å)	7.5421 (15)
c (Å)	18.827 (4)
α (°)	90.000
β (°)	109.17 (3)
γ (°)	90.000
V (Å^3); Z	2017.4 (8) ; 4
θ range (°); completeness	3.11 – 72.07 ; 0.960
Reflections: collected / independent; R_{int}	19643 / 3816 ; 0.147
μ (mm^{-1}) Abs. Corr.	1.767 Semi-empirical
R1(F); wR(F^2) [I > 2σ(I)]	0.0775; 0.1560
R1(F); wR(F^2) (all data)	0.1529; 0.1875
GoF(F^2)	0.955
Max. residual e$^-$ density	0.372 e$^-$·Å^{-3}